

# **Biodegradable Polymer-Clay Nanocomposites for Food Packaging**

**Doctoral Thesis**

submitted to obtain the academic degree of

**Doctor of Natural Sciences (Dr. rer. nat.)**

from the Bayreuth Graduate School of Mathematical and Natural  
Sciences (BayNAT) of the University of Bayreuth

**Renee Lauren Timmins**

from Philadelphia

Bayreuth, 2023



This doctoral thesis was prepared at the department of Inorganic Chemistry at the University of Bayreuth from Sept. 2019 until November 2022 and was supervised by Prof. Dr. Josef Breu.

This is a full reprint of the thesis submitted to obtain the academic degree of Doctor of Natural Sciences (Dr. rer. nat.) and approved by the Bayreuth Graduate School of Mathematical and Natural Sciences (BayNAT) of the University of Bayreuth.

Form of the dissertation: Cumulative

Date of submission: 09.03.2023

Admission by the executive board: 30.03.2023

Date of defence: 31.10.2023

Acting director: Prof. Dr. Jürgen Köhler

Doctoral committee:

Prof. Dr. Josef Breu

Prof. Dr. Seema Agarwal

Prof. Dr. Markus Retsch

Prof. Dr. Stefan Peiffer



We need acts of restoration, not only for polluted waters and degraded lands, but also for our relationship to the world. We need to restore honor to the way we live, so that when we walk through the world we don't have to avert our eyes with shame, so that we can hold our heads up high and receive the respectful acknowledgment of the rest of the earth's beings.

- Robin Wall Kimmerer

*Braiding Sweetgrass*



# Table of Contents

List of Abbreviations	- ix -
<i>1. Summary</i>	- 1 -
<i>2. Zusammenfassung</i>	- 3 -
<i>3. Introduction</i>	- 5 -
3.1. Plastic Packaging: From Its Origin to Its Pollution	- 5 -
3.2. Biodegradable polymers	- 7 -
3.2.1. Biodegradation and microplastic formation	- 8 -
3.2.2. Biodegradable commercial polymers	- 10 -
3.2.3. Addressing the drawbacks of biodegradable polymers	- 13 -
3.3. Polymer Clay Nanocomposites	- 15 -
3.3.1. Polymer barrier	- 15 -
3.3.2. Clay as a barrier filler	- 18 -
3.3.3. Synthetic hectorite and osmotic swelling	- 20 -
3.3.4. Biodegradable polymer-Hec nanocomposites	- 23 -
3.3.5. Osmotic swelling extended into organic solvents	- 24 -
3.4. Relevant Characterization Methods	- 25 -
3.4.1. X-Ray scattering and diffraction	- 25 -
3.4.2. Gas barrier measurements	- 26 -
3.4.3. Biodegradation testing	- 26 -
3.5. Preparation of Nanocomposite Coatings and Films	- 27 -
3.5.1. Spray coating	- 27 -
3.5.2. Doctor blade	- 28 -
3.5.3. Slot-die coating	- 28 -
<i>4. Synopsis</i>	- 30 -
4.1. High Barrier Nanocomposite Film with Accelerated Biodegradation by Clay Swelling Induced Fragmentation	- 32 -
4.2. Stretchable and Fast Composting Polyester Films with High-Performance Oxygen Barrier	- 33 -
4.3. Spontaneous Delamination of Affordable Natural Vermiculite as a High Barrier Filler for Biodegradable Food Packaging	- 35 -
4.4. Biodegradation in Wastewater of Water-Soluble Polymer/Clay Barrier Films from Green and Scalable Processing	- 36 -

5. <i>Literature</i>	- 38 -
6. <i>Results</i>	- 44 -
6.1. High Barrier Nanocomposite Film with Accelerated Biodegradation by Clay Swelling Induced Fragmentation	- 44 -
6.2. Stretchable and Fast Composting Polyester Films with High-Performance Oxygen Barrier	- 61 -
6.3. Spontaneous Delamination of Affordable Natural Vermiculite as a High Barrier Filler for Biodegradable Food Packaging	- 100 -
6.4. Biodegradation in Wastewater of Water-Soluble Polymer/Clay Barrier Films from Green and Scalable Processing	- 123 -
7. List of Publications	- 145 -
8. Acknowledgements	- 147 -
9. Author's statement	- 149 -

## List of Abbreviations

alg	sodium alginate	PEG	poly(ethylene glycol)
BIF	barrier improvement factor	PET	polyethylene terephthalate
CNF	Cellulose nanofiber	PLA	poly(lactide)
D	diffusion coefficient	PDLLA	poly(DL-lactide)
DDT	dichlorodiphenyltrichloroethane	PLLA	poly(L-lactide)
DSC	dynamic scanning calorimetry	PP	polypropylene
FTIR	fourier-transform infrared spectroscopy	PVC	polyvinyl chloride
GlyChit	glycol chitosan	PVDC	poly(vinylidene chloride)
GPC	gel permeation chromatography	PVOH	poly(vinyl alcohol)
Hec	synthetic sodium fluorohectorite	PVP	polyvinylpyrrolidone
HPMC	hydroxypropyl methylcellulose	RH	relative humidity
MeCN	acetonitrile	S	solubility coefficient
MP	microplastic	SAXS	small-angle x-ray scattering
NMF	N-methylformamide	SEM	scanning electron microscopy
NMR	nuclear magnetic resonance	TEM	transmission electron microscopy
OTR	oxygen transmission rate	T <sub>g</sub>	glass transition temperature
P	permeability	TR	transmission rate
PBAT	poly(butylene adipate terephthalate)	vol%	volume percentage
PBS	poly(butyl succinate)	WL	water layer
PBDMS	poly(benzenedimethylene succinate)	wt%	weight percentage
PB <sub>x</sub> BDM <sub>y</sub> S	poly(butyl benzenedimethylene succinate)	WVTR	water vapor transmission rate
PBT	poly(butylene terephthalate)	XRD	powder x-ray diffraction
PE	polyethylene	18C6	18-crown-6



## 1. Summary

Plastic pollution is everywhere. We can see the buildup growing in our landfills and oceans in the recent decades, but perhaps more dangerous is the micro-sized plastic that we cannot see. The resistance of conventional plastics to degradation means that the physical breakdown of bulk plastic in the environment leaves behind tiny plastic fragments that are mobile and hazardous to ecosystems and human health. It is this same resistance to degradation, as well as other favorable physical characteristics, that have made plastics indispensable to society.

The largest consumption of plastic is for single-use, disposable packaging. Alternative materials in this sector that would not persist in natural systems, i.e. capable of undergoing biodegradation, would mitigate meaningful amounts of plastic waste from accumulating in the environment. The challenge is matching the properties of the conventional materials with ones that are also susceptible to biodegradation.

Focusing in on single-use food packaging, the requirements of a suitable material include a barrier to gases that cause deteriorative reactions, like oxygen and water vapor, and to be mechanically apt for the given application (flexible film vs. rigid container). Moreover, for a material to be truly feasible as a replacement to conventional materials, it should be processed on a large scale and available at a reasonable cost.

In this work, the combination of biodegradable polymers with clay nanosheets was explored to meet the requirements of a food packaging material without sacrificing rapid environmental biodegradation. Nanosheets within a polymer matrix act as impermeable obstacles, creating a tortuous path against the diffusion of small molecules through the material. Synthetic sodium fluorohectorite (Hec) is particularly adapt for this purpose due to its exceptionally high aspect ratio and its rare ability to osmotically swell in water. Osmotic swelling allows for near effortless conversion from the bulk clay into individual platelets that form a stable, liquid crystalline suspension. A polymer solution can then be processed with the clay suspension to create high barrier films. The manuscripts in this thesis demonstrate strategies to process clay nanosheets with biodegradable polymers to obtain films for food packaging, and the effects that this combination may have on relevant film properties beyond barrier.

The first study sought to improve commercial poly(lactide) (PLA); a biodegradable polymer that suffers from poor barrier properties, low flexural strength, and slow biodegradation in aqueous environments. The direct combination of this hydrophobic polyester with liquid crystalline clay suspensions had been restricted by the requirement of water to achieve

osmotic swelling. By the addition of crown ethers to complex interlayer cations and provide steric pressure, osmotic delamination of Hec was achieved and finally allowed for solution processing of a PLA/Hec nanocomposite. This nanocomposite, prepared from layered slot-die coating, exhibited excellent barrier to oxygen and resistance to swelling under humid conditions, although mechanically brittle. Once immersed in water, the clay tactoids swell, physically fragmenting the film. The accelerated biodegradation rate in wastewater observed for the PLA/Hec film was in part attributed to the increased surface area after fragmentation.

The following study took a step away from commercial polymers to focus on a promising novel polyester for flexible films that exhibited rapid hydrolysis and stretchable mechanical performance, however its gas barrier was unsuitable. Rather than the direct combination of the polyester with a barrier clay, which would cause embrittlement, a nanocomposite coating was applied by spray coating an aqueous glycol chitosan/Hec suspension. The nanocomposite coated film maintained the polyethylene-like mechanical behavior and rapid biodegradation in wastewater, although slightly slower than the polyester without a coating.

Regardless of polymer choice, the high-quality synthetic Hec imparts steep prices on the nanocomposite film. To substitute the expensive synthetic Hec, a natural and abundant vermiculite clay was investigated for the production of barrier nanosheets in solution. Although vermiculite materials have historically required long procedures to obtain osmotically swollen states, by complexation of the interlayer  $Mg^{2+}$  cation with an appropriate anion, a quick and sufficient ion exchange is facilitated with yields as high as 84%. To demonstrate the effectiveness of these nanosheets as a barrier filler, a PLA/vermiculite nanocomposite coating was applied to a porous cellulose nanofiber substrate. Dramatic increase in the barrier to oxygen and water vapor were obtained and the low costs of natural vermiculite bring down the total price of the nanocomposite film.

Lastly, biodegradable packaging beyond food applications was investigated. Films applied for water-soluble packets of single portion detergents, pesticides etc., are typically made from poly (vinyl alcohol), despite its poor biodegradation in the intended medium of disposal: wastewater. Biopolymers hydroxypropyl methylcellulose and sodium alginate were investigated as replacements for this application. Sandwich layered films of each polymer were prepared with a simulated roll-to-roll processing scheme. A pure Hec center layer in the films acted as an impermeable barrier wall that also provided mechanical reinforcement. The layered structure with the barrier filler center did not significantly impede biodegradation, although only the alginate-based film exhibited rapid mineralization in wastewater.

## 2. Zusammenfassung

Die Plastikverschmutzung ist allgegenwärtig. Die Anhäufung in unseren Mülldeponien und Ozeanen hat in den letzten Jahrzehnten drastisch zugenommen, wobei die Gefahr durch Mikroplastik immer deutlicher wird. Der Zersetzungswiderstand herkömmlicher Kunststoffe hat zur Folge, dass der physikalische Abbau von Massenkunststoffen in der Umwelt winzige, mobile Fragmente zurücklässt, die eine Gefahr für Ökosysteme und die menschliche Gesundheit darstellen. Genau diese Abbaubeständigkeit sowie andere günstige physikalische Eigenschaften machen Kunststoffe für die Gesellschaft unverzichtbar.

Der Großteil des Kunststoffverbrauchs entfällt durch Einwegverpackungen. Alternative Kunststoffe, die nicht in natürlichen Systemen verbleiben, d.h. biologisch abbaubar sind, würden die Anhäufung von Kunststoffabfällen in der Umwelt erheblich verringern. Die Herausforderung besteht darin, die Eigenschaften der herkömmlichen Materialien mit denen der biologisch abbaubaren Materialien in Einklang zu bringen.

Die Anforderungen an ein geeignetes Material für Einweg-Lebensmittelverpackungen umfassen die Barriere für Gase wie Sauerstoff und Wasserdampf, die zur Nahrungsmittelverderben führen, und eine mechanische Eignung für die jeweilige Anwendung (flexible Folie vs. steifer Behälter). Damit ein Material wirklich als Ersatz für herkömmliche Materialien in Frage kommt, sollte es großtechnisch und kostengünstig verarbeitbar sein.

In dieser Arbeit wurde die Kombination von biologisch abbaubaren Polymeren mit Schichtsilikaten erforscht, um die Anforderungen einer Lebensmittelverpackung zu erfüllen, ohne die schnelle biologische Abbaubarkeit in der Umwelt zu beeinträchtigen. Schichtsilikate in einer Polymermatrix verlängern den Diffusionsweg kleiner Moleküle durch die Ausbildung eines gewundenen Pfades. Synthetisches Natriumfluorhectorit (Hec) ist aufgrund des außergewöhnlich hohen Seitenverhältnisses und seltenen Fähigkeit, in Wasser osmotisch zu quellen, für diesen Zweck besonders geeignet. Die osmotische Quellung ermöglicht eine nahezu mühelose Umwandlung des Schichtsilikates in einzelne Nanoplättchen, die eine stabile, flüssig-kristalline Suspension bilden. Diese Suspension kann dann mit einer Polymerlösung verarbeitet werden, um Hochbarrierefolien herzustellen. Die Manuskripte in dieser Arbeit zeigen Strategien zur Verarbeitung von Schichtsilikates-Nanoplättchen mit biologisch abbaubaren Polymeren, um Folien für Lebensmittelverpackungen zu erzeugen und dessen Folieneigenschaften über Barriereigenschaften hinaus zu studieren.

Handelsübliche Poly(lactid) (PLA) ist ein biologisch abbaubares Polymer, das unter schlechten Barriereigenschaften, geringer Biegefestigkeit und langsamem biologischen Abbau in wässriger Umgebung leidet. Die direkte Kombination dieses hydrophoben Polyesters mit flüssigkristallinen Schichtsilikatsuspensionen war zuvor auf wässrige Systeme eingeschränkt, welches eine Voraussetzung zur osmotischen Quellung war. Durch die Zugabe von Kronenethern, die die Zwischenschichtkationen komplexieren und für sterischen

Druck sorgen, wurde die osmotische Delaminierung von Hec erreicht und ermöglichte schließlich die Verarbeitung eines PLA/Hec-Nanokomposits in organischer Lösung. Dieses Nanokomposit, das aus einer geschichteten Slot-Die-Beschichtung hergestellt wurde, wies eine ausgezeichnete Barriere gegen Sauerstoff und eine hohe Quellbeständigkeit unter feuchten Bedingungen auf, war jedoch mechanisch spröde. Nach dem Eintauchen in Wasser quollen die Silikatkolloide auf, wodurch der Film physikalisch fragmentiert wird. Die für den PLA/Hec-Film beobachtete beschleunigte biologische Abbaugeschwindigkeit im Abwasser wurde auf die vergrößerte Oberfläche nach der Fragmentierung zurückgeführt.

Ein vielversprechender neuartiger Polyester für flexible Folien wies eine schnelle Hydrolyse und dehnbare mechanische Eigenschaften auf, die Gasbarriere war jedoch ungeeignet. Anstatt den Polyester direkt mit einem Barriersilikat zu kombinieren, was zur Versprödung führen würde, wurde eine Nanokomposit-Beschichtung durch Aufsprühen einer wässrigen Glykol-Chitosan/Hec-Suspension aufgebracht. Die mit dem Nanokomposit beschichtete Folie behielt das polyethylenähnliche mechanische Verhalten und die schnelle biologische Abbaubarkeit im Abwasser bei, wenn auch etwas langsamer als der Polyester ohne Beschichtung.

Um das teure synthetische Hec zu ersetzen, wurde ein natürlich vorkommendes Vermiculit-Silikat für die Herstellung von Barriere-Nanoplättchen in Lösung untersucht. Obwohl das Vermiculit in der Vergangenheit aufwendige Verfahren erforderte, um einen osmotisch gequollenen Zustand zu erreichen, wird durch die Komplexbildung des  $Mg^{2+}$  Zwischenschichtkationen mit einem geeigneten Anion ein schneller und ausreichender Ionenaustausch mit Ausbeuten von bis zu 84 % ermöglicht. Um die Wirksamkeit dieser Nanoplättchen als Barrierefüller zu demonstrieren, wurde eine PLA/Vermiculit-Nanokomposit-Beschichtung auf ein poröses Zellulose-Nanofasernetzwerk aufgebracht. Es wurde eine drastische Verringerung der Sauerstoff- und Wasserdampfpermeabilität erzielt, wobei die niedrigen Kosten für natürliches Vermiculit den Gesamtpreis der Nanokompositfolie senken.

Folien, die für wasserlösliche Verpackungen von einzelnen Reinigungsmittelkapseln, Pestiziden usw. verwendet werden, bestehen in der Regel aus Polyvinylalkohol, obwohl dieser im vorgesehenen Entsorgungsmedium (Abwasser) schlecht biologisch abbaubar ist. Die Biopolymere Hydroxypropylmethylcellulose und Natriumalginate wurden deshalb als Ersatzstoffe für diese Anwendung untersucht. Die Sandwich-Schichtfilme der beiden Polymere wurden mit einem simulierten Rolle-zu-Rolle-Verarbeitungsschema hergestellt. Eine reine Hec-Mittelschicht in den Filmen diente als undurchlässige Barriere, die gleichzeitig eine mechanische Verstärkung bot. Die Schichtstruktur mit dem Barrierefüllstoff in der Mitte behinderte den biologischen Abbau nicht signifikant, wobei nur der Film auf Alginatbasis eine schnelle Mineralisierung im Abwasser zeigte.

### 3. Introduction

#### 3.1. Plastic Packaging: From Its Origin to Its Pollution

Polymers constitute some of the most basic building blocks of life: DNA, proteins, carbohydrates, and cellulose. It is only in relatively recent history that humankind has harnessed the potential of this chemistry to transform daily life. The scarcity of natural resources during World War II necessitated the first surge in the production of synthetic polymers to produce military gear in the United States. For the first time, nylon was used to make ropes, parachutes, body armor, and more. Poly(methyl methacrylate), also known as Plexiglass, could replace ceramic glass for aircraft windows. Every single member of the U.S. Army received a hygiene kit containing a plastic comb.<sup>1</sup> The seemingly endless uses of this new material inspired a utopian-like vision of the future: The Plastic Man. In their 1941 book entitled 'Plastics',<sup>2</sup> British chemists Victor Yarsley and Edward Couzens envisioned a "world of color and bright shining surfaces [...] in which man, like a magician, makes what he wants for almost every need." Man would grow up surrounded by unbreakable toys, rounded corners, unscuffable walls, warpless windows, dirt-proof fabrics, and lightweight cars, planes, and boats. Then man would grow old with dignity using plastic glasses and dentures, eventually to be buried "hygienically enclosed in a plastic coffin."

With a 300% growth in plastic production by the end of the war, consumers began to reap the benefits of this new inexpensive, sanitary, and safe material as demand from the military declined. The first national Plastics Exposition took place in New York in 1946, just a few months after



**Figure 1.** LIFE Magazine article from August 1<sup>st</sup>, 1955. Reproduced with permission.

the end of the war, and brought thousands to line up and explore all the new products made available by synthetic plastics. Consumption began to ramp up after two decades of war-driven scarcity fueled by the public fascination with the futuristic products afforded by synthetic polymers; textiles and clothing that could be cleaned with only a damp cloth, suitcases light enough to lift with a finger but strong enough to carry one's weight, clear packaging that allowed the shopper to see the food inside.<sup>3</sup> Polyester was first introduced into the commercial market in 1954 and plastic production only continued to explode. Within the next 50 years, it became hard to imagine a life without plastic food containers and bags, spandex clothing, polyvinyl chloride (PVC) pipes, casing for electronics, automobile dashboards and other parts, squeeze bottles, children's toys, furniture, and disposable cutlery, cups, pens and pencils, lighters, containers for beverages and cleaning supplies, toothbrushes, packaging, and medical supplies.

The 'throwaway living' concept (**Figure 1**), previously exclusive to the wealthy, was now affordable for all due to the inexpensive mass production of disposable plastic products. Unfortunately, the idyllic vision of a world built with plastics was muddied as concerns began to emerge surrounding the dangers and pollution that accompanied the rise of plastic products. By 1976, plastic in all its forms became the most used material in the world.<sup>4</sup> Around that same time, the first reports documenting plastic pollution in marine systems and its detrimental impacts on a variety of marine life were published.<sup>5</sup>

Today, there is mounting evidence of the negative effects that plastic pollution and microplastics have on not just terrestrial and aquatic organisms, but also causing blockage of drainage and engineering systems that create a breeding ground for disease vectors.<sup>6</sup> It is estimated that 60% of all plastics ever produced, equivalent to 4,900 metric tons, were discarded and are accumulating in landfills or the natural environment. If the current global waste management trends continue, 12,000 metric tons of plastic waste would have been disposed in landfills or the natural environment by 2050.<sup>7</sup> Approximately 40% of plastic is consumed for single-use, disposable packaging applications, the most common materials for which are polyethylene (PE), polypropylene (PP), and polyethylene terephthalate (PET).<sup>8</sup> These polymers are stable against chemicals, hydrolysis, temperature, light, and microbes, which makes them great for protection of even sensitive materials. This superior stability also means that exposure to the environment does little to degrade these polymers, leaving them to persist in the environment for thousands of years. Not

surprisingly, 85% of collected litter is identified as plastic according to The Marine LitterWatch, an international database that has been collecting data since 2013.<sup>9</sup>

The commercialization of plastic products forever changed our way of life. There is no denying the positive changes that widespread plastic use has brought including the increased hygiene practices, fresher and safer food products, higher standard of living from access to inexpensive modern consumer goods, and lowered shipping costs and associated emissions due to lightweight yet effective packaging.

The 'throwaway lifestyle' of the past is no longer sustainable, which fuels the development of alternatives that would provide the indispensable benefits associated with plastics without the detrimental side effects and persistence in the environment. In this regard, materials with a relatively short functional lifespan but high production volume are of highest priority i.e., single-use packaging, particularly food packaging. Recycling of plastics is fundamentally a sound idea that directly diverts plastic waste from landfills and reduces raw material consumption. In practice, recycling rates are low and processing challenges, like isolation from contamination and avoiding deterioration of properties during reprocessing and use, has made recycling uneconomical.<sup>10</sup> Consumer interest in 'eco-friendly' materials is rising as media and marketing promote 'save the planet' strategies. Without a sacrifice of attributes such as price and taste, consumers were more inclined to prefer environmentally friendly products.<sup>11</sup>

Food packaging has a critical role in the preservation and transportation of food products through the global market. It should prevent deteriorative reactions that cause nutrient losses, color changes, off-flavor development, and microbial growth. Reduction of food waste through this mechanism is a top priority for the design of sustainable packaging since the environmental impacts of agriculture can, in terms of greenhouse gas emissions and water use, dwarf those of plastic production.<sup>12,13</sup> Matching the performance of the current packaging polymers with materials that would not persist in the environment, i.e. biodegradable polymers, has proven to be a technical challenge.

### 3.2. Biodegradable Polymers

As we dive into options for addressing the challenges of biodegradable food packaging, it is important to note that the goal is not the design of a material to be disposed of by direct release into the environment. Rather, the focus is on creating plastics that would not persist

in the environment upon accidental release, or would be suitable for disposal into standard composting conditions.

### 3.2.1. Biodegradation and microplastic formation

Biodegradation of a polymer in the environment so that it does not contribute to plastic pollution of any form will generally follow non-discrete stages (**Figure 2**). In the initial stages of environmental exposure, the polymer surface may oxidize from exposure to ultra-violet light or water. Some polymers will undergo bulk fragmentation facilitated by various mechanical or chemical factors that break the plastic into increasingly smaller pieces. Other polymers may undergo surface fragmentation where only the outermost layer of the plastic is subject to degradation mechanisms, gradually making the bulk item smaller over time. A combination of bulk and surface fragmentation mechanisms can occur in parallel. Most polymers on the market today with a C-C or C-heteroarm (e.g., oxygen, nitrogen) backbone, can remain in these stages and become increasingly smaller for decades before significant breakdown of the chemical structure. For this case, macro-plastics transition into persistent micro- and nanoplastics that are impossible to collect and are mobile enough to be found everywhere from the deep sea<sup>14</sup> to the atmosphere<sup>15</sup> and even within our own bodies.<sup>16</sup> In the

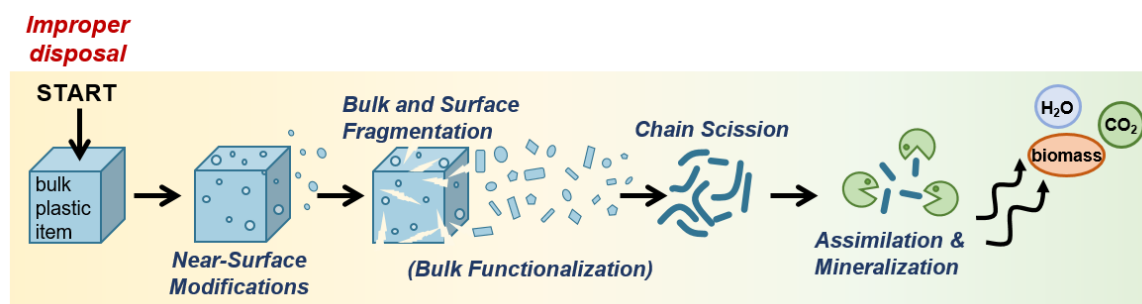


**Figure 2.** Scheme illustrating the non-discrete stages of polymer biodegradation

case of a biodegradable material, the increased surface area of the plastic allows for further functionalization of polymer chains (for certain polymer structures) and ultimately chain scission into oligomer-sized pieces. Depending on the polymer and environmental conditions, these final stages can occur as a result of several mechanisms including photo-oxidation and hydrolysis. Once the oligomers are small enough, they may be assimilated and mineralized inside microorganisms producing only CO<sub>2</sub>, CH<sub>4</sub>, H<sub>2</sub>O, and biomass.

Complete degradation of plastic hinges on its availability to chain scission by environmental factors. The formation of micro- and nanoplastic may make the plastic invisible to the eye,

but if these fragments do not break down at the molecular level, they can have harmful effects on organisms of all sizes and habitats. Henceforth, the term ‘microplastic’ will be used to encompass all plastic particles smaller than 5 mm, including nanoplastic. In marine environments, microplastics are easily accumulated by plankton and other invertebrate organisms and then can travel up the food chain. Ingestion of fish and other seafood is just one pathway that microplastics can enter humans. Microplastics often contain other chemical additives that improved the properties (e.g. processability, mechanical, UV resistance) of the original plastic material, but some of these additives can also cause disruption of the endocrine system of vertebrates, such as commonly employed bisphenol A and phthalate additives.<sup>16</sup> Other research has demonstrated that microplastic particles are able to sorb and carry other persistent and toxic organic pollutants, like dichlorodiphenyltrichloroethane (DDT), and then desorb the pollutants inside living organisms.<sup>17</sup> Although a comprehensive risk assessment is still lacking, *in vitro* studies using human cell cultures suggest that inhaled or ingested microplastic particles can cause a variety of biological effects, including oxidative stress, cellular damage, inflammatory and immune reactions, as well as neurotoxic and metabolic effects.<sup>18</sup> Further influences of microplastic pollution on terrestrial ecosystems are also of urgent concern, for example, the possible consequences of accumulated microplastics on soil texture and structure that could lead to a loss in biodiversity are currently being evaluated.<sup>19</sup>

### 3.2.2. Biodegradable commercial polymers

It is clear that plastic should not only physically fragment in the environment, but it should also undergo molecular fragmentation of polymer backbones in order to avoid dangerous environmental and health consequences. Polymers capable of biodegradation are already available commercially with a production capacity that is growing yearly.<sup>20</sup> This category is largely constituted of poly(lactide) (PLA), starch blends, poly(butylene adipate terephthalate) (PBAT, or EcoFlex), and poly(butyl succinate) (PBS). These polymers all contain ester groups within the backbone that are susceptible to hydrolysis. It is important to note that bio-based plastics is a distinct category, yet not mutually exclusive, to biodegradable plastics. Bio-based plastics are derived from renewable resources instead of the typical hydrocarbon and petroleum sources. Many non-degradable plastics like PET and PE can be bio-based, but their monomer feedstock source ultimately does not affect its properties or availability to biodegradation. PLA can be produced from corn or sugarcane-based feedstock, and is also considered to be biodegradable. On the other hand, PBAT is

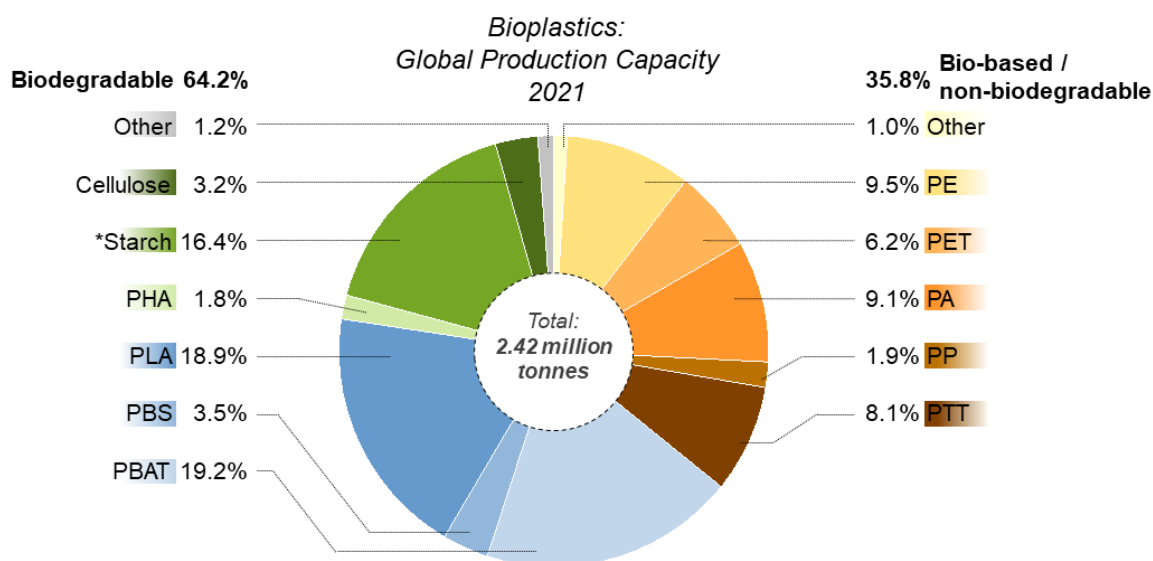


**Figure 3.** Distribution of global production capacity of biopolymers for 2021. Abbreviations: PHA - polyhydroxyalkanoates; PA - polyamide; PTT - polytrimethylene terephthalate. \*Starch blends. Reproduced from reference 20

biodegradable but produced from nonrenewable resources, and therefore is not considered to be bio-based. Bioplastics is the encompassing category for both biodegradable and bio-based polymers.<sup>21</sup>

PLA makes up 18.9% of the global production capacity for all bioplastics in 2021 (**Figure 3**). The market demand of PLA is on trend to double every 3-4 years, although production

capacity is not expected to keep the same pace.<sup>22</sup> This supply shortage, together with the relatively small production volumes, keep the prices of PLA well above other traditional plastics. As a thermoplastic polyester, PLA can be spun into fibers, stretched into rigid films, extruded into sheets for thermoformed packaging, and injected into molds.<sup>22</sup> PLA has even found its way into biomedical devices as it features zero toxicity and excellent biocompatibility.<sup>23</sup> The ease of synthesis and relatively high mechanical strength has been favorable for some food packaging applications, particularly rigid packaging, although PLA is not suitable for long-term storage due to its poor barrier to oxygen permeation. With a glass transition temperature ( $T_g$ ) around 60 °C, its major drawback is poor thermal resistance and brittleness. For flexible film applications, PLA must be blended with plasticizers or soft biodegradable polymers to improve its flexibility.

PBAT claims the largest share of the 2021 global production capacity of bioplastics at 19.2%, which is projected to grow to 30% by 2026.<sup>20</sup> One may also find PBAT under the tradename Ecoflex® produced by BASF. Unlike PLA, PBAT exhibits a high elongation at break and is very flexible, making it a popular blend component for other biodegradable materials to improve flexibility. Likewise, PBAT can be found in applications that favor flexible properties like compost bags or mulch films.<sup>24</sup> The downside of PBAT is its high price tag that keeps applications limited to specialty cases. While increasing production scale would provide some remedy, blending of PBAT with starch is a popular strategy to bring down prices in the meantime.<sup>24</sup>

The classification of PLA, PBAT, as well as other so-called biodegradable polymers as, in fact, biodegradable does not come without caveats. Biodegradation is a complex process that depends on many material and external factors including crystallinity, hydrophobicity, molar mass, pH, oxygen, light, temperature, etc.. It follows that not every biodegradable polymer would degrade under all environmental conditions. Many polymers that are classified as biodegradable actually require specific conditions and may not degrade at all in other relevant mediums. Polyesters, including PLA and PBAT, exhibit very little degradation in both fresh and salt-water systems.<sup>25</sup> While both of these polymers degrade under controlled compost conditions according to ASTM 6400 or EN 13432, their condition-dependent degradation behavior poses the question as to whether biodegradable polymers could also contribute to microplastics if not properly disposed. The breakdown of the polymer into water and gases must be rapid enough as to not allow intermediate degradation particles enough time to cause damage to the environment or organisms. Any

biodegradable packaging film proposed to replace traditional materials must maintain a robust and fast degradation across several relevant environmental conditions that it may encounter in an ‘accidental release into the environment’ scenario. Such degradation behavior has historically been at the sacrifice of mechanical or thermal properties.<sup>26</sup> This tradeoff constitutes the most challenging hurdle to the widespread implementation of biodegradable polymers as a replacement for non-degradable plastics. Not only do the inherent physical properties of biodegradable materials need to be strengthened to compete with those of PE or PET, but also the availability to biodegradation should be simultaneously improved for a more rapid biodegradation in a wider range of conditions.<sup>27</sup> There currently lacks a material that overcomes the tradeoff between high physical performance and rapid biodegradation that would also be suitable for high-volume production at low cost.

The challenge of high-performing biodegradable materials is exemplified particularly well in the following literature studies. Cross-linking or co-polymerization of PLA with flexible polymers is a logical path towards improving the toughness and stretchability of PLA as it creates a robust polymer network. Hu and coworkers employed benzoyl peroxide as a crosslinking agent for PLA/PBS blends.<sup>28</sup> With just 1% crosslinking agent and 20% PBS, the elongation of PLA increased to nearly 400% – a 40-fold improvement. However, the group also found that the physically cross-linked structure inhibited the diffusion of the degrading enzyme, proteinase K, into the bulk material, slowing its degradation kinetics relative to neat PLA. The opposite trend was observed for blends of PBAT with starch. As mentioned above, the addition of starch reduces the overall material costs and positively influences biodegradation kinetics in aqueous environments.<sup>29</sup> These improvement come at a sacrifice to the excellent stretchability of PBAT, with 30 wt% of starch in PBAT reducing elongation at break by more than 30-fold. Such property tradeoffs that plague this class of polymers prompts creative solutions from polymer chemists and material scientists in order for biodegradable plastics to be able to provide a meaningful reduction in plastic pollution.

### 3.2.3. Addressing the drawbacks of biodegradable polymers

One promising approach to improving the properties of biodegradable materials is through blending rigid and soft biodegradable polymers. With this strategy, synergetic improvements in mechanical properties and degradation can be achieved with simple processing. For example, Ecovio® is a commercial blend of PBAT and PLA that improves on the poor mechanical properties of PLA by incorporation of the flexible PBAT,

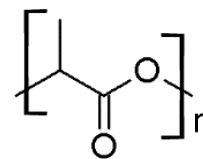


**Figure 4.** Chemical structure of PLA

and maintains rapid degradability in terrestrial systems.<sup>30,31</sup> Blending PLA with PBAT requires a compatibilizer,<sup>32</sup> which creates concerns around leaching of these smaller molecules into the environment or food items. An even simpler strategy to improve the physical and degradation properties of PLA without compatibilization additives is by optimizing the crystallinity of PLA. PLA (**Figure 4**) can be produced by the ring-opening polymerization of lactide, which is available in three different stereoisomers. As a result, three major variations of PLA exist: poly(L-lactide) (PLLA) and poly(D-lactide) (PDLA) which are semicrystalline, and poly(DL-lactide) (PDLLA) which is amorphous. Due to the different crystallinities, mechanical properties and degradation of PLA exist on a spectrum.<sup>33-35</sup> While crystalline regions impart mechanical toughness,<sup>36</sup> amorphous regions are generally more susceptible to degradation.<sup>34</sup> Through blending of PDLLA with PLLA, the Agarwal group has shown that the bulk crystallinity of PLA can be tailored to optimize the mechanical and degradation performance tradeoff.<sup>37</sup> They found that a blend of PLLA:PDLLA at a 30:70 weight ratio exhibited the fastest degradation kinetics under enzymatic conditions and the second fastest degradation in compost (with only pure PDLLA being faster) after a reduction in crystallinity to 13% from 25% of pure PLLA. Additionally, the mechanical performance of the blend films showed tensile strength and elongation at break in between the more brittle PLLA and the more flexible PDLLA.<sup>37</sup>

Another approach to new degradable polymer systems with suitable physical properties is through a synthesis route. The chemical structure of a polymer chain can be altered in order to optimize properties and ensure degradation. Consider the aliphatic PBS (Figure 5), which readily undergoes hydrolysis of its backbone ester group, however it exhibits low mechanical strength. Compare

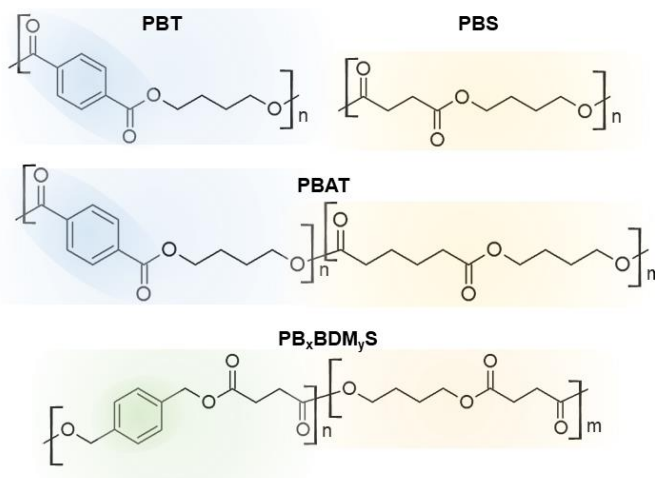


**Figure 5.** Chemical structures of several biodegradable and non-biodegradable polymers.

PBS to another polyester, poly(butylene terephthalate) (PBT), which contains an aromatic backbone group that gives it mechanical strength and chemical resistance (non-biodegradable). The inertness of PBT comes from the delocalization of electron density away from the ester group by the aromatic unit, making the carbonyl carbon less electrophilic and thus less susceptible to hydrolysis. An aromatic monomer unit could be incorporated into a copolymer with other monomer units that are susceptible to hydrolysis, as is the case with PBAT. However, as mentioned above, PBAT lacks universal degradability, which can be attributed to delocalized electron density provided by the aromatic group in the same way that makes PBT resistant to biodegradation. The Agarwal group investigated the synthesis of poly(benzenedimethylene succinate) (PBDMS) as an alternative to PBS due to its interesting structure.<sup>38</sup> The aromatic unit in the backbone is separated from the carbonyl carbon with a methylene group, which makes the delocalization of electrons by resonance not possible. By adding 1,4-butanediol as a comonomer, high yields of PB<sub>x</sub>BDM<sub>y</sub>S polyesters (x = molar ratio of 1,4-butanediol; y = molar ratio of 1,4-benzenedimethanol in the monomer feed) were obtained that were thermally processable under mild conditions. Tuning of monomer ratios gave suitable mechanical properties for food packaging while also maintaining rapid hydrolysis, with some formulations being even more rapid than PBS. Smart and simple solutions like this are critical in making improvements to biodegradable polymer systems without complex processing or synthesis strategies.

### 3.3. Polymer Clay Nanocomposites

#### 3.3.1. Polymer barrier

Possible components that can be added to a given biodegradable polymer is not limited to polymers and other organic additives. While these components impart positive changes on the bulk mechanical and thermal properties, they fall short when considering other critical physical properties like gas barrier. Packaged food items need a barrier to gasses to prolong shelf life and prevent contamination. Unfortunately, gas barrier is another property in which traditional packaging materials consistently outperform the current commercial

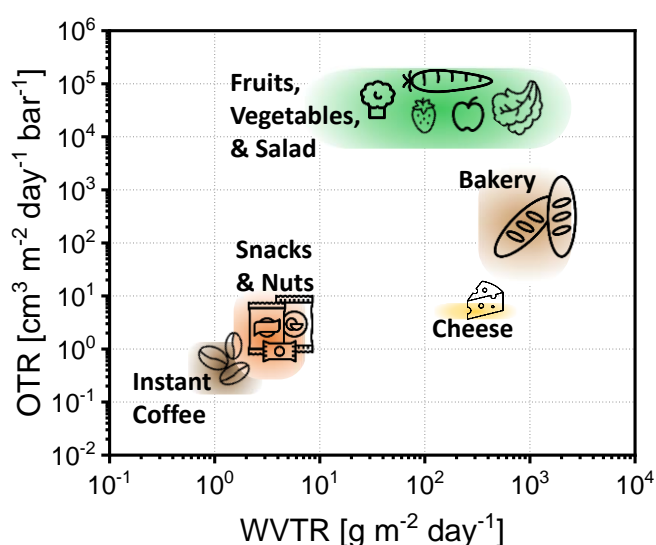


**Figure 6.** Oxygen and water vapor transmission rate ranges for various food packaging applications

biodegradable polymers.<sup>39</sup>

Without sufficient gas barrier, shelf-stable or vacuum packaging applications are out of reach for biodegradable polymers, even if suitable mechanical properties are met. Before we look at the numbers, let us first review the physical origin of polymer barrier.

The barrier of a polymer is its ability to resist transfer of a permeant through it. For food

packaging, the most relevant permeants are water vapor and oxygen as they promote deteriorative reactions and microbial growth (**Figure 6**)<sup>40,41</sup>. Gases transition from an area of low concentration to high concentration through a film in three steps: sorption to the polymer, diffusion, and desorption from the polymer.<sup>42</sup> The transmission rate (TR) defines the amount of gas that permeates per unit of area and time for a given film. Since this term does not account for film thickness, which can greatly influence the TR, the permeability coefficient can be used to compare barrier properties across varying film dimensions. The permeability coefficient is the rate of a quantity of permeant that passes through a polymer in a unit of time with a unit surface area having unit thickness with a unit pressure difference on both sides of the film.<sup>42</sup> In this work, the TR and permeability units that will be used are  $\text{cm}^3 \text{m}^{-2} \text{day}^{-1} \text{bar}^{-1}$  and  $\text{cm}^3 \mu\text{m} \text{m}^{-2} \text{day}^{-1} \text{bar}^{-1}$ , respectively. Permeability (P) of a polymer is a product of the diffusion (D) and solubility (S) coefficients.

$$P = D * S$$

D describes the kinetic movement of permeates through the polymer matrix and can be determined from Fick's first or second law. The movement of small molecules through the polymer can be driven by a concentration gradient. Fick's first law applies with the assumption that the concentration gradient is linear:

$$F = -D \frac{\partial C}{\partial x} = \frac{Q}{At}$$

Where Q represents the amount of permeate moving through unit area A, and F is the rate of mass transfer, i.e., flux. If the diffusion coefficient is independent to the concentration of the permeate (C), distance (x), or time (t), then Fick's second law applies:<sup>39</sup>

$$\frac{\partial F}{\partial x} = \frac{\partial C}{\partial t} = D \frac{\partial^2 C}{\partial x^2}$$

The solubility coefficient, S, represents how readily a permeant dissolves in a polymer, which is defined as the ratio between the equilibrium concentration of the permeate in the polymer (C) and the partial pressure of the permeant in the gas phase (p). This relationship can be expressed by Henry's law as:

$$C = S * p$$

It becomes evident that the permeability of a material will heavily depend on the environmental temperature and humidity, as well as material properties like hydrophilicity and crystallinity. Of course, these models represent only a simplified description of the complex interaction of a permeate with a polymer matrix. In practice, several other factors contribute to the true permeability of a given material. These factors include swelling of the polymer with the permeate (or other substances), which induces a nonlinear concentration gradient, additional driving forces like chemical potential or the redistribution of free volume in the polymer matrix, and interactions between the polymer chains and the permeate.<sup>39</sup> To gain a deeper understanding of these influencing factors and why they vary from polymer to polymer, let us first consider the cohesive energy density. The cohesive energy density of a substance is defined as the increase in internal energy per mole of substance if all the intermolecular forces are eliminated.<sup>43</sup> For polymers, this is estimated by additive contribution models that consider which chemical units make up the polymer chain, the strength of interaction between these units, and how this interaction changes when a different chemical unit is added to the polymer chain. The cohesive energy density

also represents the square of the solubility parameter. In other words, a high intermolecular cohesion, like in PVC due to its hydrogen bonding, will generally be more resistive to permeation compared to PE, which has relatively little intermolecular interaction.<sup>44</sup> Swelling of the polymer with moisture will negatively impact its cohesive strength, and by consequence, negatively influence barrier properties as well. It follows that despite PE having a poor barrier to gasses, its olefinic hydrophobic character makes it a better barrier to water compared to the water-soluble and highly cohesive poly(vinyl alcohol) (PVOH).

The free volume of a polymer is another factor that influences barrier properties as permeates readily travel through 'microcavities' within the polymer matrix. While related to the cohesive energy density, the free volume of a polymer is also derived from its thermal history,  $T_g$ , crystallinity, and conformational order.<sup>43</sup> Crystallinity is a particularly interesting factor to consider within the scope of high-barrier biodegradable polymers since this characteristic, depending on the polymer, can be readily tailored using thermal treatments or minor structural changes, as exemplified above by the blending of amorphous PDLLA and semicrystalline PLLA. Experimental evidence shows that crystalline regions within a polymer matrix are impermeable to transport of most low molecular weight permeants, leaving only the amorphous phase available for diffusion.<sup>42</sup> Within the amorphous phase, permeates must travel a tortuous path around the impermeable crystallites, slowing the overall transport kinetics.

Polymer crystallinity is certainly one path towards increasing the barrier of biodegradable polymers, as has been demonstrated several times in literature with PLA.<sup>45</sup> By varying the crystalline fraction, the oxygen permeability of PLA could be varied from 15,000 to 3,500  $\text{cm}^3 \mu\text{m m}^{-2} \text{day}^{-1} \text{bar}^{-1}$  at 23°C and 50% relative humidity (RH). However, this performance is still sub-par to even a low-end barrier standard like PET, which, under the same conditions, exhibits an oxygen permeability between 1,000 and 5,000  $\text{cm}^3 \mu\text{m m}^{-2} \text{day}^{-1} \text{bar}^{-1}$ . A high performance material like poly(vinylidene chloride) (PVDC) featuring oxygen permeability between 10 and 300  $\text{cm}^3 \mu\text{m m}^{-2} \text{day}^{-1} \text{bar}^{-1}$  reflects applicability in long-term food storage to oxygen-sensitive items like coffee grinds. One goal of this work is to achieve high-performance, competitive barrier using biodegradable materials.

### 3.3.2. Clay as a barrier filler

As increasing polymer crystallinity alone cannot achieve competitive barrier properties, and changes to the polymer chain composition itself could reduce availability to biodegradation, then exploration of further methods to improve the poor barrier properties of biodegradable polymers is required. Following a similar concept to the impermeable crystalline regions within a polymer matrix, impermeable inorganic fillers have been used to impart significant barrier enhancement within several polymers used for packaging, including nylon-6, PET, PE, PVC, and PVOH.<sup>46-49</sup> Namely, 2:1 phyllosilicate-type clay materials are particularly attractive filler materials due to their layered structure consisting of strong in-plane covalent bonding, but weak out-of-plane bonding that can be disrupted to produce single-layer (impermeable) silicate nanosheets. The class of so-called layered crystals includes montmorillonite, synthetic mica, vermiculite, and hectorite. Their 2:1 layers consist of two tetrahedral SiO<sub>4</sub> sheets in an edge-sharing conformation with a single octahedral plane, the composition of which depends on the type of clay. These layers are stacked together with cohesive, charge-balancing ions like Na<sup>+</sup>, Mg<sup>2+</sup>, Li<sup>+</sup>, Al<sup>3+</sup>, etc., located in the centers of the octahedra.<sup>50</sup> The aspect ratio is defined as the ratio of a platelet diameter to its thickness, where silicate nanosheets from layered crystals are typically 1 nm thick with a diameter that can range from 30 nm to over 20 microns.

In comparison to a conventional polymer-clay composite that consists of aggregated clay tactoids (i.e., silicate nanosheets stacked together having an appreciable thickness), a polymer clay nanocomposite that contains thin silicate nanosheets dispersed throughout the polymer matrix has a tremendously larger interfacial surface area that allows for greater influence on bulk properties. In terms of barrier properties, the model proposed by E.L. Cussler in 1987 has provided an accurate description of the influence that a platy filler has on the permeability of a polymer.<sup>51</sup>  $P$  is the measured permeability of the nanocomposite, and  $P_0$  is the measured permeability of the neat polymer. The ratio of these two values give the relative permeability of the nanocomposite,  $P_{rel}$ , and the inverse of  $P_{rel}$  describes the barrier improvement factor (BIF).

$$P_{rel} = \frac{P}{P_0} = \left( 1 + \mu \left( \frac{\alpha^2 \phi^2}{1 - \phi} \right) \right)^{-1}$$

Here,  $\alpha$  is the aspect ratio of the filler,  $\phi$  is the volume content of the filler in the polymer, and  $\mu$  is a geometric factor that is equal to 4/9 for nanosheets. This equation generously

assumes that the nanosheets are oriented perfectly parallel to each other and perpendicular to the direction of diffusion. From this equation, we derive a nonlinear correlation between decreasing permeability of the nanocomposite and an increasing filler aspect ratio at a given filler content. In other words, the ideal filler geometry is atomically thin platelets of infinite width (**Figure 7**). An impermeable filler of such geometry within a polymer matrix creates a dramatically convoluted maze in which permeates must navigate in order to travel through, also known as the tortuous path.

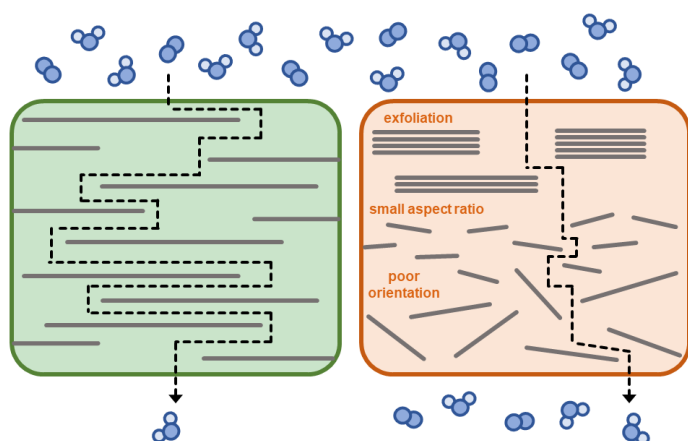


**Figure 7.** Ideal nanofiller for barrier reinforcement by formation of tortuous path (left). Poor barrier reinforcement due to exfoliation only into tactoids, using small aspect ratio platelets, and platelets with poor orientation within polymer matrix (right).

To maximize the barrier improving power of a clay filler, it should be delaminated into the thinnest possible individual nanosheets, while maintaining the large diameter inherent to the pristine material. Note that the delamination of clay tactoids specifically describes the complete separation into single-layer nanosheets, while exfoliation is the breakdown of

tactoids into thinner stacks with non-uniform thickness.<sup>52</sup> The latter being accessible to a wider range of layered clays, although producing lower quality particles of smaller aspect ratio. Exfoliation of clay nanosheets is most commonly achieved by exerting strong shear forces, e.g., with ultrasonication, on a liquid suspension to thin the cohesively bound stacks. Dispersions of clays produced this way contain single, double, and multilayer stacks of nanosheets.<sup>53</sup> Platelets may even be broken perpendicular to the stacking direction as a result of the high forces required, further reducing the aspect ratio.<sup>53</sup> A common strategy to attempt to control liquid phase exfoliation and improve the yield of single nanosheets from ionic layered materials is the exchange of the interlayer ion with a bulkier one to increase the separation distance of the sheets, i.e. d-spacing, thus weakening the cohesive forces. Similarly, solvation of the interlayer ions can also increase the d-spacing and shear lability. This phenomenon is termed crystalline swelling and will be described in more detail shortly.

Nevertheless, external energy input is still thermodynamically required to exfoliate after ion exchange in most cases and complete delamination is unattainable.<sup>59</sup>

Although liquid phase exfoliation doesn't extract the full potential of layered crystals, a small number of materials are capable of the phenomenon termed osmotic swelling, which does not require mechanical force and can give quantitative delamination into single nanosheets. Osmotic swelling of layered materials occurs when the charge carried by the individual layers is compensated by solvation of the counter ions with solvent molecules that allow gentle and complete separation. This thermodynamically allowed process requires a uniform charge density in order to be capable of uniform delayering. Such requirement is generally unfavorable towards natural minerals as synthesis temperatures below 1000 K give non-uniform charge density due to clustering of cations in the differently charged domains.<sup>54</sup> Moreover, natural minerals lack phase purity that must be remedied prior to osmotic delamination.

Not only does poor delamination of layered clays impose limits on possible barrier improvements, but the addition of inhomogeneities to a polymer matrix also impairs the mechanical performance of the nanocomposite. Clay fillers can readily impart brittleness to a polymer when interfacial adhesion is poor, for example. This trend is most apparent within the literature for PLA nanocomposites prepared by melt intercalation methods, which are favored due to being solvent-free. Melt intercalation relies on shear forces within extrusion dies to break apart clay tactoids and disperse them within the polymer matrix. Combination by force of clay into PLA has resulted in embrittlement of the nanocomposite starting at filler contents as low as 3 wt%.<sup>55-57</sup> In some reports, nanocomposites with clay contents of less than 2 wt% have higher percent elongation at break compared to pure PLA, but this improvement disappears as clay content is further increased.<sup>57-59</sup> PLA nanocomposites with such low filler contents have not displayed enough improvement in reported barrier properties due to an insufficient tortuous path to claim competitive, high-performance properties.<sup>56,58,60</sup> Therefore, a focus on high aspect ratio fillers should be made to most efficiently improve barrier performance while keeping filler content low.

### *3.3.3. Synthetic hectorite and osmotic swelling*

Synthetic layered crystals, like the synthetic sodium fluorohectorite (Hec) produced by Breu and colleagues, are advantageous for the production of high-quality barrier nanosheets as they possess superior phase purity that does not require additional purification steps and

large platelet diameters (~ 18,000 nm) (**Figure 8a**).<sup>61</sup> Hec is produced by combining melt synthesis with subsequent long-term annealing at temperatures well above 1000 K, giving a unit cell composition of  $[\text{Na}_{0.5}]^{\text{inter}}[\text{Mg}_{2.5}\text{Li}_{0.5}]^{\text{oct}}[\text{Si}_4]^{\text{tet}}\text{O}_{10}\text{F}_2$ .<sup>62</sup> In a non-hydrated state at 0% RH, the interlayer sodium is fully coordinated to an oxygen atom within the highly charged silicate layer from both above and below, giving a d-spacing of 0.96 nm. The osmotic delamination of Hec occurs in the following stages (**Figure 8b**). First, crystalline swelling begins by exposure to humidity. Below 75% RH, a one water layer (WL) state forms where three water molecules are coordinated to the sodium cation in one direction, and at the same time, form hydrogen bonds with oxygen atoms of the opposite silicate layer. In this stage, the sodium remains coordinated to one of the silicate layers and is identified by an increase in the d-spacing to 1.25 nm. Further increasing moisture content to a 2-WL structure, the sodium cation is coordinated by six water molecules that are now forming hydrogen bonds with the silicate layers on both sides, which increases the d-spacing to 1.55 nm. Within this crystalline swelling regime, there remains attractive electrostatic forces that keep the silicate layers at discrete separation distances. The transition from crystalline swelling into repulsive osmotic swelling involves further hydration, i.e., immersing into water, in which the remaining short-range attractive forces are overcome, leaving repulsive interactions between the ionic layers to dominate. Osmotic pressure between adjacent platelets pushes the platelets to increasingly large distances with further addition of water.<sup>54</sup> The homogeneous and gentle nature of this process preserves the large diameter inherent to pristine Hec in a quantitative conversion into nanosheets. With a diameter of 18  $\mu\text{m}$  and a thickness of 0.96 nm, the rotation of the negatively charged platelets in suspension is sterically hindered, forming a liquid crystalline nematic phase even in dilute conditions (< 1 vol%) with platelets being separated by more than 55 nm.<sup>54</sup>

When combined with an aqueous polymer dispersion, the liquid crystalline phase of Hec nanosheets separated to the largest allowed distance grants polymer intercalation of the interlayer space. Assuming that the polymer chains remain within the nanosheets upon removal of solvent, a highly ordered nanocomposite may be obtained where the individual Hec nanosheets are separated by regions of polymer. The intercalated structure of a polymer-clay nanocomposite forms a dramatically tortuous path to gas diffusion that can improve the barrier properties by orders of magnitude relative to the neat polymer. In practice, some degree of phase separation is thermodynamically driven. For example, a poly(ethylene glycol) (PEG)/Hec nanocomposite was prepared with different weight ratios.<sup>63</sup>

Upon drying, it was discovered that independent of clay content (20-75 wt% clay was evaluated), the d-spacing remained at 1.77 nm. Microscopic images confirmed the existence of two phases within the nanocomposite: an intercalated crystalline region that contained 75 wt% Hec, and a segregated polymer region. The growth of the polymer domains is limited as polymer mobility is hindered with removal of solvent and formation of the tortuous path.

Further studies on PVOH/Hec nanocomposites have demonstrated that drying nanocomposites at 20 °C improves polymer intercalation, and therefore the barrier properties and moisture sensitivity of the resulting nanocomposite compared to a drying temperature of 50 °C.<sup>64</sup> This study also observed that the d-spacing within the highly filled crystalline regions, also termed hybrid Bragg stacks, was measured to be smaller than the radius of gyration of the intercalating PVOH polymer. The same observation was made when using polyvinylpyrrolidone (PVP) as the polymer matrix. By careful control of the PVP/Hec ratio, Schilling et al. demonstrated that this severe confinement imposed on polymer chains contributes to further improvement of the nanocomposite barrier performance beyond what is predicted by the Cussler equation.<sup>65</sup> The excellent structural order of PVP/Hec hybrid stacks are observable with transmission electron microscopy (TEM) imaging (**Figure 8c**). Severe polymer confinement within nanosheets has been reported to influence additional properties like  $T_g$ <sup>66</sup> and segment mobility.<sup>67</sup> Highly loaded PEG/Hec nanocomposites have exhibited an extraordinary Young's modulus of up to 162 GPa in the direction parallel to clay nanosheets within hybrid Bragg stacks, suggesting ideal

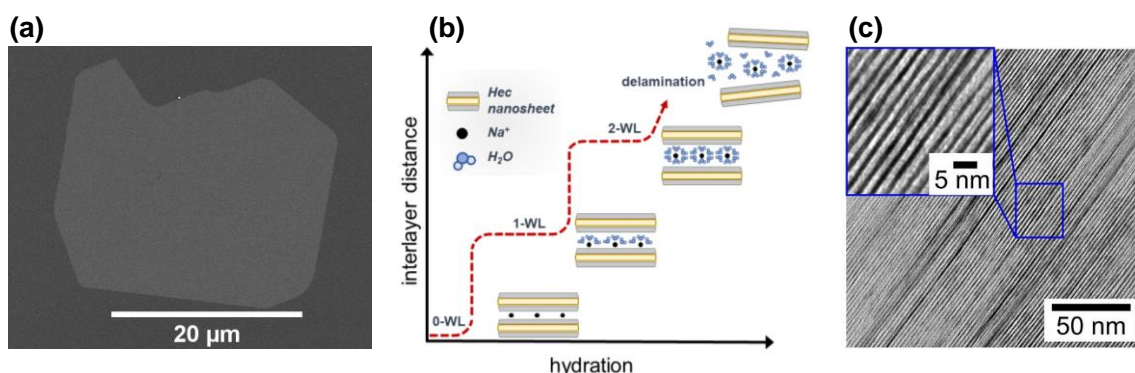


**Figure 8.** (a) SEM image of a single synthetic fluorohectorite platelet produced at the Breu research group. (b) Schematic of the osmotic swelling process of Hec. Reproduced from reference 56. (c) Cross-sectional TEM image of intercalated PVP/Hec nanocomposite containing 31 vol% Hec. [Reprinted (adapted) with permission from T. Schilling, C. Habel, S. Rosenfeldt, M. Röhr, J. Breu, *ACS Applied Polymer Materials* 2020, 2, 3010. Copyright 2020 American Chemical Society (ref 67).]

stress transfer.<sup>68</sup> The brittleness of Hec nanocomposites with clay loadings above 10 wt% remains a challenge.

#### 3.3.4. Biodegradable polymer-Hec nanocomposites

The high-quality liquid crystalline suspensions generated through the osmotic delamination of Hec has been used within the Breu group to produce waterborne polymer-clay nanocomposites coatings of superior barrier performance.<sup>65,69-71</sup> With the application of food packaging in mind, a biodegradable glycol chitosan (GlyChit) and Hec nanocomposite was spray coated onto a commercial PLA substrate.<sup>72</sup> The GlyChit matrix provided the added benefit of anti-microbial properties. A 1.4  $\mu\text{m}$  thick nanocomposite coating imparted a barrier improvement factor of  $10^4$  even at a RH of 75%, which additionally indicates a reduced tendency to swell in humid conditions.<sup>72</sup>

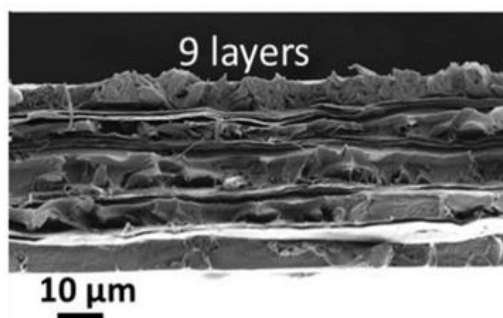


**Figure 9.** Cross-sectional SEM image of PLA/PVP-Hec layered composite film. Reprinted with permission from reference 56

With PLA being not soluble in water and thus unable to directly combine with Hec in solution, more creative means to mechanically reinforce PLA with Hec were developed.<sup>73</sup> In the work presented by Zhu et al., a solution of Hec with the water-soluble PVP was filtered through an electrospun PLA fiber mat. These bilayers could then be melt-pressed together to make multilayer films having alternating PLA and Hec/PVP layers (**Figure 9**). This film had improved tensile strength by 94% compared to neat PLA while maintaining flexibility as evaluated by the absence of cracks forming during a 100-cycle bending test. Oxygen transmission rate (OTR) was reduced by 98.9% to  $6.05 \text{ cm}^3 \text{ m}^{-2} \text{ day}^{-1} \text{ bar}^{-1}$  even at an elevated humidity of 75%. Most interestingly, the degradation performance of PLA was enhanced by the delayering of the Hec/PVP structure, which was attributed to swelling of Hec regions that increased the surface area exposed to the degradation medium. This effect was observed during both enzymatic and compost degradation mediums.<sup>74</sup>

Unfortunately, the application of a barrier coating onto a mechanically weak polymer, or the lengthy electrospinning/filter-through film preparation, amongst other work-arounds, is not enough to make PLA competitive to the traditional materials. Casting from a single solution of hydrophobic polymer and filler would allow for a simplified processing method, potential intercalation related swelling resistance, and more efficient mechanical reinforcement. Top choices of

biodegradable polymers like PLA, PBAT, and PBS are all polyesters, which thanks to their aliphatic ester units that make them susceptible to hydrolysis, also means they are hydrophobic and require organic solvents to dissolve. Although polymer/clay suspensions is a well-researched concept that has been successfully implemented in water-soluble polymers to improve their barrier, the same method was previously not translatable into organic solvents. In cases where clay

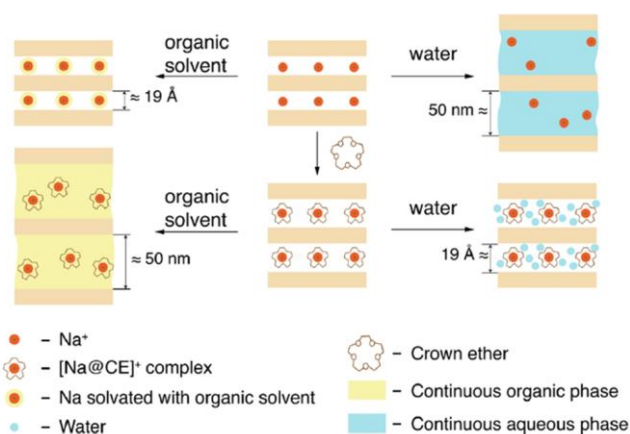


**Figure 10.** Schematic illustrating swelling behavior of synthetic fluorohectorite in organic solvent and water, and with or without crown ether-interlayer sodium complex. Separation of platelets to 19 and 50 nm represents crystalline and osmotic swelling, respectively [Reprinted (adapted) with permission from V. Dudko, K. Ottermann, S. Rosenfeldt, G. Papastavrou, J. Brey, *Langmuir* **2021**, *37*, 461. Copyright 2021 American Chemical Society (ref. 81).]

exfoliation can be adequately achieved in organic solvents, the bulky surface modifiers required are so large that the clay content becomes limited by high viscosity to contents below what would be needed for a high-performance material.<sup>75,76</sup>

### 3.3.5. Osmotic swelling extended into organic solvents

As it was clear that achieving osmotic swelling in organic solvents could unlock truly competitive barrier films made from biodegradable polymers, a high priority within the Brey research group was given to the investigation of such systems. Starting with solvent blends, acetonitrile/water mixtures were the first step towards a fully organic solvent dispersion. Up to 65 vol% acetonitrile could be used with water to achieve osmotic swelling of Hec.<sup>77</sup> This was shortly followed by a study on ternary solvent mixtures with methanol, acetonitrile, and water, which when mixed at 35 vol%, 55 vol%, and 10 vol%, respectively, still allowed for osmotic swelling of Hec.<sup>78</sup> However, this 10 vol% water content was still too much to allow for the dissolution of commercial degradable polyesters.

A huge breakthrough came with the publication of Dudko et al. where delamination of Hec was achieved in completely organic solvent systems.<sup>79</sup> Through the use of crown ethers that complex interlayer cations and render the platelet surface more hydrophobic, steric pressure is exerted on the sheets which aids in reaching the separation threshold required to trigger osmotic swelling (**Figure 10**). Water-free delamination was achieved in aprotic solvents including N-methylformamide (NMF) and N-methylacetamide. The direct combination of osmotically delaminated Hec and polyesters is now possible and will be explored later in this work.<sup>80</sup>

### 3.4. Relevant Characterization Methods

#### 3.4.1. X-Ray scattering and diffraction

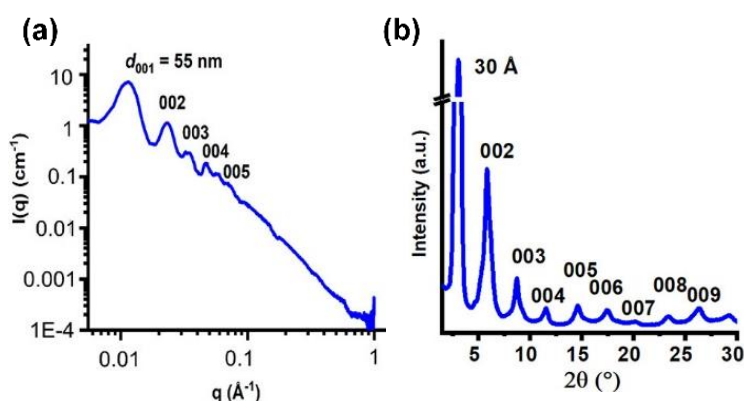


**Figure 11.** (a) SAXS of a concentrated Hec-PVP suspension illustrating the rational  $00l$ -reflections and an absence of restacked platelets in the crystalline swelling regime. (b) XRD of the resulting nanocomposite containing 31 vol% Hec that also shows  $00l$ -reflections. [Reprinted (adapted) with permission from T. Schilling, C. Habel, S. Rosenfeldt, M. Röhr, J. Breu, *ACS Applied Polymer Materials* 2020, 2, 3010. Copyright 2020 American Chemical Society (ref. 67).]

Reflections as high as the 8<sup>th</sup> order have been observed, highlighting the excellent positional order of adjacent silicate layers.<sup>54</sup> Scaling of the reflection curves following  $q^{-2}$  is consistent with two-dimensional scattering objects. Incomplete osmotic swelling can be identified by the presence of additional peaks at high  $q$  values that correspond to crystalline swelling phases.<sup>78</sup>

Similarly, powder x-ray diffraction (XRD) is used to evaluate the one-dimensional crystalline order of Hec platelets within a polymer nanocomposite (**Figure 11b**). The periodic arrangement of nanosheets is confirmed with the observation of a rational series of  $00l$ -

To evaluate a suspension of delaminated Hec platelets, small-angle X-ray scattering (SAXS) is applied. Scattering patterns of Hec contain a rational series of  $00l$ -reflections as a consequence of its coherent cofacial arrangement with large platelet separation distances (**Figure 11a**).

Reflections as high as the

reflections. Under dry conditions, deviations from the inherent d-spacing of Hec (0.96 nm) indicate long range intercalation of polymer in between nanosheets.<sup>81</sup>

#### 3.4.2. Gas barrier measurements

Several standardized testing methods exist for the measurement of gas barrier, the choice of which may depend on the type of measurement sample, the range of expected barrier values, and the choice of permeant. For the testing of food packaging films for high-performance oxygen permeation in this work, a coulometric method is applied following ASTM D3985. The patented coulometric sensor (COULOX®) applied in the MOCON measurement devices from AMETEK GmbH is absolute, providing high precision, sensitivity, and repeatability. During testing, the sample film is exposed to a flow high-purity oxygen gas on one side and a flow of nitrogen as a carrier gas on the other side. Any permeation of oxygen through the film and into the carrier gas is detected as gas flows through the coulometric sensor, where oxygen is converted into electrical energy. The quantity of oxygen permeation is obtained through conversion of the electrical signal strength. This method allows for the analysis of 100% of the carrier gas, therefore detection limits are as low as  $5 \times 10^{-4} \text{ cm}^3 \text{ m}^{-2} \text{ day}^{-1}$  for the device employed in this work, and even lower in more advanced models.<sup>82</sup>

#### 3.4.3. Biodegradation testing

The comprehensive biodegradation behavior of a given polymer requires testing under several conditions. In this work, three mediums will be employed. Since degradation rates are influenced by variations in soil conditions, temperature, water source, light, and oxygen, the degradation tests will be carried out under strictly controlled laboratory conditions defined by standardized methodologies. Enzymatic degradation under controlled conditions provide a basic understanding of how readily a polymer may undergo hydrolysis catalyzed by microorganisms. Enzymes like proteinase K and lipase are specific for polyester degradation. Following the weight loss of the sample by gravimetric analysis provides insights into bulk fragmentation kinetics, while additional analysis methods are required for determining if chain scission has occurred. These methods include, but are not limited to, gel permeation chromatography (GPC) for following changes in the molecular weight distribution, dynamic scanning calorimetry (DSC) to monitor changes in crystallinity related to degradation, and nuclear magnetic resonance (NMR) for observing changes in the chemical composition. Images produced with scanning electron microscopy (SEM) may

supplement these methods to observe changes to the sample surface as degradation progresses.<sup>37,38</sup>

Compost degradation testing provides conditions closer to those that a biodegradable polymer may encounter in its life cycle compared to the idealized enzymatic testing, although analysis is more challenging. During this test, samples are buried in locally-sourced industrial compost and stored in climate-controlled conditions following DIN EN ISO 20200 standards. Film samples are removed at specified time intervals and washed as carefully as possible. Analysis is only possible on degradation products that are collected by hand or with certain extraction techniques, and the interpretation of weight loss data and further analysis by GPC, DCS, and NMR should consider this limitation.<sup>83</sup>

CO<sub>2</sub> evolution testing is the highest standard biodegradation test available because of its ability to quantify the amount of carbon that is transformed into the smallest possible degradation products (methane, CO<sub>2</sub>). Testing procedures follow the standardized method DIN 14851:2019 with aniline as the positive standard. The current degradation medium for this test is wastewater that is obtained from the wastewater treatment plants of Bayreuth, DE for this work. Micro-Oxymax respirometers from Columbus Instruments International that were used and operate with a sensitivity of up to 0.2  $\mu\text{L h}^{-1}$  due to its closed-loop measuring with a nondispersive infrared detector.<sup>83,84</sup>

### 3.5. Preparation of Nanocomposite Coatings and Films

In this work, three different methods for preparation of coating and films were employed: spray coating, doctor blading, and slot-die coating. All of these methods involve casting from solution, as is required when working with delaminated Hec or nanosheet suspensions. Each method has their own benefits and limitations that will be discussed in the following sections.

#### 3.5.1. Spray coating

The spray coating of a substrate uses a pressurized airbrush to distribute a fine spray of suspension across a substrate that is adhered to a moving conveyor belt. The Breu research group uses a fully automated SATA 4000 LAB HVLP 1.0 mm spray gun (SATA GmbH & Co. KG, Germany) with adjustable droplet size and coating area. The spraying cycle is followed by a timed drying cycle under heat lamps. The process is repeated until a specified number of cycles is completed, or desired thickness is obtained. Creation of a fine spray gives the most uniform coating, necessitating the use of dilute suspensions (< 1 wt% solid content),

especially for the viscous nematic suspensions of clay nanosheets. Several high-performance and waterborne barrier coatings have been produced from the spray coating device in the Breu research group.<sup>65,68-70,72,81</sup> The spraying process has proven to create near perfect texture of platelets onto the substrate due to the preference for parallel positions above the substrate and the mobility afforded by the dilute suspensions.<sup>69</sup> In the current setup, only water-based solutions are spray coated because of the concern regarding aerosolized particles of organic solvents. Nevertheless, spray coating has been particularly beneficial to overcome dewetting problems in the application of the water-based suspensions of Hec onto hydrophobic substrates, attributed to the gradual buildup of quickly dried, thin wet-layers.<sup>72</sup> A single spraying cycle, depending on suspension solid content, may apply 5-10 nm at a time, requiring >200 spray/drying cycles that can total several hours. Consequently, this method is not considered scalable to industrial level and is therefore only applied when other methods of coating give unsatisfactory results.

### 3.5.2. Doctor blade

A doctor blade applies a defined wet-layer thickness by dragging a suspension across a fixed substrate. In the Breu research group, an automated device (Zehntner ZAA 2300, Zehntner GmbH Testing Instruments, Switzerland) is used for the movement of the doctor blade, and the substrate is fixed by a vacuum plate with adjustable temperature. While solution viscosity is a consideration, a much larger range of acceptable values can be applied. The solid content of the suspension can be adjusted to achieve a desired coating thickness. It should be noted that with increasing wet layer thickness or solid content, drying becomes increasingly difficult, especially in samples containing barrier nanosheets. A report from the Breu group established that doctor blading does not achieve the same degree of texture that spray coating can in the preparation of Hec nanocomposite coatings, but barrier improvement achievable with this method is nevertheless substantial.<sup>81</sup> Organic solvent-based suspensions can be coated with this method, and sequential layer addition to produce thick coatings or self-standing films is also possible, although such procedures are less favorable for large-scale production.

### 3.5.3. Slot-die coating

Preparation of highly precise coatings on the industrial scale can be done using slot-die coating devices. In this method, the suspension is delivered to the substrate from the die head with a fixed gap distance to the substrate. Up and downstream menisci, i.e., the coating

bead, form in the gap between the die head and the substrate, which is then dragged over the substrate during coating. Formation of a stable coating bead is essential to prevent coating defects. Solution delivery is metered and the speed of the moving substrate is controlled, which gives a very uniform coating thickness. The high precision allowed with slot-die coating has found applications in coatings of photographic films, paperboard, lithium-ion batteries, flexible electronics, and solar cells.<sup>85</sup> For each solution to be coated, operating parameters must be established, including coating speed, coating gap, solution viscosity, and surface tension. Determination of the operating limits for each solution can be a complex and time-consuming process, unlike the more intuitive doctor blading methods.

While being fed through the die head, the coating solution in a slot-die coating process is subjected to high shear rates. The Breu research group has demonstrated that this high shear enables flow-alignment of nematic Hec suspensions during coating with a laboratory-scale TSE Table Coater with a 1-Layer Slot Die 300 mm, AAA (TSE Troller AG, Switzerland).<sup>86</sup> This flow alignment and shear thinning of nanosheets in suspension facilitates the coating process and positively influences nanocomposite texture to produce highly effective barrier coatings. The customizable nature of the processing parameters allow for coating a wide range of velocities and organic solvent-based mixtures. Drying of the wet layer can be facilitated by the temperature-controlled substrate plate. Utilization of the slot-die coater device to produce self-standing and layered films will be demonstrated in later sections.

## 4. Synopsis

This thesis contains three publications and one manuscript regarding the preparation of biodegradable nanocomposite films as a packaging material. The work was performed in the context of the collaborative research center (Sonderforschungsbereiche, SFB) 1357 funded by the German Research Foundation (Deutsche Forschungsgemeinschaft, DFG) in 2019. SFB 1357 'Mikroplastik' has the overarching aim to study the formation and transport, biological effects, and interactions of microplastics in different ecosystems and organisms. The role of subproject Co2 (part of this thesis) was to produce a high-performing alternative to the single-use food packaging materials that produce microplastic. This aim was to be achieved with a two front strategy: by the design and synthesis of novel polymer materials with desired properties and by the processing of these polymers, as well as commercial polymers, into high performance nanocomposite films. The work reported here encompasses results from the latter focus.

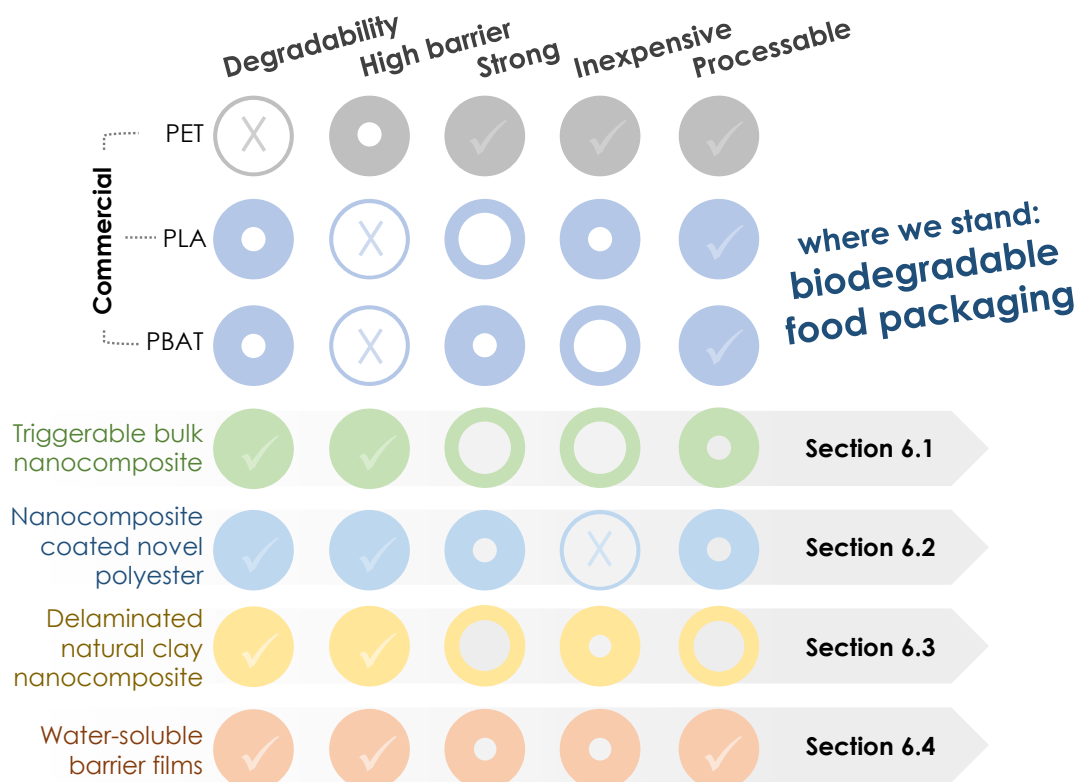


**Figure 12.** Schematic summary of the results from this thesis in comparison to commercially available materials.

General suitability as a high-performance biodegradable food packaging material involves considerations from five factors (**Figure 12**). Of course, the film should not form persistent microplastics in terrestrial and aqueous environments. The qualification as high-performance was summarized as high oxygen barrier and strong mechanical performance. For this high-volume application, low costs and capability of large scale processing are also critical factors.

Each of the enclosed manuscripts report an approach to the creation of a material that would fulfill all of these five requirements, with a varying degree of success. **Section 6.1** presents the first PLA nanocomposite film obtained from the osmotic swelling of Hec in organic solvents through complexing with crown ethers. The self-standing nanocomposite film exhibited accelerated degradation of commercial PLA due to triggered bulk fragmentation in water from swelling of clay tactoids, which acted additionally as an effective barrier to oxygen even in humid air. However, the film was quite brittle, and despite its scalable preparation with the slot die coater, the use of NMF as solvent and crown ethers detract from its feasibility in terms of price.

**Section 6.2** utilized a novel polyester with rapid hydrolysis and stretchable mechanical performance as a substrate for a waterborne Hec nanocomposite coating. With the barrier coating, the film maintained rapid degradation and strong, PE-like mechanics, although coating adhesion should be improved in future work. The substrate itself is thermally processable under mild conditions and the addition of the nanocomposite by aqueous spray coating of the polymer-Hec suspension is benign, but not scalable. Overall, the coated film exhibited great physical properties, however the novelty of the polymer employed as a substrate, the specialty of GlyChit as the nanocomposite matrix, as well as the inherently expensive synthetic Hec give this film a hefty price tag.

**Section 6.3** proposes vermiculite as the preferred nanosheet source due to its naturally abundant supply and inherently high aspect ratio. The cost of vermiculite per kg is often cheaper than that of polymers, bringing down the total cost of the system. A new and more effective delamination process was proposed that gives superior yield of single nanosheets in organic solvents. PLA was used as the polymer matrix for a vermiculite nanocomposite coating on a cellulose nanofiber substrate to demonstrate the barrier improving power of this natural clay. The coating process benefited from the porous nature of the cellulose nanofibers to remove the high boiling point solvent from both the surface and underside of the wet layer. Cellulose nanofiber substrates are inherently brittle, which the addition of the

nanocomposite did not improve. In future works, the choice of a stronger substrate or matrix material could improve the mechanical performance of vermiculite nanocomposites. Lastly, **Section 6.4** explores a polymer/Hec/polymer sandwich-structured film rather than a dispersed nanocomposite for the application of single-use water-soluble packaging. Poly(vinyl alcohol) is the current material of choice for such applications, despite its slow degradation in its intended medium of disposal: wastewater. Biopolymers (hydroxypropyl methylcellulose and alginate) were evaluated as replacement polymers. By incorporating a collapsed nematic suspension of clay platelets as the inner barrier layer, common setbacks like high processing viscosities, embrittlement, and impedance of biodegradation are avoided while high barrier even in humid conditions is ensured. Processing is scalable to roll-to-roll systems and conditions are tunable for application specific requirements.

#### 4.1. High Barrier Nanocomposite Film with Accelerated Biodegradation by Clay Swelling Induced Fragmentation

Commercialized ‘biodegradable’ polymers like PLA suffer from poor degradation in relevant environmental media, particularly aqueous environments, as introduced in more detail in **Section 3.2.2**. In this work, we aimed to improve the aqueous biodegradation kinetics of PLA by employing clay filler with a dual purpose.<sup>84</sup> Hec has demonstrated its powerful barrier improving abilities due to its high aspect ratio and osmotic swelling (**Section 3.3.2 and 3.3.3**). PLA desperately needs such massive improvements in barrier to be applicable

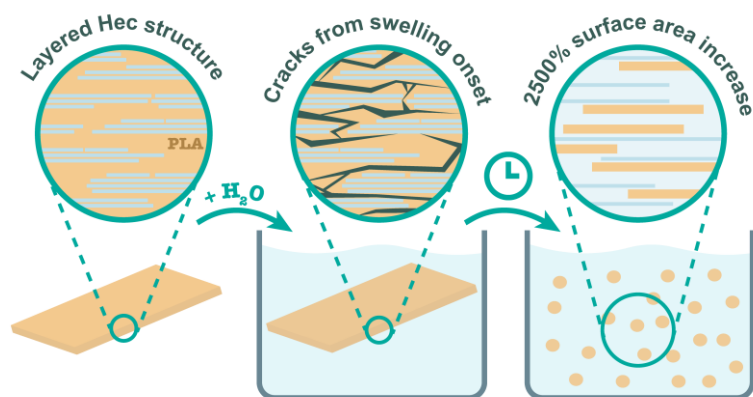


**Figure 13.** Schematic illustrating the water-triggered fragmentation of 18C6Hec/PLA films. Reprinted with permission from reference 86

for more demanding packaging applications. At the same time, clay distributed through the PLA matrix may swell upon submersion in water, which fragments the film in its entirety. The resulting increase in the surface area exposed to the degradation

medium accelerates the transition from bulk fragmentation to polymer chain scission (**Figure 13**).<sup>87</sup>

The direct combination of PLA with osmotically delaminated Hec was allowed for the first time by crown ethers, as revealed in **Section 3.3.5**. PLA dissolved in NMF can be directly added to a suspension of Hec with 18-crown-6. Casting of the film involved sequential layering using the industrially scalable slot-die coating device that allows high-precision wet layer deposition. Upon drying, approximately 120 nm thick clay tactoids were generated in-situ and separated by regions of pure PLA. The clay tactoids formed by offset stacking of single platelets, creating impermeable, through-thickness walls giving a 99.3% reduction in the oxygen permeability of PLA to  $124 \text{ cm}^3 \text{ m}^{-2} \text{ day}^{-1} \text{ bar}^{-1}$  at 65% relative humidity. An XRD study demonstrated that the tactoids are resistant to swelling even under high humidity conditions. However, the film fragmented within one hour when submerged in water, increasing its surface area by 2500%. Biodegradation of the nanocomposite film exhibited faster biodegradation relative to neat PLA under controlled enzymatic conditions and during CO<sub>2</sub> evolution testing in wastewater sludge. The starting molecular weight of the PLA in the nanocomposite was found to be lower than in the neat PLA, attributed to the high temperature dissolution in NMF. This factor may have also influenced biodegradation rate of the nanocomposite.

## 4.2. Stretchable and Fast Composting Polyester Films with High-Performance Oxygen Barrier

Synthetic routes to rapid biodegradation of polymers with strong mechanical performance by tailoring backbone structure was introduced in **Section 3.2.3**. The Agarwal group had explored the poly(1,4-benzenedimethylene succinate) (PBDMS) structure, which is a constitutional isomer of the chemically resistant poly(1,4-butylene terephthalate), but is more available to biodegradation due to separation of the ester carbonyl carbon from the aromatic unit to limit delocalization of electron density through resonance structures.<sup>38</sup> By preparation of PBDMS copolymers with 1,4-butanediol, highly stretchable (polyethylene-like) and rapidly hydrolysable PB<sub>x</sub>BDM<sub>y</sub>S polyester (x = molar ratio of 1,4-butanediol; y = molar ratio of 1,4-benzenedimethanol in the monomer feed) films were prepared with gentle thermal processing.

The PB<sub>64</sub>BDM<sub>36</sub>S polyester alone suffered from poor gas barrier, which is required to be relevant for food packaging applications. The effects of a barrier coating beyond improvement of barrier properties was evaluated. In this work, an aqueous nematic suspension of Hec and the biodegradable glycol chitosan (GlyChit) was spray coated onto PB<sub>64</sub>BDM<sub>36</sub>S as well as commercial PBS and PBAT (**Figure 14**). The highly ordered 3- $\mu$ m thick nanocomposite coating dramatically reduced the oxygen barrier of all substrates more than 200 times. Mechanical properties of the coated substrates remained highly stretchable. Biodegradation rates in compost of coated films were slightly delayed compared to uncoated films but nevertheless fell within the optimal time frame (< 8 weeks). The GlyChit-Hec coated PB<sub>64</sub>BDM<sub>36</sub>S exhibited excellent performance in mechanical, barrier and biodegradation aspects.

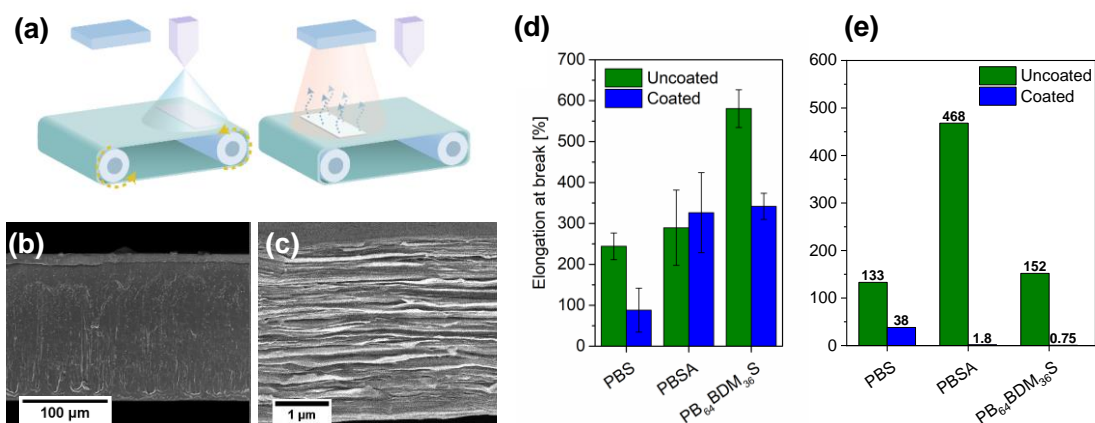


**Figure 14.** (a) Schematic of spray coating. (b) Cross-section of PB<sub>64</sub>M<sub>36</sub>S coated with GlyChitHec and (c) close up of coating. (d) Elongation at break for and (e) OTR of PBS, PBSA, and PB<sub>64</sub>M<sub>36</sub>S films with and without GlyChitHec coating. OTR compared to commercial packaging films at 65% RH and 23 C. [Reprinted (adapted) with permission from E. Sehl, R. L. Timmins, D. Ghosh, J. Breu, S. Agarwal, *ACS Applied Polymer Materials* **2022**, *4*, 6675. Copyright 2021 American Chemical Society.]

### 4.3. Spontaneous Delamination of Affordable Natural Vermiculite as a High Barrier Filler for Biodegradable Food Packaging

Up to this point, synthetic fluorhectorite has been the clay filler of choice due to its exceptionally high aspect ratio and ability to osmotically delaminate. The benefits of such traits for the preparation of nanocomposite barrier layers were discussed extensively in **Section 3.3.2 and 3.3.3**. When considering the applications of food packaging, the high cost to produce such a pristine synthetic clay raises concerns as to whether consumers are willing to pay a higher price for environmentally friendly packaging.

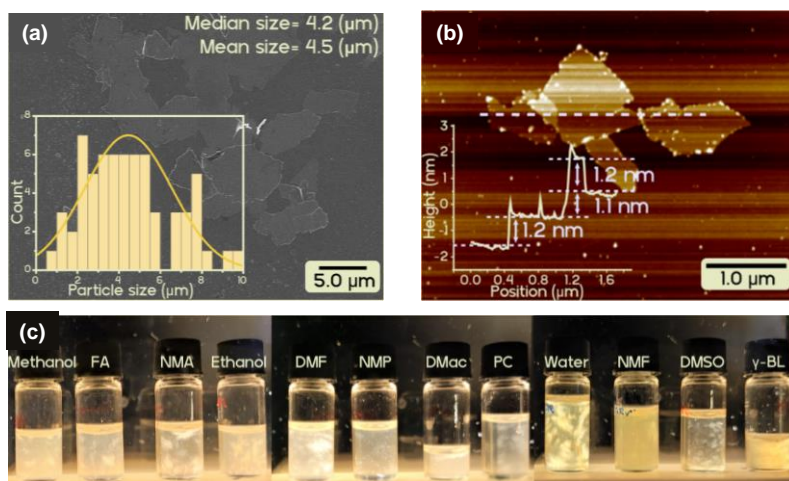


**Figure 15.** (a) SEM photo of vermiculite nanosheets on a Si wafer. *Inset*: particle size distribution measured from the SEM image indicating a mean size of  $4 \pm 1 \mu\text{m}$ . (b) Topographic AFM image of vermiculite nanosheets and height profile from the single nanosheets indicating a height of  $\sim 1.2 \text{ nm}$ . (c) Photos of nematic suspensions of vermiculite in various solvents obtained by diluting a vermiculite/NMF gel, viewed under cross-polarized light.

Natural vermiculites are another type of 2:1 layered silicates that are very abundant and have inherently large aspect ratios. Unfortunately, they are difficult to delaminate due to the high layer charge and the divalent interlayer  $\text{Mg}^{2+}$  cation. In this paper (**Figure 15**), a one-step ion-exchange is presented for the osmotic delamination

of natural vermiculite in N-methylformamide (NMF) and its mixtures with other organic solvents. A delamination yield as high as 84% was attributed to the use of butylammonium citrate. The citrate anion complexes the  $\text{Mg}^{2+}$  so that butylamine may favorably replace  $\text{Mg}^{2+}$  as the interlayer cation. A sufficient ion exchange with butylamine allows vermiculite to osmotically delaminate into single layer platelets with an aspect ratio of approximately 4,000.

The relevancy of these nanosheets as a barrier filler in inexpensive and biodegradable packaging was demonstrated by the preparation of a stable, delaminated vermiculite/PLA

suspension in a NMF/gamma-butyrolactone mixture. The suspension was doctor bladed onto a porous cellulose nanofiber substrate. The nanocomposite coated foil exhibited an oxygen transmission rate of  $1.30 \text{ cm}^3 \text{ m}^{-2} \text{ day}^{-1} \text{ bar}^{-1}$ , which competes with high-end, non-degradable poly(vinylidene dichloride) films. The cost of vermiculite is relatively lower than that of PLA, reducing the overall cost of the system.

#### 4.4. Biodegradation in Wastewater of Water-Soluble Polymer/Clay Barrier Films from Green and Scalable Processing

Water-soluble packaging films are designed to encapsulate a single portion of dishwasher or laundry detergent, pesticides, dyes, etc. to conveniently be added as a whole to the given application. The dissolved packaging is then to be released into the environment, particularly into wastewater streams. Poly(vinyl alcohol) is the most commonly employed polymer for this application, however its biodegradation in water requires acclimated microorganism that are not found in common wastewater treatment facilities.<sup>88</sup> Water-soluble bio-polymers could replace PVOH in responsibly designed packaging if their barrier and mechanical properties are improved, and biodegradation in their intended disposal medium is ensured. The high filler content (>10 wt%) that is required to obtain a suitable gas barrier of moisture-sensitive biopolymers would cause severe embrittlement if directly combined. Instead of nanocomposite formulation, creative process-based solutions were applied using the industrially scalable slot-die coater introduced in **Section 3.5.3** to prepare high-performance and biodegradable films.

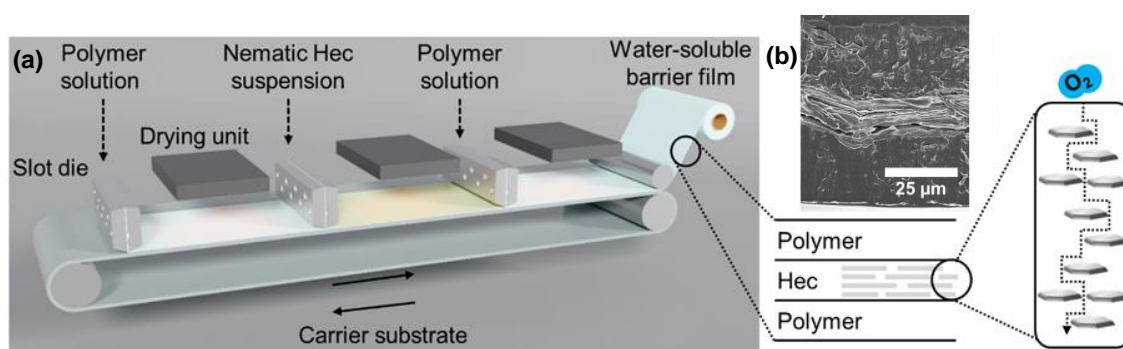


**Figure 16.** (a) 3D model of the proposed roll-to-roll processing for high-performance, water-soluble barrier films. (b) SEM image (PVOH-based film) and schematic of cross-section of sandwich-layered structure of polymer/Hec/polymer films with a tortuous path

In this work, sandwich-layered films (polymer/Hec/polymer) using either plasticized PVOH, hydroxypropyl methylcellulose (HPMC), or sodium alginate (alg) were prepared using the slot-die coater to mimic a large-scale roll-to-roll process (**Figure 16**). Isolation of the Hec and polymer solutions removes previous filler content restrictions due to high processing velocity of combined suspensions. The center layer consisting of a collapsed nematic Hec suspension created a band-like barrier wall that drastically improved barrier performance of all polymers. Inter-diffusion during processing gave a 1- $\mu\text{m}$  thick interfacial nanocomposite, ensuring strong layer adhesion. The Hec layer also acted as mechanical reinforcement, strengthening the biopolymer foils while leaving the outer polymer layers accessible to biodegradation. From monitoring  $\text{CO}_2$  evolution of the films in wastewater for 33 days, only the alg-based film was capable of significant biodegradation, while PVOH and HPMC-based films did not degrade beyond the plasticizer content.

## 5. Literature

- 1 *History and Future of Plastics*, <<https://www.sciencehistory.org/the-history-and-future-of-plastics>> (2013).
- 2 Yarsley, V. E. & Couzens, E. G. *Plastics*. (Penguin, 1945).
- 3 Freinkel, S. *Plastic: A Toxic Love Story*. (Text Publishing Company, 2011).
- 4 *A History of Plastics*, <[https://www.bpf.co.uk/plastipedia/plastics\\_history/Default.aspx](https://www.bpf.co.uk/plastipedia/plastics_history/Default.aspx)> (2008).
- 5 Ryan, P. G. in *Marine anthropogenic litter* 1-25 (Springer, Cham, 2015).
- 6 Lau, W. W. Y. *et al.* Evaluating scenarios toward zero plastic pollution. *Science* **369**, 1455-1461, doi:10.1126/science.aba9475 (2020).
- 7 Geyer, R., Jambeck, J. R. & Law, K. L. Production, use, and fate of all plastics ever made. *Sci Adv* **3**, e1700782, doi:10.1126/sciadv.1700782 (2017).
- 8 *Plastics- the Facts 2019*, <[https://www.bpf.co.uk/plastipedia/plastics\\_history/Default.aspx](https://www.bpf.co.uk/plastipedia/plastics_history/Default.aspx)> (2019).
- 9 *Marine LitterWatch*, <<https://www.eea.europa.eu/themes/water/europes-seas-and-coasts/assessments/marine-litterwatch>> (2021).
- 10 Hopewell, J., Dvorak, R. & Kosior, E. Plastics recycling: challenges and opportunities. *Philos Trans R Soc Lond B Biol Sci* **364**, 2115-2126, doi:10.1098/rstb.2008.0311 (2009).
- 11 Steenis, N. D., van Herpen, E., van der Lans, I. A., Ligthart, T. N. & van Trijp, H. C. M. Consumer response to packaging design: The role of packaging materials and graphics in sustainability perceptions and product evaluations. *Journal of Cleaner Production* **162**, 286-298, doi:10.1016/j.jclepro.2017.06.036 (2017).
- 12 Dilkes-Hoffman, L. S. *et al.* Environmental impact of biodegradable food packaging when considering food waste. *Journal of Cleaner Production* **180**, 325-334, doi:10.1016/j.jclepro.2018.01.169 (2018).
- 13 Foley, J. A. *et al.* Solutions for a cultivated planet. *Nature* **478**, 337-342, doi:10.1038/nature10452 (2011).
- 14 Van Cauwenberghe, L., Vanreusel, A., Mees, J. & Janssen, C. R. Microplastic pollution in deep-sea sediments. *Environ Pollut* **182**, 495-499, doi:10.1016/j.envpol.2013.08.013 (2013).
- 15 Enyoh, C. E., Verla, A. W., Verla, E. N., Ibe, F. C. & Amaobi, C. E. Airborne microplastics: a review study on method for analysis, occurrence, movement and risks. *Environ Monit Assess* **191**, 668, doi:10.1007/s10661-019-7842-0 (2019).
- 16 Vethaak, A. D. & Legler, J. Microplastics and human health. *Science* **371**, 672-674, doi:10.1126/science.abe5041 (2021).
- 17 Browne, M. A., Niven, S. J., Galloway, T. S., Rowland, S. J. & Thompson, R. C. Microplastic moves pollutants and additives to worms, reducing functions linked to health and biodiversity. *Curr Biol* **23**, 2388-2392, doi:10.1016/j.cub.2013.10.012 (2013).
- 18 Yong, C. Q. Y., Valiyaveetil, S. & Tang, B. L. Toxicity of Microplastics and Nanoplastics in Mammalian Systems. *Int J Environ Res Public Health* **17**, 1509, doi:10.3390/ijerph17051509 (2020).

- 19 de Souza Machado, A. A., Kloas, W., Zarfl, C., Hempel, S. & Rillig, M. C. Microplastics as an emerging threat to terrestrial ecosystems. *Glob Chang Biol* **24**, 1405-1416, doi:10.1111/gcb.14020 (2018).
- 20 *Bioplastics market data*, <<https://www.european-bioplastics.org/market/>> (2021).
- 21 Lambert, S. & Wagner, M. Environmental performance of bio-based and biodegradable plastics: the road ahead. *Chem Soc Rev* **46**, 6855-6871, doi:10.1039/c7cs00149e (2017).
- 22 Jem, K. J. & Tan, B. The development and challenges of poly (lactic acid) and poly (glycolic acid). *Advanced Industrial and Engineering Polymer Research* **3**, 60-70, doi:10.1016/j.aiepr.2020.01.002 (2020).
- 23 Singhvi, M. S., Zinjarde, S. S. & Gokhale, D. V. Polylactic acid: synthesis and biomedical applications. *J Appl Microbiol* **127**, 1612-1626, doi:10.1111/jam.14290 (2019).
- 24 Jian, J., Xiangbin, Z. & Xianbo, H. An overview on synthesis, properties and applications of poly(butylene-adipate-co-terephthalate)–PBAT. *Advanced Industrial and Engineering Polymer Research* **3**, 19-26, doi:10.1016/j.aiepr.2020.01.001 (2020).
- 25 Bagheri, A. R., Laforsch, C., Greiner, A. & Agarwal, S. Fate of So-Called Biodegradable Polymers in Seawater and Freshwater. *Glob Chall* **1**, 1700048, doi:10.1002/gch2.201700048 (2017).
- 26 Kakadellis, S. & Harris, Z. M. Don't scrap the waste: The need for broader system boundaries in bioplastic food packaging life-cycle assessment – A critical review. *Journal of Cleaner Production* **274**, 122831, doi:10.1016/j.jclepro.2020.122831 (2020).
- 27 The New Plastics Economy: Rethinking the future of plastics. (Ellen MacArthur Foundation, 2016).
- 28 Hu, X., Su, T., Li, P. & Wang, Z. Blending modification of PBS/PLA and its enzymatic degradation. *Polymer Bulletin* **75**, 533-546, doi:10.1007/s00289-017-2054-7 (2017).
- 29 Wang, X. W. *et al.* Degradability comparison of poly(butylene adipate terephthalate) and its composites filled with starch and calcium carbonate in different aquatic environments. *Journal of Applied Polymer Science* **136**, 46916, doi:10.1002/app.46916 (2019).
- 30 Weng, Y.-X. *et al.* Biodegradation behavior of poly(butylene adipate-co-terephthalate) (PBAT), poly(lactic acid) (PLA), and their blend under soil conditions. *Polymer Testing* **32**, 918-926, doi:10.1016/j.polymertesting.2013.05.001 (2013).
- 31 Gigante, V., Canesi, I., Cinelli, P., Coltelli, M. B. & Lazzeri, A. Rubber Toughening of Polylactic Acid (PLA) with Poly(butylene adipate-co-terephthalate) (PBAT): Mechanical Properties, Fracture Mechanics and Analysis of Ductile-to-Brittle Behavior while Varying Temperature and Test Speed. *European Polymer Journal* **115**, 125-137, doi:10.1016/j.eurpolymj.2019.03.015 (2019).
- 32 Arruda, L. C., Magaton, M., Bretas, R. E. S. & Ueki, M. M. Influence of chain extender on mechanical, thermal and morphological properties of blown films of PLA/PBAT blends. *Polymer Testing* **43**, 27-37, doi:10.1016/j.polymertesting.2015.02.005 (2015).

- 33 Tsuji, H. & Ikada, Y. Blends of isotactic and atactic poly(lactide). I. Effects of mixing ratio of isomers on crystallization of blends from melt. *Journal of Applied Polymer Science* **58**, 1793-1802, doi:10.1002/app.1995.070581018 (1995).
- 34 Tsuji, H. & Ikada, Y. Blends of crystalline and amorphous poly(lactide). III. Hydrolysis of solution-cast blend films. *Journal of Applied Polymer Science* **63**, 855-863, doi:10.1002/(sici)1097-4628(19970214)63:7<855::aid-app5>3.0.co;2-p (1997).
- 35 Chen, C.-C., Chueh, J.-Y., Tseng, H., Huang, H.-M. & Lee, S.-Y. Preparation and characterization of biodegradable PLA polymeric blends. *Biomaterials* **24**, 1167-1173, doi:10.1016/s0142-9612(02)00466-0 (2003).
- 36 Perego, G., Cella, G. D. & Bastioli, C. Effect of molecular weight and crystallinity on poly(lactic acid) mechanical properties. *Journal of Applied Polymer Science* **59**, 37-43, doi:10.1002/(sici)1097-4628(19960103)59:1<37::aid-app6>3.0.co;2-n (1996).
- 37 Kumar, A., Weig, A. R. & Agarwal, S. Balancing Degradability and Physical Properties of Amorphous Poly(d,l-Lactide) by Making Blends. *Macromolecular Materials and Engineering*, 2100602, doi:10.1002/mame.202100602 (2021).
- 38 Sehl, E., Eger, E. M., Himmelsbach, A. & Agarwal, S. Fast Hydrolyzable Constitutional Isomer of Poly(butylene terephthalate) and Its Copolyesters with 1,4-Butanediol. *ACS Applied Polymer Materials* **3**, 6427-6436, doi:10.1021/acsapm.1c01169 (2021).
- 39 Wu, F., Misra, M. & Mohanty, A. K. Challenges and new opportunities on barrier performance of biodegradable polymers for sustainable packaging. *Progress in Polymer Science* **117**, 101395, doi:10.1016/j.progpolymsci.2021.101395 (2021).
- 40 Wang, J. *et al.* Moisture and Oxygen Barrier Properties of Cellulose Nanomaterial-Based Films. *ACS Sustainable Chemistry & Engineering* **6**, 49-70, doi:10.1021/acssuschemeng.7b03523 (2017).
- 41 Schmid, M. *et al.* Properties of Whey-Protein-Coated Films and Laminates as Novel Recyclable Food Packaging Materials with Excellent Barrier Properties. *International Journal of Polymer Science* **2012**, 1-7, doi:10.1155/2012/562381 (2012).
- 42 Yun, X. & Dong, T. in *Food Packaging* 147-184 (Elsevier, 2017).
- 43 Lagaron, J. M., Catalá, R. & Gavara, R. Structural characteristics defining high barrier properties in polymeric materials. *Materials Science and Technology* **20**, 1-7, doi:10.1179/026708304225010442 (2013).
- 44 Van Krevelen, D. W. & Te Nijenhuis, K. *Properties of polymers: their correlation with chemical structure; their numerical estimation and prediction from additive group contributions.* (Elsevier, 2009).
- 45 Drieskens, M. *et al.* Structure versus properties relationship of poly(lactic acid). I. Effect of crystallinity on barrier properties. *Journal of Polymer Science Part B: Polymer Physics* **47**, 2247-2258, doi:10.1002/polb.21822 (2009).
- 46 Gao, F. Clay/polymer composites: the story. *Materials Today* **7**, 50-55, doi:10.1016/s1369-7021(04)00509-7 (2004).
- 47 Lim, M., Kim, D. & Seo, J. Enhanced oxygen-barrier and water-resistance properties of poly(vinyl alcohol) blended with poly(acrylic acid) for packaging applications. *Polymer International* **65**, 400-406, doi:10.1002/pi.5068 (2016).

- 48 Horst, M. F., Quinzani, L. M. & Failla, M. D. Rheological and barrier properties of nanocomposites of HDPE and exfoliated montmorillonite. *Journal of Thermoplastic Composite Materials* **27**, 106-125, doi:10.1177/0892705712443248 (2012).
- 49 Alena, K., Dagmar, M., Francois, G. J. & Miroslav, S. Polymer/clay nanocomposites and their gas barrier properties. *Polymer Composites* **34**, 1418-1424, doi:10.1002/pc.22541 (2013).
- 50 Nicolosi, V., Chhowalla, M., Kanatzidis, M. G., Strano, M. S. & Coleman, J. N. Liquid Exfoliation of Layered Materials. *Science* **340**, 1226419, doi:10.1126/science.1226419 (2013).
- 51 Cussler, E. L., Hughes, S. E., Ward, W. J. & Aris, R. Barrier membranes. *Journal of Membrane Science* **38**, 161-174, doi:10.1016/s0376-7388(00)80877-7 (1988).
- 52 Dudko, V. *et al.* Repulsive Osmotic Delamination: 1D Dissolution of 2D materials. *Advanced Materials Technologies*, doi:10.1002/admt.202200553 (2022).
- 53 Backes, C. *et al.* Guidelines for Exfoliation, Characterization and Processing of Layered Materials Produced by Liquid Exfoliation. *Chemistry of Materials* **29**, 243-255, doi:10.1021/acs.chemmater.6b03335 (2016).
- 54 Rosenfeldt, S. *et al.* In-Depth Insights into the Key Steps of Delamination of Charged 2D Nanomaterials. *Langmuir* **32**, 10582-10588, doi:10.1021/acs.langmuir.6b02206 (2016).
- 55 Darie, R. N. *et al.* Effect of Nanoclay Hydrophilicity on the Poly(lactic acid)/Clay Nanocomposites Properties. *Industrial & Engineering Chemistry Research* **53**, 7877-7890, doi:10.1021/ie500577m (2014).
- 56 Russo, P. *et al.* Physical properties of poly lactic acid/clay nanocomposite films: Effect of filler content and annealing treatment. *Journal of Applied Polymer Science* **131**, n/a-n/a, doi:10.1002/app.39798 (2014).
- 57 Gomez-Gamez, A. B., Yebra-Rodriguez, A., Peñas-Sanjuan, A., Soriano-Cuadrado, B. & Jimenez-Millan, J. Influence of clay percentage on the technical properties of montmorillonite/polylactic acid nanocomposites. *Applied Clay Science* **198**, 105818, doi:10.1016/j.clay.2020.105818 (2020).
- 58 Chang, J.-H., An, Y. U. & Sur, G. S. Poly(lactic acid) nanocomposites with various organoclays. I. Thermomechanical properties, morphology, and gas permeability. *Journal of Polymer Science Part B: Polymer Physics* **41**, 94-103, doi:10.1002/polb.10349 (2003).
- 59 Lai, S.-M., Wu, S.-H., Lin, G.-G. & Don, T.-M. Unusual mechanical properties of melt-blended poly(lactic acid) (PLA)/clay nanocomposites. *European Polymer Journal* **52**, 193-206, doi:10.1016/j.eurpolymj.2013.12.012 (2014).
- 60 Bartel, M., Remde, H., Bohn, A. & Ganster, J. Barrier properties of poly(lactic acid)/cloisite 30B composites and their relation between oxygen permeability and relative humidity. *Journal of Applied Polymer Science* **134**, doi:10.1002/app.44424 (2017).
- 61 Stöter, M. *et al.* Nanoplatelets of sodium hectorite showing aspect ratios of approximately 20,000 and superior purity. *Langmuir* **29**, 1280-1285, doi:10.1021/la304453h (2013).
- 62 Kalo, H., Möller, M. W., Ziadeh, M., Dolejš, D. & Breu, J. Large scale melt synthesis in an open crucible of Na-fluorhectorite with superb charge

- homogeneity and particle size. *Applied Clay Science* **48**, 39-45, doi:10.1016/j.clay.2009.11.014 (2010).
- 63 Habel, C. *et al.* Competition between nucleation and confinement in the crystallization of poly(ethylene glycol)/ large aspect ratio hectorite nanocomposites. *Polymer* **202**, 122734, doi:10.1016/j.polymer.2020.122734 (2020).
- 64 Röhrli, M. *et al.* Disorder-Order Transition-Improving the Moisture Sensitivity of Waterborne Nanocomposite Barriers. *ACS Appl Mater Interfaces*, doi:10.1021/acsami.1c14246 (2021).
- 65 Schilling, T., Habel, C., Rosenfeldt, S., Röhrli, M. & Breyer, J. Impact of Ultraconfinement on Composite Barriers. *ACS Applied Polymer Materials* **2**, 3010-3015, doi:10.1021/acsapm.0c00456 (2020).
- 66 Rolle, K. *et al.* Large T (g) Shift in Hybrid Bragg Stacks through Interfacial Slowdown. *Macromolecules* **54**, 2551-2560, doi:10.1021/acs.macromol.0c02818 (2021).
- 67 Eckert, A., Abbasi, M., Mang, T., Saalwächter, K. & Walther, A. Structure, Mechanical Properties, and Dynamics of Polyethylenoxide/Nanoclay Nacre-Mimetic Nanocomposites. *Macromolecules* **53**, 1716-1725, doi:10.1021/acs.macromol.9b01931 (2020).
- 68 Dorres, T. *et al.* Nanoscale-Structured Hybrid Bragg Stacks with Orientation- and Composition-Dependent Mechanical and Thermal Transport Properties: Implications for Nacre Mimetics and Heat Management Applications. *ACS Appl Nano Mater* **5**, 4119-4129, doi:10.1021/acsanm.2c00061 (2022).
- 69 Tsurko, E. S. *et al.* Can high oxygen and water vapor barrier nanocomposite coatings be obtained with a waterborne formulation? *Journal of Membrane Science* **540**, 212-218, doi:10.1016/j.memsci.2017.06.051 (2017).
- 70 Habel, C. *et al.* Lightweight Ultra-High-Barrier Liners for Helium and Hydrogen. *ACS Nano* **14**, 7018-7024, doi:10.1021/acs.nano.0c01633 (2020).
- 71 Doblhofer, E. *et al.* Structural Insights into Water-Based Spider Silk Protein-Nanoclay Composites with Excellent Gas and Water Vapor Barrier Properties. *ACS Appl Mater Interfaces* **8**, 25535-25543, doi:10.1021/acsami.6b08287 (2016).
- 72 Habel, C. *et al.* High-Barrier, Biodegradable Food Packaging. *Macromolecular Materials and Engineering* **303**, 1800333, doi:10.1002/mame.201800333 (2018).
- 73 Zhu, J. *et al.* Filter-Through Method of Making Highly Efficient Polymer-Clay Nanocomposite Membranes. *Macromolecular Materials and Engineering* **304**, 1800779, doi:10.1002/mame.201800779 (2019).
- 74 Zhu, J. *et al.* Layering-Triggered Delayering with Exfoliated High-Aspect Ratio Layered Silicate for Enhanced Gas Barrier, Mechanical Properties, and Degradability of Biodegradable Polymers. *Glob Chall* **4**, 2000030, doi:10.1002/gch2.202000030 (2020).
- 75 Rhim, J.-W., Hong, S.-I. & Ha, C.-S. Tensile, water vapor barrier and antimicrobial properties of PLA/nanoclay composite films. *LWT - Food Science and Technology* **42**, 612-617, doi:10.1016/j.lwt.2008.02.015 (2009).
- 76 Lim, S. T., Hyun, Y. H., Choi, H. J. & Jhon, M. S. Synthetic Biodegradable Aliphatic Polyester/Montmorillonite Nanocomposites. *Chemistry of Materials* **14**, 1839-1844, doi:10.1021/cm010377j (2002).

- 77 Kunz, R. *et al.* Giant Multistep Crystalline Vs. Osmotic Swelling of Synthetic Hectorite in Aqueous Acetonitrile. *Clays and Clay Minerals* **67**, 481-487, doi:10.1007/s42860-019-00046-9 (2020).
- 78 Mayr, L. *et al.* Osmotic Swelling of Sodium Hectorite in Ternary Solvent Mixtures: Nematic Liquid Crystals in Hydrophobic Media. *Langmuir* **36**, 3814-3820, doi:10.1021/acs.langmuir.0c00373 (2020).
- 79 Dudko, V., Ottermann, K., Rosenfeldt, S., Papastavrou, G. & Breu, J. Osmotic Delamination: A Forceless Alternative for the Production of Nanosheets Now in Highly Polar and Aprotic Solvents. *Langmuir* **37**, 461-468, doi:10.1021/acs.langmuir.0c03113 (2021).
- 80 Dudko, V. *et al.* Spontaneous delamination of affordable natural vermiculite as a high barrier filler for biodegradable food packaging. *Materials Advances* **3**, 9052-9062, doi:10.1039/d2ma00734g (2022).
- 81 Tsurko, E. S. *et al.* Large Scale Self-Assembly of Smectic Nanocomposite Films by Doctor Blading versus Spray Coating: Impact of Crystal Quality on Barrier Properties. *Macromolecules* **50**, 4344-4350, doi:10.1021/acs.macromol.7b00701 (2017).
- 82 OTR Permeation Analyzers, <<https://www.ametekmocon.com/products/permeationanalyzers/otr-permeation-analyzers>> (2020).
- 83 Sehl, E., Timmins, R. L., Ghosh, D., Breu, J. & Agarwal, S. Stretchable and Fast Composting Polyester Films with High-Performance Oxygen Barrier. *ACS Applied Polymer Materials* **4**, 6675-6686, doi:<https://doi.org/10.1021/acsapm.2c01040> (2022).
- 84 Timmins, R. L. *et al.* High Barrier Nanocomposite Film with Accelerated Biodegradation by Clay Swelling Induced Fragmentation. *Macromolecular Materials and Engineering* **307**, 2100727, doi:10.1002/mame.202100727 (2022).
- 85 Ding, X., Liu, J. & Harris, T. A. L. A review of the operating limits in slot die coating processes. *AIChE Journal* **62**, 2508-2524, doi:10.1002/aic.15268 (2016).
- 86 Röhrl, M. *et al.* Shear orientation of nematic phases of clay nanosheets: processing of barrier coatings. *Journal of Coatings Technology and Research*, doi:10.1007/s11998-021-00535-4
- 87 Husarova, L. *et al.* Identification of important abiotic and biotic factors in the biodegradation of poly(l-lactic acid). *Int J Biol Macromol* **71**, 155-162, doi:10.1016/j.ijbiomac.2014.04.050 (2014).
- 88 Ben Halima, N. Poly(vinyl alcohol): review of its promising applications and insights into biodegradation. *RSC Advances* **6**, 39823-39832, doi:10.1039/c6ra05742j (2016).

## 6. Results

### 6.1. High Barrier Nanocomposite Film with Accelerated Biodegradation by Clay Swelling Induced Fragmentation

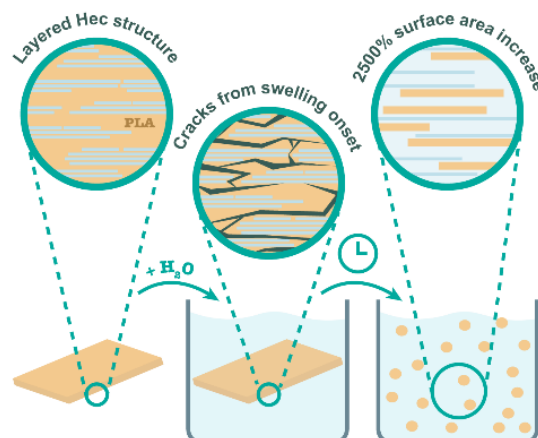
Renee L. Timmins<sup>‡</sup>, Anil Kumar<sup>‡</sup>, Maximilian Röhrle, Karel Havlíček, Seema Agarwal\*, and Josef Breu\*

<sup>‡</sup>these authors contributed equally to this work

\*corresponding author(s): josef.breu@uni-bayreuth.de, seema.agarwal@uni-bayreuth.de

Published in: *Macromolecular Materials and Engineering* **2021**, 2100727

Reprinted with permission, Copyright (2021) Wiley-VCH



Individual contribution:

Prof. Dr. Josef Breu, Prof. Dr. Seema Agarwal, and I conceptualized the paper. I developed the formulation, optimized processing, prepared the film, and conducted the XRD study. Anil Kumar performed the biodegradation testing and accompanying analysis. Karel Havlíček also performed biodegradation testing. Maximilian Röhrle performed barrier testing. The paper was written by Prof. Dr. Josef Breu, Prof. Dr. Seema Agarwal, and myself with editing and proofreading from all authors.

# High Barrier Nanocomposite Film with Accelerated Biodegradation by Clay Swelling Induced Fragmentation

Renee L. Timmins, Anil Kumar, Maximilian Röhr, Karel Havlíček, Seema Agarwal,\* and Josef Breu\*

Conventional biodegradable polymers such as poly(lactic acid) (PLA) are an attractive alternative to replace traditional nondegradable food packaging films which plague the environment. However, PLA has shown to not be degradable in some environmentally relevant conditions, including within the freshwater systems. Additionally, PLA suffers from very poor barrier properties, which could result in food spoilage. Compositing with clay has been used to improve barrier properties according to tortuous path theory. Here a synthetic, large aspect ratio Na-Hectorite is used that may be utterly delaminated in an organic solvent and composited with PLA by modification with 18-crown-6 (18C6Hec), yielding a castable, homogeneous nematic suspension. Upon drying, thermodynamics drive the suspension toward segregation into sublayers of PLA and partially restacked 18C6Hec *in situ*. This unique self-assembled nanostructure combines the best of two worlds: The aspect ratio remains high and results in a 99.3% reduction in oxygen permeability. Additionally, the film shows surprisingly high resistance to swelling at elevated humidity, but once soaked in water, clay swelling is triggered, which fragments the film and drastically increases the surface area by 2500%. Accelerated degradation is observed under controlled enzymatic conditions and in an environmentally relevant wastewater medium during CO<sub>2</sub> evolution testing.

to prevent food waste as goods are transported globally. However, with 8 million tons of plastic waste entering the ocean each year, an increasing effort is being made to replace those plastics that would persist in the environment when improperly disposed with degradable alternatives.<sup>[1-3]</sup> After all, mitigating potentially dangerous effects from micro- and nanoplastics in our ecosystem begins with material design and waste management.<sup>[4]</sup> Poly(lactic acid) (PLA) is a frontrunner for this position due to several favorable properties, including availability and low cost, zero toxicity, high mechanical strength, ease of production, and ability to derive its raw material from renewable (bio-)resources.<sup>[5,6]</sup> While PLA meets ASTM standards for compost degradation, numerous reports have shown it to have poor degradation in soil, seawater, and freshwater.<sup>[7-9]</sup> Therefore, PLA offers a limited solution to the accidental release of plastic into our water systems whose plastic litter is disproportionately composed of packaging.<sup>[10,11]</sup> Nevertheless, PLA is a weak competitor to typical packaging

materials in terms of gas barrier properties, which are necessary to prevent spoilage and extend the shelf-life of packaged food.<sup>[12]</sup>

Various attempts to accelerate PLA degradation include optimizing its microbial environment or by blending it with other more degradable or water-soluble polymers,<sup>[13-16]</sup> which increases surface area but ultimately worsens mechanical properties.<sup>[17-19]</sup> The incorporation of clay filler for this purpose stands out for its practicality and effectiveness as such layered silicate nanocomposites can provide additional improvement in the mechanical, barrier, and thermal properties.<sup>[20-23]</sup> Since natural clays are hydrophilic, modification of the clay surface via ion exchange with alkyl ammonium compounds is necessary to disperse clay into degradable, hydrophobic polyesters. While this helps disaggregation during melt compounding, delamination into single nanosheets of maximized aspect ratio is difficult, if at all possible. For these PLA/clay nanocomposites, an increase in biodegradation rate and reduction of lag time compared to PLA has been observed and is usually attributed to exposure to terminal hydroxylated edge groups.<sup>[22,24,25]</sup>

In separate reports, clay nanocomposites have also been used to address the poor barrier properties of degradable polymers for food packaging. Silicate platelets act as an impermeable

## 1. Introduction

Single-use food packaging has become an essential part of our lifestyle, for not only consumer convenience and hygiene but also

R. L. Timmins, A. Kumar, M. Röhr, S. Agarwal, J. Breu  
Bavarian Polymer Institute and Department of Chemistry  
University of Bayreuth  
Bayreuth 95447, Germany  
E-mail: agarwal@uni-bayreuth.de; josef.breu@uni-bayreuth.de  
K. Havlíček  
Institute for Nanomaterials  
Advanced Technology and Innovation  
Technical University of Liberec  
Studentská 2, Liberec 461 17, Czech Republic

 The ORCID identification number(s) for the author(s) of this article can be found under <https://doi.org/10.1002/mame.202100727>

© 2021 The Authors. Macromolecular Materials and Engineering published by Wiley-VCH GmbH. This is an open access article under the terms of the Creative Commons Attribution License, which permits use, distribution and reproduction in any medium, provided the original work is properly cited.

DOI: 10.1002/mame.202100727

barrier to diffusion, creating a tortuous path for gas molecules, including oxygen and water vapor. Previously in our group, synthetic sodium fluorohectorite (NaHec,  $[\text{Na}_{0.5}]^{\text{inter}}[\text{Mg}_{2.5}\text{Li}_{0.5}]^{\text{oct}}[\text{Si}_4]^{\text{tet}}\text{O}_{10}\text{F}_2$ ) clay has been used to create nanocomposite barrier coatings with various polymer matrices.<sup>[26–28]</sup> NaHec undergoes the rare phenomenon of repulsive osmotic delamination, which is a thermodynamically allowed process, resulting in gentle and quantitative delamination into a nematic liquid crystalline suspension. With an aspect ratio of 20000, rotation even in very dilute suspensions (<1 vol%) is sterically hindered.<sup>[29]</sup> This huge aspect ratio is preserved upon solvent evaporation, creating such an elongated diffusion pathway that with a 1.4  $\mu\text{m}$  thick glycol chitosan-intercalated NaHec coating, we have shown that the PLA oxygen barrier could outperform polyethylene terephthalate (PET) by a factor of 180 even at 75% relative humidity (RH).<sup>[26]</sup> However, similar improvements in barrier properties are challenging to achieve for a neat PLA nanocomposite due to the incompatibility of hydrophilic clays and hydrophobic polyesters, which prevents solution blending of PLA with uniform, 1 nm thick clay monolayers. Other compositing methods like melt blending trigger reaggregation or fail to assure quantitative delamination. In a study by Ray et al. where organically modified montmorillonite (OMMT) was combined with PLA via melt extrusion, an enhancement in the degradation rate of the nanocomposite in compost is observed, yet  $\text{O}_2$  permeability is hardly improved from 200  $\text{mL mm m}^{-2} \text{ day}^{-1} \text{ MPa}^{-1}$  (equivalent to 20265  $\text{cm}^3 \mu\text{m m}^{-2} \text{ day}^{-1} \text{ atm}^{-1}$ ) for neat PLA to 177  $\text{mL mm m}^{-2} \text{ day}^{-1} \text{ MPa}^{-1}$  for PLA nanocomposite. The poor barrier could be attributed to the mediocre anisotropy (and low aspect ratio of 16 for the silicate filler), creating an insufficient tortuous path to gas permeates.<sup>[23]</sup> Simply dispersing clay via melt blending into PLA to increase surface area and improve degradation without regard for microstructure misses huge potential to synergistically improve barrier properties by orders of magnitude. In our recent work, we showed a balance of high degradability and good barrier properties by preparing a PLA-layered silicate composite in which PLA and layered silicate layers alternate. This was prepared by filtering layered silicate solution through an electrospun PLA porous membrane and hot-pressing several of such layers together.<sup>[30]</sup> It would be interesting if such macro phase-separated composites could be prepared in a simple way.

Our group also recently published a method which for the first time, extends the rare phenomenon of osmotic delamination within NaHec into organic, aprotic solvents.<sup>[31]</sup> Previously limited to aqueous suspensions, osmotic delamination of NaHec was obtained spontaneously in various organic solvents, including *N*-methylformamide (NMF) by the simple addition of crown ethers. The complexation of interlayer sodium with, for example, 18-crown-6 (18C6) renders the hectorite (18C6Hec) surface more hydrophobic. This complex enables repulsive osmotic delamination where adjacent clay layers in the nematic liquid crystalline state are separated by distances large enough to be accessible for polyester macromolecules. In this work, NMF is used to create a stable, homogeneous suspension of PLA and osmotically delaminated 18C6Hec to cast films that showed phase-separated morphology by thermodynamically driven segregation into PLA domains and 18C6Hec tactoids in-situ during film preparation. The film shows surprisingly high resistance to swelling at elevated humidity, but clay swelling is triggered once soaked in water, frag-

menting the film and drastically increasing the surface area by 2500%, which might be favorable for degradation once discarded. This unique self-assembled nanostructure showed impressive barrier values competitive with state-of-the-art high-performance packaging films while also biodegrading faster than pure material in wastewater sludge (Figure 1). The details of the preparation procedure, structural characterization, and degradation behavior of nanocomposite PLA films are reported in the present work.

## 2. Results and Discussion

NaHec and 18C6 can simply be dispersed in a PLA/NMF solution, creating a homogenous and nematic phase as evidenced by the presence of a basal series in the small-angle X-ray scattering (SAXS) trace (Figure 2a). As expected for nanosheets,  $q$  values scale with  $q^{-2}$ .<sup>[32]</sup> Birefringence of the solution was observed under cross-polarized light (Figure 2a: inset), which further confirms long-range order of the liquid-crystal phase. Self-standing nanocomposite films of  $\approx 60 \mu\text{m}$  thickness were obtained by consecutively casting eight layers of this suspension via slot die coating on top of each other with intermittent drying. The substrate table was set to 60 °C to prevent the precipitation of PLA (7.2 wt% of blend solution), which is only soluble at elevated temperatures. Through the use of slot die coating, precise and uniform wet layers of suspension can be deposited onto a PET substrate from a slotted die head. Slot die coating is an industrially scalable coating method that can be particularly useful in making nanocomposite layers due to the shear-induced alignment of nanosheets within viscous solutions during processing. Resulting nanocomposite layers lack folding or crumbling defects of the nanosheets and instead present a perfect texture with all nanosheets aligned isotopically in the plane of the film.<sup>[33]</sup> The thickness of the wet layer can be tuned by machine parameters, and the dry layer thickness can be tuned by adjustment of suspension solid content (PLA + clay). Each wet layer is partially dried before the subsequent layer is coated on top, with partial solvation of the previous layer by the wet layer ensuring adhesion. Here, eight layers were deemed an optimal balance of the solution solid content and drying time of each layer.

Upon evaporation of the solvent from the coated 18C6Hec/PLA layer, the confinement of the polymer becomes ever more severe, and the concomitant entropy losses will eventually thermodynamically drive segregation of polymer and 18C6Hec nanosheets. Yet, segregation is severely hindered as mobility becomes increasingly restricted with the formation of the tortuous path. The resulting stratified nanostructure (Figure 2b) contains many randomly alternating PLA domains separating restacked 18C6Hec tactoids (i.e., 1D crystals) generated in-situ via self-assembly. According to transmission electron microscopy (TEM) micrographs (Figure 2c) obtained of the sample cross-sections prepared by cryo-ion-slicing, the segregated 18C6Hec tactoids typically have a thickness of 120 nm. Consequently, a film of 60  $\mu\text{m}$  would be comprised of some 118 tactoids separated by PLA domains of typically 414 nm thickness. The partial reaggregation creates tactoids with an aspect ratio that is reduced by a factor equal to the number of layers in the stack. Since the aspect ratio of a single nanosheet of Hec is as large as 20 000, a stack of 120 clay layers still has an appreciable aspect ratio of 166 without even considering extension in the

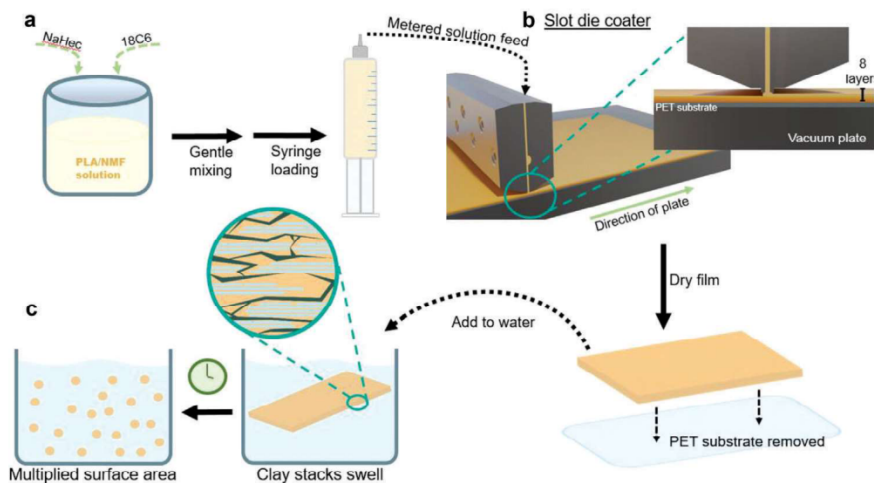


**Figure 1.** Schematic illustrating fabrication and fragmentation of PLA/18C6Hec films. a) Mixing of NaHec and 18C6 into a PLA/NMF solution. b) Suspension is loaded into a syringe which is then fed into the slot die coater where eight wet layers are coated successively onto a PET substrate. Once the film is dried, the PET substrate is removed. c) When film is immersed into water, clay swelling exerts stress-triggered fragmentation.

width of the tactoids due to the offset stacking of nanosheets (band-like aggregates). This is much larger than the aspect ratio of typical fundamental particles of montmorillonite (10–15). According to Cussler, the barrier improvement factor scales with the square of the aspect ratio.<sup>[34]</sup> The potential for barrier improvement (ratio of the permeability of the neat polymer film to the permeability of the nanocomposite) is thus expected to nevertheless be immense for the hectorite filler despite partial reaggregation. Using the aspect ratio of 166, a theoretical barrier improvement factor of 97 is expected (Equation S1, Supporting Information).

XRD patterns from the nanocomposite films taken in reflection mode show a 001 series (Figure S1, Supporting Information) with a spacing of 17.7 Å ( $2\theta = 4.99^\circ$ ), indicating that 18C6 remain complexed to the hectorite sheets during film production and that within the hectorite tactoids, there is an absence of PLA. The previously reported d-spacing of a pure 18C6Hec is even larger (18.3 Å),<sup>[31]</sup> while without a complexed 18C6, NaHec has a d-spacing of 12.5 Å.<sup>[35]</sup> Although pure NaHec is sensitive to humidity, the complexation by 18C6 reduces hydrophilicity, thus reducing its ability to swell in the presence of water vapor.<sup>[31]</sup> As water acts as a plasticizer, swelling will increase segment mobility and consequently permeability. Therefore, the moisture sensitivity of 18C6Hec stacks in the PLA nanocomposite was systematically evaluated by monitoring changes in d-spacing as a function of RH (Figure 2d). After equilibration at 90% RH, the d-spacing increased by as little as 8% relative to dry conditions, indicating minimal swelling of clay layers. Previous studies using unmodified NaHec/polyvinylpyrrolidone (PVP) nanocomposite reported that the d-spacing increased approximately 80% after exposure to the same increase in humidity.<sup>[27]</sup> This suggests little sensitivity of the PLA/18C6Hec barrier to elevated RH. At 95% RH, however, a steeper increase in d-spacing indicated the onset of more significant layer swelling.

The resistance to swelling at high humidity is indeed reflected practically in the gas barrier properties of the nanocomposite

film. Oxygen transmission rates (OTR) are of prime importance when considering films as a food packaging material. While this value is dependent on film thickness, oxygen permeability (OP) is normalized for film thickness and therefore allows for comparison between different films. OP was measured at 65% RH, as per the ISO 14663-2 standard (Figure 3a). Neat PLA film had an OP of  $17775 \text{ cm}^3 \mu\text{m}^{-2} \text{ day}^{-1} \text{ atm}^{-1}$ , which was reduced by 99.3% to  $124 \text{ cm}^3 \mu\text{m}^{-2} \text{ day}^{-1} \text{ atm}^{-1}$  by compounding with 18C6Hec. This OP outperforms reported values for the common packaging material PET and is even competitive with high-performance poly(vinylidene dichloride) (PVDC).<sup>[36]</sup> OTRs are reported in Table S1 (Supporting Information). Despite the partial restacking of 18C6Hec, the diffusion path created is nevertheless tortuous due to long, thin band-like clay structures extending along the plane of the film. This particular tactoid morphology creates impermeable walls that extend farther in the direction of the film than would be possible with individual clay sheets. Accordingly, the experimentally observed barrier improvement factor (143) is even higher than theoretical calculations.

Although this film has a tolerance for water vapor, quite surprisingly, it was found to promptly fragment when immersing it into an aqueous solution of proteinase K enzyme for degradation testing. Whenever brought into contact with water, the film disintegrated into small pieces within an hour, multiplying the surface area accessible for degradation (Figure S2, Supporting Information). According to Brunauer–Emmett–Teller (BET) analysis, the surface area of the nanocomposite after sitting in water for 24 h without external forces is  $0.372 \text{ m}^2 \text{ g}^{-1}$ , which is more than a 2500% increase from the original surface area of  $0.014 \text{ m}^2 \text{ g}^{-1}$ . The surface area has been identified as an important factor for rapid biodegradation of PLA,<sup>[37]</sup> thus the fragmentation of the PLA/18C6Hec film resulting in a dramatic increase in the surface area could be contributing to its accelerated enzymatic degradation (Figure 3b). After just 5 d, the PLA/18C6Hec film reached complete degradation at approximately 90% weight loss, con-

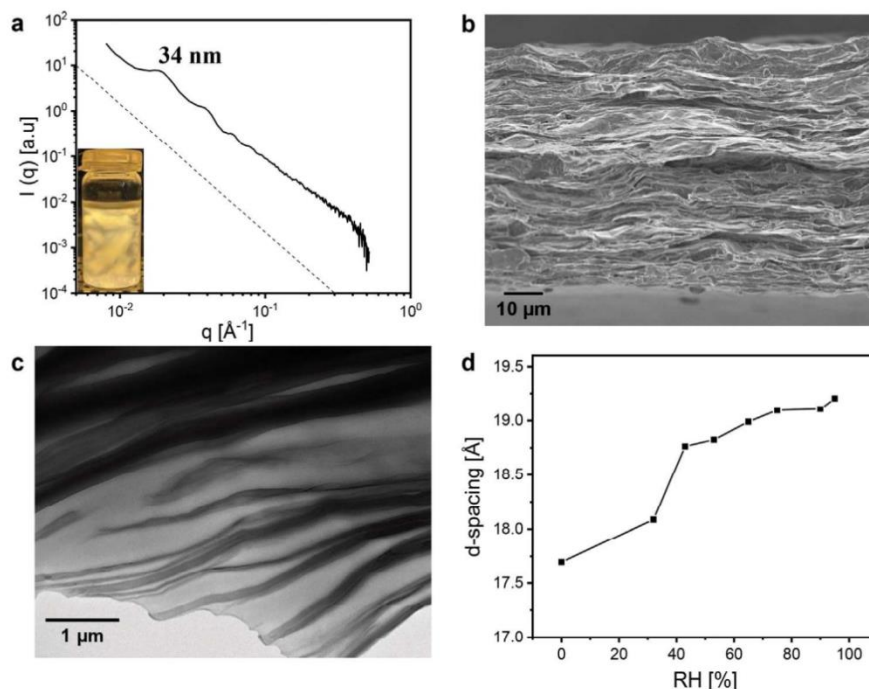


**Figure 2.** Characterization of nematic suspension and self-standing film. a) 1D SAXS pattern of concentrated PLA/18C6Hec suspension in NMF. Dotted line shows  $q^{-2}$  scale. Inset: PLA/18C6Hec suspension in NMF displaying birefringence under cross-polarized light. b) SEM image of PLA/18C6Hec film cross-section. c) TEM image of PLA/18C6Hec film cross-section. d) Swelling behavior of PLA/18C6Hec film observed from  $d_{001}$  peaks on XRD traces at an increasing relative humidity.

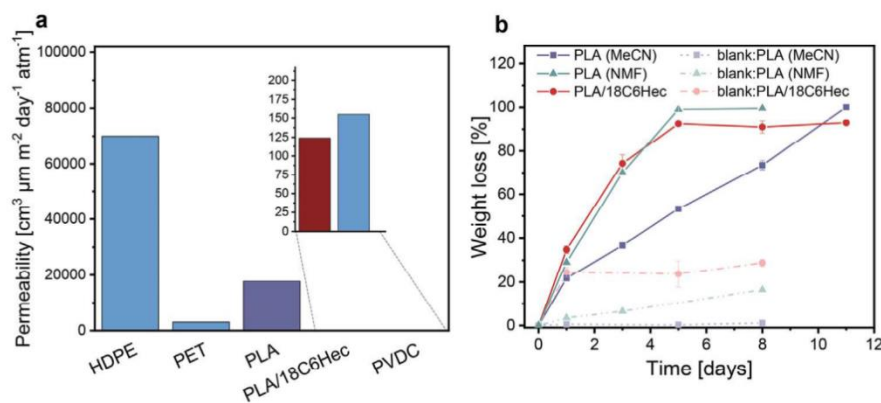


**Figure 3.** Permeability and degradation studies on PLA/18C6Hec film. a) Oxygen permeability at 65% RH and 23 °C for PLA/18C6 nanocomposite film compared to PLA and other films reported in ref. [31]. b) Weight loss measured from proteinase K enzymatic degradation. Blank trial refers to test conducted using buffer solution without enzyme.\* Permeability measured at 50% RH and 23 °C.

sidering 16 wt% of the film is hectorite clay. This is more than twice as fast as the neat PLA film that was cast from acetonitrile (MeCN), which took 11 d to reach complete degradation under similar conditions.

It is important to note that the weight loss curve of the PLA/18C6Hec film is very similar to the weight loss curve of PLA that was cast from NMF. PLA cast from NMF differs from PLA cast from MeCN in two ways. First, PLA cast from NMF

has a significantly reduced molecular weight compared to PLA cast from MeCN. This difference is apparent when comparing the day 0 molecular weight distributions from gel permeation chromatography (GPC) of PLA cast from MeCN and the PLA in the nanocomposite cast from NMF in Figure 4. The premature molecular weight shift is attributed to the high-temperature dissolution of PLA into NMF causing chain cleavage. Low initial PLA molecular weight is an additional factor contributing

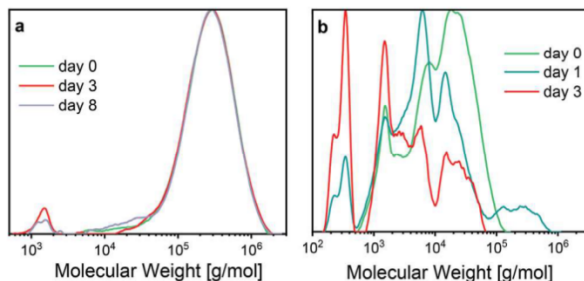


**Figure 4.** Gel-permeation chromatography traces of a) PLA (cast from MeCN) and b) PLA/18C6Hec films after enzymatic degradation for different days.

to accelerated degradation, according to the systematic study by Husárová et al.<sup>[37]</sup> Second, this low molecular weight PLA, as a result of chain cleavage, is very mechanically weak without the hectorite reinforcement and therefore does not form a self-standing film that could be peeled off its PET substrate. The PLA cast from NMF used in the enzymatic degradation test was in the form of small, flakey fragments, i.e., high surface area. Since PLA cast from NMF has both degradation accelerating factors as the PLA/18C6Hec nanocomposite (low initial molecular weight and high surface area), it would be expected that these two materials have a similar degradation rate. The addition of the clay to the low molecular weight PLA provides mechanical support and ability to form a self-standing film without losing the beneficial characteristics for rapid degradation. Due to the extremely poor structural integrity of PLA cast from NMF, a comparison between PLA cast from MeCN, which is much closer to a realistic commercial film, is perhaps more relevant.

The GPC traces of enzymatic degradation samples indicate a surface erosion mechanism of PLA cast from MeCN by showing minimal changes in molecular weight after 8 d (Figure 4). In contrast, we can confirm the further chain cleavage in the PLA/18C6Hec sample by the significant transition to lower molecular weight species appearing after just 3 d, indicating a change in mechanism to bulk degradation for the nanocomposite film. Although the PLA/18C6Hec sample had preexisting molecular weight shifts left, even the highest molecular weight species are nevertheless drastically reduced only after exposure to enzyme solution.

Scanning electron microscopy (SEM) images (Figure 5) taken from the PLA (MeCN) and PLA/18C6Hec degradation samples throughout the test show increasing surface roughness of PLA from initial to day 8, corroborating surface erosion as the primary mechanism. Contrary to PLA, the initially smooth surface of the PLA/18C6Hec nanocomposite has fallen apart into thin, open layers of clay and PLA after just 3 d. By day 8, the return of a smooth surface suggests primarily only clay platelets remain.

Degradation of PLA in the nanocomposite is further confirmed by Raman spectroscopy of degraded samples showing the disappearance of the characteristic  $1774\text{ cm}^{-1}$  PLA ester peak after 5 d (Figure S3, Supporting Information). Additionally, both differential scanning calorimetry (DSC) scans and  $^1\text{H}$  NMR could no longer detect the presence of PLA in the nanocomposite

remnants after 5 d as well (Table S2 and Figure S4, Supporting Information).

To follow the degradation of the PLA/18C6Hec films under more environmentally relevant conditions,  $\text{CO}_2$  evolution tests were performed with a respirometer according to DIN 14851 in an activated sludge wastewater medium. The kinetics of biodegradation were recorded and compared to a neat PLA film cast from MeCN since this is the more relevant comparison. Cumulative  $\text{CO}_2$  production was converted into percent biodegradation (Figure 6a). The PLA film showed minimal biodegradation (0.4%) at the end of the 45 d, while the PLA/18C6Hec nanocomposite film had significantly accelerated biodegradation (15%). Measuring only the 18C6, added as molecular complexing ligand, revealed that approximately 4% of it is biodegraded within the testing period, dismissing the possibility that this species is responsible for most of the  $\text{CO}_2$  release. After the initial phase of strongly accelerated biodegradation for the nanocomposite sample, the biodegradation continues after day 15 at a constant rate of 0.09 % biodegradation per day, which is more than the total PLA biodegradation rate in 45 d. The slowed rate of biodegradation for the nanocomposite may be due to increased crystalline fractions present after the initial rapid consumption of amorphous regions (Table S3, Supporting Information). At the end of the testing period, all that was left of the PLA/18C6Hec film was tiny fragments, while the PLA film remained visually unchanged (Figure 6b). The fragmentation, moreover, prevented any lag phase, as would typically be observed in the biodegradation of PLA and PLA nanocomposites.<sup>[38]</sup> GPC traces of the PLA sample (Figure S5, Supporting Information) show little change in molecular weight distribution postdegradation testing. Whereas significant shifts to lower molecular weights were observed postdegradation testing for the PLA/18C6Hec film, demonstrating that our nanocomposite film not only fragments in aqueous mediums but also undergoes molecular chain cleavage and accelerated biodegradation. Similar to the enzymatic degradation testing, neat PLA degrades through surface erosion, whereas the nanocomposite film undergoes a bulk biodegradation mechanism facilitated by increased surface area from the fragmentation of the film. These results were repeatable when using wastewater from treatment plants in Bayreuth, Germany, or Liberec, Czech Republic.

Mechanical testing reveals that the PLA/18C6Hec film unfortunately suffers from embrittlement due to the use of low molecular weight PLA and the incorporation of platy clay filler (Table S4, Supporting Information), as is commonly observed in similar systems.<sup>[39–41]</sup> The elastic modulus of the nanocomposite is comparable to the pure PLA (1.14 and 1.43 GPa, respectively) however the elongation at break is significantly decreased from 9.7% for pure PLLA to 3.5% for PLA/18C6Hec. Such a decrease in elongation is to be expected from an unplasticized nanocomposite containing high filler content (16 wt%). The improvement of the mechanical properties through the use of additives or blending will be the subject of future investigations.

### 3. Conclusion

In summary, our nanocomposite film addressed two major challenges facing the development of high-performance degradable polymers films: improvement of barrier properties to levels

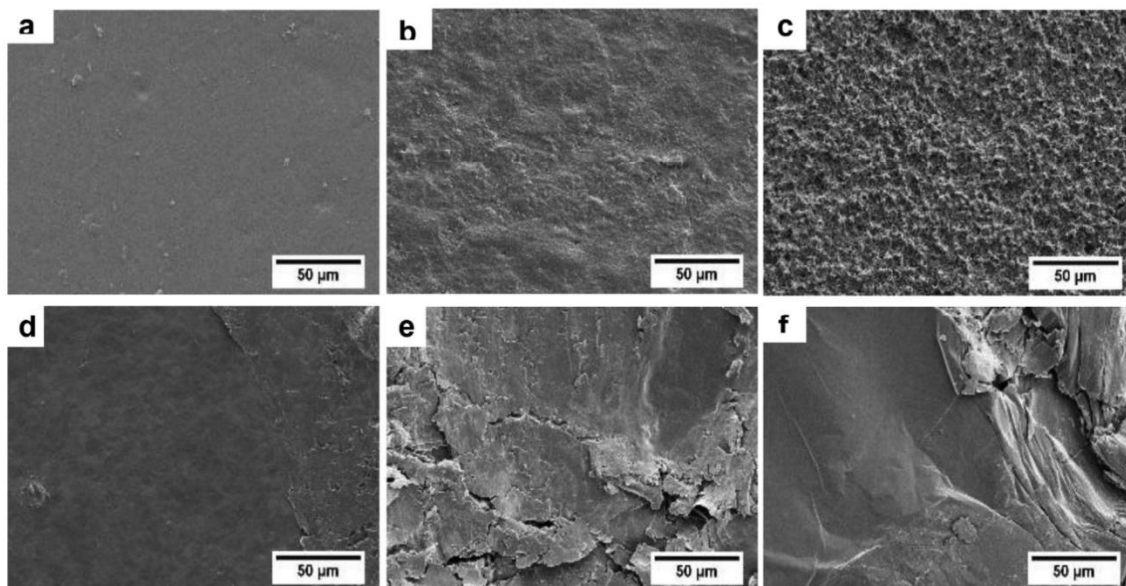


**Figure 5.** SEM images of films in enzymatic degradation test a–c) for PLA. a) Day 0 (initial), b) day 3, c) day 8. And d–f) for PLA/18C6Hec. d) Day 0 (initial), e) day 3, f) day 8.

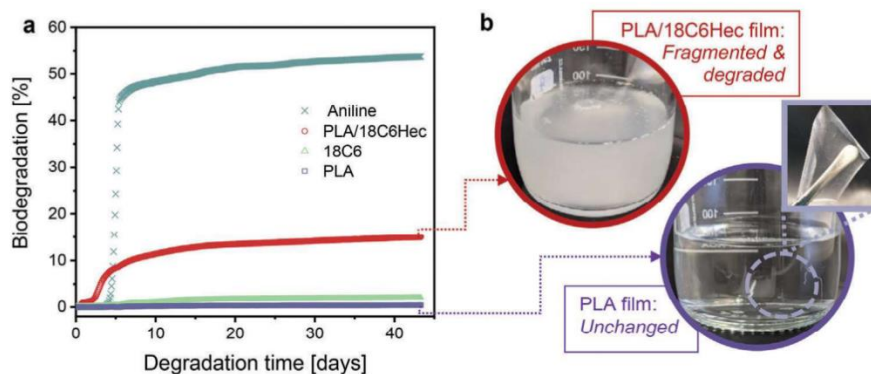


**Figure 6.** a) Percent biodegradation determined from  $\text{CO}_2$  production for degradation of PLA/18C6Hec, 18C6, and PLA (cast from MeCN) in activated sludge medium. Aniline is used as a positive standard. b) Pictures of PLA/18C6Hec and PLA films at the end of degradation testing in activated sludge.

competitive with high-performance materials and enhancement of the ability of PLA to degrade rapidly in wastewater. The water-triggered fragmentation due to the swelling of clay tactoids within the film presents a practical way to optimize the design of current degradable polymers to better suit commercial needs. Although the mechanical properties of this film are not strong enough for practical use as a self-standing material, it is instead highly promising for use as a biodegradable barrier coating. Also, the future work will include the extension of the method presented here into other degradable polymers, conducting degradation testing in different environmentally relevant mediums such as compost, and the avoidance of 18C6.

#### 4. Experimental Section

**Material:** Sodium fluorohectorite  $[\text{Na}_{0.5}]^{\text{inter}}[\text{Mg}_{2.5}\text{Li}_{0.5}]^{\text{oct}}[\text{Si}_4]^{\text{tet}}\text{O}_{10}\text{F}_2$  (Hec) was prepared by employing a synthesis procedure from the melt, as previously reported in the literature.<sup>[42]</sup> The material features a cation exchange capacity of  $1.27 \text{ mmol g}^{-1}$ . Ingeo 4043D from Natureworks was used as poly(lactic acid) (PLA). 18-crown-6 (18C6) was provided by abcr with 99% purity. N-methylformamide (NMF, 99%, Alfa Aesar) and acetonitrile (MeCN, 99%, Alfa Aesar) were used as solvent. All reagents were used as received. The polyethylene terephthalate (PET) substrate ( $36 \mu\text{m}$ ) was purchased from Bleher Folientechnik GmbH (Germany).

**Film Fabrication:** 5.2 g of PLA was dissolved in NMF (64 g) at  $100^\circ\text{C}$  in a covered round bottom flask until a clear solution was reached. Once the PLA solution was cooled to  $50^\circ\text{C}$ , 1.3 g of each NaHec and 18C6 was

added and mixed for at least one week at room temperature to ensure complete homogenization. Prior to coating, the solution was heated to 60 °C to reduce viscosity during syringe pump loading.

Films were prepared using a TSE Table Coater with a 1-Layer Slot Die 300 mm, AAA (TSE Troller AG, Switzerland). The coating width and wet layer thickness were set to 0.21 m and 88  $\mu\text{m}$ , respectively. The pump flow rate (1.5 mL  $\text{min}^{-1}$ ) and the table speed (0.08 m  $\text{min}^{-1}$ ) were adjusted accordingly. The table temperature was set to 60 °C. A PET foil was used as the base substrate onto which nanocomposite layers would be deposited. The coating gap was set to 168  $\mu\text{m}$  (36  $\mu\text{m}$  PET + 1.5  $\times$  88  $\mu\text{m}$  coating height). After each layer, the foil was left to dry for 45 min, and the coating height was increased by 10  $\mu\text{m}$ . Once eight layers were deposited, the foil was transferred to a vacuum oven at 70 °C and  $10^{-3}$  bar. After the removal of the remaining NMF, the PLA nanocomposite film was carefully peeled off the PET substrate.

For the PLA film sample cast from acetonitrile, PLA was dissolved in acetonitrile (10 wt%) at 60 °C until a clear solution was obtained. For the PLA film sample cast from NMF, PLA was dissolved in NMF (10 wt%) at 100 °C until a clear solution was obtained. Once cooled to room temperature, 18C6 was added (2 wt%) to the solution and mixed overnight. A self-standing film was produced from both of these solutions in the same manner as reported for the PLA nanocomposite, then dried for 4 d at 70 °C.

**Enzymatic Degradation:** Film samples with (approximately 2 cm  $\times$  1 cm) a weight of 40 mg were placed in a glass vial with 5 mL of 0.05 M Tris buffer solution (pH = 8.6) containing 0.2 mg  $\text{mL}^{-1}$  of Proteinase K (GeneON, Germany) and 0.2 mg  $\text{mL}^{-1}$  of sodium azide, as per a previously reported method.<sup>43</sup> The vials were then placed in incubation at 37 °C. The buffer/enzyme system was changed every 24 h to retain enzymatic activity. This was done by centrifugation of the solution and removing clear supernatant. Three samples for each experiment were taken at each time interval and were washed with distilled water three times. Collected samples were vacuum dried at room temperature for one week before being subjected to analysis. Control for each film was performed in the same medium without an enzyme.

**CO<sub>2</sub> Evolution Degradation Testing:** DIN 14851:2019 was referred to for carrying out the biodegradation test using activated sludge, after the end of the nitrification process as obtained from the wastewater treatment plant at Bayreuth, Germany. Approximately 75 mg of the film was added to 95 mL of standard medium and 5 mL of supernatant from activated sludge. Aniline was used as the positive sample. The mixture was dosed into 250 mL test bottle, and testing immediately began. The testing period was 45 d. Activated sludge (without any organic substrate) in the same concentration was used as a control. The Micro-Oxymax respirometer equipped with a paramagnetic oxygen sensor and infra-red CO<sub>2</sub> sensor (Columbus Instruments International, USA) was used for the measurements.

**Characterization: Small-Angle X-Ray Scattering (SAXS):** The small-angle X-ray "Ganesha AIR" (SAXSLAB, Denmark) equipment was used to record SAXS patterns. It is equipped with a rotating anode X-ray source (copper, MicoMax 007HF, Rigaku Corporation, Japan). The data was recorded by a position-sensitive detector (PILATUS 300K, Dectris). To cover the range of scattering vectors between 0.006 and 0.5  $\text{\AA}^{-1}$ , different detector positions were used. Prior to the measurements, the PLA/Hec/18C6 suspension was centrifuged for 1 h (10 000 rpm) to obtain a gel to enhance sensitivity. The measurement of the suspension was performed in 1 mm glass capillaries (Hilgenberg, Germany) at room temperature.

**Characterization: Scanning Electron Microscopy (SEM):** SEM images of the cross-section of the film were observed using a ZEISS LEO 1530 (Carl Zeiss AG, Germany) operating at 3 kV.

**Characterization: Transmission Electron Microscopy (TEM):** The PLA/Hec/18C6 nanocomposite film was thinly cut with an Ion Slicer EM-09100IS (JEOL GmbH, Germany). TEM images were then recorded with a JEM-2200FS (JEOL GmbH, Germany) microscope.

**Characterization: X-Ray Diffraction (XRD):** XRD patterns of the films were recorded using nickel filtered Cu-K $\alpha$  radiation ( $\lambda = 1.54187 \text{ \AA}$ ) in Bragg-Brentano-geometry on an Empyrean diffractometer (PANalytical B.V., the Netherlands) equipped with a Pixel detector. Prior to measure-

ment at 0% RH, a film sample was dried at 70 °C for one week in a vacuum oven ( $10^{-3}$  bar). For the measurements at varying RH, samples were equilibrated for at least one week either above a concentrated salt solution (MgCl<sub>2</sub> 6H<sub>2</sub>O (32% RH), K<sub>2</sub>CO<sub>3</sub> (43% RH), Mg(NO<sub>3</sub>)<sub>2</sub> (53% RH)) or in a Memmert HCP105 humidity chamber (Mettler GmBH + Co. KG, Germany) at 25 °C (65, 75, 90, and 95% RH).

**Characterization: Oxygen Transmission Rates (OTR):** OTRs were determined on a Mocon OX-TRAN 2/21 system (Mocon Inc., USA) with a lower detection limit of 0.05  $\text{cm}^3 \text{ m}^{-2} \text{ day}^{-1} \text{ atm}^{-1}$ . The measurements were performed at 23 °C and 65 % RH. A mixture of 98% nitrogen and 2% hydrogen was used as the carrier gas and pure oxygen as permeant (>99.95 %, Linde Sauerstoff 3.5). Film thickness was 59  $\mu\text{m}$  determined using a high-accuracy Digimatic micrometer (Mitutoyo, Japan) with a measuring range of 0–25 mm and a resolution of 0.0001 mm.

**Characterization: Brunauer–Emmet–Teller Surface Area Analysis (BET):** The surface area was measured with a Quantachrome Autosorb-1 using Kr as the adsorbate at 70 °K. The isotherm was evaluated using the BET method.

**Characterization: Gel Permeation Chromatography (GPC):** GPC traces were obtained using chloroform as the eluent at a flow rate of 0.5 mL  $\text{min}^{-1}$  at room temperature. A precolumn PSS SDV (particle size 5  $\mu\text{m}$ ) and a column PSS SDV XL linear (particle size 5  $\mu\text{m}$ ) calibrated against polystyrene standards (PSS) were used with a PSS SECcurity RI detector. The GPC data was analyzed by the software PSS WinGPC Unity, Build 1321.

**Characterization: Raman Spectroscopy:** Raman spectra were obtained with the WITec alpha 300 RA+ (Germany) system using a 532 nm laser line and 50 scans. The laser was focused using the maximum 10X magnification objective of the Raman microscope.

**Characterization: <sup>1</sup>H NMR:** NMR spectra were recorded on a Bruker Avance 300 NMR system operating at 300 MHz frequency at room temperature using deuterated chloroform (CDCl<sub>3</sub>) as a solvent. Chemical shifts ( $\delta$ ) are indicated in parts per million (ppm) with respect to residual solvent signals.

**Characterization: Differential Scanning Calorimetry (DSC):** DSC scans were obtained with a DSC 204 F1 Phoenix system (Netzsch) with a heating rate of 10 K  $\text{min}^{-1}$  under an N<sub>2</sub> atmosphere. The first heating cycle is used for the determination of melting peaks ( $T_m$ ), and the second heating cycle is used for the determination of glass transition ( $T_g$ ).

**Characterization: Mechanical Testing:** Stress–strain tests were performed with a tensile instrument (Zwick/Roell, BT1-FR0.5TN.D14). The samples for the tensile measurement were cut to the size of 3 mm  $\times$  30 mm for a pristine effective tensile length of 10 mm. The test was performed with crosshead speed 5 mm  $\text{min}^{-1}$  at room temperature for at least ten measurements. The slope of the linear region of the stress-strain curves was used to determine the elasticity modulus.

## Supporting Information

Supporting Information is available from the Wiley Online Library or from the author.

## Acknowledgements

R.L.T. and A.K. contributed equally to this work. The authors thank Florian Puchtl for synthesizing the synthetic hectorite, Marco Schwarzmann for preparing the samples via ion-slicing and recording the TEM and SEM images, Michael Thelen for BET measurements, Lothar Benker for Raman spectroscopy measurements, and Elmar Sehl for tensile measurements. The authors also thank Olena Khoruzhenko for the graphic design. The authors appreciate the support of the KeyLab for Optical and Electron Microscopy of the Bavarian Polymer Institute. This work was supported by the German Science Foundation (DFG) within the collaborative research projects SFB 840 and SFB 1357.

Open access funding enabled and organized by Projekt DEAL.

**Conflict of Interest**

The authors declare no conflict of interest.

**Data Availability Statement**

The data that supports the findings of this study are available in the Supporting Information of this article.

**Keywords**

clays, degradable, food packaging, nanocomposites, oxygen permeability

Received: September 30, 2021

Revised: November 10, 2021

Published online:

- [1] E. Macarthur, *Science* **2017**, 358, 843.
- [2] S. Agarwal, *Macromol. Chem. Phys.* **2020**, 221, 2000017.
- [3] J. M. Millican, S. Agarwal, *Macromolecules* **2021**, 54, 4455.
- [4] D. M. Mitrano, P. Wick, B. Nowack, *Nat. Nanotechnol.* **2021**, 16, 491.
- [5] M. Karamanlioglu, R. Preziosi, G. D. Robson, *Polym. Degrad. Stab.* **2017**, 137, 122.
- [6] S. Singha, M. S. Hedenqvist, *Polymers* **2020**, 12, 1095.
- [7] A. R. Bagheri, C. Laforsch, A. Greiner, S. Agarwal, *Global Challenges* **2017**, 1, 1700048.
- [8] H. Tsuji, K. Suzuyoshi, *Polym. Degrad. Stab.* **2002**, 75, 347.
- [9] H. Tsuji, K. Suzuyoshi, *Polym. Degrad. Stab.* **2002**, 75, 357.
- [10] A. E. Schwarz, T. N. Ligthart, E. Boukris, T. Van Harmelen, *Mar. Pollut. Bull.* **2019**, 143, 92.
- [11] C. J. Moore, *Environ. Res.* **2008**, 108, 131.
- [12] M. Zabihzadeh Khajavi, A. Ebrahimi, M. Yousefi, S. Ahmadi, M. Farhoodi, A. Mirza Alizadeh, M. Taslikh, *Food Eng. Rev.* **2020**, 12, 346.
- [13] S. Sukkhum, *J. Microbiol. Biotechnol.* **2012**, 22, 92.
- [14] Y. Tokiwa, M. Konno, H. Nishida, *Chem. Lett.* **1999**, 28, 355.
- [15] Y. Oda, A. Yonetsu, T. Urakami, K. Tonomura, *J. Polym. Environ.* **2000**, 8, 29.
- [16] A. Kumar, A. R. Weig, S. Agarwal, *Macromol. Mater. Eng.* **2021**, 2100602. <https://doi.org/10.1002/mame.202100602>.
- [17] C. Vasile, D. Pamfil, M. Răpă, R. N. Darie-Niță, A. C. Mitelut, E. E. Popa, P. A. Popescu, M. C. Draghici, M. E. Popa, *Composites, Part B* **2018**, 142, 251.
- [18] S. Dharmalingam, D. G. Hayes, L. C. Wadsworth, R. N. Dunlap, J. M. Debruyne, J. Lee, A. L. Wszelaki, *J. Polym. Environ.* **2015**, 23, 302.
- [19] W. Y. Jang, B. Y. Shin, T. J. Lee, R. Narayan, *J. Ind. Eng. Chem.* **2007**, 13, 457.
- [20] J. K. Pandey, K. Raghunatha Reddy, A. Pratheep Kumar, R. P. Singh, *Polym. Degrad. Stab.* **2005**, 88, 234.
- [21] H. C. Koh, J. i. S. Park, M. i. A. e. Jeong, H. Y. Hwang, Y. T. Hong, S. Y. Ha, S. Y. Nam, *Desalination* **2008**, 233, 201.
- [22] K. Fukushima, C. Abbate, D. Tabuani, M. Gennari, G. Camino, *Polym. Degrad. Stab.* **2009**, 94, 1646.
- [23] S. Sinha Ray, K. Yamada, M. Okamoto, K. Ueda, *Nano Lett.* **2002**, 2, 1093.
- [24] E. Castro-Aguirre, R. Auras, S. Selke, M. Rubino, T. Marsh, *Polymers* **2018**, 10, 202.
- [25] S. Sinha Ray, M. Okamoto, *Macromol. Mater. Eng.* **2003**, 288, 936.
- [26] C. Habel, M. Schöttle, M. Daab, N. J. Eichstaedt, D. Wagner, H. Bakhshi, S. Agarwal, M. A. Horn, J. Breu, *Macromol. Mater. Eng.* **2018**, 303, 1800333.
- [27] T. Schilling, C. Habel, S. Rosenfeldt, M. Röhr, J. Breu, *ACS Appl. Polym. Mater.* **2020**, 2, 3010.
- [28] C. Habel, E. S. Tsurko, R. L. Timmins, J. Hutschreuther, R. Kunz, D. D. Schuchardt, S. Rosenfeldt, V. Altstadt, J. Breu, *ACS Nano* **2020**, 14, 7018.
- [29] S. Rosenfeldt, M. Stöter, M. Schlenk, T. Martin, R. Q. Albuquerque, S. Förster, J. Breu, *Langmuir* **2016**, 32, 10582.
- [30] J. Zhu, C. Habel, T. Schilling, A. Greiner, J. Breu, S. Agarwal, *Macromol. Mater. Eng.* **2019**, 304, 1800779.
- [31] V. Dudko, K. Ottermann, S. Rosenfeldt, G. Papastavrou, J. Breu, *Langmuir* **2021**, 37, 461.
- [32] L. Boldon, F. Laliberte, L. Liu, *Nano Rev.* **2015**, 6, 25661.
- [33] M. Röhr, J. H. Mettke, S. Rosenfeldt, H. Schmalz, U. Mansfeld, R. L. Timmins, C. Habel, J. Breu, F. Durst, *J. Coat. Technol. Res.* **2021**, 1. <https://doi.org/10.1007/s11998-021-00535-4>.
- [34] E. L. Cussler, S. E. Hughes, W. J. Ward, R. Aris, *J. Membr. Sci.* **1988**, 38, 161.
- [35] H. Kalo, W. Milius, J. Breu, *RSC Adv.* **2012**, 2, 8452.
- [36] C. Maes, W. Luyten, G. Herremans, R. Peeters, R. Carleer, M. Buntinx, *Polym. Rev.* **2018**, 58, 209.
- [37] L. Husárová, S. Pekařová, P. Stloukal, P. Kucharczyk, V. Verney, S. Commereuc, A. Ramone, M. Koutny, *Int. J. Biol. Macromol.* **2014**, 71, 155.
- [38] P. Stloukal, S. Pekařová, A. Kalendova, H. Mattausch, S. Laske, C. Holzer, L. Chitu, S. Bodner, G. Maier, M. Slouf, M. Koutny, *Waste Manage.* **2015**, 42, 31.
- [39] A. B. Gomez-Gamez, A. Yebra-Rodriguez, A. Peñas-Sanjuan, B. Soriano-Cuadrado, J. Jimenez-Millan, *Appl. Clay Sci.* **2020**, 198, 105818.
- [40] Y. Guo, K. Yang, X. Zuo, Y. Xue, C. Marmorat, Y. Liu, C. - C. Chang, M. H. Rafailovich, *Polymer* **2016**, 83, 246.
- [41] P. Russo, S. Cammarano, E. Bilotti, T. Peijs, P. Cerruti, D. Acierno, *J. Appl. Polym. Sci.* **2014**, 131, 39798.
- [42] H. Kalo, M. W. Möller, M. Ziadeh, D. Dolejš, J. Breu, *Appl. Clay Sci.* **2010**, 48, 39.
- [43] S. Li, A. Girard, H. Garreau, M. Vert, *Polym. Degrad. Stab.* **2000**, 71, 61.

**[M]** acro-  
olecular  
Materials and Engineering

Supporting Information

for *Macromol. Mater. Eng.*, DOI 10.1002/mame.202100727

High Barrier Nanocomposite Film with Accelerated Biodegradation by Clay Swelling Induced Fragmentation

*Renee L. Timmins, Anil Kumar, Maximilian Röhl, Karel Havlíček, Seema Agarwal\* and Josef Breu\**

**High barrier nanocomposite film with accelerated biodegradation by clay swelling induced fragmentation**

*Renee L. Timmins, Anil Kumar, Maximilian Röhr, Karel Havlíček, Seema Agarwal\*, and Josef Breu*

Cussler's theory for permeability [1]:

$$P_{rel} = \frac{P}{P_0} = \left( 1 + \mu \left( \frac{\alpha^2 \phi^2}{1 - \phi} \right) \right)^{-1} = \frac{1}{BIF} \quad \text{Equation S1}$$

Where  $P$  is the permeability of the nanocomposite,  $P_0$  is the permeability of the neat polymer,  $\phi$  is the filler content (volume fraction),  $\alpha$  is the aspect ratio of the filler,  $\mu$  is a geometrical factor dependent on filler shape, and BIF is barrier improvement factor.

To calculate theoretical barrier improvement factor for the PLA/18C6Hec nanocomposite:  $\mu$  is 4/9, aspect ratio is 166 (approximated using height of 120 nm for clay tactoids and the width for NaHec platelets of 20,000 nm), and filler content is 8.5 vol%.

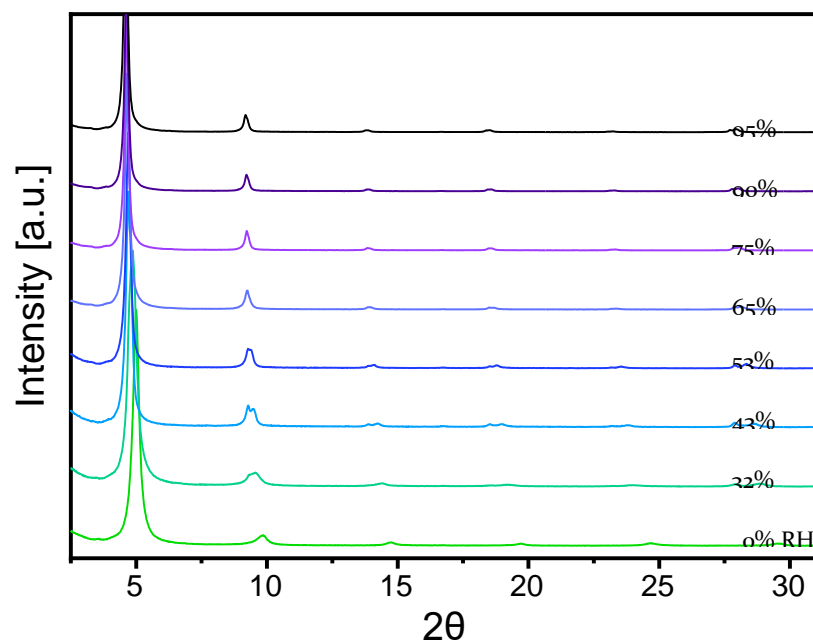


**Figure S1.** XRD spectra of PLA/18C6Hec films at different humidities

**Table S1.** Oxygen transmission rates (OTR) and permeability for PLA and PLA nanocomposite films at 23 °C and 65 % RH

Sample	Thickness (μm)	OTR (cm <sup>3</sup> m <sup>-2</sup> day <sup>-1</sup> atm <sup>-1</sup> )	Permeability (cm <sup>3</sup> μm m <sup>-2</sup> day <sup>-1</sup> atm <sup>-1</sup> )
PLA	25	711	17 775
PLA/18C6Hec	59	2.10	124

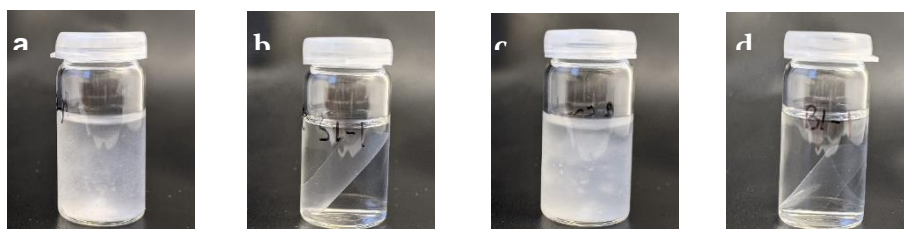


**Figure S2.** Film samples immersed in buffer solution for 1 hour at 37°C for **a**, PLA/18C6 without enzyme **b**, PLA without enzyme **c**, PLA/18C6 with enzyme **d**, PLA with enzyme.

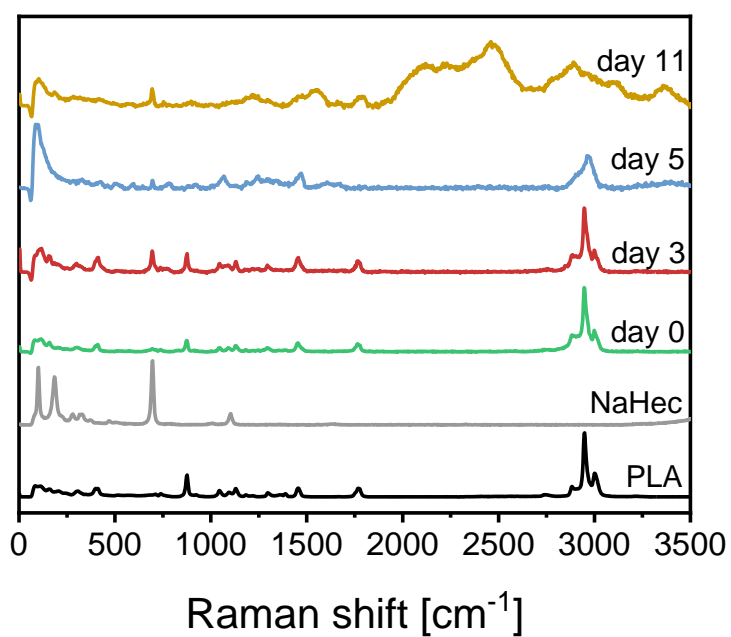


**Figure S3.** Raman spectra of PLA, NaHec, and PLA/18C6Hec nanocomposite after day 0 (initial), day 3, day 5, and day 11 after enzymatic degradation

**Table S2.** DSC data for PLA and PLA/18C6Hec films pre and post enzymatic degradation testing

Sample	$T_g$ (°C)	$T_m$ (°C)	$\Delta H_m$ (J $g^{-1}$ )	$\Delta H_c$ (J $g^{-1}$ )	Wt% PLA	$\chi$ (%)
PLA	60	150	29	n.d.	100	31
PLA- degradation (day 8)	59	147	33	n.d.	100	35
PLA/18C6Hec	n.d.	130	33	n.d.	66	53
PLA/18C6Hec- post degradation (day 3)	n.d.	129	22	n.d.	n.d.	n.d.
PLA/18C6Hec- post degradation (day 5)	n.d.	n.d.	n.d.	n.d.	n/a	n/a

n.d. = not determined

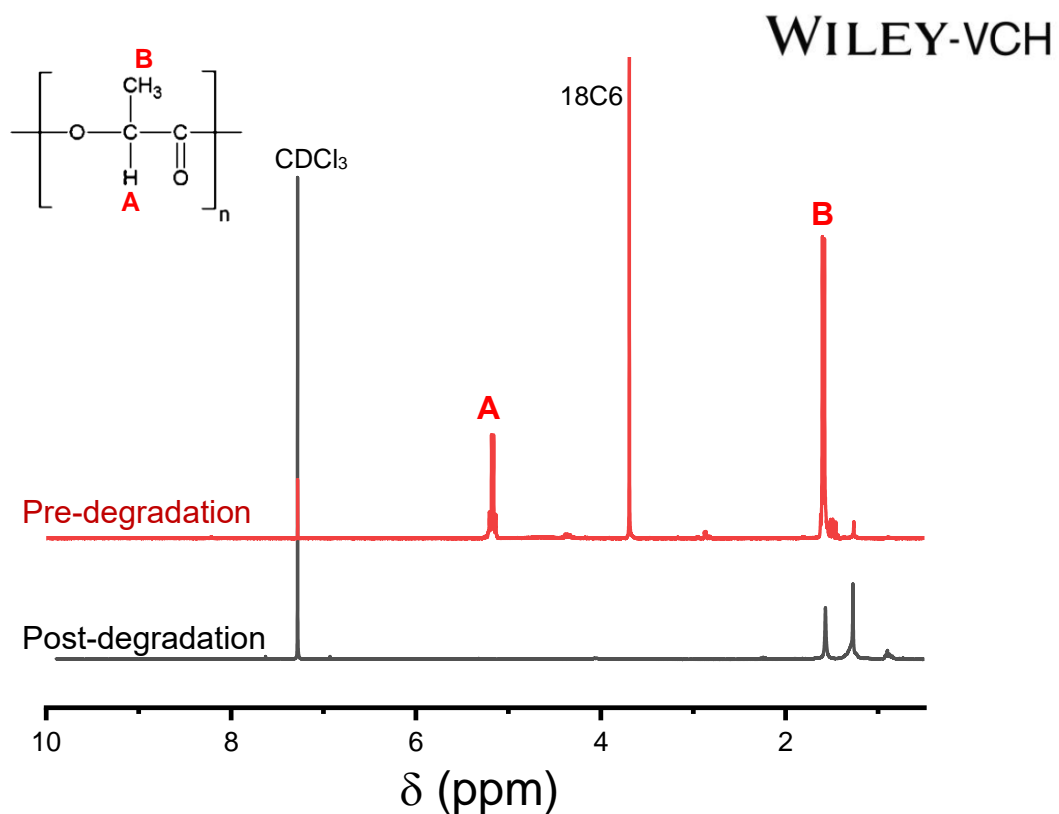


**Figure S4.**  $^1\text{H-NMR}$  spectra of PLA/18C6Hec film, pre- and post-enzymatic degradation testing period of 5 days

**Table S3.** DSC data for PLA and PLA/18C6Hec films pre- and post-degradation testing in activated sludge for 45 days

Sample	$T_g$ (°C)	$T_m$ (°C)	$\Delta H_m$ (J g $^{-1}$ )	$\Delta H_c$ (J g $^{-1}$ )	Wt% PLA	$\chi$ (%)
PLA	60	150	29	n.d.	100	31
PLA- degradation <sup>post</sup>	59	148	35	n.d.	100	37
PLA/18C6Hec	n.d.	130	33	n.d.	66	53
PLA/18C6Hec- post degradation	n.d.	141	44	n.d.	n.d.	n.d.

n.d. = not determined

**Calculation of % Crystallinity:**

$$\% \chi (\text{Norm.}) = \frac{\Delta H_m - \Delta H_{cc}}{\Delta H^{\circ f}} \times \frac{100}{w} \quad \text{Equation S2}$$

Where  $\Delta H_m$  is the observed enthalpy of fusion obtained from the first heating process of DSC measurement,  $\Delta H_{cc}$  is the enthalpy of crystallization,  $\Delta H^{\circ f}$  is the enthalpy of fusion of the completely crystalline materials and the  $w$  is the PLLA weight ratio in polymer blends. Here,  $\Delta H^{\circ f}$  is 93 J/g for PLA.<sup>[2]</sup>

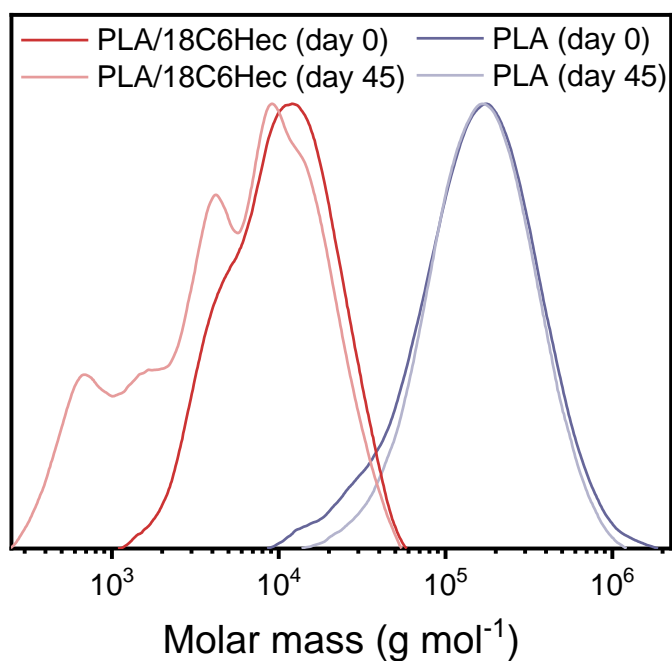


**Figure S5.** Gel-permeation chromatography traces of PLA (cast from MeCN) and PLA/18C6Hec films before and after degradation in activated sludge wastewater medium

**Table S4.** Mechanical testing data for PLA and PLA/18C6Hec films

Sample	Elastic Modulus (GPa)	Tensile Strength (MPa)	Elongation at break (%)
PLA	1.43	63.3	9.7
PLA/18C6Hec	1.14	26.1	3.5

References

- [1] E. L. Cussler, S. E. Hughes, W. J. Ward, R. Aris, *Journal of Membrane Science* **1988**, 38, 161.
- [2] E. W. Fischer, H. J. Sterzel, G. Wegner, *Kolloid-Zeitschrift und Zeitschrift für Polymere* **1973**, 251, 980.

## 6.2. Stretchable and Fast Composting Polyester Films with High-Performance Oxygen Barrier

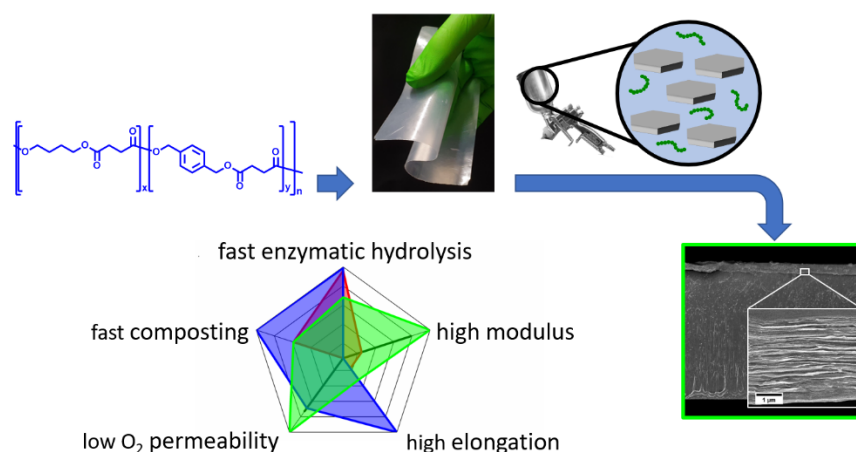
Elmar Sehl<sup>‡</sup>, Renee L. Timmins<sup>‡</sup>, Dipannita Ghosh, Josef Breu, Seema Agarwal\*

<sup>‡</sup>these authors contributed equally to this work

\*corresponding author(s): seema.agarwal@uni-bayreuth.de

Published in: *ACS Applied Polymer Materials* **2022**, 4 (9), 6675-6686

Reprinted with permission. Copyright 2022 American Chemical Society



Individual contribution:

Prof. Dr. Josef Breu and Prof. Dr. Seema Agarwal conceptualized the paper. Elmar Sehl synthesized the polymers, prepared the substrate films, and performed enzymatic and compost degradation testing with accompanying polymer analysis. I prepared the coating suspension, coated the substrates, and performed oxygen barrier testing. Dipannita Ghosh performed CO<sub>2</sub> evolution testing. The paper was written through contribution of all coauthors.

## Stretchable and Fast Composting Polyester Films with High-Performance Oxygen Barrier

Elmar Sehl,<sup>§</sup> Renee L. Timmins,<sup>§</sup> Dipannita Ghosh, Josef Breu, and Seema Agarwal\*Cite This: <https://doi.org/10.1021/acscapm.2c01040>

Read Online

ACCESS |

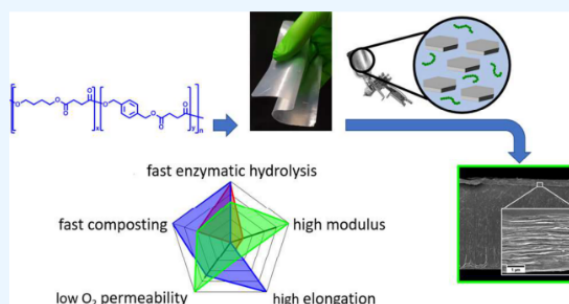
Metrics &amp; More

Article Recommendations

Supporting Information

**ABSTRACT:** This work presents one of the fastest composting aliphatic–aromatic polyesters with a good balance of mechanical and barrier properties, making it a sustainable alternative for low-density polyethylene in packaging. The polyesters (PB<sub>x</sub>BDM<sub>y</sub>S) are prepared by melt polycondensation of 1,4-butanediol (B), 1,4-benzenedimethanol (BDM), and succinic acid (S). One composition exhibited a tensile strength of  $20 \pm 2$  MPa, a modulus of  $150 \pm 8$  MPa, and a very high elongation at break of  $581 \pm 46\%$ . The low oxygen transmission rate ( $152 \text{ cm}^3 \cdot \text{m}^{-2} \cdot \text{day}^{-1} \cdot \text{bar}^{-1}$ ) measured at 65% relative humidity and 23 °C confirms excellent barrier performance. A 3 μm water-borne nanocomposite coating of glycol chitosan and sodium fluorohectorite further reduced the gas permeability to a value of  $0.75 \text{ cm}^3 \cdot \text{m}^{-2} \cdot \text{day}^{-1} \cdot \text{atm}^{-1}$ , which is competitive with materials suitable for demanding packaging applications such as poly(vinylidene chloride) while maintaining good mechanical properties and high stretchability. After studying the enzyme-catalyzed hydrolysis under controlled conditions, the full fragmentation, assimilation, and mineralization in thermophilic, aerobic composting could be confirmed in less than 5 weeks using a combination of different analytical methods. The mechanism of degradation was proven to be bulk degradation.

**KEYWORDS:** polyester, food packaging, biodegradable, layered silicates, nanocomposite



## INTRODUCTION

The easy functionalization, processability, lightweight, and low cost of commodity polymers provide a sustainable choice among several material classes for a variety of applications. There is a continuous increase in plastic production, and figures like global plastic production being over 350 million metric tons (Mt) per year are no longer a surprise.<sup>1</sup> Problems associated with the increased production and use of plastics are waste management and the occurrence of plastic fragments (microplastics; MP) in different environmental segments.<sup>2–7</sup> The packaging sector is one of the biggest consumers of plastics, utilizing more than 40% of the total plastics in Europe.<sup>1</sup> The packaging sector also greatly contributes to plastic pollution and MP in the environment. It is estimated that 4800 Mt of plastic, representing 60% of all of the plastic ever produced, has been disposed of in a landfill or the natural environment. Current projects predict this number to increase to 12,000 Mt by 2050.<sup>8</sup> Circular approaches are being promoted to reduce plastic waste.<sup>9,10</sup> The use of biodegradable packaging, especially for short-term/single-use food packaging, is considered one strategy toward zero plastic pollution.<sup>11</sup> Poly(L-lactide) (PLA) could be a promising biodegradable alternative for polyolefins, yet it suffers from many drawbacks that limit its practical use as a packaging material. This includes poor mechanical properties and low melt stability that make

processing more difficult.<sup>12</sup> Also, PLA is not fully degradable in some relevant environmental conditions<sup>13</sup> and takes a long time for degradation in compost.<sup>14,15</sup> Unfortunately, there seems to be a trade-off between thermomechanical properties and degradability in polyesters. Considering the chemical structure of the common packaging materials poly(1,4-butylene terephthalate) (PBT) and poly(ethylene terephthalate) (PET), the aromatic unit in their backbones provide high thermal transition temperatures, thermomechanical stability, and chemical resistance,<sup>16</sup> making them widely used materials.<sup>1</sup> Without the aromatic backbone, as in poly(1,4-butylene succinate) (PBS), the polymer loses thermomechanical stability due to its low melting point yet becomes readily degradable compared to PBT and PET.<sup>17,18</sup>

The trade-off between the mechanical properties and the rate of composting and the inherently poor barrier properties in the existing degradable polymers make their use in real applications difficult.<sup>19</sup> Therefore, efforts combining all

Received: June 17, 2022

Accepted: August 1, 2022

properties into one material are appreciable. For example, aromatic monomer units could be combined with degradable aliphatic units in a single polymer, as is the case for the commercial poly(butylene adipate-co-butylene terephthalate) (PBAT), but such polymers still display slow degradation kinetics in many environmental conditions.<sup>13,20</sup> The combination of hydrolyzable ester groups and an aromatic group into the backbone of a polymer in a way that maintains degradability and desirable mechanical properties was recently investigated by us. Poly(1,4-benzenedimethylene succinate) (PBDMS) is a constitutional isomer of PBT in which the carbonyl carbon is more electrophilic due to the aromatic unit being separated from the ester carbonyl carbon, thus limiting the delocalization of electron density through resonance structures.<sup>21</sup> PBDMS and its copolymers with 1,4-butanediol were prepared, showing fast hydrolysis under basic conditions, good mechanical properties, and thermal stability. Such material has great potential to be a suitable replacement as a biodegradable food packing material if only it also demonstrated the other requirements of fast degradation and high barrier performance.

The most successful attempts at improving barrier properties of polymers are by incorporating two-dimensional (2D) impermeable filler such as graphene, layered double hydroxides, and clays.<sup>22–24</sup> The latter presents a particular advantage due to its commercial availability, environmental inertness, and simplicity in processing. Due to their natural hydrophobicity, obtaining a clay nanocomposite film with many commercially available biodegradable polymers has been a challenge. Common processing methods like melt blending often fail to achieve full delamination of the clay and a high degree of orientation;<sup>25–27</sup> these two factors heavily contribute to the elongation of a diffusion path for permeates through the film, i.e., the formation of a tortuous path, and thus improved barrier properties.<sup>28</sup> Yet, the most important consideration is the aspect ratio (ratio of width to height) of the clay filler used. Common montmorillonite clays have aspect ratios below 300, requiring very high filler content to reduce gas transmission into a somewhat relevant range.

Multilayered systems are one method that researchers have used to improve montmorillonite barrier performance. For example, Svagan et al. built up a barrier nanocomposite on a poly(lactic acid) (PLA) substrate with a layer-by-layer dip-coating setup that reduced PLA oxygen permeability by up to 99% with 70 alternating bilayers of chitosan and montmorillonite.<sup>29</sup> Using a similar layer-by-layer dip-coating method, anionic and cationic polymers combined with montmorillonite yielded impressive barrier improvement of nonbiodegradable films due to its “nano-brick” microstructure.<sup>30,31</sup> Such time-consuming or complex processing methods are not a realistic path toward greater implementation of fully biodegradable alternatives to current food packaging materials.

Our group has shown that we can achieve the barrier improvement that one would expect from a multilayered system with just a single nanocomposite coating. Hectorite clay (Hec) as a filler material provides an exceptional aspect ratio of 20,000 and maintains the unique ability to osmotically swell in water, giving gentle and quantitative delamination into single nanosheets. Hec can form highly ordered, intercalated nanostructures that impart drastic barrier improvements even as a coating in water-borne systems.<sup>24,32,33</sup>

This work presents a high-performance polyester film that combines impressive barrier properties with appropriate

mechanical properties and processability while showing very fast biodegradability in industrial compost (5–8 weeks). The Hec clays improved the barrier performance keeping a good balance between mechanical properties and degradation time in compost without leaving behind any MP.

## EXPERIMENTAL SECTION

**Materials.** Chloroform-*d*<sub>1</sub> (CDCl<sub>3</sub>, 99.8%) and dimethyl sulfoxide-*d*<sub>6</sub> (99.8%) were purchased from Deutero. Disodium phosphate (99%) was purchased from Grüssing. Hydrochloric acid (37%) was purchased from VWR. Sodium azide (99%) was purchased from Alfa Aesar. Aniline (≥99.5%) was purchased from Carl Roth. Avicel PH-101 (particle size ~50 μm) was purchased from Sigma-Aldrich. BioPBS FZ91PM (PBS) and BioPBS FD92PM [poly(1,4-butylene succinate-co-1,4-butylene adipate), PBSA] were kindly provided by MCPP Germany GmbH (a group company of Mitsubishi Chemical). Esterase EL-01 suspension (27.9 mg/mL protein content, origin: *Thermomyces lanuginosus*, EC 3.1.1.3) was purchased from ASA Spezialenzyme GmbH. The active compost was kindly provided by Veolia Umweltservice Süd GmbH & Co. KG. The activated wastewater sludge after the nitrification step was kindly provided by the wastewater treatment plant of the Stadtbauhof Bayreuth. Glycol chitosan (GlyChit) was purchased from Santa Cruz Biotechnology, had a polymerization degree of ≥400 (crystalline, 73% deacetylated), and was used as received. All solvents were purchased in technical grade from local suppliers and purified via rotatory evaporation. Sodium fluorohectorite [Na<sub>0.5</sub>]<sup>inter</sup>[Mg<sub>2.5</sub>Li<sub>0.5</sub>]<sup>oct</sup>[Si<sub>4</sub>]<sup>tet</sup>O<sub>10</sub>F<sub>2</sub> (Hec) was prepared by employing a synthesis procedure from the melt, as previously reported in the literature.<sup>34</sup> The material features a cation exchange capacity of 1.27 mmol g<sup>-1</sup>. According to our recently published procedure, the polyesters were synthesized in a two-step melt polymerization process using 1,4-butanediol, 1,4-benzenedimethanol, and succinic acid.<sup>21</sup> The polymers are designated as PB<sub>x</sub>BDM<sub>y</sub>S, where *x* and *y* are the molar ratios of the 1,4-butanediol and 1,4-benzenedimethanol in the feed, respectively. Phosphate-buffered saline was produced by pH titration of aqueous disodium phosphate solution against concentrated hydrochloric acid.

**Analytical Methods.** <sup>1</sup>H (300 MHz) and <sup>13</sup>C (75 MHz) NMR spectra were recorded on an Ultrashield-300 spectrometer (Bruker) in CDCl<sub>3</sub>, using the residue peak of the undeuterated solvent as an internal standard. ACD/NMR Processor Academic Edition, version 12.01, was used to analyze NMR spectra.

Gel permeation chromatography (GPC) was used for the measurement of molar masses and molar mass distribution (*D*) on a 1260 Infinity (Agilent Technologies). The instrument was equipped with a pre-column SDV 5 μm, the main column SDV linear XL 5 μm (PSS, Mainz, Germany), and a refractive index detector (RI, Agilent Technologies). The autosampler injected 20 μL of the sample, and CHCl<sub>3</sub> (HPLC grade) was used as a solvent with a flow rate of 0.5 mL·min<sup>-1</sup> at 23 °C. Polystyrene (PSS calibration kit, PSS, Mainz, Germany) was used as a calibration standard for 630 to 2,580,000 Da. The polymers were dissolved in CHCl<sub>3</sub> (HPLC grade) with Toluene (HPLC grade) as an internal standard in a concentration of 2 mg·mL<sup>-1</sup> and filtered through a 0.22 μm PTFE filter before injection. The program PSS WinGPC Unity was used to process the results.

Thermogravimetric analysis was performed at a TG 209 F1 Libra (Netzsch). Approximately 10 mg of the sample was precisely weighed into an 85 μL Al<sub>2</sub>O<sub>3</sub> crucible (Thepro) by the internal balance of the machine. The sample was measured in the range of 25–1100 °C under synthetic air (80 vol % N<sub>2</sub>, 20 vol % O<sub>2</sub>) with a flow rate of 50 mL·min<sup>-1</sup>. The program Proteus Analysis version 8.0 was used to process the results.

Differential scanning calorimetry (DSC) was performed at a DSC 204 F1 Phoenix (Netzsch). Approximately 5 mg of the sample was weight in a 30/40 μL aluminum crucible with a pierced lid (Thepro). The sample was measured with a heating rate of 10 K·min<sup>-1</sup> in the range of –80 to 220 °C under nitrogen 5.3, with a flow rate of 20 mL·min<sup>-1</sup>. The program Proteus Analysis version 8.0 was used to process the results.

Polyester films were produced with a 25-12-2HC hot press (Carver). The polyesters were dried in a vacuum at 40 °C overnight and pressed in between two Nowoflon PFA foil or glass fiber reinforced PTFE foil-covered stainless steel plates using a 130 mm × 130 mm × 0.1 mm mold at a temperature of 130–180 °C for 3 min. The pressure was increased from 0 to 5 t after 1 min. Subsequent thermal quenching was performed on a LaboPress P150H manual lever cold press (Vogt Maschinenbau, Berlin, Germany) until room temperature was reached. Annealing was performed according to a previously published procedure.<sup>19</sup> PB<sub>44</sub>BDM<sub>56</sub>S, PBS, and PBSA were not annealed.

X-ray diffraction (XRD) of the uncoated polymer films was performed on a D8 ADVANCE diffractometer (Bruker). The Cu K $\alpha$  irradiation ( $\lambda = 1.54187 \text{ \AA}$ ) source was operated at 40 kV and 40 mA. Five annealed polyester films were stacked, and the pattern was recorded in the  $2\theta$  range of 5–45° (0.025 °·min<sup>-1</sup>) at room temperature. The program DIFFRAC.EVA V4.0 was used to process the data. XRD patterns of the coated films were recorded using nickel filtered Cu K $\alpha$  radiation ( $\lambda = 1.54187 \text{ \AA}$ ) in Bragg–Brentano geometry on an Empyrean diffractometer (PANalytical B.V., the Netherlands) equipped with a Pixel detector. Before measurement, the films were equilibrated at room temperature for 1 week.

Oxygen transmission rates (OTR) were measured with a Mocon OX-TRAN 2/21 system (Mocon, Inc.) with a lower detection limit of 0.05 cm<sup>3</sup>·m<sup>-2</sup>·day<sup>-1</sup>·bar<sup>-1</sup>. OTR for the coated films was measured on a Mocon OX-TRAN 2/21 XL instrument (Minneapolis) with a lower detection limit of 0.0005 cm<sup>3</sup>·m<sup>-2</sup>·day<sup>-1</sup>·bar<sup>-1</sup>. The measurements were performed at 23 °C and 65% RH. A 98% nitrogen and 2% hydrogen mixture was used as the carrier gas and pure oxygen as permeant (Linde Sauerstoff 3.5). Film thickness was determined using a high-accuracy Digimatic micrometer (Mitutoyo, Japan) with a measuring range of 0–25 mm and a resolution of 0.0001 mm.

The mechanical performance was determined by uniaxial stress–strain testing on a BT1-FR 0.STND14 (Zwick/Roell) at room temperature. The samples were produced by a pneumatic puncher (Coesfeld, Dortmund, Germany) according to DIN 53 504 S3A. The thickness of every specimen was measured with a Series 293 (0–25 mm) digital micrometer (Mitutoyo, Neuss, Germany), taking the average of three different positions in the gauge area as the final width. The specimens were conditioned at room temperature for 24 h before testing. The test speed applied to the samples was 10 mm·min<sup>-1</sup> at a grip to grip separation of 30 mm. The elastic modulus was determined by the slope of the linear region of the stress–strain curves. All samples were measured at least five times, and the statistical average is given as the result.

Scanning electron microscopy (SEM) images were taken on a Zeiss LEO 1530 (FE-SEM, Schottky field emission cathode; in-lens and SE 2 detector) at an accelerating voltage of 3 kV. The samples were sputtered with platinum (1.3 nm) before imaging using an HR208 sputter coater (Cressington, Dortmund, Germany) with an MTM20 thickness controller (Cressington).

FTIR spectroscopy was performed on Spectrum Two (PerkinElmer) equipped with a UATR-unit (diamond), KBr optics, and a DTGS MIR detector. The spectra were recorded in the range of 4000–450 cm<sup>-1</sup> with a resolution of 4 cm<sup>-1</sup> and an accumulation of four scans. The software Spectrum 10 was used to process the data.

Elemental analysis was performed on a CHNS elemental analyser vario EL cube (Elementar Analysensysteme GmbH, Langensfeld, Germany).

Ultrapure water was prepared by a Milli-Q direct water purification system (Merck, Germany) with a resistivity of 18.2 M $\Omega$ ·cm at 25 °C and a TOC of  $\leq 1$  ppm.

Composting experiments were carried out in a constant climate chamber HPP110 (Mettler, Schwabach, Germany) equipped with a compressed air dehumidification system at 58  $\pm$  0.5 °C and 70  $\pm$  2% relative humidity in the interior.

The pH titration of the phosphate-buffered saline was controlled with a SevenCompact pH meter S220 (Mettler Toledo) equipped with a pH electrode InLine Expert at room temperature. The device

was calibrated with three different standard buffer solutions before use.

Micro-Oxymax Respirometer (Columbus Instruments International) was used for wastewater degradation experiments. The machine was equipped with a nondispersive infrared detector and operates with a sensitivity up to 0.2  $\mu\text{L}\cdot\text{h}^{-1}$  due to a closed loop measuring method. The sensors were calibrated with gas standard mixtures before use. Additionally, a gas drying unit ( $\geq 98\%$  CaSO<sub>4</sub>,  $< 2\%$  CoCl<sub>2</sub>), as well as 0.2  $\mu\text{m}$  particle filters and condensers for each channel, were attached.

**Nanocomposite Coating.** Hec (1 g, 1 wt %) was delaminated by immersing it into doubled-distilled water (99 g) and mixing in an overhead shaker for 2 days. GlyChit was dissolved in double-distilled water (1 wt %) and let mix in an overhead shaker until a clear solution was obtained. The Hec and GlyChit solutions were mixed in a 1:1 (wt %) ratio. The total solid content was adjusted to 0.7 wt % by adding additional double-distilled water. After mixing overnight, the solution underwent speedmixing (Hauschild & Co. KG) under a vacuum to remove gas bubbles (5 min, 100 mbar). The solution was then spray-coated using a SATA 4000 LAB HVLP 1.0 mm spray gun (SATA GmbH & Co. KG, Germany) onto the polymer substrates for a total of 80 spray cycles with a 120 s drying time under a heat lamp at 28 °C.

**Enzymatic Hydrolysis.** For the enzymatic hydrolysis, films of PB<sub>3</sub>BDM<sub>3</sub>S, PBDMS, PBS, and PBSA, and the GlyChitHec-coated PB<sub>64</sub>BDM<sub>36</sub>S and PBSA were used. The films were cut into 10 mm × 10 mm pieces and immersed in phosphate-buffered saline (4 mL, pH = 7.40, 0.10 mol·L<sup>-1</sup>) containing Esterase EL-01 (0.01 mg·L<sup>-1</sup>) and sodium azide (0.1 g·L<sup>-1</sup>). All samples were incubated in a KS 3000 control incubator (IKA) at 37 °C and 60 rpm. Samples were taken in triplicate at various time intervals. Each sample was washed with methanol (1 mL), Milli-Q water (2 × 1 mL), and methanol (1 mL) for at least 5 min with subsequent drying in a high vacuum at room temperature until a constant weight was recorded. Samples showing disintegration were carefully decanted to 1 mL, transferred to tared centrifugation vials ( $V = 2 \text{ mL}$ ), and centrifuged (10,000 rpm, 5 min, 20 °C). The supernatant was carefully decanted, followed by washing with methanol (1 mL), Milli-Q water (2 × 1 mL), and methanol (1 mL) for 5 min with centrifugation and decantation after each step. The samples were dried under a high vacuum at room temperature until a constant weight was recorded. The samples were analyzed by gravimetry, GPC, SEM, and <sup>1</sup>H NMR spectroscopy. Additionally, blank experiments were conducted under the same conditions without enzyme.

**Degradation Test in Wastewater Sludge.** The degradation in wastewater sludge under an aerobic environment was carried out according to DIN EN ISO 14852 in triplicate using  $\sim 70$  mg polymer film, and 100 mL activated wastewater sludge as the test medium. Aniline (40  $\mu\text{L}$ ) was used as the positive sample. An Avicel PH-101 (75.35 mg, microcrystalline cellulose, particle size  $\sim 50 \mu\text{m}$ ) was also tested for comparison. The percentage of biodegradation was calculated by monitoring carbon dioxide production using the following eq 1.

$$\text{biodegradation} = \frac{m(\text{CO}_2)_T - m(\text{CO}_2)_B}{m(\text{CO}_2)_{Th}} \times 100 \quad (1)$$

Here,  $m(\text{CO}_2)_T$  is the amount of carbon dioxide evolved from the test medium,  $m(\text{CO}_2)_B$  is the amount of carbon dioxide evolved in blank medium between the start and the end of the test, and  $m(\text{CO}_2)_{Th}$  is the theoretical amount of carbon dioxide produced by the test material, which is calculated by eq 2.

$$m(\text{CO}_2)_{Th} = \frac{m_{\text{sample}} \cdot (C\%)_{EA} \cdot M(\text{CO}_2)}{100 \cdot M(C)} \quad (2)$$

Here,  $m_{\text{sample}}$  is the mass of the tested sample,  $(C\%)_{EA}$  is the carbon content of the sample determined by elemental analysis,  $M(\text{CO}_2)$  is the molar mass of carbon dioxide, and  $M(C)$  is the molar mass of carbon.

C

<https://doi.org/10.1021/acscapm.2c01040>  
ACS Appl. Polym. Mater. XXXX, XXX, XXX–XXX

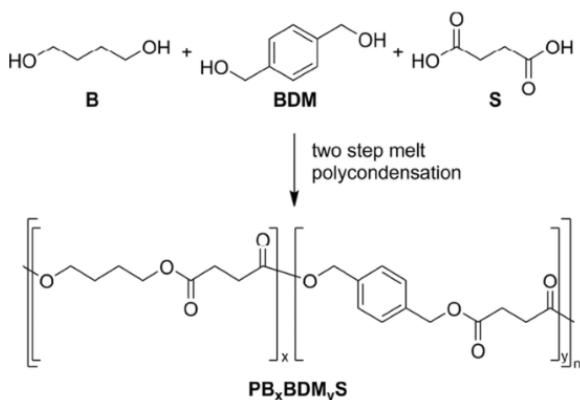
**Composting.** Controlled composting was performed under aerobic conditions. The test method was based on DIN EN ISO 20200. For composting experiments, uncoated and GlyChitHec-coated films of PB<sub>64</sub>BDM<sub>36</sub>S, PBS, and PBSA were used. The films were cut into 19 mm × 25 mm pieces (~100 mg) and mounted to an 18 mm × 24 mm frame. Each film was incubated in compost (160 g, 50% dry solid content) together with low-density polyethylene (50 μm thickness) and cellulose filter paper (110 μm thickness) reference of the same size. The setup for each sample is shown in Figure S25. A detailed description of the compost origin, preparation, and analysis is given in the Supporting Information (SI). The samples were incubated in a constant climate chamber at 58 ± 0.5 °C and 70 ± 2% relative humidity. Twice a week, deionized water was added to keep the compost constant at 50 ± 5% dry solid content. Samples were taken at various time intervals. The samples were carefully washed with methanol, deionized water, and methanol again with subsequent drying under a high vacuum at room temperature until a constant weight was recorded. The samples were analyzed by GPC, SEM, DSC, and optical imaging.

**Compost Extraction.** After removing the samples, the remaining compost after eight weeks of thermophilic incubation was extracted with a CHCl<sub>3</sub>/MeOH mixture (9:1, v/v, 100 mL, 2 × 80 mL) for more than 1 h per extraction step, followed by subsequent filtration. The solvent was removed under reduced pressure. The residue was analyzed by <sup>1</sup>H NMR spectroscopy. The compost was extracted a second time with methanol (100 mL, 2 × 80 mL) for more than 1 h per extraction step, followed by subsequent filtration. The solvent was removed under reduced pressure. The residue was analyzed by <sup>1</sup>H NMR spectroscopy. Also, a blank compost sample was treated in the same way.

## RESULTS AND DISCUSSION

The detailed synthetic procedure and structural characterization of poly(1,4-benzenedimethylene succinate) and the random copolyesters poly(1,4-butylene succinate-co-1,4-benzenedimethylene succinate) (PB<sub>x</sub>BDM<sub>y</sub>S;  $x$  = molar ratio of 1,4-butanediol and  $y$  = molar ratio of 1,4-benzenedimethanol in the feed) based on 1,4-butanediol (B), 1,4-benzenedimethanol (BDM), and succinic acid (S) by a two-step melt polycondensation (Scheme 1) and the procedure for their processing into films via hot pressing followed by annealing are described in our recent work.<sup>21</sup> The same technique was used

**Scheme 1.** Reaction Scheme of the Melt Polycondensation of 1,4-Butanediol (B), 1,4-Benzenedimethanol (BDM), and Succinic Acid (S) for the Formation of Poly(1,4-butanediol succinate-co-1,4-benzenedimethylene succinate) (PB<sub>x</sub>BDM<sub>y</sub>S)



in the present work. The exact molecular composition of the films is stated in Table S1, and the thermal data in Table S2.

All of the prepared polyester films are highly translucent (Figure 1a). The processed films were analyzed regarding molar mass and dispersity via gel permeation chromatography (GPC). Polyester films with high molecular weights up to 56000 for PB<sub>83</sub>BDM<sub>17</sub>S were produced (Table 1). The crystallinity of the polyester films was examined via X-ray diffraction (XRD). The crystallinity index was calculated as the quotient of the crystalline area and total area from the XRD profiles (Figure S1). It varied from 0.16 to 0.42, depending on the copolymer composition (Table 1).

The polymer films were screened for enzymatic hydrolysis under controlled conditions to study the effect of structure and copolymer composition on macromolecular chain scission. The enzyme Esterase EL-01 from *T. lanuginosus*, a fungus present in compost piles and agricultural soil, was chosen.<sup>35</sup> This lipase is known for its robust character, long-term retention of activity, and a wide range of suitable pH and temperature. The hydrolysis assay was performed at 37 °C in phosphate-buffered saline at pH 7.40, with the addition of small amounts of sodium azide to prevent microbial growth. Figure 1b plots the residue mass against time. All compositions showed a linear mass loss over time. The rate of enzymatic hydrolysis (the percentage change in mass per hour) was calculated by the slope of the linear fit of each data set (Figure S2). The fastest rate of hydrolysis of around -4.9%·h<sup>-1</sup> was shown by PB<sub>64</sub>BDM<sub>36</sub>S, PB<sub>54</sub>BDM<sub>46</sub>S, and PBSA (Table 1).

Interestingly, the hydrolysis rate significantly decreased in both directions of composition change away from PB<sub>64</sub>BDM<sub>36</sub>S and PB<sub>54</sub>BDM<sub>46</sub>S, i.e., for PB<sub>83</sub>BDM<sub>17</sub>S and PB<sub>20</sub>BDM<sub>80</sub>S, the rate of hydrolysis was -0.81 ± 0.01 and -0.170 ± 0.005%·h<sup>-1</sup>, respectively. In general, high crystallinity and hydrophobicity are important parameters for the slow rate of enzymatic hydrolysis. For PB<sub>83</sub>BDM<sub>17</sub>S, the slight decrease in the hydrolysis rate (-0.170 ± 0.005%·h<sup>-1</sup>) might be due to the high crystallinity (crystallinity index: PB<sub>83</sub>BDM<sub>17</sub>S 0.42; PB<sub>64</sub>BDM<sub>36</sub>S 0.25; and PB<sub>54</sub>BDM<sub>46</sub>S 0.16) (Table 1). Although PB<sub>20</sub>BDM<sub>80</sub>S has a crystallinity (crystallinity index 0.30) in the range of other fast degrading copolyesters (crystallinity index; PB<sub>64</sub>BDM<sub>36</sub>S 0.25, PBSA 0.31), the slowed hydrolysis is assigned to a very large content of aromatic units that make the polymer more hydrophobic. The homopolymer PBDMS showed slower enzymatic hydrolysis with a rate of -0.0234 ± 0.0005%·h<sup>-1</sup> for the same reason. So, the rate-determining factor depends on an interplay between hydrophobicity and crystallinity for this system. All weight losses during the enzymatic hydrolysis were validated by running blank experiments in which films were placed in the buffer system without enzymes. No significant weight losses were seen in blank experiments (Table 1).

Samples at different enzymatic hydrolysis stages were analyzed with GPC, <sup>1</sup>H NMR spectroscopy, and scanning electron microscopy (SEM). The representative characterization for one of the samples (PB<sub>64</sub>BDM<sub>36</sub>S) is shown in Figure 2. For other samples, a detailed analysis is available in the Supporting Information. No relevant changes in the molecular weights of the polyesters could be observed till about 24% residue mass, as determined by overlapping elution curves from GPC measurements during hydrolysis (Figures 2b and S3). The <sup>1</sup>H NMR spectra also could not indicate any differences between eroded and pristine polyester films (Figures 2a and S4–S10). SEM images showed the surface-

D

<https://doi.org/10.1021/acsapm.2c01040>  
ACS Appl. Polym. Mater. XXXX, XXX, XXX–XXX

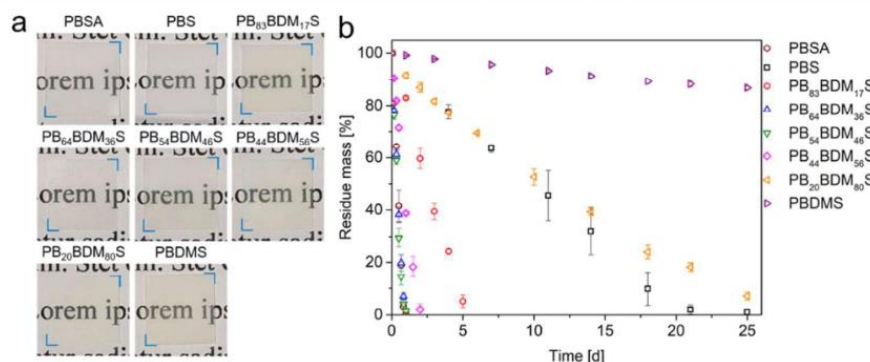


**Figure 1.** (a) Photographs of the pristine polyester films (10 mm × 10 mm) used for enzymatic hydrolysis in front of the text (font: Times, font size: 12). The blue angles indicate the edges of each film. (b) Enzymatic hydrolysis of the pristine polyester films with esterase EL-01 (0.01 mg·mL<sup>-1</sup>) in phosphate-buffered saline (0.1 mol·L<sup>-1</sup>, pH = 7.40) at 37 °C.

**Table 1.** GPC Data, Crystallinity Indices, Rates of Enzymatic Hydrolysis, and Residue Masses after Enzymatic Hydrolysis Blank Experiments

polyester	$M_n^a$	$D^a$	$X_c^b$	rate of enzymatic hydrolysis <sup>c</sup> [%·h <sup>-1</sup> ]	residue mass of blank <sup>d</sup> [%]
PBS	74,000	2.4	0.44 <sup>e</sup>	-0.205 ± 0.002	99.0 ± 0.3
PBSA	77,000	2.6	0.31	-4.8 ± 0.1	99.3 ± 0.2
PB <sub>63</sub> BDM <sub>17</sub> S	56,000	2.0	0.42 <sup>e</sup>	-0.81 ± 0.01	99.85 ± 0.08
PB <sub>64</sub> BDM <sub>36</sub> S	45,000	2.0	0.25 <sup>e</sup>	-4.94 ± 0.09	99.72 ± 0.12
PB <sub>54</sub> BDM <sub>46</sub> S	55,000	2.0	0.16 <sup>e</sup>	-5.0 ± 0.2	99.61 ± 0.08
PB <sub>44</sub> BDM <sub>56</sub> S	49,000	2.0	0.17	-2.17 ± 0.05	99.62 ± 0.09
PB <sub>20</sub> BDM <sub>80</sub> S	23,000	2.2	0.30 <sup>e</sup>	-0.170 ± 0.005	98.9 ± 0.2
PBDMS	34,000	2.4	0.31 <sup>e</sup>	-0.0234 ± 0.0005	99.89 ± 0.04
PBS+Hec	71,000	2.5			98.8 ± 0.2
PBSA+Hec	77,000	2.6		-3.7 ± 0.1	98.65 ± 0.07
PB <sub>64</sub> BDM <sub>36</sub> S+Hec	55,000	2.1		-3.4 ± 0.1	99.0 ± 0.3

<sup>a</sup>GPC (CHCl<sub>3</sub>, room temperature, PS standard). <sup>b</sup>Crystallinity index was calculated as the quotient of the crystalline area and total area from the XRD profiles (Figure S1). <sup>c</sup>Rates of enzymatic hydrolysis were calculated by the slope of the linear fit of each data set (Figures S2 and S16). <sup>d</sup>Residue mass of the polyester films without the addition of enzyme sampled after the last measuring point of each composition. <sup>e</sup>Data was taken from ref 21.

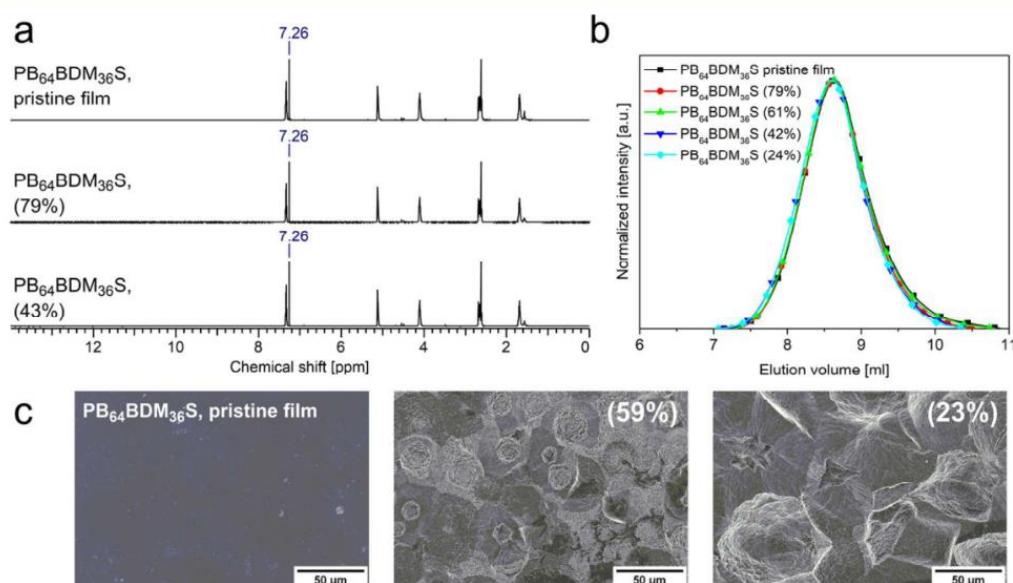


**Figure 2.** (a) <sup>1</sup>H NMR spectra, (b) GPC elution curves, and (c) SEM images of pristine PB<sub>64</sub>BDM<sub>36</sub>S films and at different stages of enzymatic hydrolysis (the residue mass is stated in parentheses) confirming the hydrolysis mechanism as surface erosion.

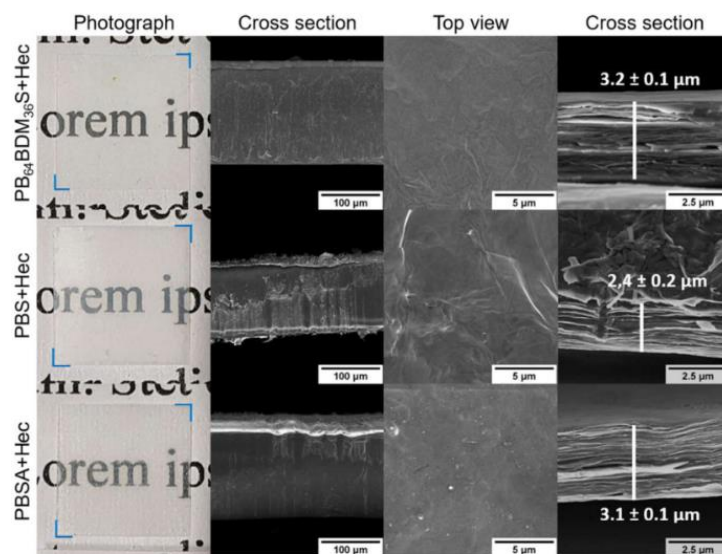


**Figure 3.** Photographs and SEM images of (top row)  $PB_{64}BDM_{36}S+Hec$ , (middle row)  $PBS+Hec$ , and (bottom row)  $PBSA+Hec$  showing from left to right pictures of the coated polyester films (10 mm  $\times$  10 mm) in front of the text (font: Times, font size: 12), the cross section of the films, a top view onto the Hec coatings, and the cross section of the coatings.

eroded structures with an absence of cavities penetrating into the bulk material (Figures 2c and S11). From these observations, a surface erosion mechanism was confirmed during the enzymatic hydrolysis for all synthesized samples, PBS, and PBSA.

For applications in food packaging, the gas barrier properties of the polymer films are of utmost importance since it is the most influential factor in determining the shelf life of the packaged item. Biodegradable polyesters generally do not provide a sufficient barrier to permeable gases like oxygen and thus require reinforcement to be relevant for long-term and shelf-stable packaging applications. Polymer barrier improvement can be achieved by adding impermeable filler materials due to the consequential elongation of the diffusion path (i.e., tortuous path) for permeates.<sup>28</sup> The synthetic sodium hectorite clay (Hec) has proven to be an excellent material for barrier reinforcement due to the single-layer nano silicate platelets that are spontaneously obtained upon immersion in water via osmotic swelling. The gentle nature of osmotic swelling allows for the preservation of the exceptional 20,000 aspect ratio inherent to the bulk material. Platelets in solution are wide enough so that their rotation is sterically hindered and are separated to distances large enough to accommodate polymer macromolecules.<sup>36</sup> In this work, we use glycol chitosan (GlyChit) as the nontoxic polymer matrix for Hec for barrier improvement.

Based on the enzymatic hydrolysis test results, we chose the composition  $PB_{64}BDM_{36}S$  to be coated with GlyChitHec because of its fast rate of enzymatic hydrolysis and mechanical properties close to low-density polyethylene.<sup>16</sup> PBS and PBSA films were also coated using the same conditions to serve as commercial reference materials. The GlyChitHec solution was prepared by combining an aqueous suspension of delaminated Hec and an aqueous solution of GlyChit in a 1:1 ratio. A fully automated spray coating setup was used to coat the substrates to promote superior nanocomposite texture for maximum barrier improvement.<sup>32</sup> After 80 spray cycles and sufficient

drying, the final coating thickness of the GlyChitHec nanocomposite was 3  $\mu\text{m}$ . SEM images of the cross section and coating surface of the coated  $PB_{64}BDM_{36}S$ , PBS, and PBSA films are reported in Figure 3, which demonstrates the coating uniformity. Because of the thin layer thickness, the GlyChitHec coating has just a minor effect on the optical properties of the coated films that maintain their high translucency (Figure 3).

The microstructure of the nanocomposite coating was evaluated with XRD (Figure S12). A nanocomposite with 50 wt % of Hec in GlyChit corresponds to 36 vol% of filler using densities of 2.7 and 1.5  $\text{g cm}^{-3}$  for Hec and GlyChit, respectively. For a 1D crystalline and translationally homogeneous nanocomposite with 36 vol % filler, we expect a basal spacing of 2.7 nm, which is indicated in Figure S12 with a dotted line. Reflections of the nanocomposite coatings on all substrates show a basal spacing within 0.05 nm of this expected value. Therefore, we confirm all nanocomposite coatings consist of a 1D crystalline, highly orientated, and intercalated structure with little to no segregated domains, as visible in the SEM images of the film cross sections provided in Figure 3 as well as in the inset of Figure S12. A basal spacing of 2.7 nm corresponds to a structure consisting of 0.96 nm thick Hec sheets separated by 1.8 nm of GlyChit volume. A polymer subjected to such confinement positively influences barrier properties of a nanocomposite due to reduced segment mobility, in addition to the tortuous path created by impermeable clay filler.<sup>33</sup> This confinement is also thought to be responsible for a hydrophobization effect observed in previous work with GlyChitHec nanocomposites that delayed the moisture-induced swelling of the polymer and consequential degradation of barrier performance with increasing humidity.<sup>19</sup> The GlyChitHec-coated samples were designated in this article with “+Hec” after the polymer name.

The GlyChitHec-coated films were thermally characterized by TGA and compared to the uncoated films (Table S2). After thermal degradation under synthetic air, the coated films show

F

<https://doi.org/10.1021/acscapm.2c01040>  
ACS Appl. Polym. Mater. XXXX, XXX, XXX–XXX

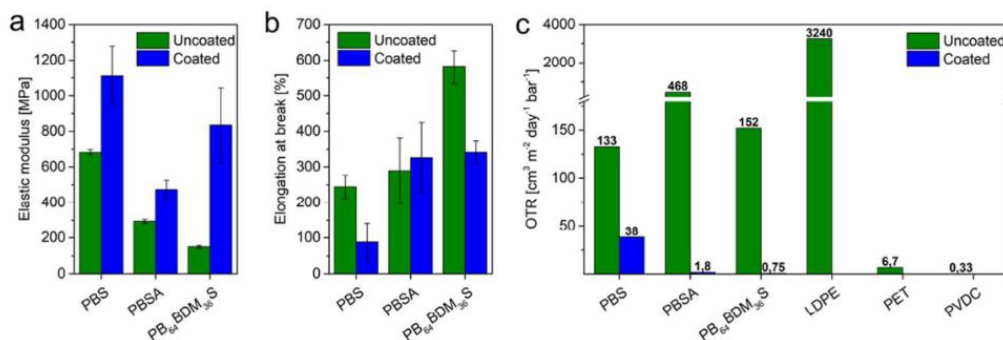


**Figure 4.** Statistical results of (a) elastic modulus and (b) elongation at break from the mechanical testing of the uncoated and coated PB<sub>64</sub>BDM<sub>36</sub>S, PBS and PBSA films. (c) Oxygen transmission rates (OTR) (65% RH, 23 °C) for polyester substrates, neat and with a 3 μm GlyChitHec coating. Values are compared to commercial films measured at 50% RH and 23 °C. Film thicknesses: PB<sub>64</sub>BDM<sub>36</sub>S, PBS, and PBSA ~150 ± 10 μm, LDPE ~54 μm,<sup>37</sup> PET ~100 μm,<sup>38</sup> PVDC ~100 μm.<sup>39</sup>

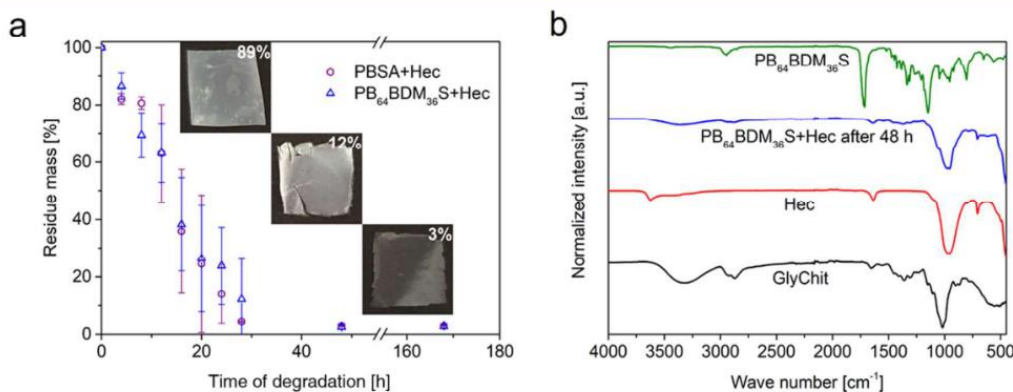


**Figure 5.** (a) Enzymatic hydrolysis of PB<sub>64</sub>BDM<sub>36</sub>S+Hec and PBSA+Hec films with esterase EL-01 (0.01 mg·mL<sup>-1</sup>) in phosphate-buffered solution (0.1 mol·L<sup>-1</sup>, pH = 7.40). The three photographs show PB<sub>64</sub>BDM<sub>36</sub>S+Hec films at different stages of the hydrolysis with the corresponding residue mass. (b) FTIR spectra of GlyChit, Hec, the remaining layer of PB<sub>64</sub>BDM<sub>36</sub>S+Hec after 48 h of enzymatic hydrolysis, and the pristine PB<sub>64</sub>BDM<sub>36</sub>S film.

a residue mass at 1100 °C ( $m_{1100}$ ) of approximately 2%, corresponding to the remaining Hec. The uncoated films showed no pertinent  $m_{1100}$ . Also, no relevant differences in onset temperature or curve progression could be observed between the pristine and coated polyesters (Figure S13). These results indicate that the GlyChitHec coating does not affect the thermal degradation behavior of the polyester substrates.

The melting and crystallization behavior was analyzed by DSC. No significant differences in the bulk material properties were observed regarding characteristic temperatures, enthalpies (Table S2), and curve progression (Figure S14) between uncoated and coated films. During DSC measurements, a cooling rate of 10 K/min is used, which is too fast to let PB<sub>64</sub>BDM<sub>36</sub>S crystallize. Therefore, in the second heating cycle, no melting peak was seen. Therefore, before using polyester films for any testing in this work, as mentioned in the experimental part, annealing was performed according to a previously published procedure.<sup>21</sup>

The mechanical performance of uncoated and coated polyester films was compared using uniaxial tensile testing. The elastic modulus and the elongation at break are shown in Figure 4a,b, the values are summarized in Table S3, and stress–strain curves are plotted in Figure S15. The elastic modulus of PB<sub>64</sub>BDM<sub>36</sub>S was increased after coating by 456%

to 834 ± 210 MPa. The polyester, even after coating, showed moderate tensile strength with a very high elongation of 342 ± 32% before breaking. The mechanical properties of PB<sub>64</sub>BDM<sub>36</sub>S (elastic modulus 150 ± 8 MPa, tensile strength 20 ± 2 MPa, elongation at break 581 ± 46%) were close to that of low-density polyethylene (LDPE, elastic modulus: 102–310 MPa, tensile strength: 9–15 MPa, elongation at break: 100–800%).<sup>16</sup>

Upon assessing the oxygen barrier performance of the films, the powerful effect of a highly ordered nanocomposite is evident (Figure 4c). In a previous publication, a neat coating of GlyChit on PLA reduced oxygen transmission rate (OTR) by 14 times at 33% relative humidity (RH), but this effect broke down once the humidity level rose above 50%.<sup>19</sup> For food packaging applications, even lower OTRs are required, and this barrier performance must be maintained at more relevant humidity levels (>50%). Therefore, barrier measurements for this work are measured at 23 °C and 65% RH, which is well above the moisture-induced swelling threshold for pure GlyChit.

The GlyChitHec coating reduced the OTR of PBSA by 260 times from 468 to 1.81 cm<sup>3</sup>·m<sup>-2</sup>·day<sup>-1</sup>·atm<sup>-1</sup> (Figure 4c). PB<sub>64</sub>BDM<sub>36</sub>S showed a similar reduction after coating by 202 times to the lowest OTR observed from all of the coated films of 0.75 cm<sup>3</sup>·m<sup>-2</sup>·day<sup>-1</sup>·atm<sup>-1</sup>. These oxygen barrier values

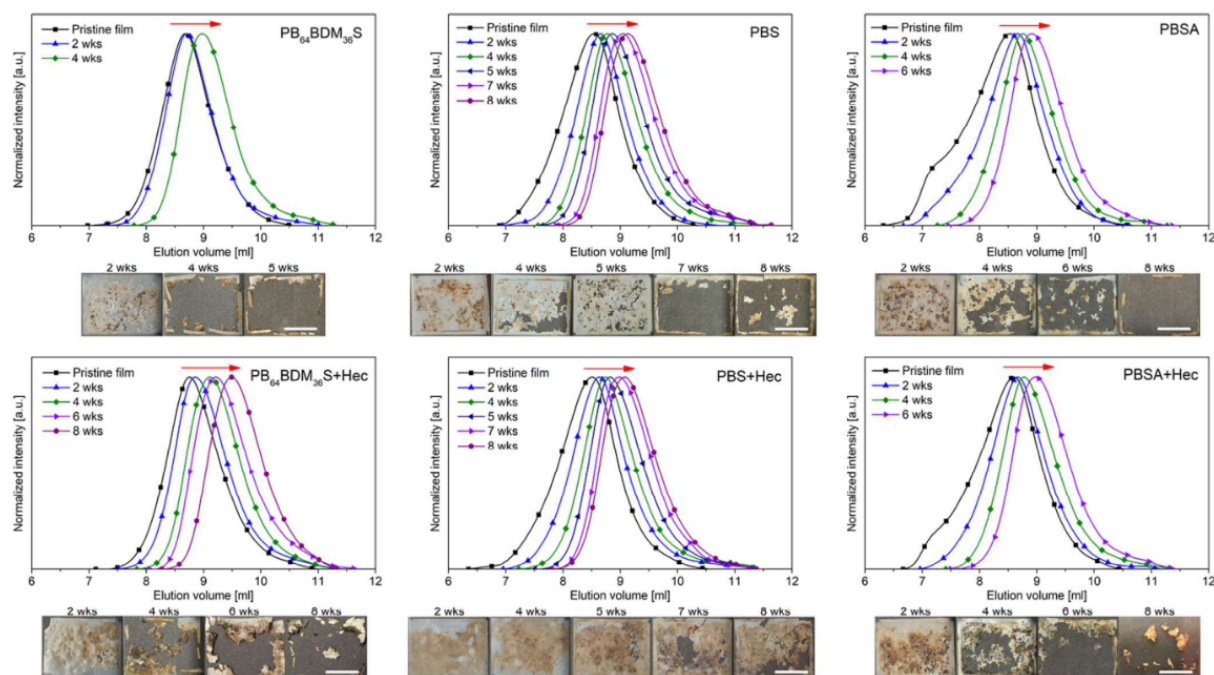


**Figure 6.** Elution curves of the (upper line) uncoated and (lower line) GlyChitHec-coated  $PB_{64}BDM_{36}S$ , PBS, and PBSA films, as well as photographs of the corresponding isolated films (white scale bar 10 mm) after different intervals of compost incubation.

outcompete the standard poly(ethylene terephthalate) (PET) and are competitive with the high-performing barrier material, poly(vinylidene chloride) (PVDC).<sup>40</sup> With the mechanical properties of  $PB_{64}BDM_{36}S$  competitive with LDPE, a comparison of their OTR shows that even before coating,  $PB_{64}BDM_{36}S$  is a much more suitable packaging material than LDPE. This translates to longer shelf life for food items packaged with  $PB_{64}BDM_{36}S$  compared to current LDPE films. When coated with GlyChitHec,  $PB_{64}BDM_{36}S$  could even be suitable for long-term food storage (e.g., vacuum-packed dry goods). GlyChitHec-coated  $PB_{64}BDM_{36}S$  provides a high-performance barrier to the film while maintaining its similar tensile strength and elongation at break compared to LDPE.

The residue mass recorded during enzymatic hydrolysis tests of GlyChitHec-coated  $PB_{64}BDM_{36}S$ , and PBSA films are plotted against the time in Figure 5a. These two substrates were chosen because of the fast enzymatic hydrolysis observed for the pristine films. There was no effect of the GlyChitHec coating on polyesters in terms of the completion of hydrolysis. A rate of enzymatic hydrolysis of  $-3.4 \pm 0.1\% \cdot h^{-1}$  was observed for the coated  $PB_{64}BDM_{36}S$  film and  $-3.7 \pm 0.1\% \cdot h^{-1}$  for the coated PBSA (Figure S16). Although these rates are slightly lower than for the uncoated  $PB_{64}BDM_{36}S$  and PBSA, the hydrolysis is still very fast and complete. The slightly decreased hydrolysis rate might be due to the reduction in the exposed polymer surface for the enzymatic attack as the GlyChitHec coating slows diffusion into the polymer substrate.

For both  $PB_{64}BDM_{36}S$  and PBSA, a residue mass of 2–3% was recorded after 2 and 7 days of the hydrolysis experiment. Figure 5a shows photographs of a  $PB_{64}BDM_{36}S$ +Hec film at an early stage (residue mass 89%), late stage (residue mass 12%), and the leftover GlyChitHec layer after 48 h of enzymatic hydrolysis (residue mass 3%). The undisintegrated fragments leftover after this testing period are confirmed using FTIR as

the GlyChitHec layer. Figure 5b compares the FTIR spectrum of the remaining solids from  $PB_{64}BDM_{36}S$ +Hec after 48 h of enzymatic hydrolysis with GlyChit, Hec, and pristine  $PB_{64}BDM_{36}S$ . The spectrum of the remaining solids shows a cumulative spectrum of GlyChit and Hec. Additionally, the absence of the prominent ester carbonyl stretching band at  $1713 \text{ cm}^{-1}$  confirms the complete hydrolysis of the polyester. Both polyesters showed no change in the GPC elution curves during hydrolysis (Figure S17). SEM images at different stages of the hydrolysis depicted a uniform erosion of the surface with an absence of any bulk penetrating cavities (Figure S18). No differences in the  $^1\text{H}$  NMR spectra could be determined between the pristine and eroded films (Figures S19 and S20). These observations confirm a surface erosion mechanism for the  $PB_{64}BDM_{36}S$ +Hec as well as PBSA+Hec.

The preliminary experiments also showed biodegradation in wastewater as studied using a combination of analytical methods (Figures S21 and S22). Although eroded surfaces were visible by SEM, degradation was very slow ( $\sim 1\%$  in 28 days; cellulose  $\sim 10\%$  in 28 days).

Under aerobic conditions, the biodegradation in industrial compost was tested for the uncoated, and GlyChitHec-coated  $PB_{64}BDM_{36}S$ , PBS, and PBSA films based on the standard test method DIN EN ISO 20200. A detailed description of the composting origin and the required analytics is given in the Supporting Information (Table S4, Figures S23–S27). The composting was performed at  $58 \pm 0.5 \text{ }^\circ\text{C}$  and  $50 \pm 5\%$  humidity for eight weeks. LDPE was used as a negative sample (Figure S27). Samples were taken in regular intervals, and the visually identified polymer pieces were isolated, cleaned, and dried. Gravimetric analysis of the degradation process was not performed, as manual isolation of degradation fragments is highly error-prone and impossible for very small pieces. In the later stages of the degradation test, it was especially difficult to

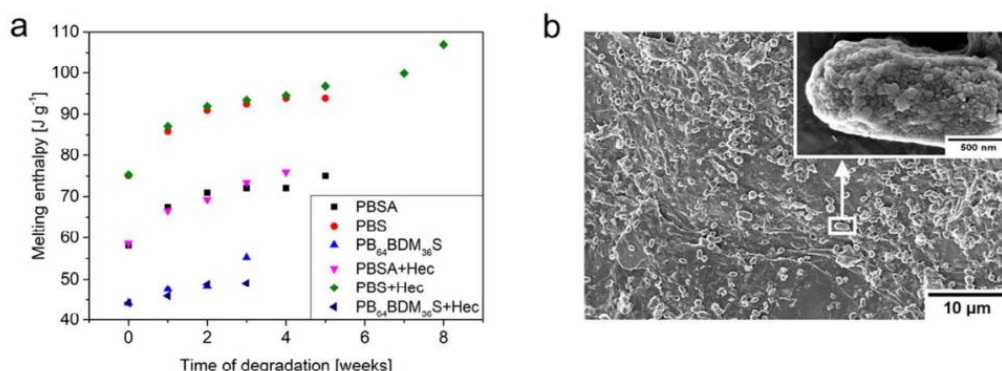


Figure 7. (a) Melting enthalpy of the uncoated and GlyChitHec-coated PB<sub>64</sub>BDM<sub>36</sub>S, PBS, and PBSA films at different stages of the composting experiment. (b) B<sub>64</sub>BDM<sub>36</sub>S+Hec film after 4 weeks of compost incubation. The polymer side is shown.

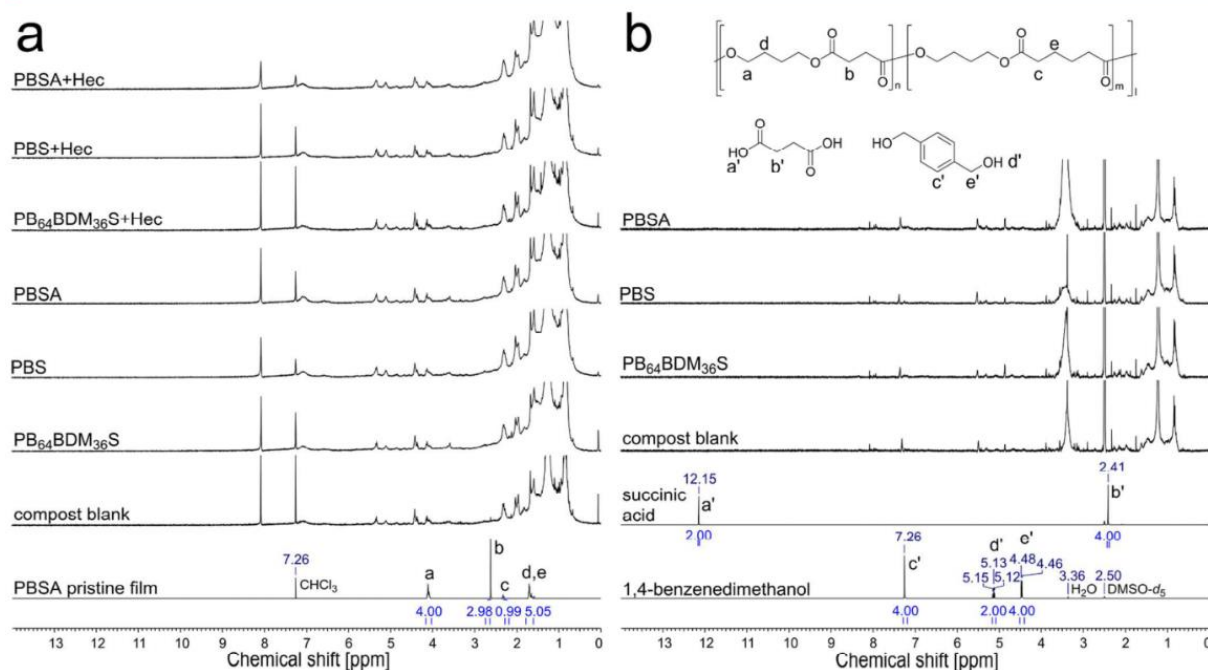


Figure 8. (a) <sup>1</sup>H NMR spectra (chloroform-*d*<sub>1</sub>) of the obtained residue after compost extraction with chloroform:methanol (9:1, v/v) of the uncoated and GlyChitHec-coated films after 8 weeks of thermophilic incubation. Additionally, the spectra of the pristine PBSA film are shown for comparison. (b) <sup>1</sup>H NMR spectra (dimethyl sulfoxide-*d*<sub>6</sub>) of the obtained residue after the second compost extraction with methanol of uncoated films after 8 weeks of thermophilic incubation. The spectra of succinic acid and 1,4-benzenedimethanol are shown for comparison.

make a clear differentiation between polymer, GlyChitHec, and components of the compost within a single isolated piece. Therefore, we relied on analytical techniques to follow the degradation of the films, given that polymer separation from inorganics was still possible. For the sample preparation of GPC measurements, the isolated pieces were mixed with chloroform overnight. While the polymer dissolved, the insoluble content could be separated by filtration through a 0.22 μm PTFE filter before injection. Figure 6 shows the GPC traces and images of the corresponding films that were isolated at different intervals of thermophilic incubation.

The decrease in molecular weight with progressing degradation time is observable for all compositions by the shift of the GPC traces to higher elution volumes. PB<sub>64</sub>BDM<sub>36</sub>S showed full fragmentation after 5 weeks. The

only remaining pieces were from the area sandwiched between the sample frame that had no direct contact with the compost. PBSA showed a full fragmentation within eight weeks, while fragments of PBS were still visible after the amount of same time. For PB<sub>64</sub>BDM<sub>36</sub>S+Hec and PBSA+Hec, only a few small fragments could be isolated after 8 weeks of compost incubation, while for PBS+Hec, the majority of the film was still visible. We hypothesize that the GlyChitHec layer supports the structural integrity of the polymer substrates and slows down the fragmentation of the bulk material. By taking the increase in the peak elution volumes, summarized in Table S5, as a sign of decreasing molar mass, we found that the GlyChitHec coating doesn't affect reductions in molar mass observed in the macroscopic bulk material.

Potential changes in crystallinity during composting were analyzed by DSC, and the melting enthalpies are reported in Figure 7a as a function of the composting time. The enthalpy increased for all compositions with increasing time of degradation. A significant influence of the coating on changes in the melting enthalpy over time was not observed. This data supports a mechanism involving fast degradation of the amorphous regions and fragmentation of the remaining highly crystalline domains. With the increasing time of thermophilic compost incubation, more and larger cavities were observed via SEM on the film surfaces that penetrate into the polymer bulk (Figure S28). Based on these observations, a bulk degradation mechanism under composting conditions was confirmed for all tested compositions.

SEM images reported in Figures 7b and S29 and S30 show the surface of the polyester films at different stages of thermophilic incubation, where the colonialization of microorganisms is visible. This colonialization was observed in all polymer samples and on both the polyester substrate and the nanocomposite coating surface, confirming the affinity of the polymer surface for microorganisms leading to biodegradation.

To confirm full biodegradation after eight weeks of thermophilic incubation, the compost was extracted with a mixture of chloroform and methanol (9:1, v/v) after the visible samples were removed. The extracted solid was analyzed via  $^1\text{H}$  NMR spectroscopy (Figure 8a). The spectra of the extracted compost where the uncoated and GlyChitHec-coated PB<sub>64</sub>BDM<sub>36</sub>S, PBS, and PBSA were incubated show very high accordance with the extracted compost blank sample. No traces of the polyesters or additional molecules were visible. This proves the complete and fast degradation of the polyesters once they have disintegrated into very small pieces. The compost samples were extracted a second time with methanol, in which succinic acid and 1,4-benzenedimethanol degradation products have sufficient solubility.  $^1\text{H}$  NMR spectra of the solid residue from this extraction for each polyester are compared to the spectra of a blank compost experiment, succinic acid, and 1,4-benzenedimethanol in Figure 8b. The spectra of the residue from compost extraction used for polymer incubation are equal to the compost blank and lack identifiable monomer signals. We can conclude that mono- or oligomers formed by the macromolecular chain scission could undergo bio-assimilation and mineralization by microorganisms and do not remain in the compost.

## CONCLUSIONS

The PB<sub>x</sub>BDM<sub>y</sub>S copolyester films showed composition-dependent enzymatic hydrolysis under controlled conditions. The fast and complete hydrolysis of some of the compositions, such as PB<sub>64</sub>BDM<sub>36</sub>S, even at very low enzyme concentrations was possible within one day (rates up to  $-5.0\% \cdot \text{h}^{-1}$ ). The selected polyester (PB<sub>64</sub>BDM<sub>36</sub>S) was completely degraded in industrial compost using the method prescribed in DIN EN ISO 20200 in less than 5 weeks. The commercial PBSA showed complete degradation under similar conditions after 8 weeks, while fragments of PBS were still visible after the same time. Mechanical properties in the same range as LDPE but much lower OTR value ( $152 \text{ cm}^3 \cdot \text{m}^{-2} \cdot \text{day}^{-1} \cdot \text{bar}^{-1}$ ) make the present polyester a degradable substitute to LDPE. Further, a 3  $\mu\text{m}$  thick GlyChitHec nanocomposite coating could decrease the OTR of PB<sub>64</sub>BDM<sub>36</sub>S more than 200 times to  $0.76 \text{ cm}^3 \cdot \text{m}^{-2} \cdot \text{day}^{-1} \cdot \text{bar}^{-1}$ , maintaining the good mechanical properties and optimum degradation time in compost (<8 weeks),

making this material suitable for high-performance food packaging.

## ASSOCIATED CONTENT

### Supporting Information

The Supporting Information is available free of charge at <https://pubs.acs.org/doi/10.1021/acsapm.2c01040>.

Molecular composition of the polyesters; XRD pattern of PBSA, PB<sub>44</sub>BDM<sub>56</sub>S, and the GlyChitHec coating; linear fits of the enzymatic hydrolysis; GPC traces, SEM images, and  $^1\text{H}$  NMR spectra of the enzymatically hydrolyzed polyesters; TGA, DSC, and mechanical data of the polyesters; biodegradation in wastewater, information, and analytics of the compost; and GPC peak elution volumes and SEM images of the composted polyesters (PDF)

## AUTHOR INFORMATION

### Corresponding Author

Seema Agarwal — *Macromolecular Chemistry II and Bavarian Polymer Institute, University of Bayreuth, 95447 Bayreuth, Germany*; [orcid.org/0000-0002-3174-3152](https://orcid.org/0000-0002-3174-3152); Email: [agarwal@uni-bayreuth.de](mailto:agarwal@uni-bayreuth.de)

### Authors

Elmar Sehl — *Macromolecular Chemistry II and Bavarian Polymer Institute, University of Bayreuth, 95447 Bayreuth, Germany*

Renee L. Timmins — *Inorganic Chemistry I and Bavarian Polymer Institute, University of Bayreuth, 95447 Bayreuth, Germany*

Dipannita Ghosh — *Macromolecular Chemistry II and Bavarian Polymer Institute, University of Bayreuth, 95447 Bayreuth, Germany*

Josef Breu — *Inorganic Chemistry I and Bavarian Polymer Institute, University of Bayreuth, 95447 Bayreuth, Germany*; [orcid.org/0000-0002-2547-3950](https://orcid.org/0000-0002-2547-3950)

Complete contact information is available at: <https://pubs.acs.org/doi/10.1021/acsapm.2c01040>

### Author Contributions

<sup>§</sup>E.S. and R.L.T. contributed equally to this work. The manuscript was written through contributions of all authors. All authors have given approval to the final version of the manuscript.

### Funding

This study was funded by the Deutsche Forschungsgemeinschaft (DFG, German Research Foundation)—SFB 1357—391977956.

### Notes

The authors declare no competing financial interest.

## ACKNOWLEDGMENTS

The authors acknowledge the Bavarian Polymer Institute (BPI) for the use of the infrastructure of the KeyLabs “Small Scale Polymer Processing” and “Electron and Optical Microscopy”. They thank Florian Puchler for synthesizing the synthetic hectorite, and Marco Schwarzmann for the SEM images. Furthermore, the authors thank Manfred Bauer and the composting plant Veolia Umweltservice Süd GmbH & Co. KG in Pegnitz for providing the compost. They also thank the

J

<https://doi.org/10.1021/acsapm.2c01040>  
ACS Appl. Polym. Mater. XXXX, XXX, XXX–XXX

wastewater treatment plant of the Stadtbauhof Bayreuth for providing activated wastewater.

## REFERENCES

- (1) Plastics Europe, Plastics - the Facts 2021. An analysis of European plastics production, demand and waste data. Plastics Europe, 2021. [https://plasticseurope.org/wp-content/uploads/2021/12/AF-Plastics-the-facts-2021\\_250122.pdf](https://plasticseurope.org/wp-content/uploads/2021/12/AF-Plastics-the-facts-2021_250122.pdf) (accessed July 20, 2022).
- (2) Agarwal, S. Biodegradable Polymers: Present Opportunities and Challenges in Providing a Microplastic-Free Environment. *Macromol. Chem. Phys.* **2020**, *221*, No. 2000017.
- (3) Millican, J. M.; Agarwal, S. Plastic Pollution: A Material Problem? *Macromolecules* **2021**, *54*, 4455–4469.
- (4) Akdogan, Z.; Guven, B. Microplastics in the environment: A critical review of current understanding and identification of future research needs. *Environ. Pollut.* **2019**, *254*, No. 113011.
- (5) Baldwin, A. K.; Corsi, S. R.; Mason, S. A. Plastic Debris in 29 Great Lakes Tributaries: Relations to Watershed Attributes and Hydrology. *Environ. Sci. Technol.* **2016**, *50*, 10377–10385.
- (6) Peeken, I.; Primpke, S.; Beyer, B.; Gütermann, J.; Katlein, C.; Krumpfen, T.; Bergmann, M.; Hehemann, L.; Gerdt, G. Arctic sea ice is an important temporal sink and means of transport for microplastic. *Nat. Commun.* **2018**, *9*, No. 1505.
- (7) Piehl, S.; Leibner, A.; Löder, M. G. J.; Dris, R.; Bogner, C.; Laforsch, C. Identification and quantification of macro- and microplastics on an agricultural farmland. *Sci. Rep.* **2018**, *8*, No. 17950.
- (8) Geyer, R.; Jambeck, J. R.; Law, K. L. Production, use, and fate of all plastics ever made. *Sci. Adv.* **2017**, *3*, No. e1700782.
- (9) Varghese, H.; Chandran, A. Triboelectric Nanogenerator from Used Surgical Face Mask and Waste Mylar Materials Aiding the Circular Economy. *ACS Appl. Mater. Interfaces* **2021**, *13*, 51132–51140.
- (10) Jin, K.; Banerji, A.; Kitto, D.; Bates, F. S.; Ellison, C. J. Mechanically Robust and Recyclable Cross-Linked Fibers from Melt Blown Anthracene-Functionalized Commodity Polymers. *ACS Appl. Mater. Interfaces* **2019**, *11*, 12863–12870.
- (11) Lau, W. W. Y.; Shiran, Y.; Bailey, R. M.; Cook, E.; Stuchtey, M. R.; Koskella, J.; Velis, C. A.; Godfrey, L.; Boucher, J.; Murphy, M. B.; Thompson, R. C.; Jankowska, E.; Castillo Castillo, A.; Pilditch, T. D.; Dixon, B.; Koerselman, L.; Kosior, E.; Favoino, E.; Gutberlet, J.; Baulch, S.; Atreya, M. E.; Fischer, D.; He, K. K.; Petit, M. M.; Sumaila, U. R.; Neil, E.; Bernhofen, M. V.; Lawrence, K.; Palardy, J. E. Evaluating scenarios toward zero plastic pollution. *Science* **2020**, *369*, 1455–1461.
- (12) Endres, H.-J.; Siebert-Raths, A. *Technische Biopolymere: Rahmenbedingungen, Marktsituation, Herstellung, Aufbau und Eigenschaften*, Hanser Verlag, 2009; p 188.
- (13) Bagheri, A. R.; Laforsch, C.; Greiner, A.; Agarwal, S. Fate of So-Called Biodegradable Polymers in Seawater and Freshwater. *Global Challenges* **2017**, *1*, No. 1700048.
- (14) Stloukal, P.; Pekařová, S.; Kalendová, A.; Mattausch, H.; Laske, S.; Holzer, C.; Chitu, L.; Bodner, S.; Maier, G.; Slouf, M.; Koutny, M. Kinetics and mechanism of the biodegradation of PLA/clay nanocomposites during thermophilic phase of composting process. *Waste Manage.* **2015**, *42*, 31–40.
- (15) Kalita, N. K.; Bhasney, S. M.; Mudenur, C.; Kalamdhad, A.; Katiyar, V. End-of-life evaluation and biodegradation of Poly(lactic acid) (PLA)/Polycaprolactone (PCL)/Microcrystalline cellulose (MCC) polyblends under composting conditions. *Chemosphere* **2020**, *247*, No. 125875.
- (16) Mark, J. E., Ed. *Polymer Data Handbook*, 2nd ed.; Oxford University Press, 2009.
- (17) Wu, S.; Zhang, Y.; Han, J.; Xie, Z.; Xu, J.; Guo, B. Copolymerization with Polyether Segments Improves the Mechanical Properties of Biodegradable Polyesters. *ACS Omega* **2017**, *2*, 2639–2648.
- (18) Kunioka, M.; Ninomiya, F.; Funabashi, M. Biodegradation of poly(butylene succinate) powder in a controlled compost at 58 °C evaluated by naturally-occurring carbon 14 amounts in evolved CO<sub>2</sub> based on the ISO 14855-2 method. *Int. J. Mol. Sci.* **2009**, *10*, 4267–4283.
- (19) Habel, C.; Schöttle, M.; Daab, M.; Eichstaedt, N. J.; Wagner, D.; Bakhshi, H.; Agarwal, S.; Horn, M. A.; Breu, J. High-Barrier, Biodegradable Food Packaging. *Macromol. Mater. Eng.* **2018**, *303*, No. 1800333.
- (20) Qi, R.; Jones, D. L.; Liu, Q.; Li, Z.; Yan, C. Field test on the biodegradation of poly(butylene adipate-co-terephthalate) based mulch films in soil. *Polym. Test.* **2021**, *93*, No. 107009.
- (21) Sehl, E.; Eger, E. M.; Himmelsbach, A.; Agarwal, S. Fast Hydrolyzable Constitutional Isomer of Poly(butylene terephthalate) and Its Copolyesters with 1,4-Butanediol. *ACS Appl. Polym. Mater.* **2021**, *3*, 6427–6436.
- (22) Yang, Y.-H.; Bolling, L.; Priolo, M. A.; Grunlan, J. C. Super gas barrier and selectivity of graphene oxide-polymer multilayer thin films. *Adv. Mater.* **2013**, *25*, 503–508.
- (23) Yu, J.; Ruengkajorn, K.; Crivoi, D.-G.; Chen, C.; Buffet, J.-C.; O'Hare, D. High gas barrier coating using non-toxic nanosheet dispersions for flexible food packaging film. *Nat. Commun.* **2019**, *10*, No. 2398.
- (24) Habel, C.; Tsurko, E. S.; Timmins, R. L.; Hutschreuther, J.; Kunz, R.; Schuchardt, D. D.; Rosenfeldt, S.; Altstädt, V.; Breu, J. Lightweight Ultra-High-Barrier Liners for Helium and Hydrogen. *ACS Nano* **2020**, *14*, 7018–7024.
- (25) Okamoto, K.; Sinha Ray, S.; Okamoto, M. New poly(butylene succinate)/layered silicate nanocomposites. II. Effect of organically modified layered silicates on structure, properties, melt rheology, and biodegradability. *J. Polym. Sci., Part B: Polym. Phys.* **2003**, *41*, 3160–3172.
- (26) Bartel, M.; Remde, H.; Bohn, A.; Ganster, J. Barrier properties of poly(lactic acid)/cloisite 30B composites and their relation between oxygen permeability and relative humidity. *J. Appl. Polym. Sci.* **2017**, *134*, No. 44424.
- (27) Li, F.; Zhang, C.; Weng, Y. Improvement of the Gas Barrier Properties of PLA/OMMT Films by Regulating the Interlayer Spacing of OMMT and the Crystallinity of PLA. *ACS Omega* **2020**, *5*, 18675–18684.
- (28) Cussler, E. L.; Hughes, S. E.; Ward, W. J.; Aris, R. Barrier membranes. *J. Membr. Sci.* **1988**, *38*, 161–174.
- (29) Svagan, A. J.; Åkesson, A.; Cárdenas, M.; Bulut, S.; Knudsen, J. C.; Risbo, J.; Plackett, D. Transparent films based on PLA and montmorillonite with tunable oxygen barrier properties. *Biomacromolecules* **2012**, *13*, 397–405.
- (30) Priolo, M. A.; Gamboa, D.; Holder, K. M.; Grunlan, J. C. Super gas barrier of transparent polymer-clay multilayer ultrathin films. *Nano Lett.* **2010**, *10*, 4970–4974.
- (31) Hagen, D. A.; Box, C.; Greenlee, S.; Xiang, F.; Regev, O.; Grunlan, J. C. High gas barrier imparted by similarly charged multilayers in nanobrick wall thin films. *RSC Adv.* **2014**, *4*, 18354–18359.
- (32) Tsurko, E. S.; Feicht, P.; Nehm, F.; Ament, K.; Rosenfeldt, S.; Pietsch, I.; Roschmann, K.; Kalo, H.; Breu, J. Large Scale Self-Assembly of Smectic Nanocomposite Films by Doctor Blading versus Spray Coating: Impact of Crystal Quality on Barrier Properties. *Macromolecules* **2017**, *50*, 4344–4350.
- (33) Schilling, T.; Habel, C.; Rosenfeldt, S.; Röhr, M.; Breu, J. Impact of Ultraconfinement on Composite Barriers. *ACS Appl. Polym. Mater.* **2020**, *2*, 3010–3015.
- (34) Kalo, H.; Möller, M. W.; Ziadeh, M.; Dolejš, D.; Breu, J. Large scale melt synthesis in an open crucible of Na-fluorohectorite with superb charge homogeneity and particle size. *Appl. Clay Sci.* **2010**, *48*, 39–45.
- (35) Maheshwari, R.; Bharadwaj, G.; Bhat, M. K. Thermophilic fungi: their physiology and enzymes. *Microbiol. Mol. Biol. Rev.* **2000**, *64*, 461–488.
- (36) Stöter, M.; Kunz, D. A.; Schmidt, M.; Hirsemann, D.; Kalo, H.; Putz, B.; Senker, J.; Breu, J. Nanoplatelets of sodium hectorite

showing aspect ratios of  $\approx 20,000$  and superior purity. *Langmuir* **2013**, *29*, 1280–1285.

(37) Hong, S.-I.; Krochta, J. M. Whey protein isolate coating on LDPE film as a novel oxygen barrier in the composite structure. *Packag. Technol. Sci.* **2004**, *17*, 13–21.

(38) Müller, K. Faster results, permeation measurement of films. *Kunststoffe Int.* **2011**, *101*, 62–67.

(39) Mohr, J. M.; Paul, D. R. Comparison of gas permeation in vinyl and vinylidene polymers. *J. Appl. Polym. Sci.* **1991**, *42*, 1711–1720.

(40) Lange, J.; Wyser, Y. Recent innovations in barrier technologies for plastic packaging – a review. *Packag. Technol. Sci.* **2003**, *16*, 149–158.

Supporting Information

Stretchable and Fast Composting Polyester  
Films with High Performance Barrier

*Elmar Sehl<sup>†</sup>, Renee L. Timmins<sup>‡</sup>, Dipannita Ghosh<sup>†</sup>, Josef Breu<sup>‡</sup>, Seema Agarwal<sup>†\*</sup>*

<sup>†</sup>Macromolecular Chemistry II and Bavarian Polymer Institute, University of Bayreuth,  
Universitätsstraße 30, 95447 Bayreuth, Germany

<sup>‡</sup>Inorganic Chemistry I and Bavarian Polymer Institute, University of Bayreuth,  
Universitätsstraße 30, 95447 Bayreuth, Germany.

**Corresponding Author**

\*E-mail: agarwal@uni-bayreuth.de

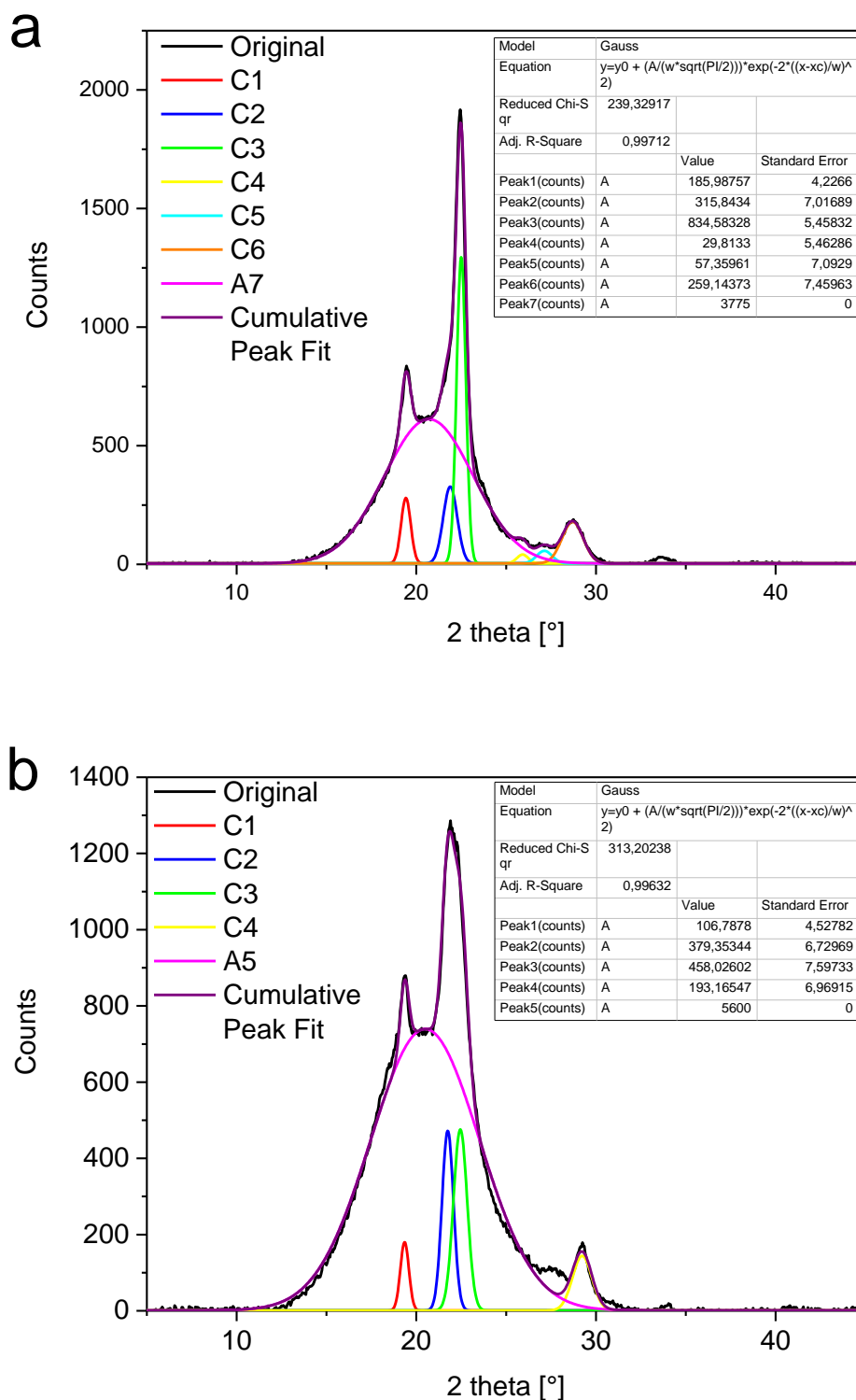


**Figure S1.** Nonlinear multiple peak fit of the XRD patterns of (a) PBSA and (b) PB<sub>44</sub>BDM<sub>56</sub>S using the program Origin Pro 9.1 (Gaussian method). Peak numbering for crystalline peaks starting at small angles.

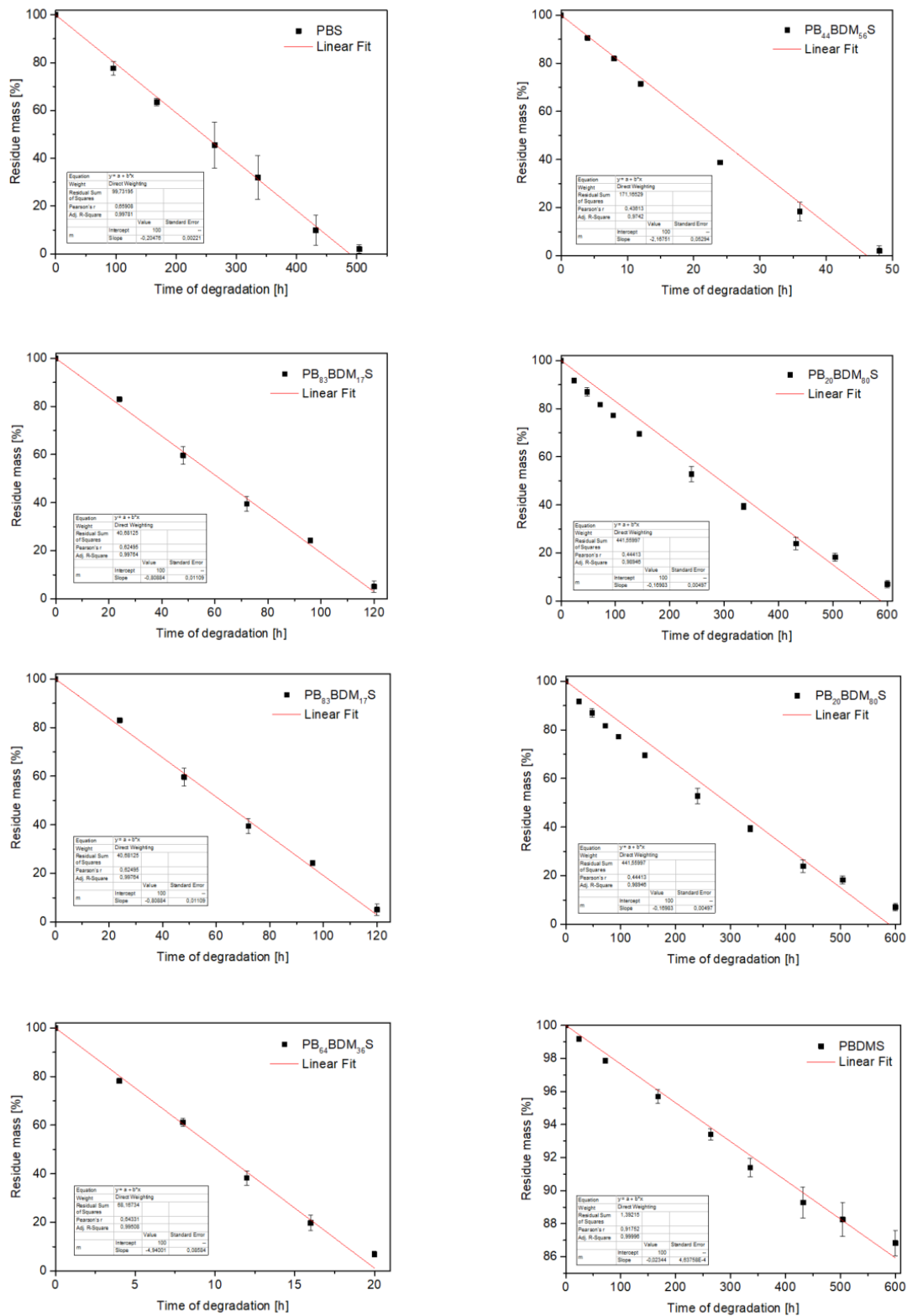
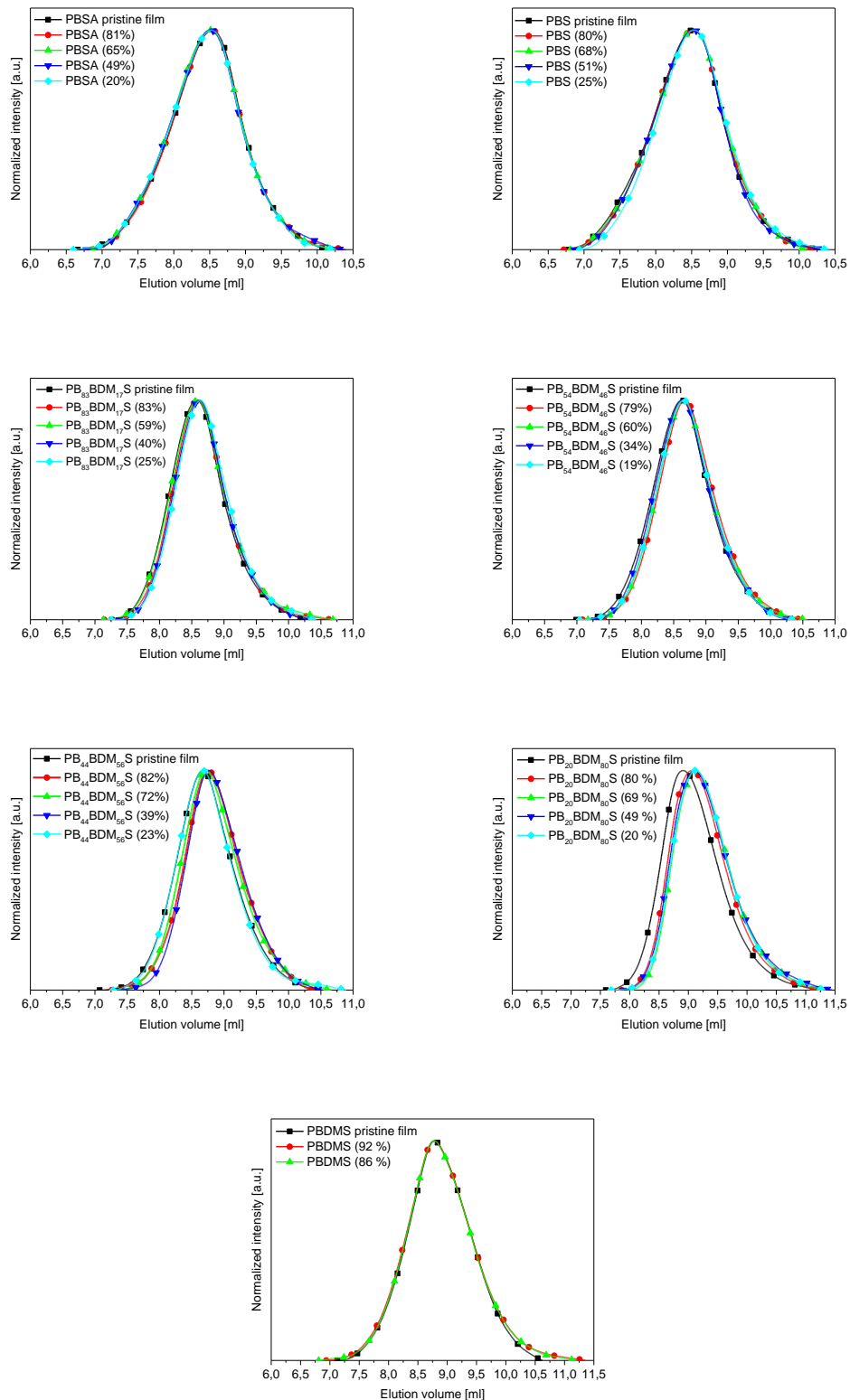
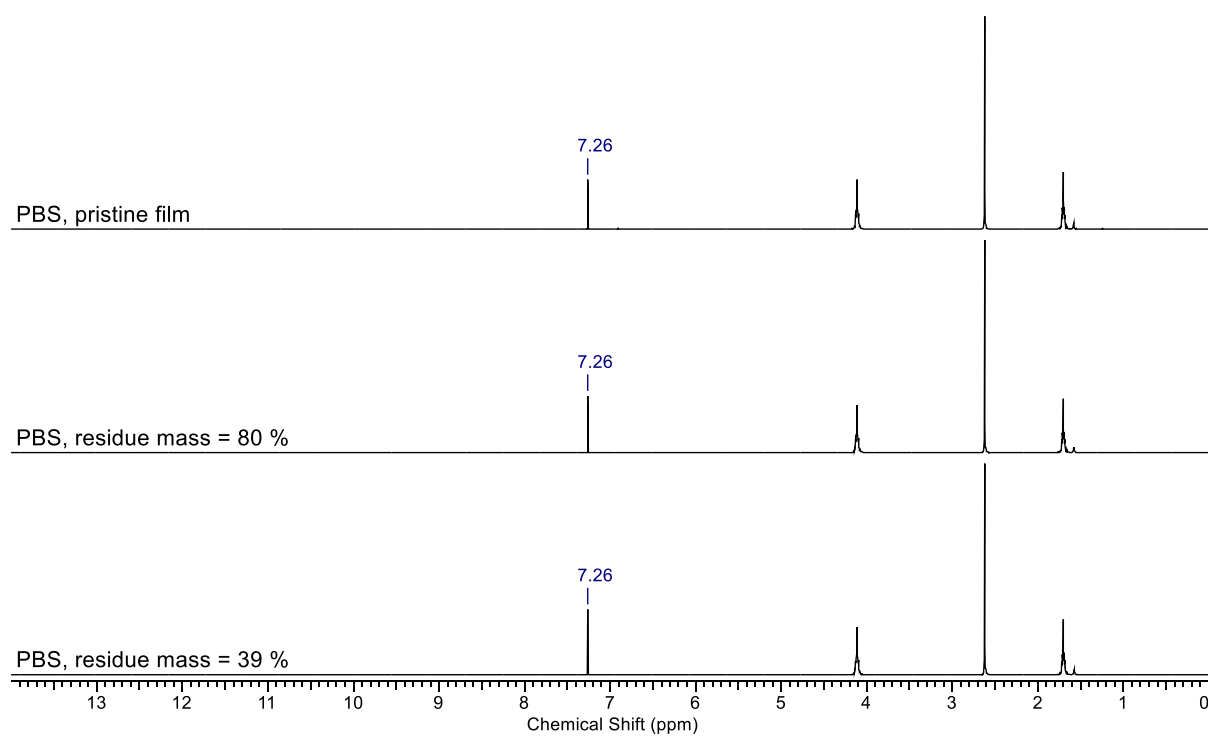


Figure S2. Rate determination of enzymatic hydrolysis of the uncoated polyester films.



**Figure S3:** Normalized elution volumes of the polyester films PBSA, PBS, PB<sub>x</sub>BDM<sub>y</sub>S, and PBDMS, taken at different intervals of the enzymatic degradation (CHCl<sub>3</sub>, 23 °C, PS-standard). Residue mass of the measured films is stated in parenthesis.



**Figure S4.** <sup>1</sup>H NMR spectra of pristine films and films at different stages of the enzymatic hydrolysis of PBS.

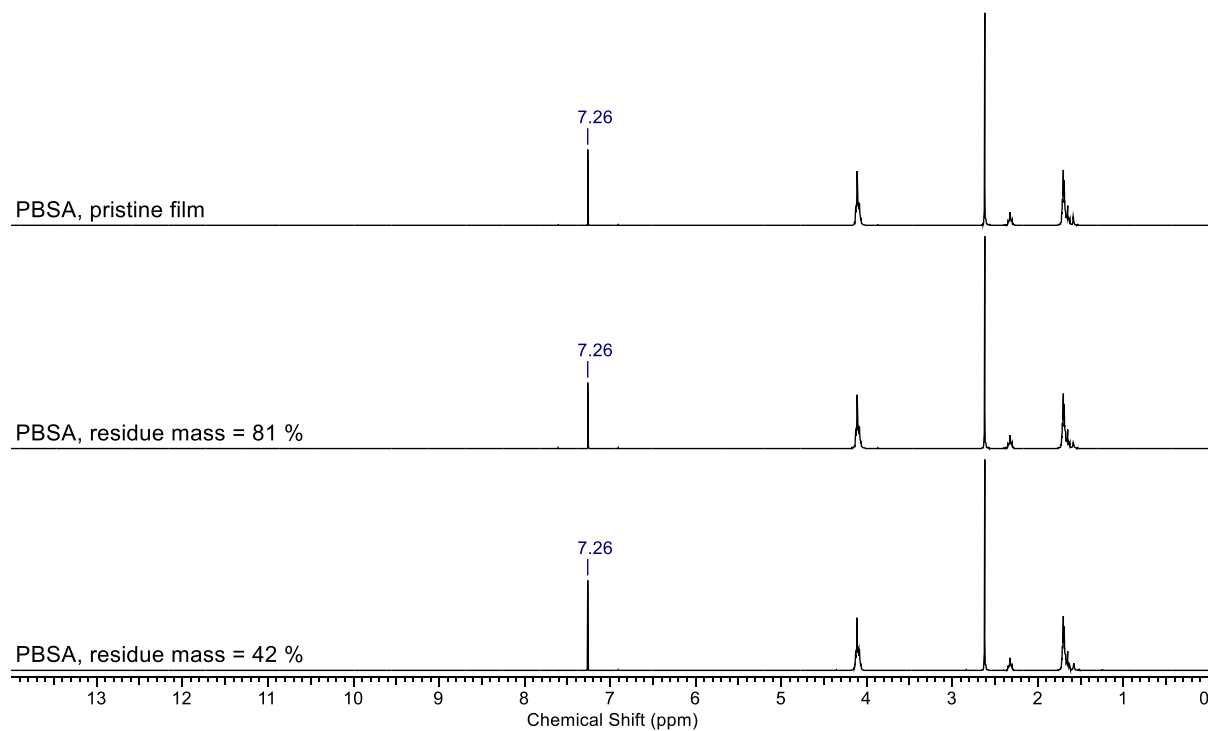


**Figure S5.** <sup>1</sup>H NMR spectra of pristine films and films at different stages of the enzymatic hydrolysis of PBSA.

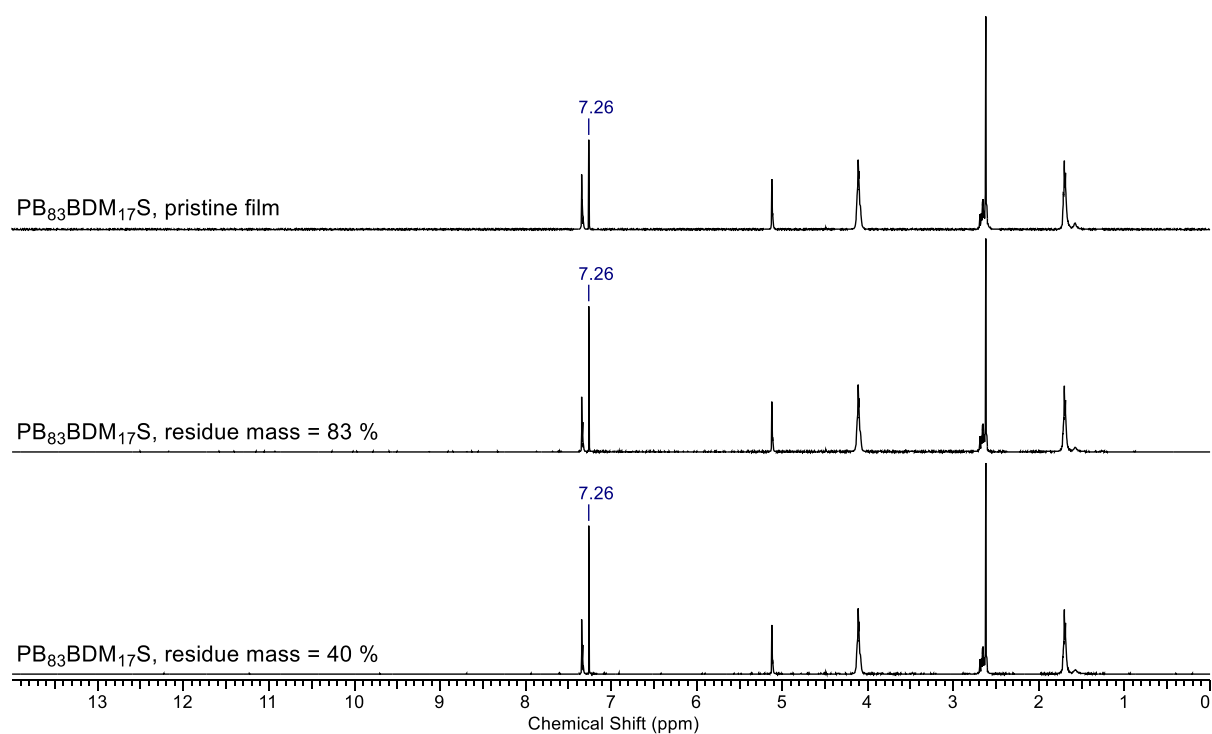


**Figure S6.**  $^1\text{H}$  NMR spectra of pristine films and films at different stages of the enzymatic hydrolysis of  $\text{PB}_{83}\text{BDM}_{17}\text{S}$ .

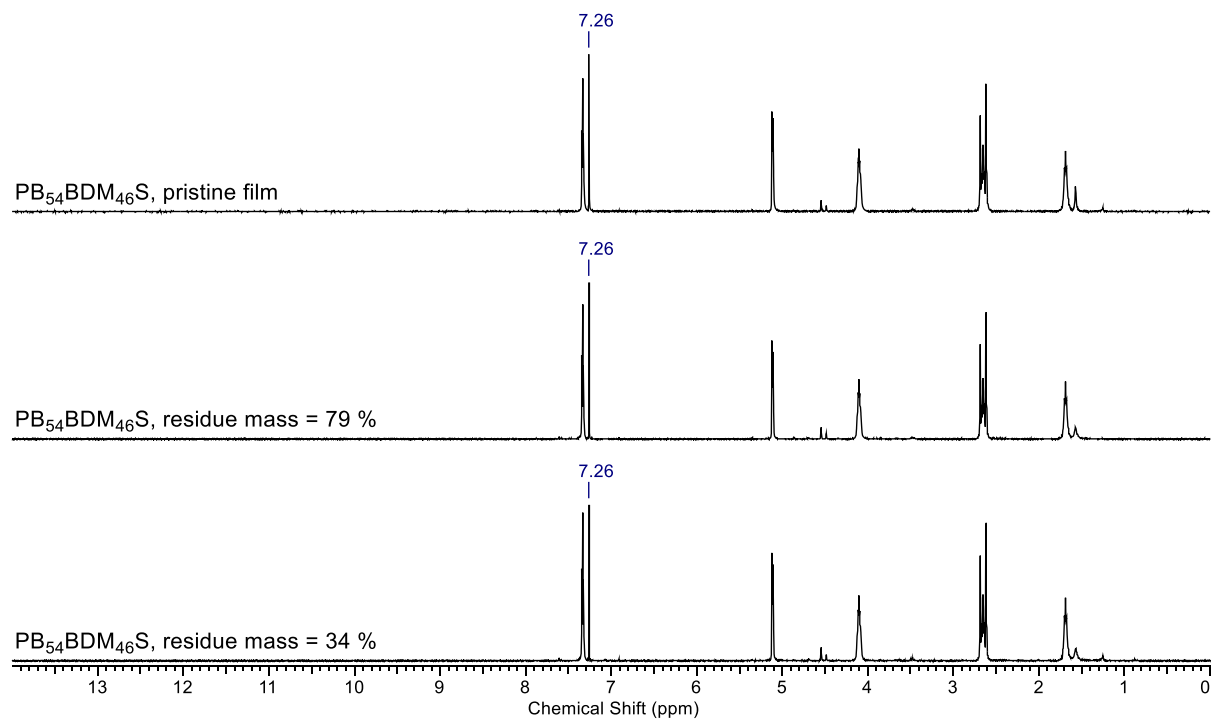


**Figure S7.**  $^1\text{H}$  NMR spectra of pristine films and films at different stages of the enzymatic hydrolysis of  $\text{PB}_{54}\text{BDM}_{46}\text{S}$ .

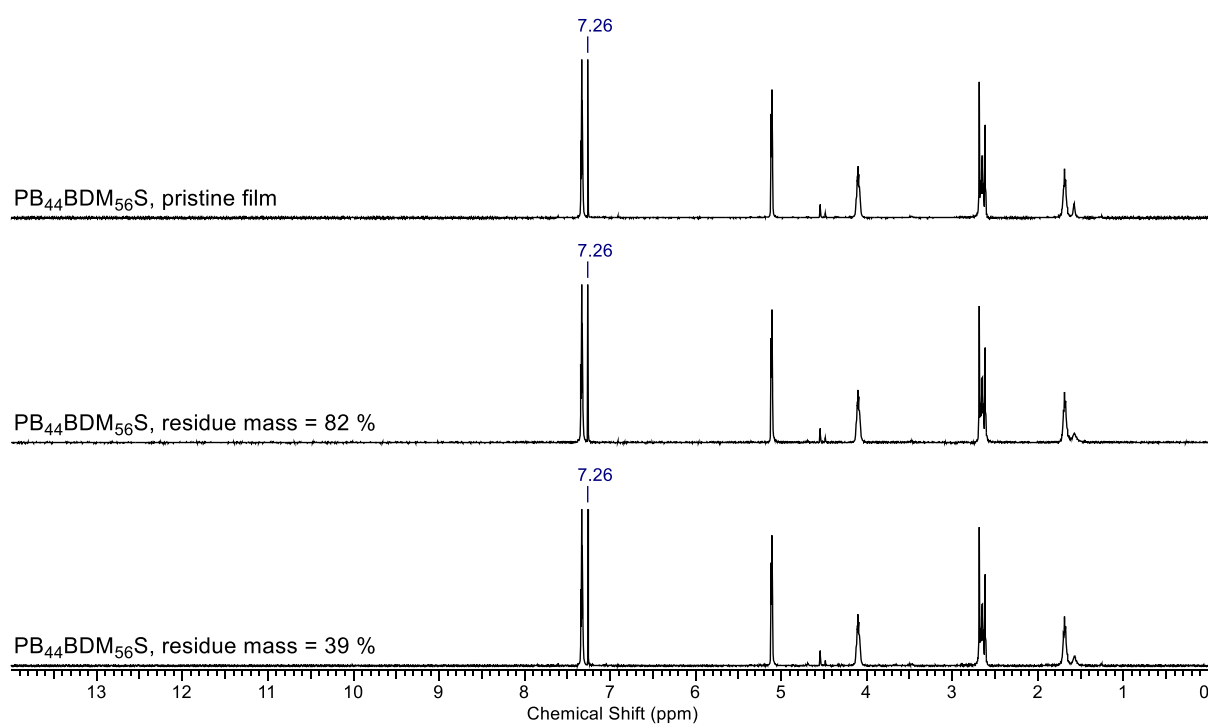


**Figure S8.**  $^1\text{H}$  NMR spectra of pristine films and films at different stages of the enzymatic hydrolysis of  $\text{PB}_{44}\text{BDM}_{56}\text{S}$ .

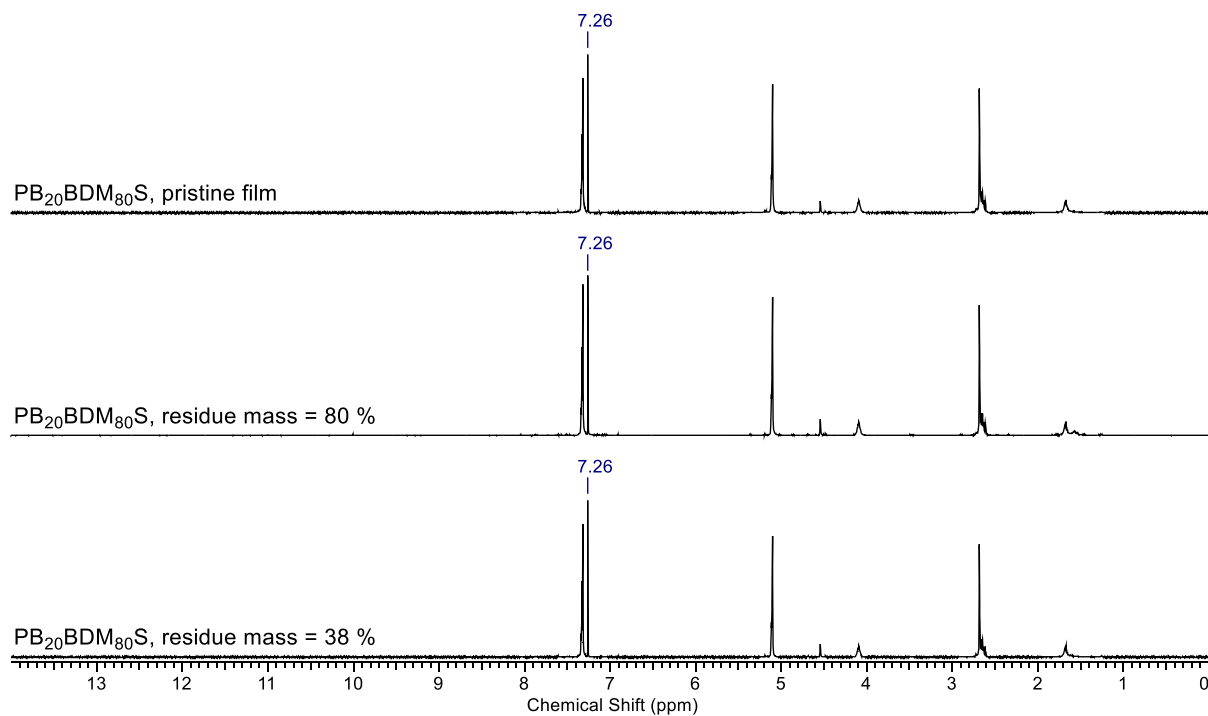


**Figure S9.**  $^1\text{H}$  NMR spectra of pristine films and films at different stages of the enzymatic hydrolysis of  $\text{PB}_{20}\text{BDM}_{80}\text{S}$ .

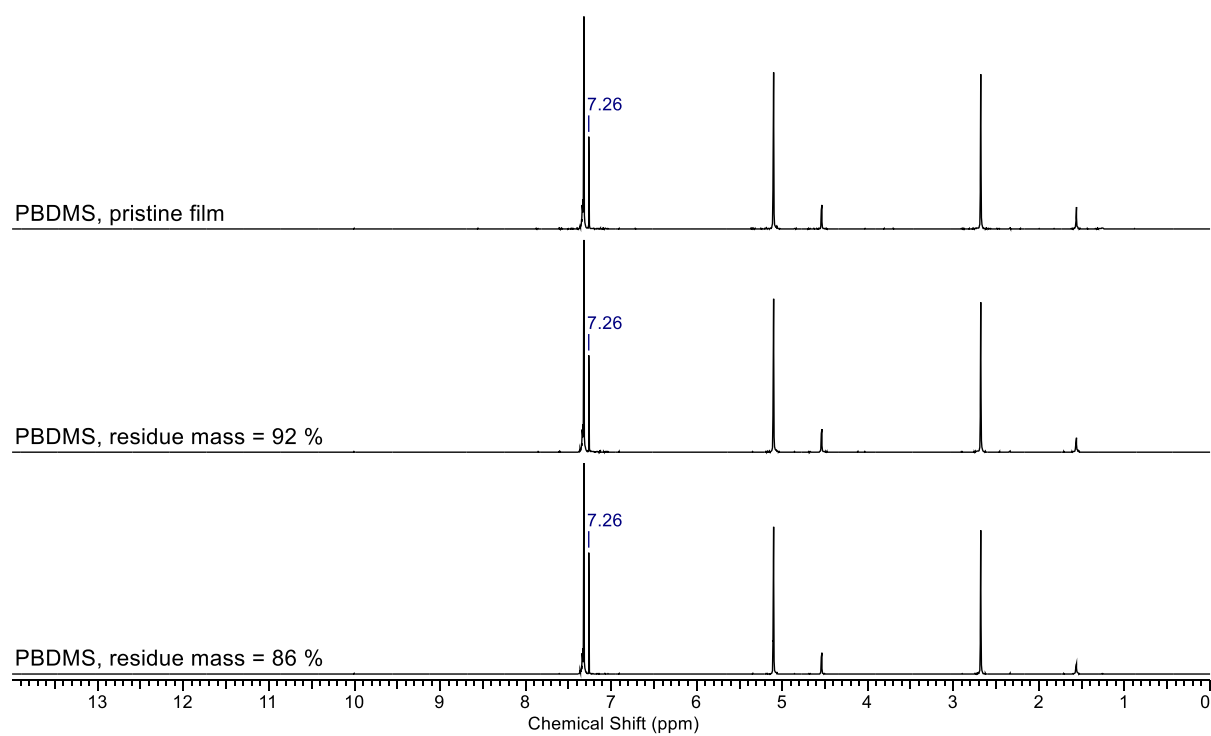


**Figure S10.**  $^1\text{H}$  NMR spectra of pristine films and films at different stages of the enzymatic hydrolysis of  $\text{PB}_{44}\text{BDM}_{56}\text{S}$ .

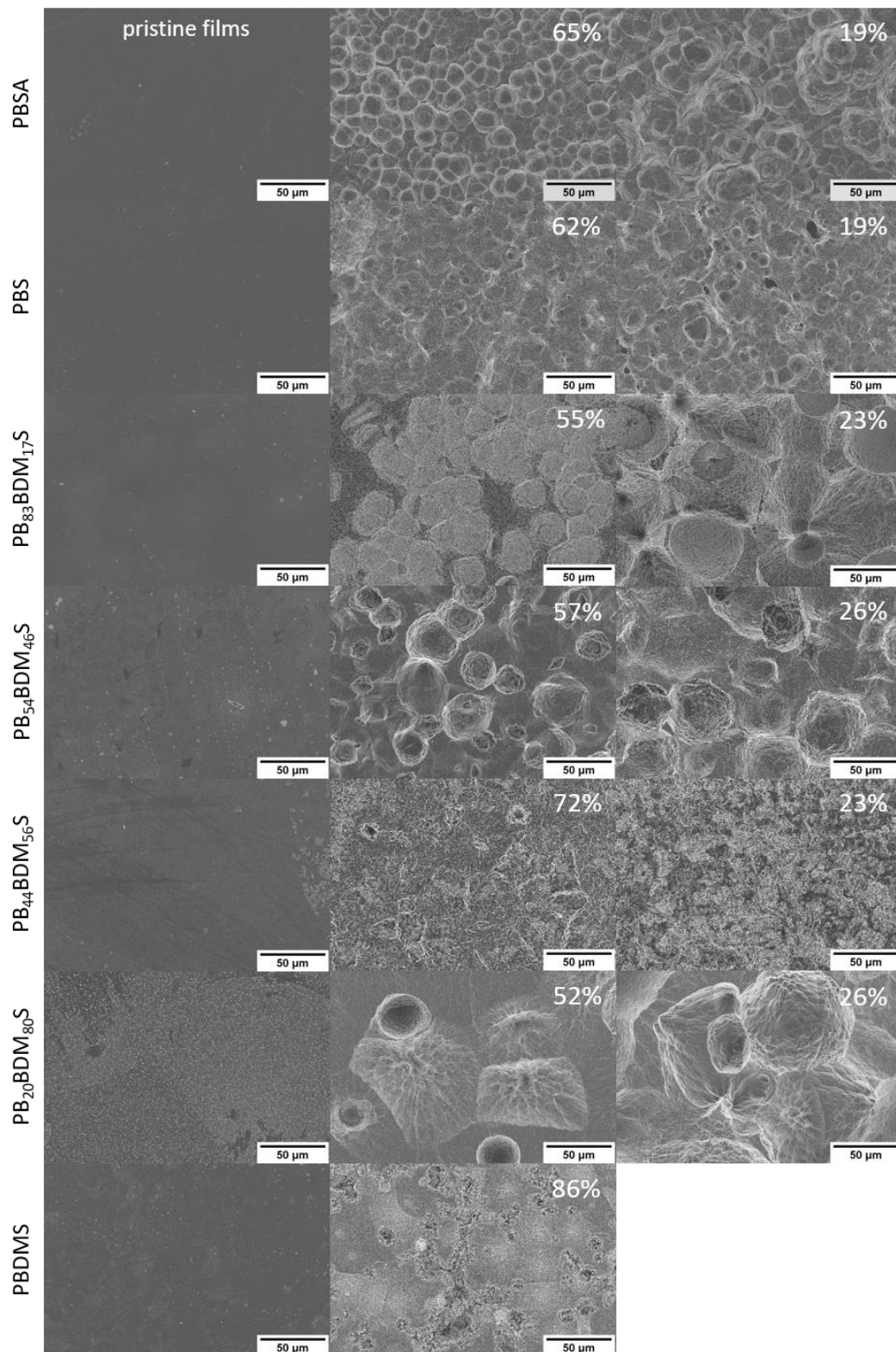


**Figure S11.** SEM images of the pristine (1<sup>st</sup> column) and eroded films of uncoated PB<sub>x</sub>BDM<sub>y</sub>S, PBDMS, PBS and PBSA before and at different intervals of the enzymatic hydrolysis. Residual mass of the measured film is stated in each image. The scale bar is 50 μm.

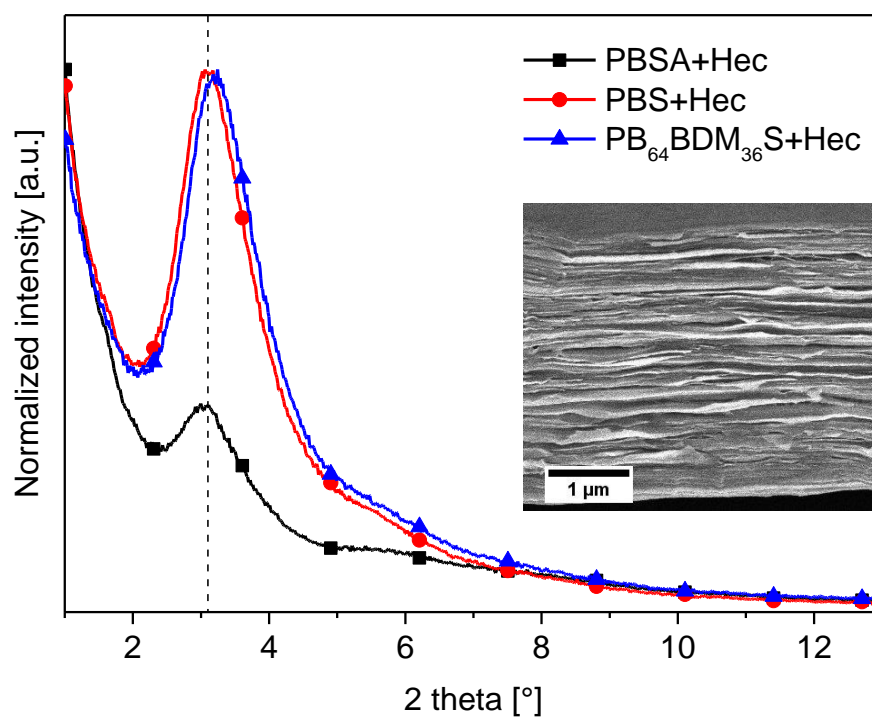


**Figure S12.** XRD of the GlyChitHec coating on PB<sub>64</sub>BDM<sub>36</sub>S, PBS and PBSA.

**Table S1.** TGA and DSC data of pristine and Hec coated PB<sub>64</sub>BDM<sub>36</sub>S, PBS and PBSA.

polyester	TGA			DSC					
	synthetic air			1 <sup>st</sup> heating <sup>d</sup>		cooling <sup>d</sup>		2 <sup>nd</sup> heating <sup>d</sup>	
	$T_{\text{onset}}^{\text{a}}$	$m_{1100}^{\text{b}}$	$T_{\text{g}}^{\text{c}}$	$T_{\text{m}}$	$\Delta H_{\text{m}}$	$T_{\text{c}}$	$\Delta H_{\text{c}}$	$T_{\text{m}}$	$\Delta H_{\text{m}}$
	[°C]	[%]	[°C]	[°C]	[J·g <sup>-1</sup> ]	[°C]	[J·g <sup>-1</sup> ]	[°C]	[J·g <sup>-1</sup> ]
PBS	369	-0.14	-32	115	75 <sup>e</sup>	74	-66	114	75 <sup>f</sup>
PBSA	366	-0.05	-45	88	59	43	-46	87	57
PB <sub>64</sub> BDM <sub>36</sub> S	354	0.01	-21	43/68	45	-	-	-	-
PBS+Hec	368	1.68	-32	117	74 <sup>g</sup>	74	-63	115	73 <sup>h</sup>
PBSA+Hec	372	2.23	-45	87	58	42	-48	87	58
PB <sub>64</sub> BDM <sub>36</sub> S+Hec	355	1.99	-21	43/70	44	-	-	-	-

<sup>a</sup> $T_{\text{onset}}$  is the extrapolated onset temperature according to ISO 11358-1. <sup>b</sup>Residue mass at 1100 °C. <sup>c</sup>Glass transition temperature taken from 2<sup>nd</sup> heating cycle at a rate of 10 K·min<sup>-1</sup>. <sup>d</sup>Melting temperature ( $T_{\text{m}}$ ), crystallization temperature ( $T_{\text{c}}$ ), melting enthalpy ( $\Delta H_{\text{m}}$ ) and crystallization enthalpy ( $\Delta H_{\text{c}}$ ) at a rate of  $\pm 10$  K·min<sup>-1</sup>. <sup>e</sup> $\Delta H_{\text{c}} = -9$  J·g<sup>-1</sup> was added to  $\Delta H_{\text{m}}$  ( $T_{\text{c}} = 91$  °C). <sup>f</sup> $\Delta H_{\text{c}} = -7$  J·g<sup>-1</sup> was added to  $\Delta H_{\text{m}}$  ( $T_{\text{c}} = 99$  °C). <sup>g</sup> $\Delta H_{\text{c}} = -6$  J·g<sup>-1</sup> was added to  $\Delta H_{\text{m}}$  ( $T_{\text{c}} = 92$  °C). <sup>h</sup> $\Delta H_{\text{c}} = -2$  J·g<sup>-1</sup> was added to  $\Delta H_{\text{m}}$  ( $T_{\text{c}} = 99$  °C).

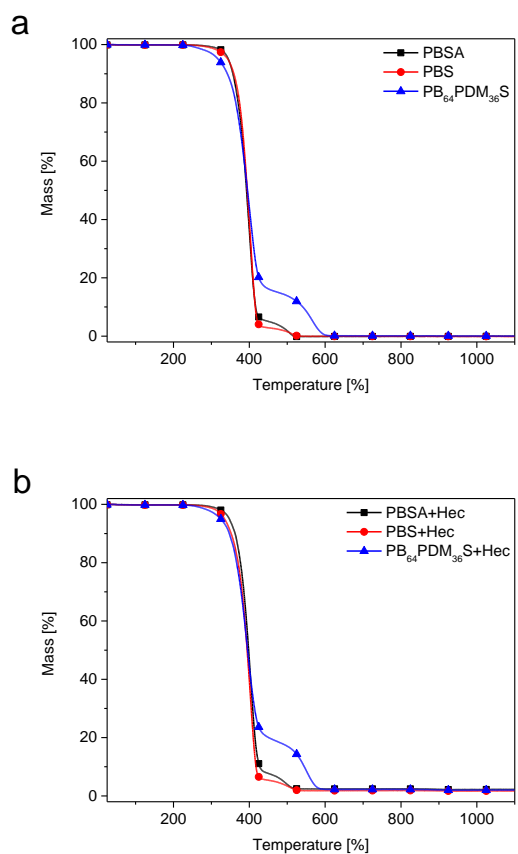


**Figure S13.** TGA curves of PBSA, PBS and  $PB_{64}BDM_{36}S$  films (a) uncoated and (b) Hec coated under synthetic air.

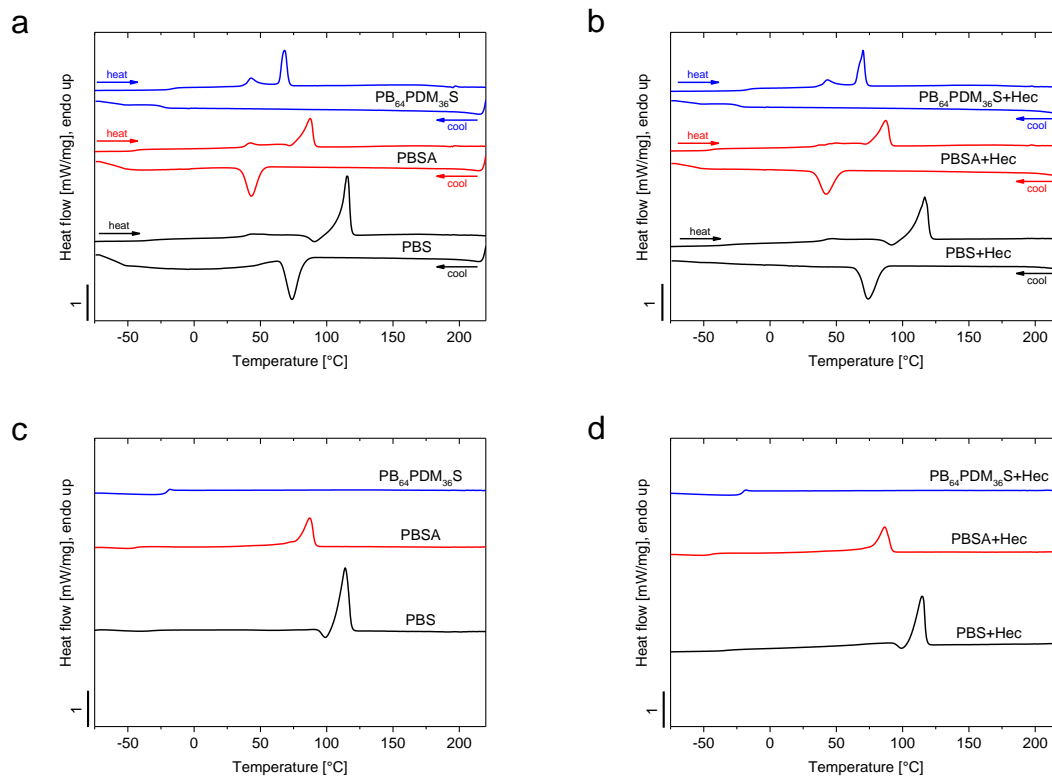


**Figure S14.** DSC curves of the uncoated and GlyChitHec coated polyesters films of PB<sub>64</sub>BDM<sub>36</sub>S, PBSA, and PBS showing (a,b) the 1<sup>st</sup> heating and cooling curve and (c,d) the 2<sup>nd</sup> cooling curve.

**Table S2.** Mechanical properties of the uncoated and hectorite coated PB<sub>64</sub>BDM<sub>36</sub>S, PBS and PBSA.

polyester	elastic modulus [MPa]	tensile strength [MPa]	elongation at break [%]
PBS <sup>a</sup>	683 ± 15	37 ± 3	244 ± 33
PBSA <sup>a</sup>	295 ± 11	20 ± 2	290 ± 92
PB <sub>64</sub> BDM <sub>36</sub> S <sup>a</sup>	150 ± 8	20 ± 2	581 ± 46
PBS+Hec	1110 ± 168	28 ± 1	88 ± 54
PBSA+Hec	474 ± 52	19 ± 3	326 ± 98
PB <sub>64</sub> BDM <sub>36</sub> S+Hec	834 ± 210	15 ± 1	342 ± 32

<sup>a</sup>Values from reference.<sup>1</sup>

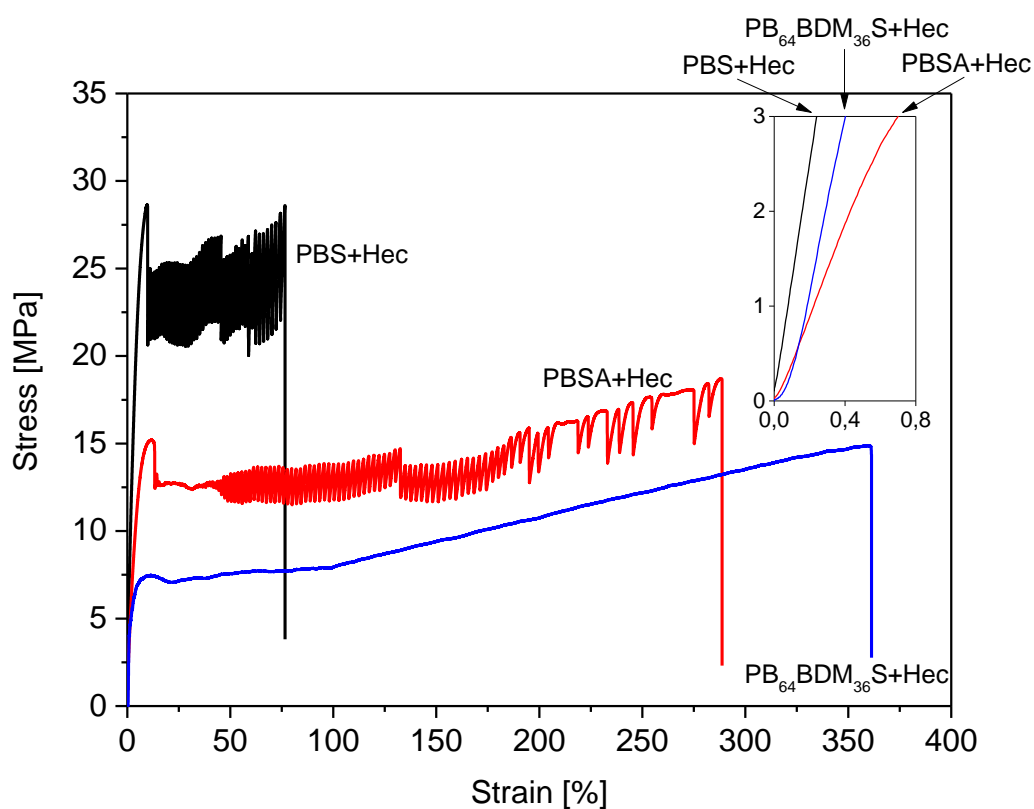


**Figure S15.** Stress-strain curve of the hectorite coated polyester films. The phenomenon of the sawtooth type curve of PBS and PBSA is described in the literature.<sup>1</sup>

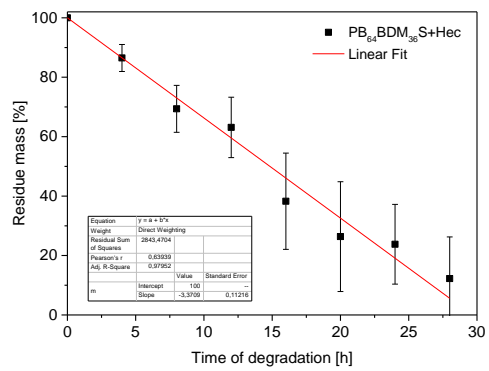
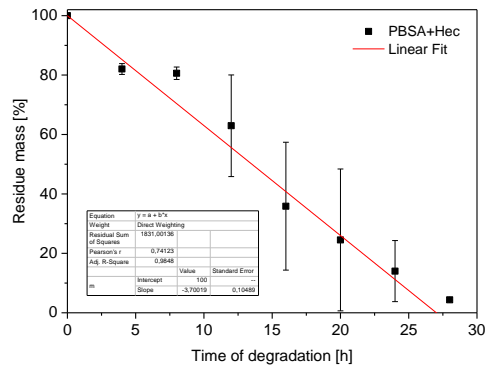


**Figure S16.** Rate determination of enzymatic hydrolysis of the coated polyester films.

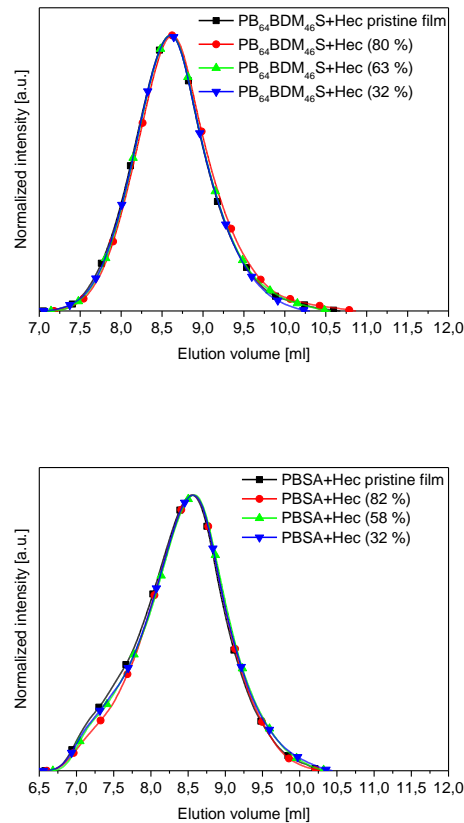


**Figure S17.** Normalized elution volumes of the hectorite coated polyester films PB<sub>64</sub>BDM<sub>36</sub>S+Hec and PBSA+Hec taken at different intervals of the enzymatic degradation (CHCl<sub>3</sub>, 23 °C, PS-standard). Residue mass of the measured films is stated in parenthesis.

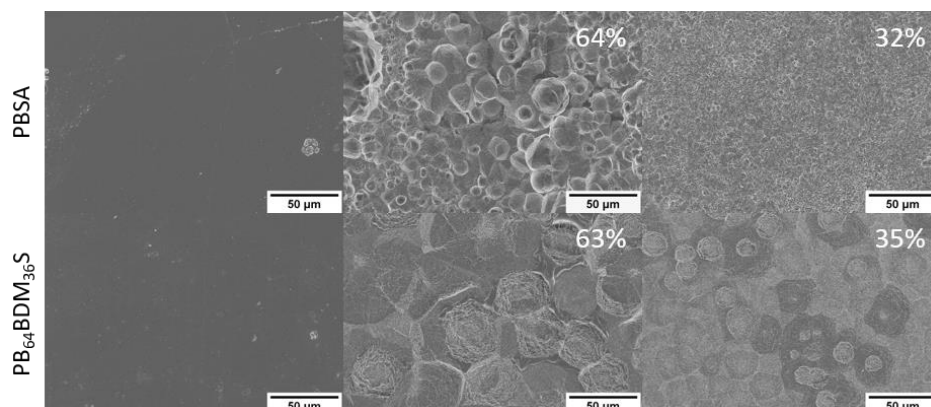


**Figure S18.** SEM images of the pristine (1<sup>st</sup> column) and eroded films of Hec-coated PB<sub>64</sub>BDM<sub>36</sub>S and PBSA before and at different intervals of the enzymatic hydrolysis. Residual mass of the measured film is stated in each image.

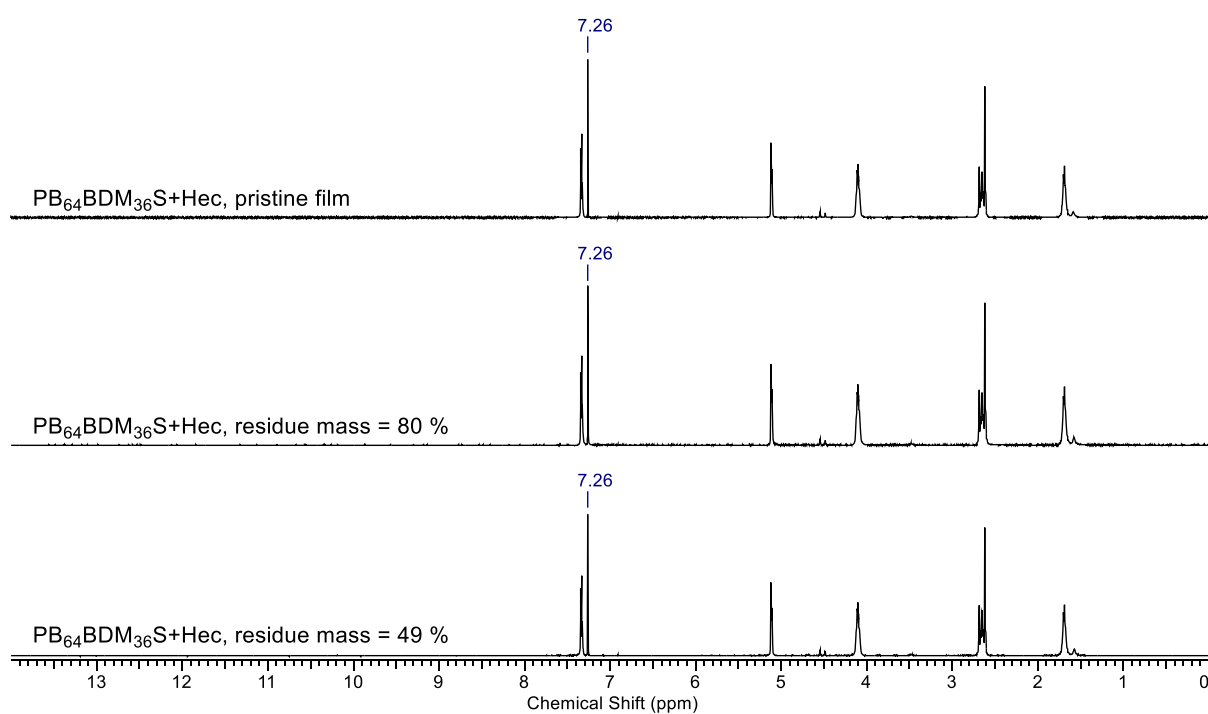


**Figure S19.**  $^1\text{H}$  NMR spectra of pristine films and films at different stages of the enzymatic hydrolysis of  $\text{PB}_{64}\text{BDM}_{36}\text{S}+\text{Hec}$ .

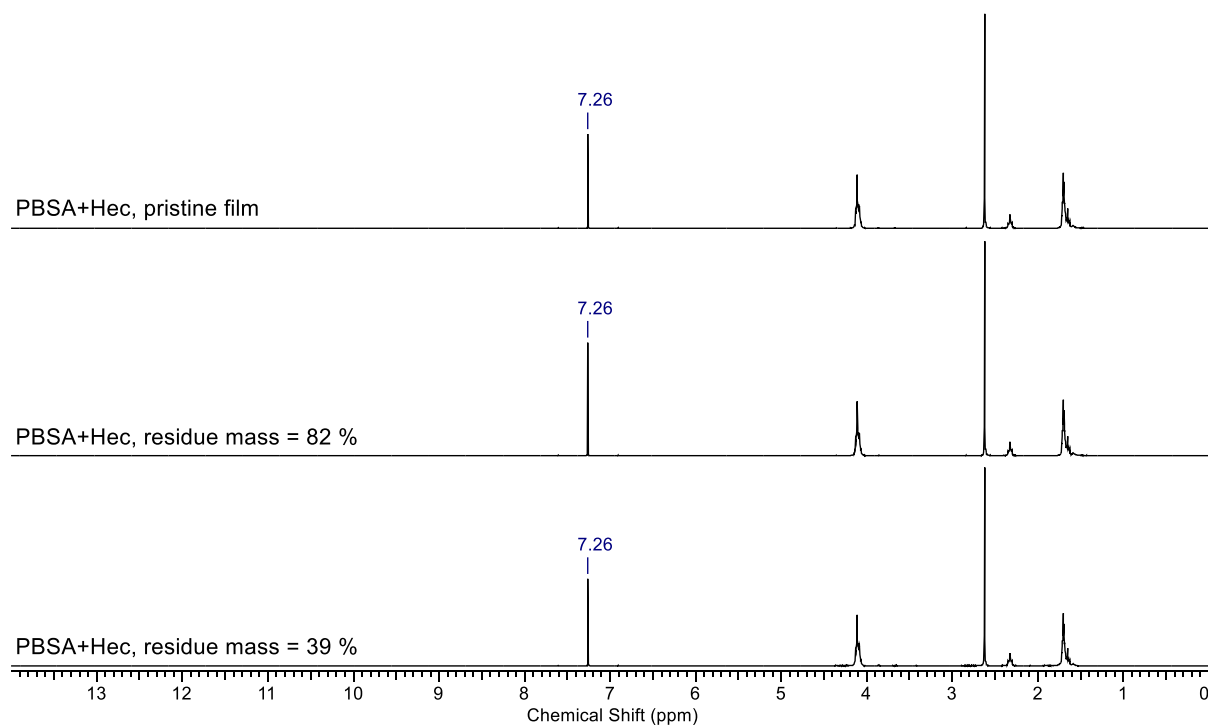


**Figure S20.**  $^1\text{H}$  NMR spectra of pristine films and films at different stages of the enzymatic hydrolysis of  $\text{PBSA}+\text{Hec}$ .

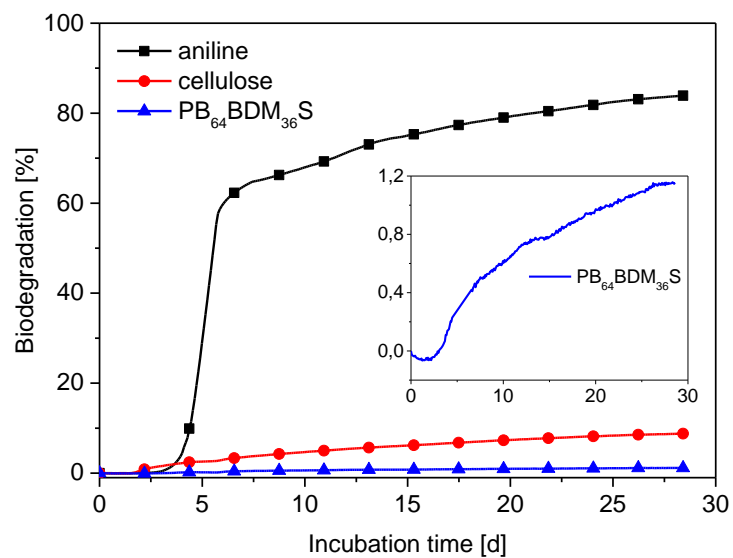


**Figure S21.** Calculated percentage of biodegradation from carbon dioxide produced after 28 days in aerobic wastewater sludge according to the process in DIN EN ISO 14852.

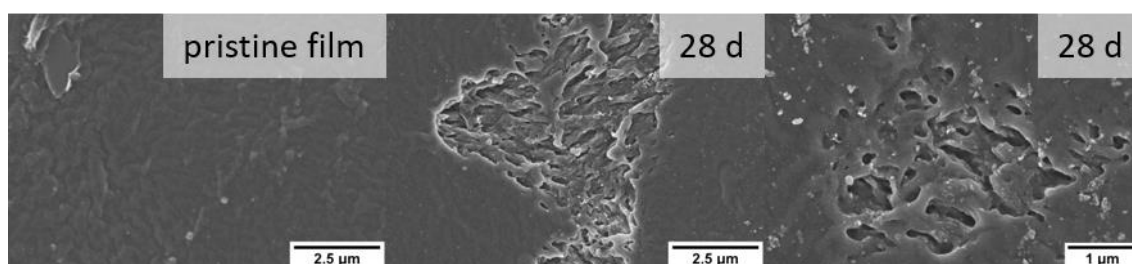


**Figure S22.** SEM images of PB<sub>64</sub>BDM<sub>36</sub>S before and after 28 d of degradation in aerobic wastewater sludge using the Micro-Oxymax respirometer.

**Origin and analytics of the compost:**

The compost was collected from the compost plant Veolia Umweltservice Süd GmbH & Co. KG in Pegnitz, Germany.

The compost contains household biowaste (50 vol%) and green waste (50 vol%), acting as structural material, from the month of July 2021. The compost piles were rearranged and watered once a week. The material was taken from the core of the pile two months after the start of the intensive rotting in open composting. The core temperature profile during this time is shown in Figure S23. The compost was sieved with a 10 mm and 4 mm sieve. Photographs of the material structure after sieving are shown in Figure S24. The compost parameters are in good agreement with the requirements according DIN EN ISO 14855, DIN EN ISO 20200, DIN EN 14045 or ASTM D5338. The important parameters are stated in Table S3. Before the start of the composting experiment, deionized water was added under mixing to reach a dry solid content of 50%.

The cellulose reference showed similar signs of degradation in every sampling interval of thermophilic composting, ensuring that each compost batch is active (Figure S26). The low density polyethylene reference was unaffected in every case (Figure S27).

**Table S3.** Analytics of the compost material <4 mm.

	<b>Compost</b>
<b>pH<sup>a</sup></b>	7.4 ± 0.2
<b>dry solid content<sup>b</sup> [wt%]</b>	58.3 ± 0.2
<b>ash content [wt%]<sup>c</sup></b>	32.6 ± 0.2
<b>C/N ration<sup>d</sup></b>	10.4 ± 0.7
<b>total C content<sup>d</sup> [%]</b>	16 ± 2
<b>total N content<sup>d</sup> [%]</b>	1.6 ± 0.4

<sup>a</sup>Compost (100 g) and distilled water 1:5 (*w/w*) were mixed. The pH was measured with pH-indicator strips in triplicate. The error was given according to the accuracy of the stripes.

<sup>b</sup>Dry solid content was measured as the weight ratio from the sample heated to 105 °C until constant weight and the initial weight (~100 g). The statistical average of five samples is given as a result.

<sup>c</sup>Ash content was measured as the weight ratio from the sample calcinated at 550 °C for 24 h under air and the initial weight (~100 g). The statistical average of five samples is given as a result.

<sup>d</sup>The C/N ration was determined by elemental analysis (CHNS elemental analyser vario EL cube [Elementar Analysensysteme GmbH]). The statistical average of five samples is given as a result.

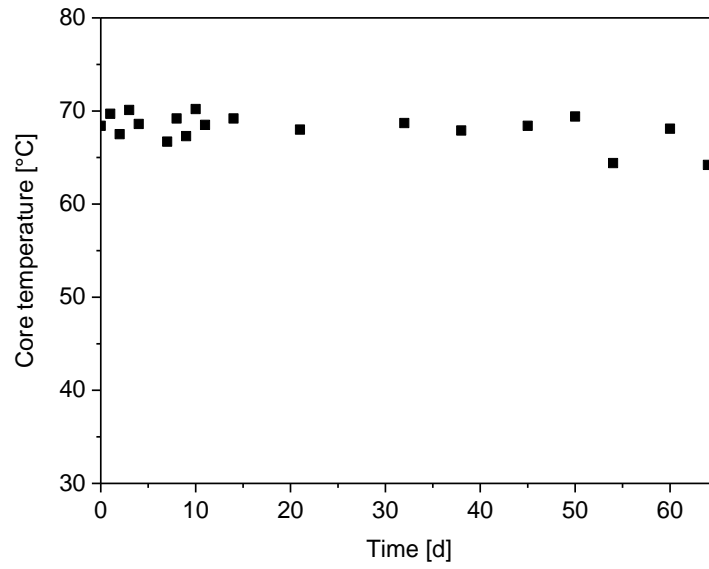


**Figure S23.** Core temperature profile of the compost in open composting under aerobic conditions at the compost plant in Pegnitz, Germany.



**Figure S24.** Compost sieved to <10 mm (left) and <4 mm (right).

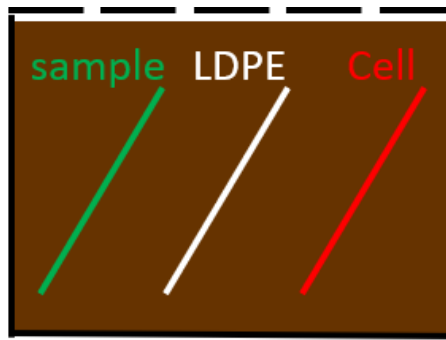


**Figure S25.** Scheme of a 250 mL sample box used for composting. The frames with the sample, the low density polyethylene reference (LDPE), and cellulose reference (Cell) are placed in the compost (brown) as shown.



**Figure S26.** Cellulose (Cell) reference in pristine state and after 4 and 8 weeks of thermophilic compost incubation.

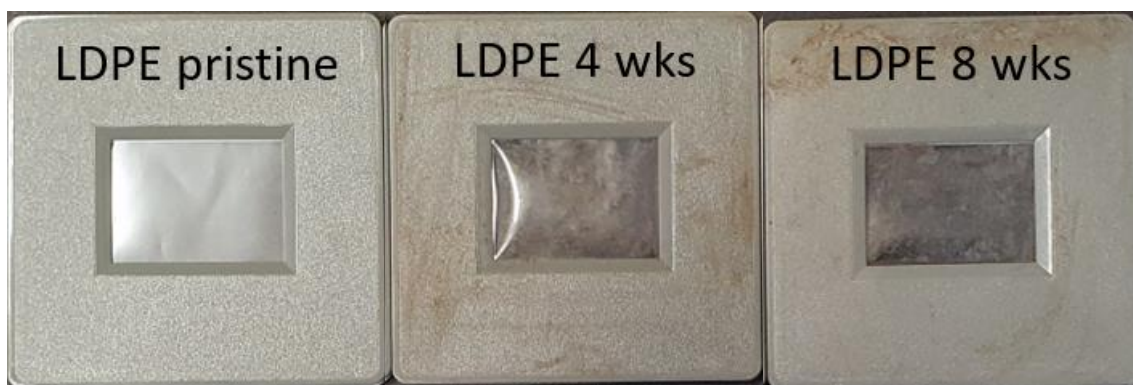


**Figure S27.** Low density polyethylene (LDPE) reference in pristine state and after 4 and 8 weeks of thermophilic compost incubation.

**Table S4.** Peak elution volume after different compost incubation times.

polyester	peak elution volume [ml]						
	0 wks	2 wks	4 wks	5 wks	6 wks	7 wks	8 wks
PBS	8.54	8.66	8.77	8.86	n.d.	9.04	9.13
PBSA	8.54	8.67	8.75	n.d.	8.92	n.d.	n.d.
PB <sub>64</sub> BDM <sub>36</sub> S	8.69	8.71	8.97	n.d.	n.d.	n.d.	n.d.
PBS+Hec	8.51	8.63	8.74	8.82	n.d.	8.98	9.08
PBSA+Hec	8.59	8.67	8.77	n.d.	8.98	n.d.	n.d.
PB <sub>64</sub> BDM <sub>36</sub> S+Hec	8.76	8.86	9.11	n.d.	9.21	n.d.	9.49

n.d. = not determined.

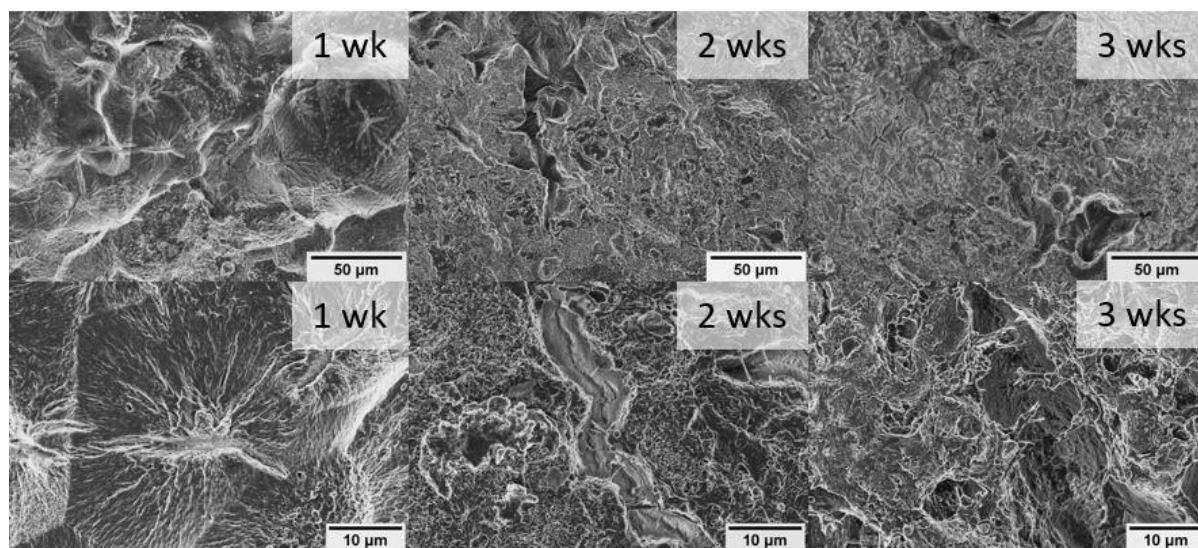


**Figure S28:** SEM image of PB<sub>64</sub>BDM<sub>36</sub>S films a one, two and three weeks of thermophilic compost incubation.

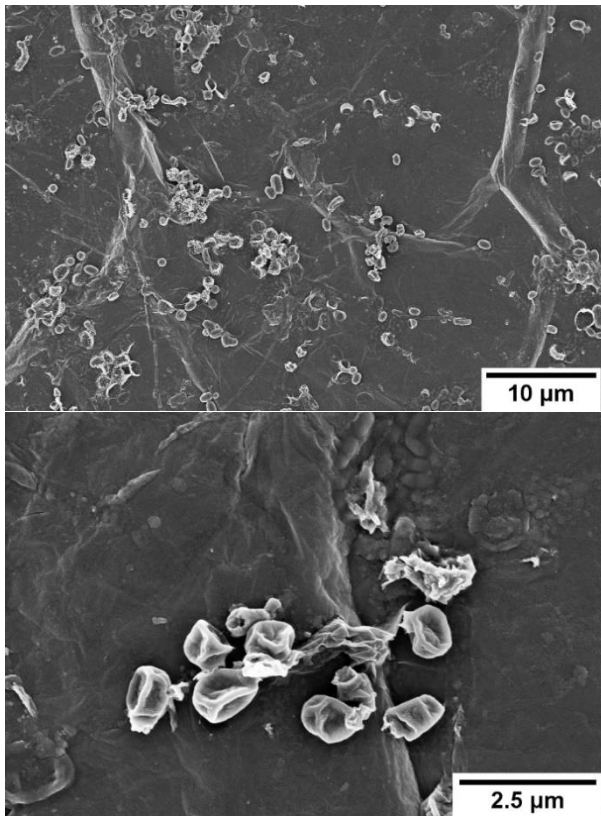


**Figure S29:** PBS+Hec film after 8 weeks of compost incubation. Hec side is shown.

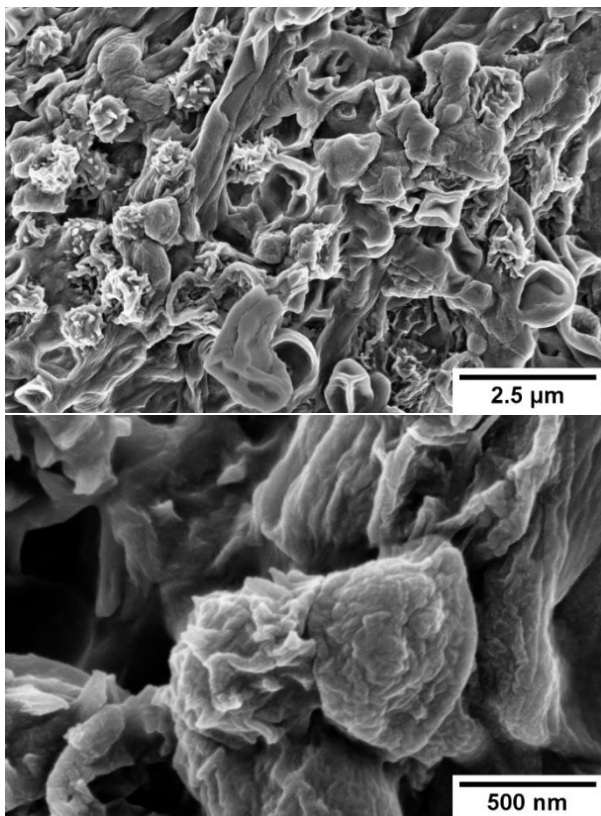


**Figure S30.** PBSA+Hec film after 4 weeks of compost incubation. Hec side is shown.

**References**

(1) Sehl, E.; Eger, E. M.; Himmelsbach, A.; Agarwal, S. Fast Hydrolyzable Constitutional Isomer of Poly(butylene terephthalate) and Its Copolyesters with 1,4-Butanediol. *ACS Appl. Polym. Mater.* 2021, 3 (12), 6427–6436. DOI: 10.1021/acsapm.1c01169.

### 6.3. Spontaneous Delamination of Affordable Natural Vermiculite as a High Barrier Filler for Biodegradable Food Packaging

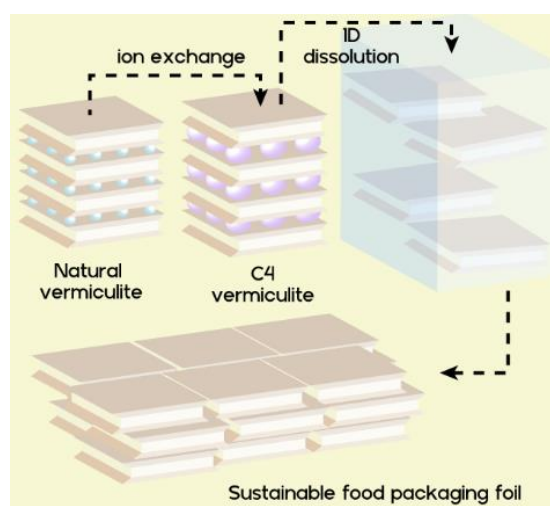
Volodymyr Dudko<sup>‡</sup>, Renee L. Timmins<sup>‡</sup>, Olena Khoruzhenko, Maximilian Röhr, Christopher Greve, Sabine Rosenfeldt, Tekla Tammelin, Seema Agarwal, Eva M. Herzig, Josef Breu\*

<sup>‡</sup>these authors contributed equally to this work

\*corresponding author(s): josef.breu@uni-bayreuth.de

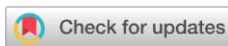
Published in: *Materials Advances* 2022, 3 (24), 9052-9062.

Reprinted with permission. Copyright 2022 Royal Society of Chemistry



Individual contribution:

Prof. Dr. Josef Breu and Volodymyr Dudko conceptualized the paper. Volodymyr Dudko developed the vermiculite delamination protocol and performed accompanying analysis. I prepared the nanocomposite coating and performed gas barrier measurements and shelf life calculations. Olena Khoruzhenko contributed to data analysis. Maximilian Röhr assisted with barrier measurements. Tekla Tammelin provided the cellulose nanofiber substrate and scientific discussion. Christopher Greve, Sabine Rosenfeldt, and Eva M. Herzig provided SAXS measurements and interpretation. Seema Agarwal provided technical expertise. The paper was written by Volodymyr Dudko, Prof. Dr. Josef Breu, and myself with editing and proofreading from all authors.



Cite this: DOI: 10.1039/d2ma00734g

## Spontaneous delamination of affordable natural vermiculite as a high barrier filler for biodegradable food packaging†

Volodymyr Dudko,<sup>‡a</sup> Renee L. Timmins,<sup>‡a</sup> Olena Khoruzhenko,<sup>a</sup> Maximilian Röhl,<sup>a</sup> Christopher Greve,<sup>id c</sup> Sabine Rosenfeldt,<sup>a</sup> Tekla Tammelin,<sup>id b</sup> Seema Agarwal,<sup>a</sup> Eva M. Herzig<sup>id c</sup> and Josef Breu<sup>id \*a</sup>

Expensive biodegradable packaging as a preventative measure against continued accumulation of plastic waste in our environment is often in conflict with the need for high performing packaging materials that prevent food waste. Compounding with delaminated vermiculite nanosheets is a compelling concept to simultaneously improve barrier properties through creation of a 'tortuous path' while also decreasing the price of the system due to its natural abundance. However, an effective delamination process that captures the full barrier improvement potential of this natural filler has been lacking. Here, we present a superior protocol for vermiculite delamination based on reducing the intrinsic hydrophobicity due to interlayer  $Mg^{2+}$  cations and the transfer of this osmotically swollen, liquid crystalline state into organic solvents. Nanocomposite coatings of degradable polyesters on nanocellulose exhibited oxygen and water transmission rates of  $1.30 \text{ cm}^3 \text{ m}^{-2} \text{ day}^{-1} \text{ atm}^{-1}$  and  $1.74 \text{ g m}^{-2} \text{ day}^{-1}$ , respectively, which competes with high-end, non-degradable poly(vinylidene dichloride) films.

Received 23rd June 2022,  
Accepted 25th October 2022

DOI: 10.1039/d2ma00734g

rsc.li/materials-advances

### Introduction

Innovative packaging plays a critical role in preventing loss of precious food products, yet presents a massive problem when considering their end-of-life scenarios. The United Nations Food and Agricultural Organisation estimates the global food wastage to be equivalent to 1.3 billion tons, which results in an unnecessary 3.3 billion tonnes of  $CO_2$  equivalent of greenhouse gases being released into the atmosphere per year.<sup>1</sup> Materials like polyethylene, poly(vinylidene dichloride) (PVDC), and polyamide possess a high barrier to relevant permeants, including water vapour, carbon dioxide, and oxygen, which prevents food waste by protecting from contamination and preserving freshness, taste, and colour of the products. Despite these critical functions, the growing concerns and awareness of consumers towards plastic pollution and ubiquitous microplastic contamination was reflected in a major Ipsos poll conducted

in 2019, which found that 71% of global consumers believe that single use plastic products should be banned as soon as possible.<sup>2</sup> More recently, directives came from both the European Union and Canada to ban the use of certain single-use plastics,<sup>3,4</sup> spearheading a growing movement to replace traditional plastics with biodegradable alternatives in the interest of environmental preservation and human health.<sup>5,6</sup> Current coated and chemically treated paper alternatives only present an unrecyclable and non-compostable burden on waste management systems.<sup>7</sup> There still lacks an environmentally friendly packaging option that provides the lightweight and convenient protection to which we have become accustomed.

Accordingly, one must consider the overall environmental impact of a packaged food product including the life cycle of the packaging material as well as the food. Implementation of bio-based and biodegradable packaging is an important step, but without high-performance properties that reduce food waste, the net environmental impact of the entire system is not improving.<sup>8</sup> Moreover, most consumers are unwilling to pay a higher price for an item to have environmentally friendly packaging.<sup>9</sup> A material substitution may become more attractive as the cost of certain biobased materials, e.g. cellulose and cellulose-based materials, decreases with increased production volumes while the rising price of petroleum threatens the rock-bottom price tag of conventional polymers.<sup>10</sup> Practical and low cost solutions required to tackle the challenge of the poor and

<sup>a</sup> Bavarian Polymer Institute and Department of Chemistry, University of Bayreuth, Universitätsstr. 30, 95440 Bayreuth, Germany. E-mail: Josef.Breu@uni-bayreuth.de

<sup>b</sup> VTT Technical Research Centre of Finland Ltd, VTT, PO Box 1000, FI-02044 Espoo, Finland

<sup>c</sup> Physikalisches Institut, Dynamik und Strukturbildung-Herzig Group, Universität Bayreuth, Universitätsstr. 30, 95447, Bayreuth, Germany

† Electronic supplementary information (ESI) available. See DOI: <https://doi.org/10.1039/d2ma00734g>

‡ Equal contribution.

moisture susceptible barrier properties of these bio-based and biodegradable materials are through multilayer strategies or surface hydrophobisation strategies.<sup>11–13</sup> These methods indeed decrease moisture sensitivity of hydrophilic materials, but still fails to provide barrier levels acceptable for food packaging. Another such approach is by the application of a thin nanocomposite barrier coating using clay nanosheets. Nanocomposite foils have barrier performance improved by orders of magnitude compared to the neat substrate.<sup>14–16</sup> The use of natural clays offers the additional benefit of being an inexpensive and sustainable filler that reduces the overall cost of the packaging.

As barrier improvement scales with the square of the platelet aspect ratio (diameter/thickness ratio) due to elongation of the diffusion path for permeates,<sup>17</sup> the most commonly applied clay minerals, montmorillonite and LAPONITE<sup>®</sup><sup>18,19</sup> with an aspect ratio of <150 and 20, respectively, are insufficient. Particularly when considering the inherently poor barrier performance of biodegradable polymer matrixes,<sup>19,20</sup> much larger aspect ratios are required. Layered fillers with promising diameters are synthetic hectorites<sup>21</sup> or natural vermiculites. While efficient delamination protocols for the former have already been established (*i.e.*, osmotic swelling),<sup>21</sup> the same cannot be said for the latter.

Osmotic swelling<sup>22</sup> is an exceptionally effective method for the production of barrier nanosheets since it is a thermodynamically allowed process that does not require any mechanical force as opposed to ultrasound driven liquid-phase exfoliation methods. Being repulsive<sup>23,24</sup> in nature allows for an utter and most gentle delamination into the thinnest possible nanosheets, while liquid phase exfoliation provides only nanosheets with a range of thicknesses (for a definition of delamination *versus* exfoliation, see: Gardolinsky and Lagay).<sup>25</sup> Consequently, only delamination *via* osmotic swelling preserves the aspect ratio inherent in the platelet diameter of the non-delaminated starting material.

Considering the polymer component of a nanocomposite coating, commercially produced biodegradable polymers like poly lactic acid (PLA), poly(butylene succinate-*co*-butylene adipate) (PBBSA), and poly(butylene adipate terephthalate) (PBAT) are attractive options, but only soluble in organic solvents. Until recently, osmotic delamination was restricted to a very small number of layered compounds in water.<sup>26–30</sup> Water soluble biodegradable polymers like poly(vinyl alcohol) (PVOH) are highly susceptible to swelling even under ambient conditions, significantly deteriorating the barrier performance.<sup>31,32</sup> Fortunately, osmotic swelling of a synthetic hectorite could recently be extended into applicable organic solvents.<sup>33</sup>

Natural vermiculites are 2 : 1 layered silicates are particularly appealing as a clay component in a nanocomposite barrier system, in contrast to a synthetic hectorite, because vermiculite deposits are abundant with global production at over 500 k tons per year<sup>34</sup> and cost around 20 ct per kg. Thermally expanded vermiculites are well-known in chemistry laboratories as the standard adsorbent for spilled organic solvents (Fig. 1a). Moreover, vermiculites have the same layer structure as the commonly applied

montmorillonite but with a much larger diameter, and hence a higher potential aspect ratio.<sup>35–37</sup> Vermiculites unfortunately have a significantly higher charge density compared to montmorillonite, which renders osmotic swelling much more difficult.<sup>38</sup> Vermiculite swelling is not only impeded by the high charge density, but also by the dominant divalent interlayer cation  $Mg^{2+}$  that forms a strong and symmetrical electrostatic interaction with the adjacent nanosheets, pinning them together. Yet upon exchange with bulky organocations, vermiculite is known to swell osmotically in water.<sup>39–42</sup> Due to the large diameter of nanosheets, gels obtained by swelling are not isotropic but rather viscous, liquid crystalline, nematic phases even at low concentrations of 1 vol%. It follows that in order to efficiently incorporate vermiculite into a biodegradable polymer matrix for use in sustainable food packaging, obtaining osmotic swelling in organic solvents is a critical hurdle. More specifically, for solution casting in a roll-to-roll production of nanocomposite coatings, osmotic swelling of vermiculite is required in a solvent that also dissolves biodegradable polyesters.

In this paper, we report a simple one-step ion exchange strategy for repulsive osmotic delamination of natural vermiculite in the organic solvent *N*-methyl formamide (NMF) and its mixtures that results in a high delamination yield (80 wt%) and preservation of the high aspect ratio of the nanosheets compared to ultrasonication-assisted methods.<sup>43</sup> Solution blending with biodegradable polymers like PLA becomes straightforward. Nanocomposite coatings obtained by the doctor blading of a polymer/clay suspension improved gas barrier performance of a natural, fully biodegradable,<sup>13</sup> and highly hydroscopic wood-based nanocellulose paper substrate by 90.2% and 97.8%, respectively. The PLA-vermiculite coated nanocellulose system presents a biodegradable alternative to traditional high-performance food packaging with oxygen and water transmission rates of  $1.30 \text{ cm}^3 \text{ m}^{-2} \text{ day}^{-1} \text{ atm}^{-1}$  and  $1.74 \text{ g m}^{-2} \text{ day}^{-1}$ , respectively. Moreover, our manufacturing strategy involves only facile and scalable unit operations positively contributing to the future implementation at a commercial scale.

## Results and discussion

### Repulsive osmotic delamination of natural vermiculites

Osmotic swelling of highly charged clays occurs when the interlayer cation is completely exchanged for select bulky and hydrophilic organocations.<sup>39–42</sup> Cations are solvated by the solvent molecules, increasing the separation between nanosheets and boosting translational entropy within the interlayer space. Upon reaching a separation threshold, osmotic swelling sets in, allowing for a most gentle delamination process while preserving the aspect ratio inherent to the pristine platelet diameter.<sup>23,24,38,44</sup>

Vermiculites are the weathering products of biotite, where the  $K^+$  cations are replaced by  $Mg^{2+}$  while at the same time the layer charge is reduced somewhat by oxidation of structural iron with oxygen in the air.<sup>45</sup> Due to the high hydration enthalpy of  $Mg^{2+}$ , vermiculites are hydrated. Hydration of

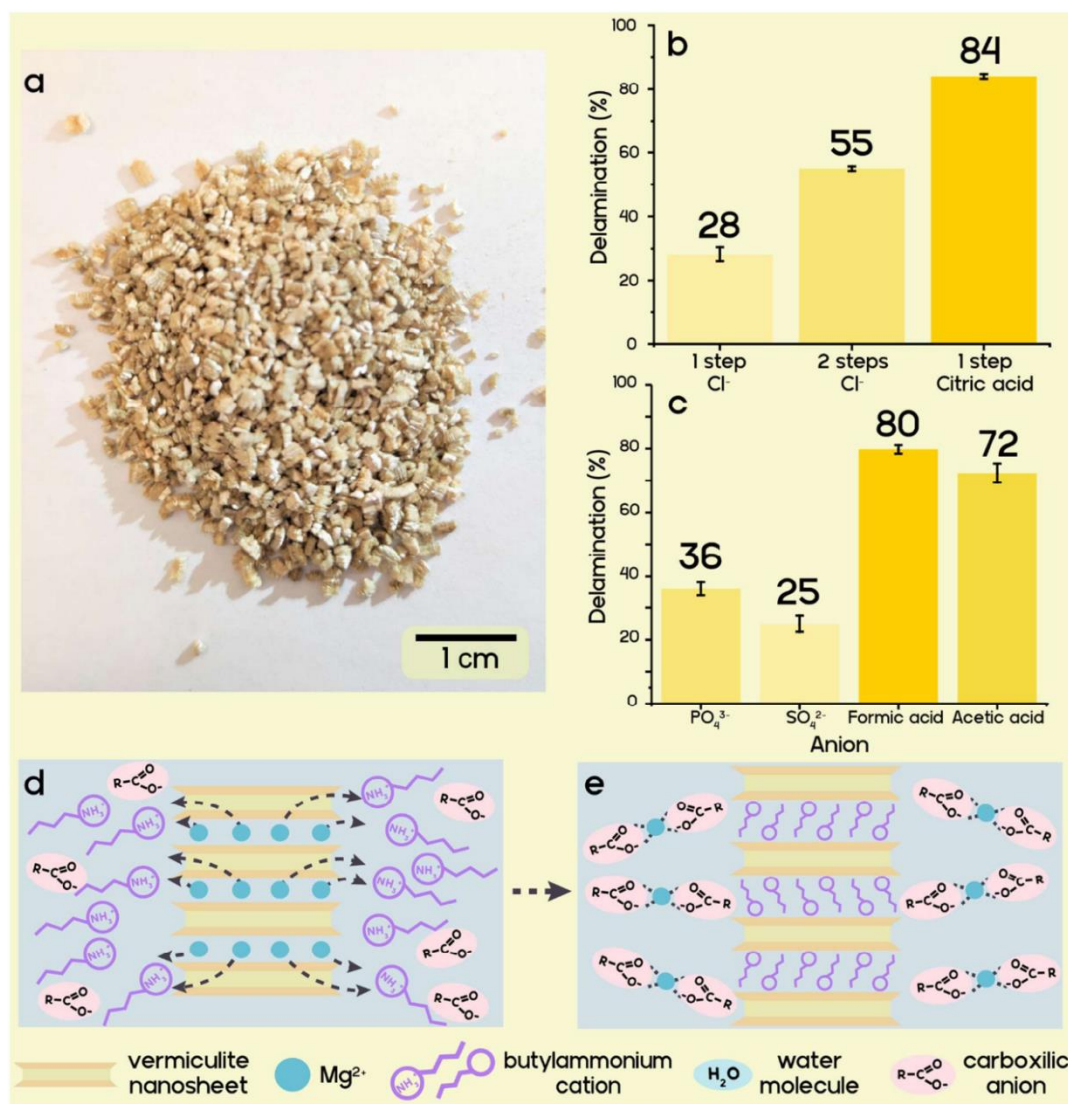


Fig. 1 Schematic representation of osmotic swelling of natural vermiculites. (a) Photo of thermally expanded natural vermiculite. (b) Delamination yield observed by a one-step ion exchange with butylammonium chloride or citrate as compared to a two-step ion exchange first to Na<sup>+</sup> followed by butylammonium chloride. (c) Delamination yield observed by a one-step ion exchange with different inorganic and organic salts of butylammonium. (d) Schematic of ion exchange process in presence of carboxylic acid anions (e). The proposed process of ion exchange that leads to enhanced delamination yield. Magnesium cations form complexes with carboxylic acid anions, increasing the hydrophilicity and reducing the tendency to re-enter the interlayer space.

pristine vermiculites, however, is limited to a two-layer hydrate even when immersed into water because of the high charge density. Owing to the natural origins of such vermiculites, contamination with pristine biotite mica impurities (which have an inaccessible interlayer space and do not exhibit any swelling behaviour) is inevitable. We cannot expect to achieve a 100% yield of delaminated nanosheets from the raw mined material because of this remaining accessory mineral.

Divalent interlayer cations like Mg<sup>2+</sup>, as found in the pristine vermiculite, impede osmotic swelling. Complete exchange of

divalent interlayer cations with monovalent cations of higher hydration energy (*e.g.*, Li<sup>+</sup>)<sup>46</sup> or one capable of inducing steric pressure (*e.g.*, butylamine)<sup>39</sup> is essential for osmotic swelling to set in. The high selectivity in the interlayer space of vermiculite makes the direct and complete exchange of Mg<sup>2+</sup> for Li<sup>+</sup> or protonated butylamine difficult and time-consuming. According to Walker *et al.*, butylamine vermiculites that produce gels upon swelling have been obtained by repeated ion exchange of Mg<sup>2+</sup> with Na<sup>+</sup> over a period of one year.<sup>40</sup> Only then in a second step can Na<sup>+</sup> be sufficiently replaced by butylammonium. Needless to

say, such a lengthy two-step ion exchange process is unsuitable for high-volume applications.<sup>39</sup>

We hypothesise that by removing the  $Mg^{2+}$  cation from an exchange equilibrium through complexation, a high yield of ion-exchanged vermiculite in a single-step ion exchange is possible. Complexation is supplemented by the hydrophobicity of incoming organocations.<sup>47</sup> Carboxylic acids can be used for protonation of butylamine, while at the same time they can form stable complexes with  $Mg^{2+}$ , decreasing its activity to a level where butylammonium favourably enters the interlayer space. Vermiculite must first be activated for osmotic swelling by ion exchange in water. A series of ion exchanges were performed using butylamine in combination with one of several protonating acids to determine the most efficient pairing for maximizing the yield of the nematic phase consisting of delaminated nanosheets, and to compare with the published two-step ion exchange (Fig. 1b and c).<sup>40</sup> Direct ion exchange with butylammonium chloride gives only 28 wt% delamination yield, while the two-step method involving sequential exchange of  $Mg^{2+}$  for  $Na^+$ , and then for butylammonium, provided a higher yield of 55 wt%. Butylammonium phosphate, sulfate, formate, and acetate produced yields of 36 wt%, 25 wt%, 80 wt%, and 72 wt%, respectively. The higher complex building constant for  $Mg^{2+}$  and the citrate anion compared to monodentate anions gives a superior yield of 84 wt% for butylammonium citrate (Fig. 1d and e).<sup>48,49</sup> Moreover, it was found that the concentration of the butylamine solution can be decreased 10-fold without a dramatic reduction of the delamination yield (from 84% at 1 M to 75% at 0.1 M, Fig. S1, ESI†). As high ionic strength hampers repulsive osmotic swelling, the delamination yields were determined after washing in ethanol followed by redispersion into water. CHN analysis of butylammonium citrate exchanged vermiculite confirms the highest organic content out of all exchanged vermiculites, which corresponds to 91% of the cation exchange capacity, indicating a high degree of ion exchange (Table S1, ESI†).

#### Characterization of nematic phases and delaminated vermiculite nanosheets

Coarse-grained, non-delaminated mica may be removed through sedimentation by centrifugation, which also gives a concentrated gel of delaminated vermiculite in the supernatant. The small-angle X-ray scattering (SAXS) (Fig. 2a red dots) of gel in NMF confirms the separation to the single layers to 62.8 nm (corresponding to  $q = 0.01 \text{ \AA}^{-1}$ ). Nematic ordering is confirmed by the presence of a rational  $00l$  series and an absence of Bragg reflexes at high  $q$  values (Fig. 2a red line), which would correspond to the swollen intercalation compound of 1.4 nm.<sup>50</sup> The pattern can be modelled with the disk shape structure factor (Fig. 2a blue dotted line) having a diameter of 2000 nm and thickness of 1.8 nm.<sup>44,51,52</sup>

Static light scattering (SLS) gave a mean particle size of about 4.9  $\mu\text{m}$  (Fig. 2b), which corresponds to the hydrodynamic diameter of the nanosheets. Since SLS measurements were performed in aqueous dispersions, the particle size distribution is representative of the bulk material.<sup>53</sup> This value was cross-checked by assessing a large number of vermiculite

nanosheets with SEM micrographs (Fig. 2c), which gave a mean diameter of  $4 \pm 1 \mu\text{m}$ , in agreement with the SLS value.

While SAXS probes the bulk suspension, delamination of vermiculite may be confirmed at the level of individual nanosheets with atomic force microscopy (AFM). The average height of three nanosheets was  $1.2 \pm 0.1 \text{ nm}$  (Fig. 2d and Fig. S2, ESI†). Since AFM images were recorded under ambient conditions, counter ions attached to the basal surface will be solvated, which adds to the true thickness of 1 nm for a 2:1 layered material.<sup>21</sup> Taking this systematic error into account, it can safely be concluded that all imaged nanoplatelets are single layers because observed heights are significantly smaller than 2 nm.

Considering a nanosheet thickness of 1 nm and a 4  $\mu\text{m}$  median lateral extension of the clay particles, delaminated natural vermiculite from Eucatex, Brazil offers a mean aspect ratio of 4000. This aspect ratio is more than an order of magnitude higher than the typical value for montmorillonite and is comparable to synthetic sodium tetrasilic mica.<sup>54</sup> Such a high aspect ratio filler in a nanocomposite is expected to have a considerable impact on the barrier properties in combination with biodegradable polymers (Fig. S3 and eqn (S1), ESI†).

#### Nematic suspension of vermiculite in organic solvents

As most biodegradable polymers of commercial interest are non-water soluble polyesters (PLA, PBBSA, PBAT, poly( $\epsilon$ -caprolactone)), the nematic aqueous vermiculite suspensions were freeze-dried before being re-suspended in organic solvents. Of the solvents tested, NMF proved to be capable of osmotic swelling butylammonium vermiculite yielding nematic suspensions. The greatest advantage of NMF over the other solvents is its exceptionally high dielectric constant ( $\epsilon_r = 171$ ).<sup>55</sup> Unfortunately, NMF has been reported to considerably reduce the molecular weight of PLA during dissolution, which in turn ruins the mechanical integrity of PLA composites.<sup>16</sup> Therefore, the suspension of vermiculite in NMF was concentrated by centrifugation to a gel with 9 wt% vermiculite. The gel is then diluted to 1 wt% with various other organic solvents yielding mixtures with less than 10 wt% NMF. Most low dielectric solvents instantly trigger flocculation. However, some moderately polar solvents that are used in the industrial coating preparation, including dimethylformamide (DMF), dimethylacetamide (DMAc), dimethyl sulfoxide (DMSO), *N*-methyl-2-pyrrolidone (NMP), ethanol, and  $\gamma$ -butyrolactone ( $\gamma$ -BL), preserve the nematic nature of the vermiculite suspension as indicated by birefringence under cross-polarised light (Fig. 2e).

Out of the various solvent parameters evaluated, only a high dielectric constant displays a correlation with the stability of the liquid crystal phase (Table S2, ESI†). The only clear outliers are acetonitrile and ethanol, where the former has a lower dielectric constant than expected, but still induces swelling. Assuming the wt% of NMF to be 10%, the threshold value for the dielectric constant of a co-solvent in a solvent mixture appears to be 36. The flocculated samples are shown in Fig. S4 (ESI†).

The solubility of biodegradable polymers may be estimated by applying the Hansen parameters<sup>56</sup> (Table S2, ESI†). Out of the listed solvents capable of osmotic swelling,  $\gamma$ -BL has Hansen

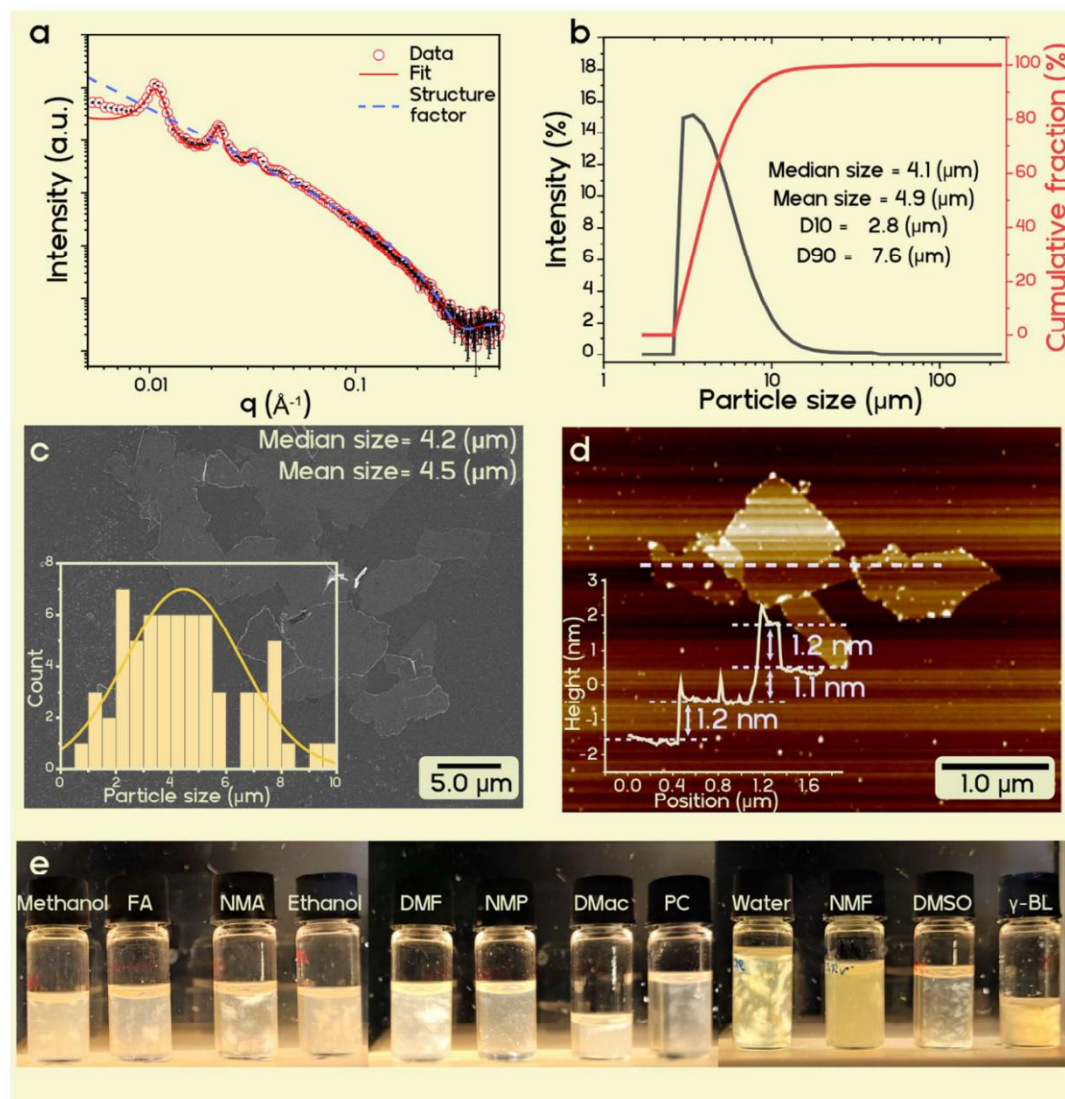


**Fig. 2** Characterization of nematic suspensions and delaminated vermiculite nanosheets (a). SAXS intensity of vermiculite gel, indicating a liquid crystalline order in the nematic suspension in NMF. (b) Static light scattering number weighted size distribution indicating a mean size of  $4.9 \mu\text{m}$  (c) SEM photo of vermiculite nanosheets on a Si wafer. Inset: Particle size distribution measured from the SEM image indicating a mean size of  $4 \pm 1 \mu\text{m}$ . (d) Topographic AFM image of vermiculite nanosheets and height profile from the single nanosheets indicating a height of  $\sim 1.2 \text{ nm}$ . (e) Photos of nematic suspensions of vermiculite in various solvents obtained by diluting a vermiculite/NMF gel, viewed under cross-polarized light, and reducing the tendency to re-enter the interlayer space.

parameters which indicate that it will also be capable of dissolving biodegradable polyesters (Hansen parameters for PLA are 18.9, 4.6 and  $7.6 \text{ MPa}^{1/2}$  for  $\delta D$ ,  $\delta P$ , and  $\delta H$ , respectively), as required for the preparation of high-performance, degradable nanocomposites *via* solution blending and roll-to-roll processing.

#### Fabrication of biodegradable food packaging foils

Cellulose nanofiber (CNF) paper has recently been established as an inexpensive, wood-based, sustainable, and completely

biodegradable substrate. Previous work has established the ability of this CNF substrate to degrade in compost within 4 weeks, which was comparable with other chemically unmodified cellulose variants.<sup>13,57,58</sup> The CNF paper used, which was prepared from unmodified birch kraft pulp, was reported to show a pore size of approximately 5 nm and has even been applied for the purpose of organic solvent nanofiltration.<sup>59</sup> Physical characterizations of the film have been thoroughly studied in Lee *et al.* and others.<sup>13,60,61</sup> Highly hydroscopic CNF

provides extremely poor barrier performance, especially in the presence of water vapour, making it alone unsuitable as a packaging material; therefore, we chose this substrate to demonstrate the barrier performance power of a vermiculite-filled nanocomposite. PLA was dissolved at 10 wt% in  $\gamma$ -BL. This solution was mixed with a 5 wt% suspension of vermiculite in the  $\gamma$ -BL/NMF mixture, obtained as described above, at a 50/50 weight ratio of PLA to vermiculite nanosheets. PLA addition does not compromise colloidal stability nor trigger flocculation as evidenced by no significant changes in the SAXS curves upon PLA addition (Fig. S5, ESI<sup>†</sup>). The nematic character of the mixture was confirmed by birefringence. The suspension with a total solid content (PLA + vermiculite) of 6.7 wt% was coated by doctor blading onto a CNF substrate. A wet coat thickness of 250  $\mu\text{m}$  resulted in a  $5 \pm 0.5 \mu\text{m}$  thick dry coating (PLA-verm/CNF) (Fig. S6, ESI<sup>†</sup>). Due to the porous nature of the CNF substrate, complete solvent removal could be achieved despite the high boiling point of NMF as solvent is allowed to permeate through the substrate while the larger clay particles and polymer chains are not. The area in which solvent molecules have to escape effectively doubles and prevents the trapping of solvent molecules within the coating as the wet layer dries from the outside inwards.

The dried nanocomposite coating resists cracking upon bending due to the highly flexible nanosheets, which is in agreement with previous work on coatings that employ high aspect ratio clay nanosheets.<sup>15</sup> The coating also withstood scratching using a pencil of 2H hardness. For comparison, a CNF paper was coated with only PLA using the same procedure (PLA/CNF).

The oxygen transmission rate (OTR) of the PLA-verm/CNF foil was measured at 23 °C and an elevated 65% relative humidity (RH) and compared to the OTR of both the uncoated CNF paper (35  $\mu\text{m}$ ) and the PLA/CNF foil with a coating thickness of 10  $\mu\text{m}$ . OTRs of the neat and the PLA/CNF foils were 13.3 and 13.2  $\text{cm}^3 \text{m}^{-2} \text{day}^{-1} \text{atm}^{-1}$ , respectively. A coating layer of PLA on CNF paper has essentially zero effect on the oxygen barrier performance even as a thick coating, as expected, due to its exceptionally poor performance even as a bulk material (711  $\text{cm}^3 \text{m}^{-2} \text{day}^{-1} \text{atm}^{-1}$ , 25  $\mu\text{m}$  thickness). With or without a PLA coating, CNF oxygen barrier is not suitable for food packaging (Fig. 3a).<sup>62</sup> The use of a PLA-vermiculite nanocomposite coating on CNF is a game-changer in this regard. A dramatic drop in the oxygen transmission rate for the PLA-verm/CNF foil to a value of 1.30  $\text{cm}^3 \text{m}^{-2} \text{day}^{-1} \text{atm}^{-1}$  was observed, equating to a barrier improvement factor of 3,484 (eqn (S2), ESI<sup>†</sup>) and a reduction in oxygen transmission by 90.2% as compared to the neat cellulose paper. This coating brings the oxygen barrier of a paper material (PLA-verm/CNF) into competition with non-degradable and high-performance materials like PVDC and metallized polyethylene terephthalate/polyethylene (PET/Met/PE) laminates, which reports OTR values in the range of 1–2  $\text{cm}^3 \text{m}^{-2} \text{day}^{-1} \text{atm}^{-1}$ <sup>63,64</sup> (Fig. 3b). Even more impressive was the drop in the water vapour transmission rate (WVTR) due to the PLA-vermiculite nanocomposite coating. CNF paper, being a hydroscopic substrate, naturally has a poor barrier to water

vapour, especially at an elevated 75% RH, which is well beyond what would be needed for swelling to set in and further deteriorate barrier performance.<sup>65</sup> The neat CNF paper reports a WVTR of 79.6  $\text{g m}^{-2} \text{day}^{-1}$ , which is slightly improved by the addition of a PLA coating (40.1  $\text{g m}^{-2} \text{day}^{-1}$ ) due to its hydrophobicity, but nevertheless remains unsuitable for demanding food packaging applications. The PLA-verm/CNF foil recorded a dramatically reduced WVTR of 1.74  $\text{g m}^{-2} \text{day}^{-1}$ , corresponding to a barrier improvement of 91 and a reduction in the CNF transmission rate by 97.8%. Other water soluble, high-barrier polymers like PVOH struggle to maintain WVTR values below 2  $\text{g m}^{-2} \text{day}^{-1}$  at RH above 50%.<sup>31</sup> With a single degradable coating layer, our PLA-verm/CNF foil again outperforms PET/PE laminates having conventional barrier layers of ethylene vinyl alcohol (EVOH) or PVDC, and rather approaches a WVTR comparable to PET/Met/PE laminates<sup>64</sup> (Fig. 3b). The overall barrier performance of our PLA-verm/CNF foil sits well within the range expected for demanding applications like instant coffee packaging.

The nanocomposite coating imparts such dramatic barrier improvements due to the formation of a 'tortuous path' by impermeable clay nanosheets. The exceptional improvement observed for this vermiculite nanocomposite can be attributed to the preservation of a high aspect ratio during repulsive osmotic delamination and the high degree of orientation of the clay nanosheets that is promoted through solvent casting of osmotically swollen suspensions. These attributes increase the diffusion path of gas molecules, leading to enhanced barrier properties. In addition, the XRD pattern of the nanocomposite coating (Fig. S7, ESI<sup>†</sup>) indicates the intercalation of the PLA chains within the interlayer space of vermiculite, reflected by the increase in  $d$ -spacing from approximately 1.3 nm for butylamine vermiculite to 2.8 nm for the PLA nanocomposite. Previously we have demonstrated that the intercalation of polymer chains can improve the barrier properties of nanocomposite coatings and positively influence the barrier behaviour under increased relative humidity conditions.<sup>32,66</sup> Previous attempts for a CNF nanocomposite film using montmorillonite could not achieve the high performing barrier values that we observed here. Despite a non-biodegradable cross-linked PVOH and poly(acrylic acid) polymer matrix that inherently has better barrier properties than PLA, without the use of a completely delaminated and high aspect ratio filler, the range of achievable barrier performance is limited.<sup>67</sup>

Our method for vermiculite nanocomposites makes bio-based and sustainable materials like cellulose paper a viable option for even ambitious food packaging applications like crispy snacks or instant coffee packaging. While other platy fillers of synthetic origin are expensive and not environmentally benign, vermiculite is provided in bulk by nature for an appealing low price, rendering it attractive for high-volume applications such as food packaging. The coated foil also fulfills consumer preference for transparent packaging (Fig. 3c). The haze and clarity of the coated CNF is improved relative to the uncoated CNF substrate, although transparency decreases slightly from 91.7% to 85.1% for the PLA-verm/CNF foil (Fig. S7, ESI<sup>†</sup>).

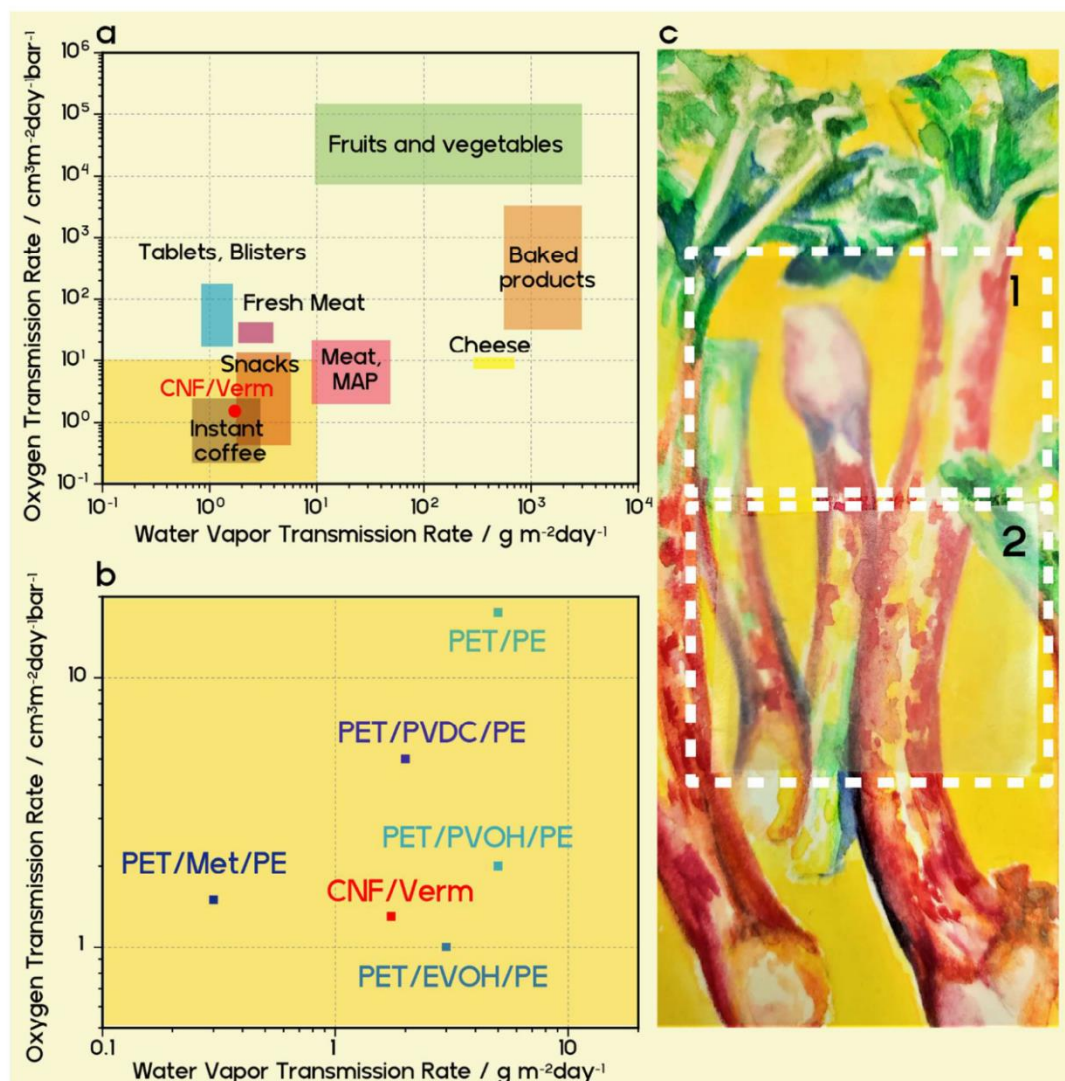


Fig. 3 Barrier properties of nanocomposites. (a) Barrier requirements for packaging of selected foods according to [62], and the barrier properties of PLA-verm/CNF foil. (b) OTR and WTR of commercial non-biodegradable high-performance multilayer packaging according to [64] in comparison with our PLA-verm/CNF foil. (c) Painting covered with the CNF substrate foil (1) and the PLA-verm/CNF foil (2).

High-performance food packaging plays a role in reducing food waste by extending the shelf life of packaged items. To explore the real life consequences of water transmission rate values, we can consider 500 g of a powdered food item (*e.g.* flour) that has a density of 1 g cm<sup>-3</sup> and initial moisture content of 2 wt% with a critical moisture content of 8 wt% at which the food is regarded spoiled. This food item is packaged in a 3 cm × 15 cm × 10 cm rectangular plastic film pack that is exposed to 75% RH at 23 °C. If the film pack were to be made of neat CNF, the corresponding shelf life would be only 9 days. With a neat 10 μm PLA coating on CNF, the shelf life would be 18 days, making it only suitable for short-term use. Our PLA-verm/CNF foil has the shelf life of an outstanding 416 days,

opening up opportunities for long-term packaging applications (detailed calculation provided in ESI<sup>†</sup>).<sup>68,69</sup> Such a shelf life extension has dramatic implications on the ability of biodegradable materials to not only reduce the amount of plastic waste entering the environment, but also to reduce food waste and contribute to a more sustainable food production cycle.

## Conclusions

Our studies suggest that the modification procedure for vermiculite delamination and transfer to organic solvents provides the ideal nanosheet filler for biodegradable food packaging.

These nanosheets simultaneously addresses two major problems facing widespread implementation of biodegradable polymers: poor barrier properties and high price. Our estimation suggests that the price of 1 kg of delaminated vermiculite on the lab scale is below 1 USD, which is cheaper than PBSA or PLA (\$3.5 and \$2 per kg in 2019). In this way, we resolve difficulties in the implementation of biodegradable materials by employing a strategy that the packaging industry already uses for commodity polymers, in which almost half of the mass of material consists of inert filler (carbon black or CaCO<sub>3</sub>) to decrease the price of the final product. A nanocomposite with 50 wt% vermiculite is expected to have a price close to \$2 per kg for PBSA and \$1.5 per kg for PLA, making it comparable to polyethylene and polypropylene, which are commonly used in the packaging industry.

## Experimental section

### Materials

Unless otherwise stated, all the chemicals used in the present work were purchased from Sigma Aldrich and directly used without further purification. Butylamine (99.5%), phosphoric acid ( $\geq 85$  wt% in H<sub>2</sub>O), sulphuric acid (95.0–98.0%), hydrochloric acid (37 wt% in H<sub>2</sub>O), NMF. Citric acid (99%), formic acid (99%), glacial acetic acid (99%).

The PBSA used in this work was purchased from Mitsubishi Chemicals (BioPBS FD92PM). PLA was supplied by Nature Works, USA as the Ingeo 4043D grade semi-crystalline poly-L-lactide.

Mechanically disintegrated CNF was prepared from bleached birch kraft pulp obtained from the Finnish pulp mill. The pulp suspension was pre-refined in a Masuko grinder (Supermasscolloider MKZA10-15J, Masuko Sangyo Co., Japan) at 1500 rpm and fluidized with six passes through a Microfluidizer (Microfluidics M-7115-30 Microfluidics Corp.) at 1800 bar. Self-standing CNF films were produced by solvent casting method and they were manufactured on a semipilot scale Coatema Coating Machinery GmbH with the patented method.<sup>61,70,71</sup> A 1.6 wt% CNF dispersion, including sorbitol (30 wt% solids in dry film from Sigma), was casted on polypropylene substrate. After evaporation of water, the CNF film with a thickness of 35  $\mu\text{m}$  was separated from the plastic substrate and cut into A4 sheets. The grammage and density of the CNF film is 60 g m<sup>-2</sup> and 0.93 g cm<sup>-3</sup>, respectively.

Starting material was Eucatex vermiculite. The structural formula of half unit cell is [Mg<sub>0.35</sub>]<sup>inter</sup>[Mg<sub>2.475</sub> Al<sub>0.075</sub> Fe<sub>0.305</sub> Ti<sub>0.04</sub> Mn<sub>0.005</sub>]<sup>oct</sup>[Si<sub>3.11</sub> Al<sub>0.89</sub>]<sup>tet</sup>O<sub>10</sub>H<sub>2</sub> and cation exchange capacity of 147 m equiv./100 g. Natural vermiculite flakes were ground into crystals of 50  $\mu\text{m}$  size. A larger crystal size impedes swelling.

### Preparation of ion exchange solutions

Butylamine was titrated in Millipore water to pH = 7 with appropriate acid to obtain the desired counter anion. The solutions were diluted to 1 mol L<sup>-1</sup>.

**Ion exchange procedure.** 2 g of the clay was suspended in 200 mL of a 1 M solution of the organic salt (> 25-fold excess of the CEC, delamination is prevented by the high ionic strength) and refluxed for 12 h. Then the clay was washed 5 times with 50/50 vol% water/ethanol mixture and dried in the vacuum oven at 70 °C.

### Delamination experiment

A known amount of ion-exchanged vermiculite powder was added to 10 mL of MilliQ water in a 15 mL centrifuge tube and was equilibrated in an overhead shaker for 24 h. The vermiculite was then centrifuged at 3000 g for 10 minutes, and the supernatant with the delaminated nanosheets was poured into a Petri dish with a known weight. The water from the supernatant was completely evaporated at 120 °C, and then the Petri dish was equilibrated at 43% RH for 24 h. After weighing the Petri dish, the delamination yield was determined by the ratio between the weight of the nanosheets left after evaporation to the initial weight of vermiculite added for the delamination experiment.

### SAXS measurements

SAXS data was collected with a “Double Ganesha AIR” (SAXSLAB, Denmark). In this laboratory-based system, a focused X-ray beam is provided by a rotating copper anode (MicoMax 007HF, Rigaku Corporation, Japan). A position-sensitive detector (PILATUS 300 K, Dectris) was used in different positions to cover the range of the scattering vector  $q = 0.004\text{--}0.6 \text{ \AA}^{-1}$ . Before the measurement, the clay suspensions were added to 1 mm glass capillaries (Hilgenberg, code 4007610). The circularly averaged data was normalized to the incident beam, sample thickness, and measurement time. The scattering of a solvent filled capillary was used for background subtraction. Further evaluation was done with the software Scatter (version 2.5).<sup>72</sup> The measurements for ESI† are performed in vacuum at room temperature on a Xeuss 3.0 (Xenocs SAS, Grenoble, France) equipped with a Cu K $\alpha$  source (wave length of  $\lambda = 1.54 \text{ \AA}$ ) and a Dectris EIGER 2R 1M detector. Different sample to detector distances (50, 350, 900, 1200 and 1800 mm) were used to cover a wider range of scattering vectors  $q$ .

### AFM measurements

The surface topography has been determined by atomic force microscopic measurements. The images were acquired with a Dimension Icon (Bruker Nano Inc.) in PeakForce tapping mode in air. ScanAsyst Air cantilever (Bruker Nano Inc.) with a typical spring constant of 0.4 N m<sup>-1</sup> and a resonant frequency of 70 kHz was used. The PeakForce amplitude was 60 nm and the PeakForce frequency was 2 kHz. The AFM images were processed with NanoScope Analysis 1.80 (Bruker Nano Inc.). The topography was flattened by subtracting a first-order polynomial background using a threshold to exclude platelets from flattening. Platelet heights were determined by means of ‘step tool’ in NanoScope Analysis software. The samples were prepared by slow evaporation of a few drops of a diluted suspension (0.02 g L<sup>-1</sup>) on a Si-wafer under ambient conditions.

### Particle size distribution

Particle size distribution was recorded by static light scattering (SLS) of aqueous dispersions using a Retsch Horiba LA-950 SLS instrument. The refractive index of the solid phase was set to a value of 1.5. A measurement routine called “mica in water” supplied by the manufacturer (Horiba) was applied. The routine determines transmission rates and optimizes the concentration of the suspensions.

**Scanning electron microscopy (SEM).** SEM images of the cross-section of the film were observed using a ZEISS LEO 1530 (Carl Zeiss AG, Germany) operating at 3 kV.

### Foil fabrication

PLA-vermiculite solution was prepared by mixing 2.5 g of a 10 wt% PLA solution in  $\gamma$ -BL with 5 g of a 5 wt% vermiculite dispersion in a  $\gamma$ -BL/NMF (90:10) mixture. Total solid content was 6.67 wt%. This solution was mixed overnight on an overhead mixer before being coated onto a CNF substrate using a doctor blading unit (Zehntner ZAA 2300, Zehntner GmbH Testing Instruments, Switzerland). The substrate temperature was 60 °C, the blade speed was 1.5 cm s<sup>-1</sup>, and the blade height was 250  $\mu$ m. For the PLA/CNF foil, the PLA solution was coating directly onto the CNF foil using the same conditions. The coated foils were dried overnight at room temperature then in 40 °C oven for two days. Complete solvent removal was confirmed using thermal gravimetric analysis (Fig. S9, ESI<sup>†</sup>).

Coating thickness of 5  $\mu$ m was determined using a high-accuracy Digimatic micrometer (Mitutoyo, Japan) with a measuring range of 0–25 mm and a resolution of 0.0001 mm. Thickness was also confirmed with SEM imaging (Fig. S6, ESI<sup>†</sup>).

### Oxygen transmission rates (OTR)

OTR was determined on a Mocon OX-TRAN 2/21 M10x system (Mocon Inc., USA) with a lower detection limit of  $5 \times 10^{-4}$  cm<sup>3</sup> m<sup>-2</sup> day<sup>-1</sup> atm<sup>-1</sup>. The measurements were performed at 23 °C and 65% RH. A mixture of 98 vol% nitrogen and 2 vol% hydrogen was used as the carrier gas and pure oxygen as the permeant (>99.95%, Linde Sauerstoff 3.5).

### Water vapor transmission rates (WVTR)

WVTR was determined on a HiBarSens HBS 2.0 HT (Sempa Systems GmbH, Dresden, Germany) with a lower detection limit of  $10^{-6}$  g m<sup>-2</sup> day<sup>-1</sup>. The tests were conducted at 23 °C at a relative humidity of 75%.

### Thermal gravimetric analysis (TGA)

Thermogravimetric analysis was performed at a TG 209 F1 Libra (Netzsch). Approximately 8 mg of the sample was precisely weighed into an aluminum crucible (Concavus) by the internal balance of the machine. The sample was measured in the range of 25–600 °C under nitrogen. The program Proteus Analysis version 8.0 was used to process the results.

### X-Ray diffraction (XRD)

XRD patterns were obtained on a Bragg–Brentano-type diffractometer (Empyrean, Malvern Panalytical BV, The Netherlands) equipped with a PIXcel-1D detector using Cu K $\alpha$  radiation ( $\lambda = 1.54187$  Å). All patterns were analyzed using Malvern Panalytical's HighScore Plus software.

### Optical properties

Transmittance, haze, and clarity were measured on a BYK-Gardner Haze-Gard Plus (BYK-Gardner GmbH, Germany). An average of five measurements per film sample were taken.

## Author contributions

V. D. and R. T. contributed equally to this work. J. B., S. A., T. T. conceived and supervised the research. V. D. optimized the vermiculite delamination and performed the transfer to organic solvents. V. D. and O. K. performed the characterization of the nanosheets. Investigation of delamination progress by SAXS was done by V. D. and S. R. R. T. and M. R. performed foil fabrication and barrier measurements. V. D., R. T., O. K., and J. B. wrote the manuscript. All authors discussed the results and commented on the manuscript.

## Conflicts of interest

There are no conflicts to declare.

## Acknowledgements

V. Dudko and R. Timmins contributed equally to this work. The project has been funded by the Deutsche Forschungsgemeinschaft (DFG, German Research Foundation) – project number 391977956 –SFB1357/C02. V. D. thanks the Elite Network of Bavaria for support. Tekla Tammelin gratefully acknowledges the Academy of Finland's Flagship Competence Center for Materials Bioeconomy, FinnCERES. The authors thank Marco Schwarzmann for preparing and taking the transmission electron microscopy images, Michael Thelen for AFM measurements, and Dr Matthias Daab for useful discussions. We appreciate the support of the Keylabs for Polymer Additives and Fillers, Optical and Electron Microscopy, Mesoscale Characterization: Scattering Techniques, Surface and Interface Characterization of the Bavarian Polymer Institute (BPI).

## Notes and references

- 1 Food waste footprint Impacts on natural resources, Food and Agriculture Organization of the United Nations, 2013.
- 2 S. Atkinson and I. Payne, A Throwaway World: the challenge of plastic packaging and waste, <https://www.ipsos.com/en/throwaway-world-challenge-plastic-packaging-and-waste>, 2022).

- 3 Single-Use Plastics Prohibition Regulations, <https://www.gazette.gc.ca/rp-pr/p1/2021/2021-12-25/html/reg2-eng.html>, 2022).
- 4 Single-use plastics, [https://ec.europa.eu/environment/topics/plastics/single-use-plastics\\_en](https://ec.europa.eu/environment/topics/plastics/single-use-plastics_en), 2022).
- 5 C. J. Moore, *Environ. Res.*, 2008, **108**, 131–139.
- 6 N. D. Steenis, E. van Herpen, I. A. van der Lans, T. N. Ligthart and H. C. M. van Trijp, *J. Cleaner Prod.*, 2017, **162**, 286–298.
- 7 F. Riedewald, E. Wilson, Y. Patel, D. Vogt, I. Povey, K. Barton, L. Lewis, T. Caris, S. Santos and M. O'Mahoney, *Waste Manage.*, 2022, **138**, 172–179.
- 8 M. C. Heller, S. E. M. Selke and G. A. Keoleian, *J. Ind. Ecol.*, 2018, **23**, 480–495.
- 9 M. van Birgelen, J. Semeijn and M. Keicher, *Environment and Behavior*, 2008, **41**, 125–146.
- 10 H. Shaghaleh, X. Xu and S. Wang, *RSC Adv.*, 2018, **8**, 825–842.
- 11 G. de Souza, M. N. Belgacem, A. Gandini and A. J. F. Carvalho, *Cellulose*, 2021, **28**, 1617–1632.
- 12 P. Willberg-Keyrilainen, J. Vartiainen, J. Pelto and J. Ropponen, *Carbohydr. Polym.*, 2017, **170**, 160–165.
- 13 I. Leppänen, M. Vikman, A. Harlin and H. Orelma, *J. Polym. Environ.*, 2019, **28**, 458–470.
- 14 J.-W. Rhim, H.-M. Park and C.-S. Ha, *Prog. Polym. Sci.*, 2013, **38**, 1629–1652.
- 15 C. Habel, M. Schöttle, M. Daab, N. J. Eichstaedt, D. Wagner, H. Bakhshi, S. Agarwal, M. A. Horn and J. Breu, *Macromol. Mater. Eng.*, 2018, **303**, 1800333.
- 16 R. L. Timmins, A. Kumar, M. Röhrli, K. Havlíček, S. Agarwal and J. Breu, *Macromol. Mater. Eng.*, 2021, 2100727, DOI: [10.1002/mame.202100727](https://doi.org/10.1002/mame.202100727).
- 17 Y. Cui, S. Kumar, B. Rao Kona and D. van Houcke, *RSC Adv.*, 2015, **5**, 63669–63690.
- 18 B. Tan and N. L. Thomas, *J. Membr. Sci.*, 2016, **514**, 595–612.
- 19 F. Wu, M. Misra and A. K. Mohanty, *Prog. Polym. Sci.*, 2021, **117**, 101395.
- 20 S. Singha and M. S. Hedenqvist, *Polymers*, 2020, **12**(5), 1095.
- 21 M. Stöter, D. A. Kunz, M. Schmidt, D. Hirsemann, H. Kalo, B. Putz, J. Senker and J. Breu, *Langmuir*, 2013, **29**, 1280–1285.
- 22 L. J. Michot, I. Bihannic, S. Maddi, S. S. Funari, C. Baravian, P. Levitz and P. Davidson, *Proc. Natl. Acad. Sci. U. S. A.*, 2006, **103**, 16101–16104.
- 23 M. Daab, N. J. Eichstaedt, A. Edenharter, S. Rosenfeldt and J. Breu, *RSC Adv.*, 2018, **8**, 28797–28803.
- 24 M. Daab, N. J. Eichstaedt, C. Habel, S. Rosenfeldt, H. Kalo, H. Schießling, S. Förster and J. Breu, *Langmuir*, 2018, **34**, 8215–8222.
- 25 J. E. F. C. Gardolinski and G. Lagaly, *Clay Miner.*, 2005, **40**, 547–556.
- 26 W. J. Roth, T. Sasaki, K. Wolski, Y. Song, D.-M. Tang, Y. Ebina, R. Ma, J. Grzybek, K. Kałahurska, B. Gil, M. Mazur, S. Zapotoczny and J. Cejka, *Sci. Adv.*, 2020, **6**, eaay8163.
- 27 L. Wang and T. Sasaki, *Chem. Rev.*, 2014, **114**, 9455–9486.
- 28 P. Davidson, C. Penisson, D. Constantin and J.-C. P. Gabriel, *Proc. Natl. Acad. Sci. U.S.A.*, 2018, **115**, 6662–6667.
- 29 J.-C. P. Gabriel, F. Camerel, B. J. Lemaire, H. Desvaux, P. Davidson and P. Batail, *Nature*, 2001, **413**, 504–508.
- 30 R. Liu, T. Gong, K. Zhang and C. Lee, *Sci. Rep.*, 2017, **7**, 1–9.
- 31 E. S. Tsurko, P. Feicht, C. Habel, T. Schilling, M. Daab, S. Rosenfeldt and J. Breu, *J. Membr. Sci.*, 2017, **540**, 212–218.
- 32 T. Schilling, C. Habel, S. Rosenfeldt, M. Röhrli and J. Breu, *ACS Applied Polymer Materials*, 2020, **2**, 3010–3015.
- 33 V. Dudko, K. Ottermann, S. Rosenfeldt, G. Papastavrou and J. Breu, *Langmuir*, 2021, **37**, 461–468.
- 34 T. J. Brown, N. E. Idoine, C. E. Wrighton, E. R. Raycraft, S. F. Hobbs, R. A. Shaw, P. Everett, E. A. Deady and C. Kresse, *World Mineral Production 2015–2019*, British Geological Survey, Nottingham, UK, 2021.
- 35 H. Kalo, M. W. Möller, D. A. Kunz and J. Breu, *Nanoscale*, 2012, **4**, 5633–5639.
- 36 A. Meunier, *Clay Miner.*, 2006, **41**, 551–566.
- 37 S. Taruta, R. Obara, N. Takusagawa and K. Kitajima, *J. Mater. Sci.*, 2005, **40**, 5597–5602.
- 38 M. Daab, S. Rosenfeldt, H. Kalo, M. Stöter, B. Bojer, R. Siegel, S. Förster, J. Senker and J. Breu, *Langmuir*, 2017, **33**, 4816–4822.
- 39 W. G. Garrett and G. F. Walker, *Clays Clay Miner.*, 1960, **9**, 557–567.
- 40 G. F. Walker and W. G. Garrett, *Science*, 1967, **156**, 385–387.
- 41 J. A. Rausell-Colom and P. S. Salvador, *Clay Miner.*, 1971, **9**, 139–149.
- 42 L. F. Braganza, R. J. Crawford, M. V. Smalley and R. K. Thomas, *Clays Clay Miner.*, 1990, **38**, 90–96.
- 43 J. L. Pérez-Rodríguez, F. Carrera, J. Poyato and L. A. Pérez-Maqueda, *Nanotechnology*, 2002, **13**, 382–387.
- 44 S. Rosenfeldt, M. Stöter, M. Schlenk, T. Martin, R. Q. Albuquerque, S. Förster and J. Breu, *Langmuir*, 2016, **32**, 10582–10588.
- 45 M. J. Wilson, *Clay Miner.*, 1999, **34**, 7–25.
- 46 J.-J. Shao, K. Raidongia, A. R. Koltonow and J. Huang, *Nat. Commun.*, 2015, **6**, 1–7.
- 47 B. Rotenberg, J.-P. Morel, V. Marry, P. Turq and N. Morel-Desrosiers, *Geochim. Cosmochim. Acta*, 2009, **73**, 4034–4044.
- 48 K. N. Pearce, *Aust. J. Chem.*, 1980, **33**, 1511–1517.
- 49 J. W. Bunting and K. M. Thong, *Can. J. Chem.*, 1970, **48**(11), 1654–1656.
- 50 N. T. Skipper, A. K. Soper and J. D. C. McConnell, *J. Chem. Phys.*, 1991, **94**, 5751–5760.
- 51 L. Boldon, F. Laliberte and L. Liu, *Nano Rev.*, 2015, **6**(1), 25661.
- 52 E. Paineau, I. Bihannic, C. Baravian, A.-M. Philippe, P. Davidson, P. Levitz, S. S. Funari, C. Rochas and L. J. Michot, *Langmuir*, 2011, **27**, 5562–5573.
- 53 D. Goossens, *Sedimentology*, 2008, **55**, 65–96.
- 54 P. Das, J.-M. Malho, K. Rahimi, F. H. Schacher, B. Wang, D. E. Demco and A. Walther, *Nat. Commun.*, 2015, **6**, 1–14.
- 55 J. Barthel, R. Buchner and B. Wurm, *J. Mol. Liq.*, 2002, **98–99**, 51–69.
- 56 C. M. Hansen, *Hansen Solubility Parameters*, CRC Press, 2007.
- 57 K. Missoum, P. Sadoeco, J. Causio, M. N. Belgacem and J. Bras, *Mater. Sci. Eng., C*, 2014, **45**, 477–483.
- 58 M. Lassoued, F. Crispino and E. Loranger, *Carbohydr. Polym.*, 2021, **254**, 117411.

## Materials Advances

## Paper

- 59 A. Mautner, K. Y. Lee, P. Lahtinen, M. Hakalahti, T. Tammelin, K. Li and A. Bismarck, *Chem. Commun.*, 2014, **50**, 5778–5781.
- 60 K.-Y. Lee, T. Tammelin, K. Schulfter, H. Kiiskinen, J. Samela and A. Bismarck, *ACS Appl. Mater. Interfaces*, 2012, **4**, 4078–4086.
- 61 T. Mäkelä, M. Kainlauri, P. Willberg-Keyriläinen, T. Tammelin and U. Forsström, *Microelectron. Eng.*, 2016, **163**, 1–6.
- 62 H. C. Langowski, Presented in part at the Permeation durch Packstoffe, Freising, 2008.
- 63 J. E. Samuels, *High-barrier flexible polyvinylidene chloride composite applications*, ASTM International, 1986.
- 64 J. Lange and Y. Wyser, *Packag. Technol. Sci.*, 2003, **16**, 149–158.
- 65 M. Putkonen, P. Sippola, L. Svrđ, T. Sajavaara, J. Vartiainen, I. Buchanan, U. Forsström, P. Simell and T. Tammelin, *Philos. Trans. R. Soc., A*, 2018, **376**, 20170037.
- 66 M. Röhrli, L. K. S. Federer, R. L. Timmins, S. Rosenfeldt, T. Dörres, C. Habel and J. Breu, *ACS Appl. Mater. Interfaces*, 2021, **13**, 48101–48109.
- 67 S. Spoljaric, A. Salminen, N. Dang Luong, P. Lahtinen, J. Vartiainen, T. Tammelin and J. Seppälä, *Polym. Compos.*, 2014, **35**, 1117–1131.
- 68 G. L. Robertson, *Food packaging: principles and practice*, CRC press, 2005.
- 69 G. L. Robertson, *Food packaging and shelf life: a practical guide*, CRC Press, 2009.
- 70 T. Tammelin, A. Harlin, M. Vehviläinen, P. Nousiainen and K. Kolppo, *BioResources*, 2011, **6**, 2386–2398.
- 71 T. Tammelin, A. Salminen and U. Hippi, *WIPO (PCT)*, WO2013/060934, 2012.
- 72 S. Förster, S. Fischer, K. Zielske, C. Schellbach, M. Sztucki, P. Lindner and J. Perlich, *Adv. Colloid Interface Sci.*, 2011, **163**, 53–83.

## Supporting Information

Spontaneous Delamination of Affordable Natural Vermiculite as a High Barrier Filler for Biodegradable Food Packaging

Volodymyr Dudko, Renee L. Timmins, Olena Khoruzhenko, Maximilian Röhl, Christopher Greve, Sabine Rosenfeldt, Tekla Tammelin, Seema Agarwal, Eva M. Herzig, Josef Breu\*

*Materials Advances* **2022**, 3 (24), 9052-9062.

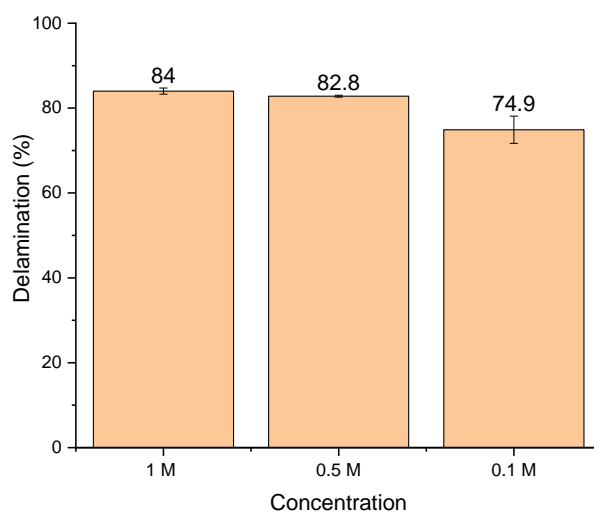


**Figure S1.** Comparison of the delamination yield depending on concentration of the cation.

**CHN analysis****Table S1.** Experimental wt% of C and N in exchanged organoclays

	C <sub>4</sub> Cl <sup>-</sup>	Na to C <sub>4</sub> Cl <sup>-</sup>	C <sub>4</sub> Ac <sup>2-</sup>
C, wt %	3.9	4.78	7.6
N, wt %	1.08	1.31	2.21

C<sub>4</sub> Cl<sup>-</sup> is the sample prepared via single exchange using butylammonium cation and chlorine as a counter anion.

Na to C<sub>4</sub> Cl<sup>-</sup> denotes the two step sequential exchange with sodium and then with C<sub>4</sub> Cl<sup>-</sup>.

C<sub>4</sub> Ac<sup>2-</sup> denotes the single exchange using the butylammonium cation and citrate as a counter anion.

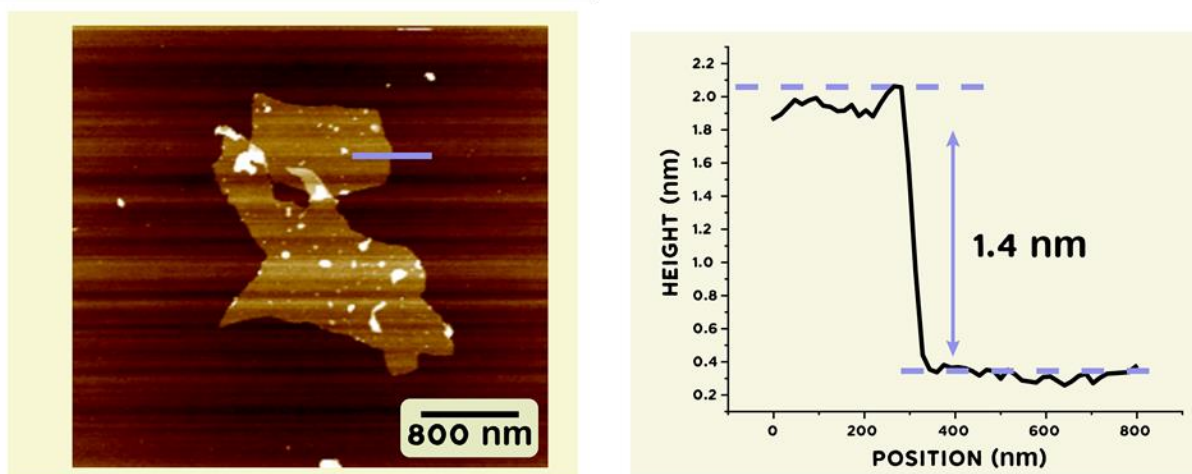


**Figure S2.** Topographic AFM image of a single nanosheet from an aqueous suspension with the height profile

**Cussler's theory for permeability:**

$$P_{rel} = P/P_0 = \left(1 + \mu \left(\frac{\alpha^2 \phi^2}{1-\phi}\right)\right)^{-1} \quad \text{Equation S1}$$

Where P is the permeability of the nanocomposite,  $P_0$  is the permeability of the neat polymer,  $\phi$  is the filler content (volume fraction),  $\alpha$  is the aspect ratio of the filler,  $\mu$  is a geometrical factor dependent on filler shape (in case of platelet shape filler it is  $4/9$ )<sup>1</sup>

To calculate theoretical improvement factor for different nanosheet sizes:  $\mu$  is  $4/9$ , aspect ratio is 30 for Laponite, 150 for Montmorillonite, 4000 for Vermiculite.

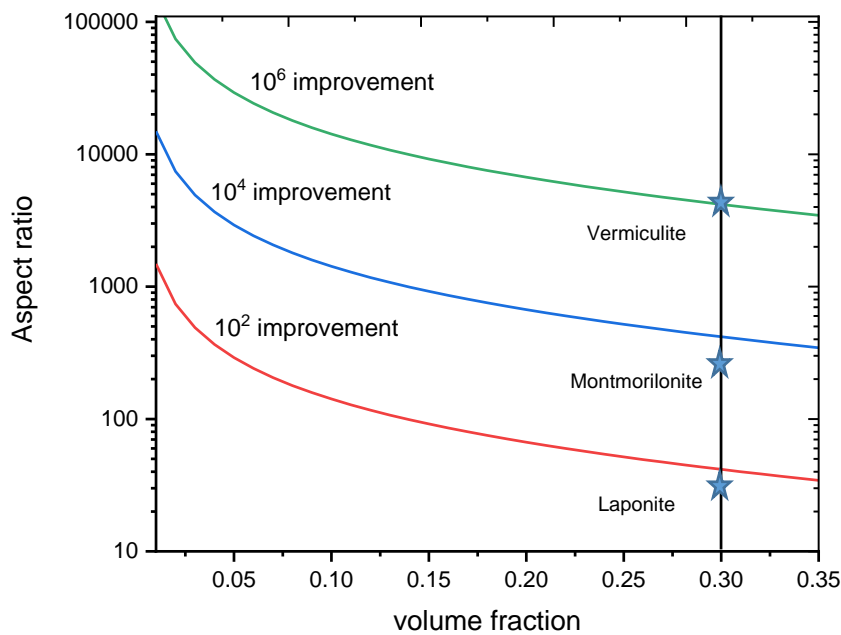


**Figure S3.** Improvement based on different aspect ratio nanosheets. The vertical line corresponds to a filler content as applied in the PLA-verm/CNF foil stressing the superiority of the vermiculite nanosheets compared to more common clay fillers.

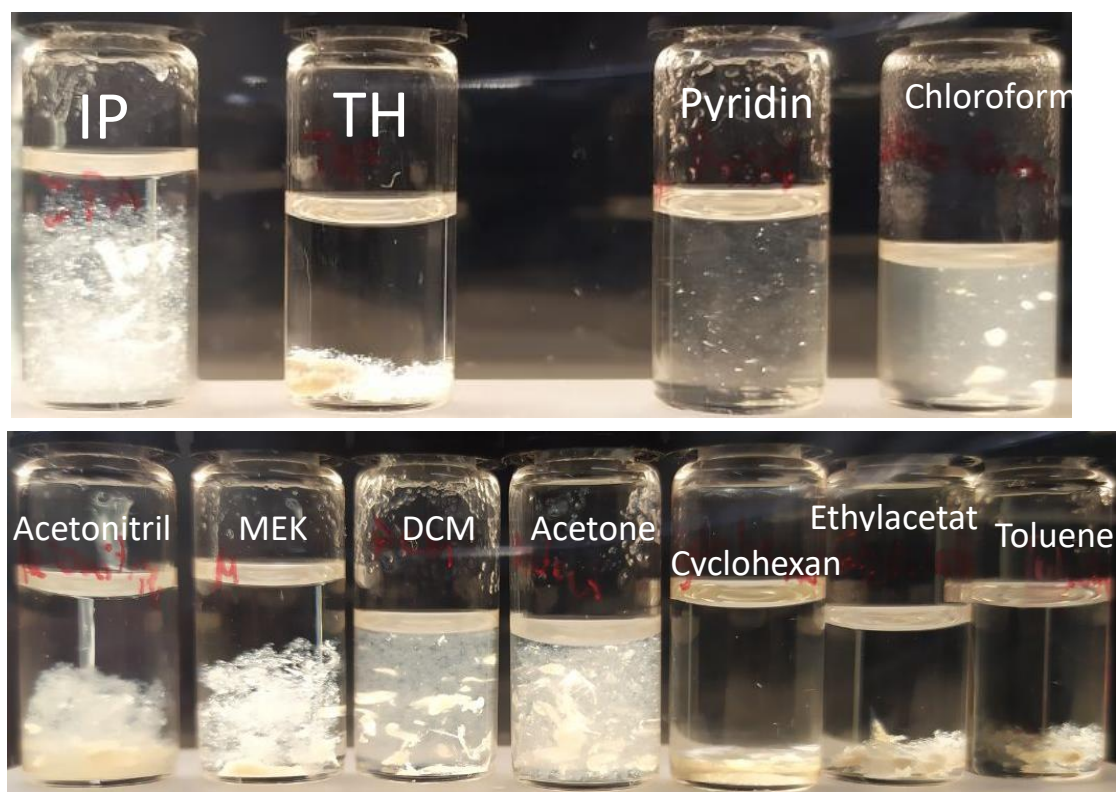


**Figure S4.** Photos of flocculated vermiculite samples in different solvents

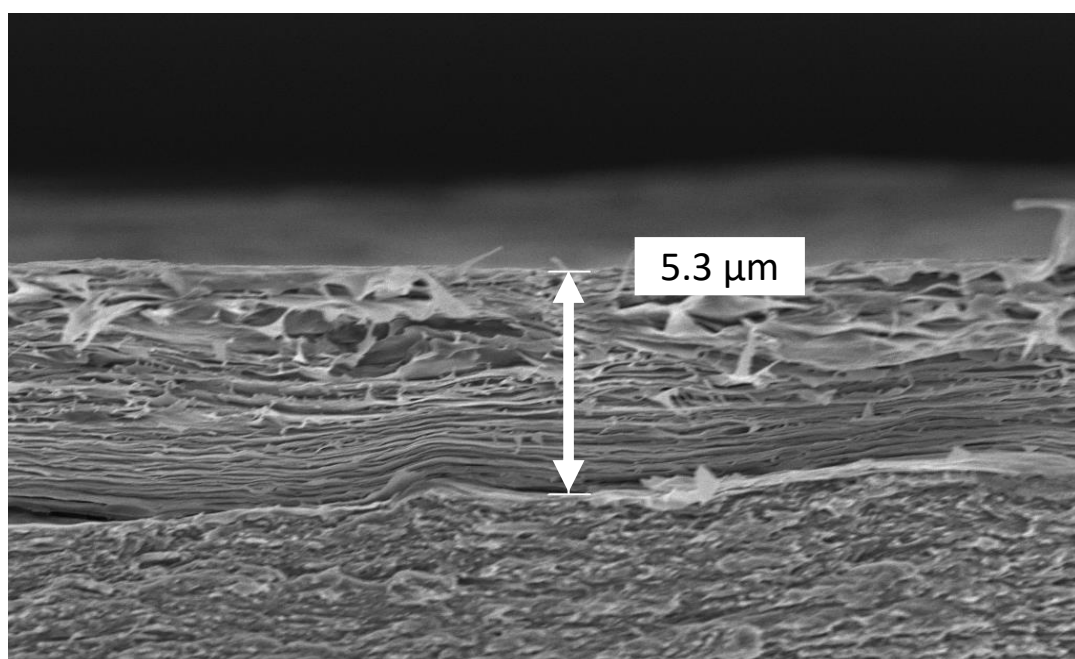


**Figure S5.** SEM photo of PLA-verm/CNF foil cross section. Marked bar denotes the thickness of the coating

**Table S2.** Summary of the solvent properties of the solvents used in the studies of natural vermiculite swelling

Solvents	Relative dielectric constant <sup>2</sup>	Dipole moment, D <sup>2</sup>	$\delta D^3$ [Mpa <sup>1/2</sup> ]	$\delta P$ [Mpa <sup>1/2</sup> ]	$\delta H$ [Mpa <sup>1/2</sup> ]	Swelling
Ethanol	24.5	1.66	15.8	8.80	19.4	yes
Methanol	32.6	2.87	14.7	12.3	22.3	yes
DMac	37.8	3.72	16.8	11.5	9.40	yes
DMSO	46.7	4.10	18.4	16.4	10.2	yes
NMF	171 <sup>4</sup>	3.83	17.4	18.8	15.9	yes
Water	80.1	1.87	15.5	16.0	42.3	yes
N-methyl-acetamide	179 <sup>4</sup>	4.12	16.9	17.0	13.0	yes
FA	111	3.71	17.2	26.2	19.0	yes
$\gamma$ -BL	41.0	4.27	18	16.6	7.40	yes
Propylene carbonate	64.9 <sup>5</sup>	4.94	20	18.0	4.10	yes
NMP	32.2	4.09	18	12.3	7.20	yes
DMF	36.7	3.79	17.4	13.7	11.3	yes
Isopropanol	19.9	1.59	15.8	6.10	16.4	no
Cyclohexane	1.88	0	16.8	0	0.20	no
Pyridine	12.5	2.37	19.0	8.80	5.90	no
Acetonitrile	38.8	3.44	15.3	18.0	6.10	no
Methylethyl ketone	18.5	2.78	16.0	9.00	5.10	no
Acetone	21.4	2.69	15.5	10.4	7.00	no
Toluene	2.38	0.31	18.0	1.4	2.00	no
Chloroform	4.81	1.15	17.8	3.1	5.70	no
Dichloro-methane	8.93	1.14	17.0	7.3	7.10	no
Tetra-hydrofuran	7.58	1.69	16.8	5.7	8.00	no
Ethylacetate	6.40	1.88	15.8	5.3	7.20	no

DMac-Dimethylacetamide, DMSO- Dimethyl sulfoxide, NMF- N-Methylformamide, FA- Formamide,

$\gamma$ -BL- gamma-Butyrolactone, NMP- N-Methyl-2-pyrrolidone, DMF- Dimethylformamide,  $\delta D$  dispersive,  $\delta P$  polar,  $\delta H$  hydrogen bond component of Hansen parameters.

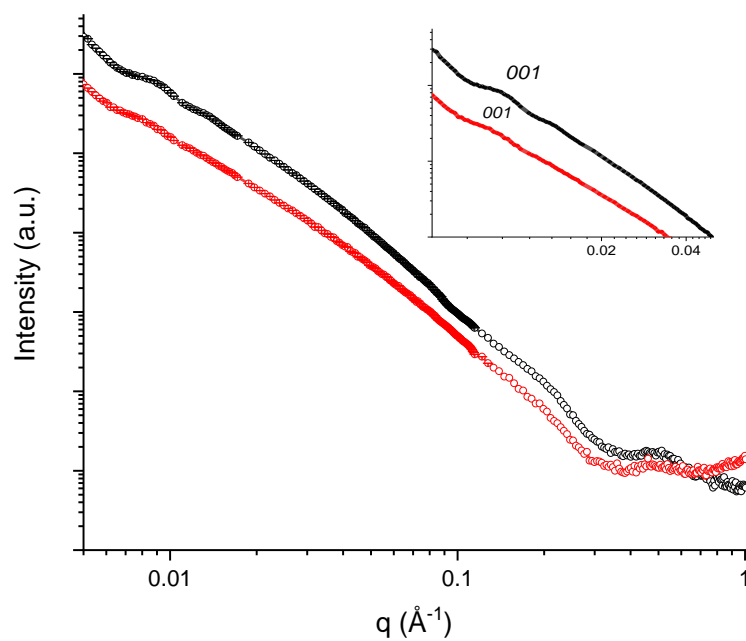


**Figure S5.** SAXS pattern of the vermiculite in gamma-bl (black) and vermiculite + PLA in gamma-bl (red), showing the *001* oscillation in similar position of  $q$ , showing that addition of PLA to vermiculite suspension do not compromise the colloidal stability of nanosheets. Insert shows the  $q$  range from 0.005 to 0.05 Å<sup>-1</sup> with higher magnifications.

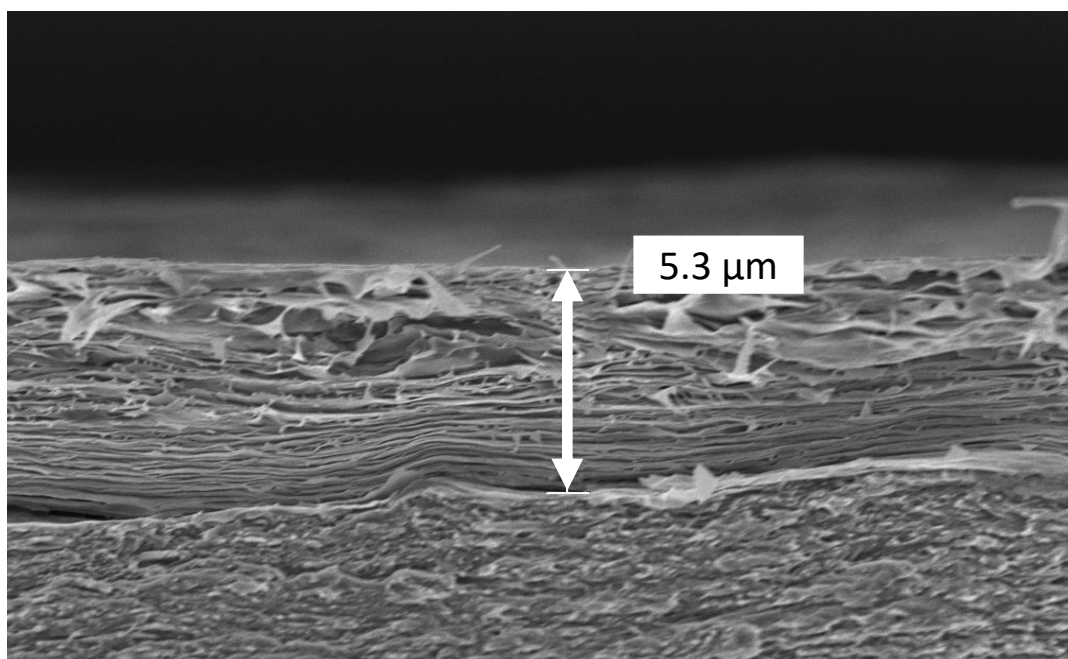


**Figure S6.** SEM photo of PLA-verm/CNF foil cross section. Marked bar denotes the thickness of the coating

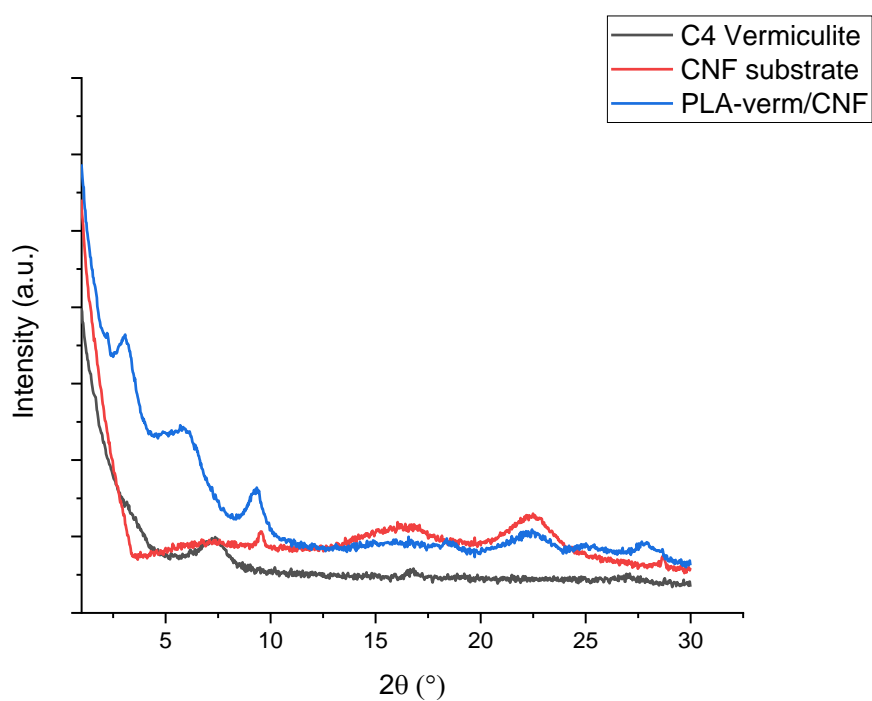


**Figure S7.** XRD pattern of the C4 exchanged vermiculite, CNF foil and PLA-verm/CNF nanocomposite.

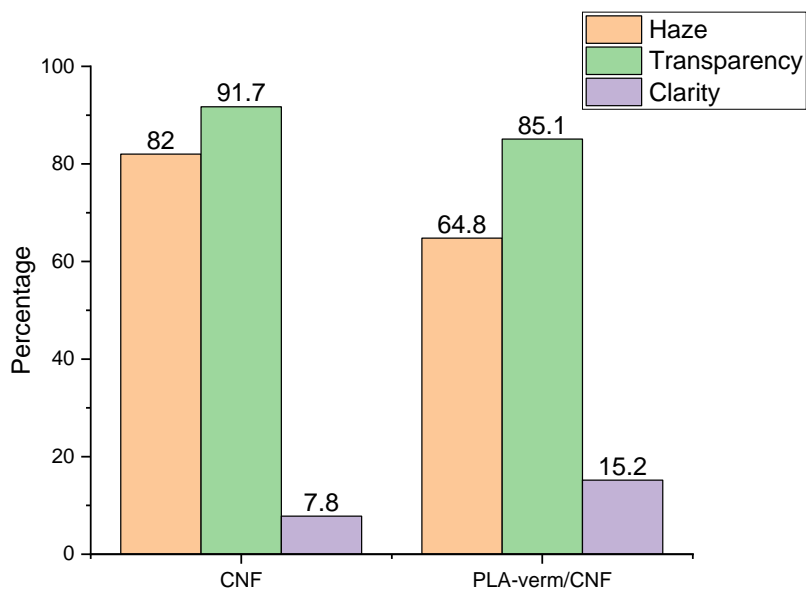


**Figure S8.** Optical properties (transmittance, haze, clarity) of the neat CNF substrate and CNF/Verm foil.

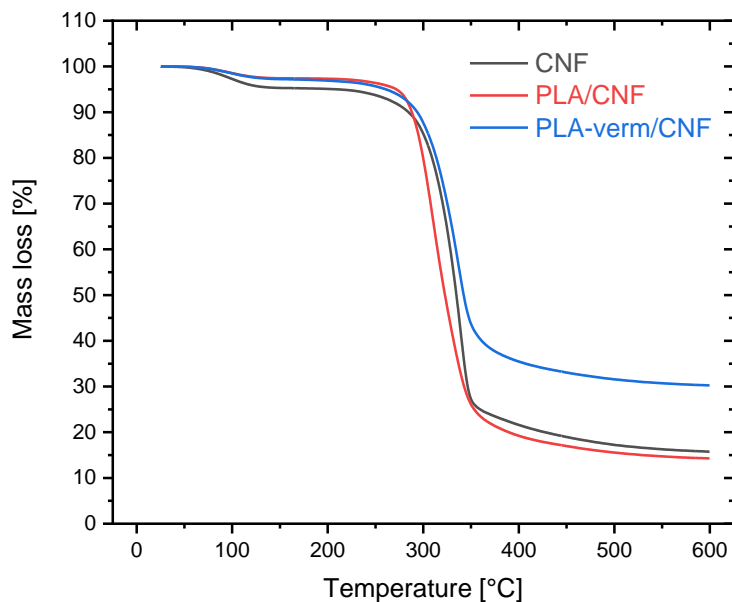


**Figure S9.** Thermal gravimetric analysis of CNF substrate (black), CNF coated with PLA (red), and CNF coated with PLA-verm nanocomposite (blue)

**Calculation for barrier improvement factor**

The OTRs for the coatings can be calculated by;

$$OTR_{coating} = \frac{1}{\frac{1}{OTR_{total}} - \frac{1}{OTR_{substrate}}}$$

Permeability ( $P$ ) of both the neat polymer coating and the nanocomposite coating are calculated using their respective thicknesses ( $d$ );

$$P = OTR * d$$

For water vapor permeability, the water vapor partial pressure ( $\Delta p$ ) must be considered. At 100% RH and 23°C,  $\Delta p$  is 0.0277 atm, which corresponds to  $\Delta p = 0.020775$  atm at 75% RH and 23 °C. The new equation is;

$$P = \frac{OTR * d}{\Delta p}$$

Barrier improvement factor (BIF) is the ratio of the permeability of the neat polymer coating ( $P_{neat}$ ) to the permeability of the nanocomposite coating ( $P_{nc}$ );

$$BIF = \frac{P_{neat}}{P_{nc}} \quad \text{Equation S2}$$

**Calculation for theoretical shelf life<sup>6</sup>:**

For 500 g of powder material that is 2 wt% water content,

$$weight_{dry} = 500 * 0.98 = 490 \text{ g}$$

$$weight_{water} = 500 * 0.02 = 10 \text{ g}$$

For a critical moisture content of 8 wt%, the final weight of water in the powder is,

$$weight_{max} = \frac{490}{0.92} - 490 = 42.6 \text{ g}$$

The weight of water to permeate into the powder is,

$$42.6 - 10 = 32.6 \text{ g}$$

For a rectangular package of dimensions 3 x 15 x 10 cm, the surface area is 0.045 m<sup>2</sup>

The amount of water permeating into the package per day is

$$weight_{water \text{ per day}} = 0.045 \text{ m}^2 * OTR$$

The time to reach the critical moisture content (i.e. shelf life) is,

$$shelf \text{ life} = \frac{32.6 \text{ g}}{weight_{water \text{ per day}}}$$

References:

- [1] E. L. Cussler, S. E. Hughes, W. J. Ward, R. Aris, *J. Membr. Sci.* **1988**, 38, 161.
- [2] W. M. Haynes, *CRC Handbook of Chemistry and Physics*, CRC Press, **2011**.
- [3] C. M. Hansen, *Hansen Solubility Parameters*, CRC Press, **2007**.
- [4] J. Barthel, R. Buchner, B. Wurm, *J. Mol. Liq.* **2002**, 98-99, 51.
- [5] Y. Chernyak, *J. Chem. Eng. Data* **2006**, 51, 416.
- [6] G. L. Robertson, *Food packaging and shelf life: a practical guide*, CRC Press, **2009**.

## 6.4. Biodegradation in Wastewater of Water-Soluble Polymer/Clay Barrier Films from Green and Scalable Processing

Maximilian Röhl<sup>‡</sup>, Renee L. Timmins<sup>‡</sup>, Dipannita Ghosh, Dominik D. Schuchardt, Sabine Rosenfeldt, Simon Nürnberger, Uwe Bölz, Seema Agarwal, and Josef Breu\*

<sup>‡</sup>these authors contributed equally to this work

\*corresponding author(s): josef.breu@uni-bayreuth.de



Individual contribution:

Prof. Dr. Josef Breu, Maximilian Röhl, and I conceptualized the paper. Maximilian Röhl prepared the films and performed gas barrier and optical property measurements. I performed mechanical testing and contributed to data processing and interpretation. Dipannita Ghosh performed biodegradation testing, Dominik D. Schuchardt provided scientific discussion, and Sabine Rosenfeldt performed the SAXS measurement. Simon Nürnberger performed the water solubility testing. Uwe Bölz provided scientific discussion. Prof. Dr. Seema Agarwal assisted with experimental design and scientific input regarding biodegradation testing. The paper was written by Maximilian Röhl, Prof. Dr. Josef Breu, and myself with editing and proofreading from all authors.

# Green and scalable processing of water-soluble, biodegradable polymer/clay barrier films

Maximilian Röhr1 | Renee L. Timmins1 | Dipannita Ghosh2 |  
 Dominik D. Schuchardt1 | Sabine Rosenfeldt3 | Simon Nürnberger1 |  
 Uwe Bölz4 | Seema Agarwal2 | Josef Breu1 

<sup>1</sup>Bavarian Polymer Institute, Department of Chemistry, University of Bayreuth, Bayreuth, Germany

<sup>2</sup>Macromolecular Chemistry II, Bavarian Polymer Institute, Department of Chemistry, University of Bayreuth, Bayreuth, Germany

<sup>3</sup>Physical Chemistry I, Bavarian Polymer Institute, Department of Chemistry, University of Bayreuth, Bayreuth, Germany

<sup>4</sup>HPX Polymers GmbH, Tutzing, Germany

## Correspondence

Josef Breu, Bavarian Polymer Institute and Department of Chemistry, University of Bayreuth, Bayreuth 95447, Germany. Email: [josef.breu@uni-bayreuth.de](mailto:josef.breu@uni-bayreuth.de)

## Funding information

H2020 Marie Skłodowska-Curie Actions, Grant/Award Number: 860720; Deutsche Forschungsgemeinschaft, Grant/Award Number: SFB 1357-391977956

## Abstract

Poly(vinyl alcohol) (PVOH) based water-soluble packaging with intentional disposal into wastewater provides great convenience for both households and industry. In this paper, we demonstrate with CO<sub>2</sub> evolution testing that only insignificant fractions (~2%) of PVOH biodegrade in wastewater within 33 days. To avoid unintentional environmental build-up and the accompanying consequences to marine life, alternative materials with a suitable balance of performance and biodegradability are needed. Until now, the barrier properties of biodegradable biopolymers could not compete with state-of-the-art water-soluble packaging materials like PVOH films. In this paper, we report on waterborne, sandwich-structured films using hydroxypropyl methylcellulose or alginate produced with an industrially scalable slot-die coater system. The inner layer of the film consists of a collapsed nematic suspension of high aspect ratio synthetic clay nanosheets that act as an impermeable wall. Such a film structure not only allows for barrier filler loadings capable of sufficiently reducing oxygen and water vapor permeability of alginate to 0.063 cm<sup>3</sup> mm m<sup>-2</sup> day<sup>-1</sup> bar<sup>-1</sup> and 53.8 g mm m<sup>-2</sup> day<sup>-1</sup> bar<sup>-1</sup>, respectively, but also provides mechanical reinforcement to the biopolymer films facilitating scalable processing. Moreover, the films disintegrated in water in less than 6 min while rapid biodegradation of the dissolved polymer was observed.

## KEYWORDS

biodegradable and water-soluble packaging, microplastic, oxygen and water vapor barrier, slot die coating, sustainability

Maximilian Röhr1 and Renee L. Timmins contributed equally to this study.

This is an open access article under the terms of the [Creative Commons Attribution-NonCommercial](https://creativecommons.org/licenses/by-nc/4.0/) License, which permits use, distribution and reproduction in any medium, provided the original work is properly cited and is not used for commercial purposes.

© 2023 The Authors. *Journal of Applied Polymer Science* published by Wiley Periodicals LLC.

They are designed to dissolve and be released into the environment during use—particularly into wastewater streams. Poly(vinyl alcohol) (PVOH) is the most commonly employed polymer for such packaging as it is widely accepted as biodegradable. However, the kinetics of degradation in conventional wastewater are so slow that PVOH is actually considered a recalcitrant pollutant.<sup>2</sup>

Removal of PVOH from industrial wastewater is not accomplished through standard procedures, which consist of biological treatment with microbial stems that are commonly encountered in communal sewage plants to break down organic matter contaminants. The persistence of PVOH has led some to suggest the addition of advanced oxidation processes (ozonation, persulfate oxidation, electrochemical oxidation, etc.) to wastewater treatment facilities to reduce the level of contamination.<sup>3–5</sup> Unfortunately, this suggestion does not address the root of the problem and overlooks the poor worldwide accessibility to state-of-the-art wastewater treatment facilities.

Certain microorganisms, such as *Pseudomonas* (Sphingomonads) strains, are capable of biodegrading PVOH after acclimating in heavily contaminated waters, but the conditions for sufficient acclimation are highly specific. Such wastewater streams are primarily those of paper and textile treatment plants that continuously expel PVOH in large quantities.<sup>2,6,7</sup> Even with acclimated microorganisms, the kinetics of PVOH removal depends on various additional factors, including molecular weight, degree of hydrolysis, and the presence of salts.<sup>8,9</sup> PVOH contamination in natural water bodies has already brought consequences including increases in the chemical oxygen demand and inhibition of aerobic microorganisms, suffocating surface foam, and mobilization of heavy metals within water streams.<sup>5,10,11</sup>

Products that employ water-soluble films having an intentional disposal into the environment should be designed in a more responsible manner that does not contribute to wastewater pollution. The challenge is matching the excellent properties that PVOH provides with a more readily biodegradable alternative that meets the requirements during usage while allowing for being washed away. An ideal sustainable, water-soluble packaging film would exhibit biodegradability in wastewater, high gas barrier, flexible mechanical properties, transparent optical properties, as well as being suitable for high-volume manufacturing.

While natural biopolymers, including cellulose, alginate, whey protein, and so forth,<sup>12</sup> are quite attractive for use as alternative packaging material because they are readily water-soluble as well as biocompatible, nontoxic, and renewable,<sup>13</sup> they lack sufficient gas barrier and mechanical toughness. Both water vapor and oxygen barrier performance are critical considerations for commercial packaging

materials to prevent the breakdown of the film under ambient conditions and degradation of oxygen or water vapor sensitive products.<sup>14</sup> Some successful attempts to fabricate biopolymer films with properties relevant to water-soluble packaging offering a considerable water vapor barrier have been made at the lab scale, however, the fabrication techniques, including solvent casting or electrospinning, would not be practical for large-scale production.<sup>15,16</sup>

Improving the barrier of natural biopolymers can be accomplished effectively by the use of barrier fillers. The synthetic clay sodium hectorite (Hec) has imparted massive barrier improvements to biodegradable polymers in the past thanks to its exceptional aspect ratio and complete intercalation by water-soluble polymers.<sup>17,18</sup> Our group reported recently that band-like aggregates of Hec, even without an intercalated polymer matrix, provide an excellent barrier to oxygen due to the perfect clay nanosheet alignment induced during application by slot die coating.<sup>19</sup>

Slot die coating is a relatively unexplored lab-scale film preparation method that can easily be translated into a large-scale and low-cost roll-to-roll process. The instrument uses a die head having a thin slot from which metered solution exits onto a moving substrate. The encountered shear thinning on the applied solution is particularly useful to improve barrier properties due to the alignment of polymer chains and suspended barrier filler in the resulting film.<sup>20,21</sup>

In this work, we report a slot die coating method that can be translated into large-scale roll-to-roll manufacturing of high-barrier, self-standing biodegradable films for water-soluble packaging applications. Waterborne layered films made of Hec with either PVOH, hydroxypropyl methylcellulose (HPMC), or sodium alginate (alginate) were evaluated as a packaging material in terms of water solubility, gas barrier properties, mechanical performance, and optical properties. CO<sub>2</sub> evolution of the layered films in wastewater is compared to the same polymer film without Hec to ensure improvements in physical properties do not come at a sacrifice to biodegradability.

A roll-to-roll process easily enables the incorporation of multiple functional layers, unlike traditional solvent casting which is practically limited to a single monolayer. The layered structure of these films prevents complications that come with compounding a nematic Hec suspension with biopolymers like high viscosities, aggregation of filler, or embrittlement that limits high clay loadings.<sup>19</sup> At the same time, the exceptional barrier enhancement expected from the use of high aspect ratio nanosheets is ensured, producing biodegradable, high-performance, and scalable packaging films. With water being the only solvent employed, the production of the films aims to fulfill the 12 Principles of Green Chemistry.<sup>22</sup>

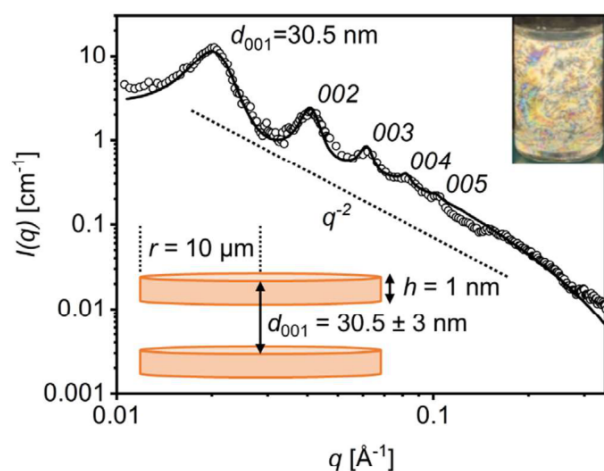


**FIGURE 1** Small angle x-ray scattering (SAXS) pattern of a 6 wt% ( $\approx 2.3$  vol%) aqueous Hec suspension with nanosheets uniformly separated to 30.5 nm ( $\circ$ -measured,  $-$ calculated). The top inset shows birefringence of the diluted nematic Hec suspension between crossed polarizers. The bottom inset displays the model of disks used for the calculated SAXS intensity. [Color figure can be viewed at [wileyonlinelibrary.com](http://wileyonlinelibrary.com)]

## 2 | RESULTS AND DISCUSSION

### 2.1 | Film fabrication

A quantitatively delaminated suspension of Hec can be prepared by simply mixing the bulk clay in water. The rare phenomenon of thermodynamically allowed one-dimensional dissolution (i.e., osmotic swelling) that is accessible to this material provides single layers of negatively charged nanosheets without the use of mechanical force.<sup>23</sup> Fully delaminated Hec nanosheets have a preserved platelet diameter of  $\approx 20,000$  nm with a single layer thickness of 1 nm, yielding an exceptionally large aspect ratio (ratio of platelet diameter to thickness).<sup>24</sup> Such a high aspect ratio of  $\approx 20,000$  hinders rotation of adjacent Hec nanosheets in solution even at concentrations as low as 1 vol%,<sup>25</sup> giving a nematic liquid crystalline phase as indicated by the birefringence observed under cross-polarized light (Figure 1, top inset). Under closer inspection employing small angle x-ray scattering (SAXS), we can confirm a highly ordered liquid crystal structure with single Hec nanosheets separated to 30.5 nm corresponding to a 6 wt% ( $\approx 2.3$  vol%) aqueous Hec suspension (Figure 1). The  $q^{-2}$ -dependence of the SAXS curve at the low and intermediate  $q$ -range is characteristic for platy two-dimensional objects.<sup>26</sup> This geometry is further corroborated by applying a calculated model of disks with a radius of 10,000 nm ( $\pm 15\%$ ) and a thickness of 1 nm ( $\pm 7\%$ ) separated to a  $d$ -spacing of

$30.5 \pm 3$  nm using a Gaussian distribution (Figure 1, bottom inset). Observable reflexes up to 005 and an absence of peaks in the high  $q$  region that would indicate an undelaminated fraction verifies the presence of a translationally homogeneous nematic phase. The nematic nature of the Hec suspension is a critical aspect to obtain superior barrier properties since coated Hec nanosheets should lie parallel to the substrate and perpendicular to the direction of gas diffusion.<sup>27</sup> Retention of this structural order during processing will be ensured by employing a slot die coating instrument.

Separate polymer solutions of PVOH, HPMC, and Alginate were prepared by mixing the respective polymers with the plasticizers sorbitol and glycerol in a weight ratio of 80/10/10 (polymer/sorbitol/glycerol) in water. Plasticizers were added to obtain soft and flexible films as required for single-serving pouch applications. Solution concentrations and wet-coat heights were adjusted to warrant viscosities appropriate for slot die coating.

Due to the repulsive nature of the nanosheets that constitute liquid crystalline, delaminated Hec, suspensions of this material are highly viscous even at solid contents as low as 3 wt%.<sup>28</sup> The Hec suspension was prepared as 6 wt% in double distilled water, reflecting the maximum viscosity processible with the in-house slot die coater.

The polymer blends and the Hec suspension were then applied sequentially onto a PLA carrier substrate using a slot-die coater. The choice of material for the carrier substrate is inconsequential, as it will be removed from the layered films prior to analysis. In a similar fashion to the production of commercial layered films, the lab-scale slot-die coater provides precise and programmable solution deposition to make customizable layer structures. For this work, we chose a sandwich structure consisting of three layers arranged as polymer/Hec/polymer. With this structure, a suitable Hec content can be added without the concern of increasing viscosity of the polymer solution into ranges unsuitable for processing, as would be the case when working with a single, combined polymer/Hec suspension. Unlocking filler restrictions also gives access to properties of biopolymer nanocomposites that are unattainable with a homogeneous blend. A sandwich structure produced on a large-scale roll-to-roll process would consist of three sequential slot die heads, separated by drying units, and a collecting roll to remove the film from the carrier substrate when the addition of layers is complete (Figure 2a).

In our current laboratory setup, we are limited to a single slot die head, so the roll-to-roll process is stimulated by drying coated layers with a lamellar airflow dryer, then exchanging the solution in the slot die and

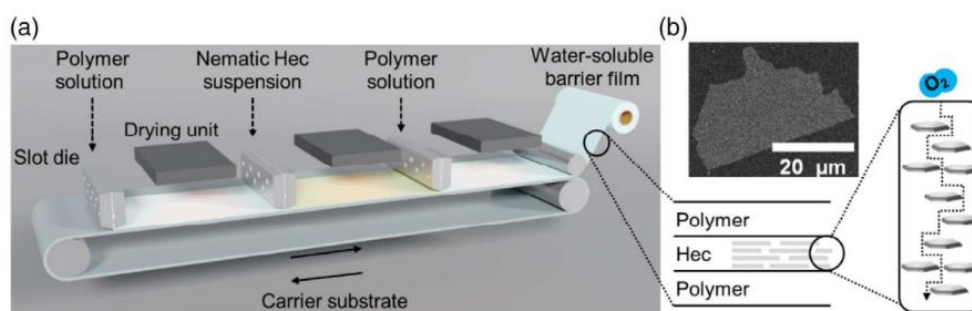


**FIGURE 2** (a) Sketch of the potential roll-to-roll processing method employing three consecutive slot die heads and drying units. In this way, a multi-layered film can be fabricated in-line and at high throughput by applying different coating solutions. Here we propose a layered sandwich structure with a first inner layer of water-soluble polymer, a second barrier layer of Hec and a third sealing layer of water-soluble polymer on top. The layered film is peeled-off and rolled-up while the carrier substrate can be reused. The inset highlights the tortuous path that a sandwiched Hec barrier layer provides against gas permeation. (b) Scanning electron microscopy (SEM) image of a single Hec nanosheet with a diameter  $>20\ \mu\text{m}$ . [Color figure can be viewed at [wileyonlinelibrary.com](http://wileyonlinelibrary.com)]

coating the next layer on top of the dry one. Given a desired dry film thickness and solution solid content, the wet coating thickness is adjusted by means of the pump flow rate, table speed, and coating gap. The final dry film can be easily peeled from the carrier substrate for analysis. A sandwich polymer film was produced from each of the three polymer solutions prepared. Due to the staggered stacking of platelets within a nematic Hec suspension and the large lateral extension of these sheets, we expect that the collapse of the structure upon drying will create a solid and nearly impermeable wall with a band-like structure and a diffusion path for permeates that is dramatically tortuous (Figure 2b).<sup>29</sup>

The final clay content of the PVOH, HPMC, and alginate layered films was determined from the residue that remains after a temperature ramp during thermal gravimetric analysis (Figure S1) as 21, 22, and 40 wt%, respectively. For comparison, monolayer films of each polymer (without Hec) were also prepared from the same polymer/plasticizer solution to ensure identical plasticizer content.

## 2.2 | Imaging

Cross-sections of each of the prepared films were observed with scanning electron microscopy (SEM) (Figure S2). The consecutive coating of individual layers provides highly uniform outer polymer layers of  $\approx 30\ \mu\text{m}$  sandwiching the inner Hec layer. The slight detachment of the top layer of polymer from the Hec layer is an artifact from preparation for imaging. The center Hec layer, which exhibits the proposed barrier wall structure, is  $\approx 6\ \mu\text{m}$  thick, neglecting the area of detachment. The ideal parallel alignment of the nanosheets can be attributed to the shear forces that

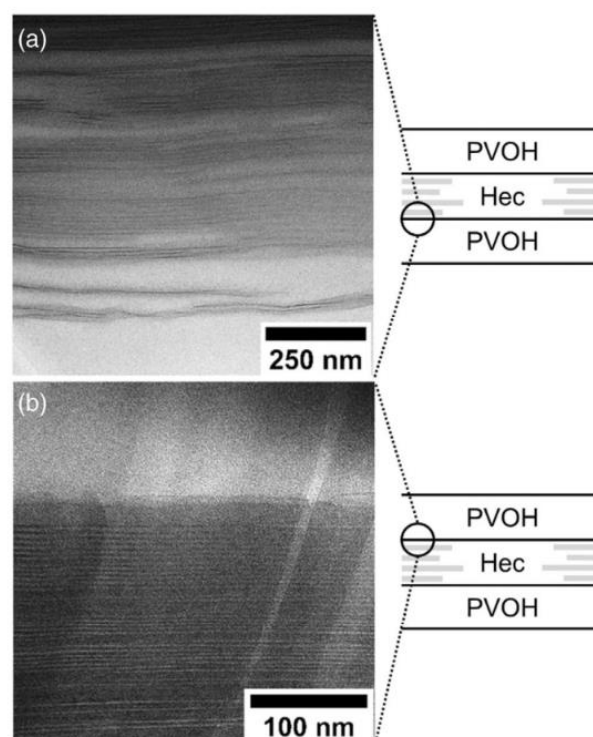


**FIGURE 3** Transmission electron microscope (TEM) cross-sections of the PVOH/Hec/PVOH film. (a) Interface between first PVOH sublayer and second Hec barrier layer. (b) Interface between second Hec barrier layer and top PVOH layer.

suspensions are subjected to within the slot die coating head, which retains the highly ordered, liquid crystalline Hec structure during processing.<sup>28</sup> Electron dispersive x-ray (EDX) element mapping of the film cross-sections with silicon from Hec represented in cyan and carbon from the PVOH represented in red aid in distinguishing the defined layer structure.

The layer interfaces within the PVOH/Hec/PVOH film were further investigated by transmission electron microscope (TEM) of the cross-sections prepared by cryo-ion-slicing (Figure 3). Observation of HPMC/Hec/HPMC and alginate/Hec/alginate films with TEM imaging was not possible as the ion beam used to prepare ultra-thin slices damages the biopolymers.

It appears that coating an aqueous Hec suspension onto the water-soluble PVOH sublayer leads to a partial re-dissolution of the dried polymer layer. This mobilizes the polymer, allowing it to diffuse between adjacent nanosheets that are separated to 30.5 nm in the liquid nematic state. The in-situ formed nanocomposite interface reaches only 1  $\mu\text{m}$  into the Hec layer due to the tortuosity imparted by the impermeable nanosheets that restrict further diffusion as drying progresses (Figure 3a). Such a structure at the interface provides excellent layer adhesion between the Hec and polymer domains. The amount of diffusion from the top layer of PVOH into the Hec region is less than the bottom layer of PVOH (Figure 3b), which explains its higher susceptibility to delayering as observed in the SEM image. Such behavior is not a surprise as a Hec layer is less prone to swelling upon removal of water and restacking of platelets. This suggests that the size of the nanocomposite interface could be modified by the drying treatment of the layers. Earlier studies have also demonstrated that the degree of PVOH intercalation into Hec can be modified by decreasing the drying temperature.<sup>20</sup>

The formation of an interfacial nanocomposite is assumed to form in the HPMC and alginate layered films as well due to their XRD patterns (Figure S3), which reflect a *d*-spacing of 1.6 and 1.4 nm, respectively. These values are substantially higher than the basal spacing of neat Hec ( $d_{001} = 0.96$  nm).<sup>24</sup> The PVOH layered film also exhibits a *d*-spacing of 1.6 nm.

## 2.3 | Characterization and application

### 2.3.1 | Water solubility tests

The desired time for a water-soluble packaging film to disintegrate depends upon the mode of application. For household use, like in detergent pods, dissolution within minutes is desired, but it must be balanced with some degree of resistance to moisture or water vapor that may be encountered during transport and storage.

To evaluate film behavior when exposed to water, each film underwent water solubility testing according to the MSTM-205 testing standard (Figure S4). Films were held still in vigorously mixing water at room temperature. Disintegration time is defined as the time it takes until film breakage is observed, and dissolution time as

**TABLE 1** Disintegration and dissolution time of water-soluble films according to the method “MSTM-205 Solubility Test with Plastic Holder” in distilled water at a temperature of 23°C.

Film	Disintegration time (min)	Dissolution time (min)
PVOH/Hec/PVOH	5.7 $\pm$ 1.3	9.7 $\pm$ 2.1
HPMC/Hec/HPMC	5.9 $\pm$ 2.1	7.4 $\pm$ 2.1
Alginate/Hec/ Alginate	2.9 $\pm$ 0.9	4.3 $\pm$ 0.6
PVOH	0.3 $\pm$ 0.1	0.4 $\pm$ 0
HPMC	0.3 $\pm$ 0.1	0.5 $\pm$ 0.1
Alginate	0.1 $\pm$ 0	0.1 $\pm$ 0

the time it takes until fragments of the film are no longer detectable by eye. Comparative tests were performed with neat polymer films (Table 1).

All of the plasticized polymer films exhibited disintegration in 0.3 min or less and underwent complete dissolution in no longer than 0.5 min, with HPMC taking the longest to do so. This is an expected result for these highly hydrophilic and water-soluble polymers. As a sandwich layered film, the time to disintegration was delayed to 2.9 min for alginate and 5.7 and 5.9 min for PVOH and HPMC, respectively. The time to disintegration, comparable to the time it would take for a pouch to release its contents, could be characterized for the desired application, for example, rapid release pouch (alginate film) or a standard release time (PVOH and HPMC film). Dissolution time of the three films ranged from 4.3 min for the alginate/Hec/alginate film to 9.7 min for the PVOH/Hec/PVOH film. The sandwich film structure proved able to provide some hydrophobicity when added to water-soluble polymers without totally hindering their ability to disintegrate rapidly. Hydrophobization has also been observed in intercalated Hec nanocomposites with other water-soluble polymers by means of an increased resistance to swelling and the improved water vapor barrier.<sup>17,30</sup> This slight modification of film properties makes them much more practical for real-world use where accidental exposure to water should not cause premature disintegration and exposure to humid conditions should not initiate excessive swelling that ruins film integrity and barrier. Films of the plasticized polymers themselves disintegrate within 20 s of exposure to water, which would lead to much wasted product if storage conditions are not strictly monitored. Although the layering of Hec within these same plasticized polymers increases their disintegration time, their ability to dissolve fully under 10 min at room temperature was not impeded. A range of disintegration and dissolution times could be customized by altering the film layer structure and by using different polymers to match expected packaging conditions.

Films/polymers	OP at 23°C and 50% RH (cm <sup>3</sup> mm m <sup>-2</sup> day <sup>-1</sup> bar <sup>-1</sup> )	WVP at 23°C and 85% RH (g mm m <sup>-2</sup> day <sup>-1</sup> bar <sup>-1</sup> )
PVOH/Hec/PVOH	0.008 (65% RH)	8.4
HPMC/Hec/HPMC	0.001 (65% RH)	12.5
Alginate/Hec/Alginate	0.063 (65% RH)	53.8
PVOH <sup>a</sup>	0.02 (0% RH)	1260
Poly(ethylene terephthalate) (PET) <sup>a</sup>	1–5	21–84
Polypropylene (PP) <sup>a</sup>	50–100	8–17
Polyethylene (PE) <sup>a</sup>	50–200	21–84
Poly(vinyl chloride) (PVC) <sup>a</sup>	2–8	42–84
Poly(lactic acid) (PLA) <sup>b</sup>	3–15 (0%/50% RH)	158–855
Poly(butylene adipate terephthalate) (PBAT) <sup>b</sup>	61	3450 (100% RH)
EVOH 32 mol% <sup>c</sup>	0.01 (65% RH)	-
Exceval <sup>d</sup>	0.002 (65% RH)	-

Note: Unless otherwise stated, the OP and WVP are given at test conditions of 23°C and 50% RH, 85% RH, respectively. Values are partially converted from their originally reported units allowing a consistent comparison.

<sup>a</sup>Lange and Wyser.<sup>31</sup>

<sup>b</sup>Wu et al.<sup>40</sup>

<sup>c</sup>Mitsubishi Gas Chemical.<sup>41</sup>

<sup>d</sup>Kuraray.<sup>32</sup>

### 2.3.2 | Gas barrier properties

Despite being water-soluble, the layered films provide exceptional protection against permeates, like oxygen and water vapor, that cause deteriorative reactions in many products. Oxygen transmission rate (OTR) and water vapor transmission rate (WVTR) values recorded for our layered films were converted into oxygen permeability (OP) and water vapor permeability (WVP) to normalize for film thickness and allow comparison across commercial and literature reports (Table 2). At a 65% relative humidity (RH), the PVOH, and HPMC layered films have an OP of 0.008 and 0.001 cm<sup>3</sup> mm m<sup>-2</sup> day<sup>-1</sup> bar<sup>-1</sup>, respectively. These values are comparable to the high-performance Exceval and outperform other common non-degradable packaging materials like polyethylene terephthalate (PET), polyethylene (PE), and poly(vinyl chloride) (PVC) measured at a lower 50% RH.<sup>31,32</sup> WVP values at a challenging 85% RH for PVOH and HPMC layered films are 8.4 and 12.5 g mm m<sup>-2</sup> day<sup>-1</sup> bar<sup>-1</sup>, respectively, once again outperforming the same commercial films.

While hydrophilic polymers like Exceval and ethylene vinyl alcohol (EVOH) swell at elevated RH, which degrades barrier performance,<sup>30,33</sup> the Hec barrier layer blocks diffusion of absorbed water and slows the swelling

TABLE 2 Oxygen permeability (OP) and water vapor permeability (WVP) of the water-soluble films compared with common polymers used for packaging and biodegradable polymers.

process. This becomes evident when comparing the WVP of 1260 g mm m<sup>-2</sup> day<sup>-1</sup> bar<sup>-1</sup> for neat water-soluble PVOH with the low WVP of 8.4 g mm m<sup>-2</sup> day<sup>-1</sup> bar<sup>-1</sup> found for the Hec loaded PVOH layered film at a demanding high 85% RH.<sup>31</sup> The incorporated Hec barrier layer hampers swelling and concomitant breakdown of barrier as indicated by a barrier improvement factor of 150.

Our processing strategy easily achieves top OP and WVP performance for HPMC among other HPMC systems reported in literature across various fillers and blends.<sup>34</sup> Although the layered alginate film falls slightly behind our other layered films and Exceval, it nevertheless outperforms several commercial packaging films and is competitive with the same materials in terms of WVP. The OP and WVP values for the alginate layered film of 0.063 cm<sup>3</sup> mm m<sup>-2</sup> day<sup>-1</sup> bar<sup>-1</sup> and 53.8 g mm m<sup>-2</sup> day<sup>-1</sup> bar<sup>-1</sup>, respectively, surpass previously reported barrier values for this material, even compared to other nanocomposites or crosslinked structures.<sup>35–39</sup> All of our layered films are orders of magnitude better in both OP and WVP when compared to commercial biodegradable films like PLA and poly(butylene adipate terephthalate) (PBAT). In general, the high barrier requirements for packaging are usually out of range for unfilled biodegradable materials.<sup>40</sup>

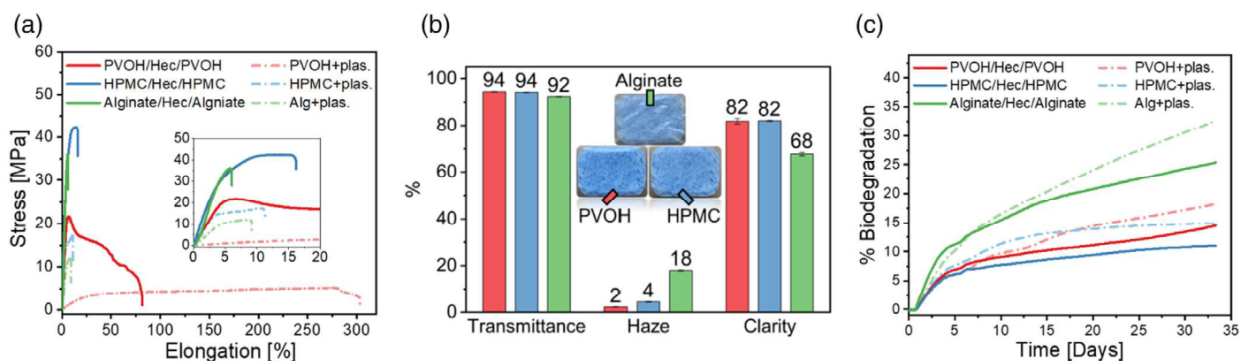


**FIGURE 4** Characterization of the films. (a) Mechanical properties of the plasticized polymers (10 wt% of each plasticizer, sorbitol, and glycerol) and their layered films with Hec. (b) Optical properties of layered films. (c) Biodegradation measured in terms of conversion to  $\text{CO}_2$  of the plasticized polymers (10 wt% of each plasticizer, sorbitol, and glycerol) and their layered films with Hec. [Color figure can be viewed at [wileyonlinelibrary.com](http://wileyonlinelibrary.com)]

### 2.3.3 | Mechanical properties

With an excellent barrier to permeating gases, the evaluation of these layered films as a packaging material continues with the examination of mechanical performance. These water-soluble polymer layered films also exhibited excellent tensile properties suitable for flexible packaging films (Figure 4a, Table S1). The addition of the Hec layer improved the elastic modulus of all three of the plasticized polymers, establishing further functionality as a structural reinforcement. For alginate, the Hec layer boosts its elastic modulus from 35 to 1100 MPa. HPMC layered films exhibited nearly a 300% increase in its tensile strength. Naturally, percent elongation at break was reduced in all samples from the clay layer, however, severe embrittlement that is often observed in dispersed nanocomposite systems, even at much lower clay loadings than reported here, was avoided.<sup>38,42,43</sup> Moreover, the stretchability of PVOH is retained despite 22 wt% Hec, although delamination of the film layers was observed starting around 40% elongation.

A balance of suitable mechanical performance and suitable barrier properties has plagued degradable clay nanocomposites in the past due to how the same rigid, impermeable fillers that elongate the diffusion pathway for permeates also cause embrittlement of the polymer matrix.<sup>44</sup> These competing effects limited clay loading to below 5 wt% in dispersed nanocomposites and thus limited barrier performance. In this way, achieving high performance regarding both barrier and mechanical properties in a single material presented a huge hurdle to the implementation of biodegradable packaging materials with competitive performance. By the addition of common plasticizers and a sandwich-layered structure, we have evidently succeeded in mitigating

this embrittlement effect. The simple and scalable method of producing barrier films that we report here provides a promising solution to such critical hurdles of the past.

### 2.3.4 | Optical properties

Characterization of the optical properties of the layered films was performed to demonstrate how these films also meet the consumer preference for transparent packaging (Figure 4b). The PVOH layered film provides the most transparent film, while the alginate layered film suffers from slight haziness. Nevertheless, all three of the layered materials exhibit excellent optical properties that are suitable for transparent packaging needs, as displayed in an example of packaged dishwasher tablets (Figure 4b, inset).

### 2.3.5 | $\text{CO}_2$ evolution testing for biodegradation

Dissolution of polymers can favor biodegradation kinetics since, in the dissolved state, polymers have a maximized exposed surface area available to chain scission via hydrolysis. The oligomeric pieces may then be mineralized by microbial assimilation. However, this assimilation by microbes is not guaranteed simply by dissolution but additionally requires an appropriate match of enzymes and chain functionalities.

Therefore, the sandwich layered films and the plasticized polymer films were evaluated for their biodegradation in wastewater sludge by monitoring conversion into  $\text{CO}_2$  for 33 days. Wastewater sludge was sourced from

the local wastewater treatment plant in Bayreuth, Germany. Cumulative CO<sub>2</sub> production was converted into percent biodegradation (Figure 4c), and aniline was used as the positive control. As additional references, the neat plasticizers were also evaluated under the same conditions (Figure S5). Sorbitol biodegraded 92% by the end of the 33 days, while glycerol degraded just 27% in the same time. With 10 wt% of each sorbitol and glycerol added to all films, we can therefore assume that ~12% of their total biodegradation in 33 days can be attributed to that of the plasticizers.

Taking a closer look at the biodegradation behavior of the plasticized polymer films reveals that PVOH and HPMC degradation reaches 14% and 11%, respectively. This biodegradation should be primarily, if not entirely, attributed to the plasticizers, exemplifying that although dissolved in water, these materials are incapable of degradation by microorganisms encountered in a typical communal sewage plant (or degrade too slowly to be non-persistent). As reported in the introduction, PVOH biodegradation requires a specialized environment with adapted microbes that are not common for communal sewage plants.<sup>2</sup> HPMC has shown to be biodegradable in soil,<sup>45</sup> however, this behavior is evidently not directly translatable to wastewater on a relevant timescale.

On the other hand, biodegradation on day 33 for the plasticized alginate and alginate/Hec/alginate of 33% and 25%, respectively, was recorded. Given that only 12% of the plasticizers would be assimilated at that point, the degradation of both the alginate samples substantially exceeds what could be attributed to the plasticizers. Clearly, alginate films are not only dissolved in freshwater but are also biodegraded in this wastewater environment.

Similarly to the dissolution kinetics, the biodegradation kinetics are slightly slowed down by the incorporation of a Hec layer into the center of the polymer films, likely attributed to its barrier effect. These biodegradation curves confirm that a sandwich-layered film with the barrier reinforcement material in the center provides optimal improvement in physical properties while also leaving the polymer accessible to biodegradation.

### 3 | CONCLUSION

Water-soluble packaging films provide unmatched convenience for dispensing both household and commercial products. In this work, we demonstrated the insignificant biodegradation of a commonly employed material, PVOH, in the disposal medium that it is designed for: wastewater. Similarly, and somewhat surprisingly, even a bio-based HPMC film showed no significant biodegradation, while the alginate films demonstrated up to 33% biodegradation

in 33 days. With rapid biodegradation and low production costs,<sup>46</sup> sodium alginate could make a viable commercial alternative to PVOH.

However, biopolymers, like alginate, cannot compete alone in demanding packaging applications due to their weak barrier and mechanical properties. By employing an industrially scalable slot die coating system (roll-to-roll processing), sandwich-structured films containing an inner hectorite clay barrier layer were obtained. This barrier layer could impart competitive properties to films of sodium alginate, including an OP and WVP of 0.063 cm<sup>3</sup> mm<sup>-2</sup> day<sup>-1</sup> bar<sup>-1</sup> and 53.8 g mm<sup>-2</sup> day<sup>-1</sup> bar<sup>-1</sup>, respectively. The layered film architecture, moreover, lifts previously encountered limitations on hectorite content related to rapidly increasing viscosity even at low filler contents. The shear-induced alignment of hectorite platelets during processing creates a highly ordered 6 μm thick impermeable barrier wall. An interfacial nanocomposite with the outer polymer layers that formed in situ during processing provided excellent layer adhesion and polymer confinement-induced barrier improvement. Possibilities of increasing the size of this nanocomposite area by varying the drying treatment have implications on further tuning interfacial adhesion, dissolution behavior, barrier properties, and possibly even mechanical properties to meet application-specific needs, which motivates a follow-up study.

## 4 | EXPERIMENTAL

### 4.1 | Materials and sample preparation

#### 4.1.1 | Materials

The synthetic clay sodium fluorohectorite (Hec) with the formula [Na<sub>0.5</sub>]<sup>inter</sup>[Mg<sub>2.5</sub>Li<sub>0.5</sub>]<sup>oct</sup>[Si<sub>4</sub>]<sup>tet</sup>O<sub>10</sub>F<sub>2</sub> was synthesized according to a published literature procedure and features a cation exchange capacity of 1.27 mmol g<sup>-1</sup>.<sup>24,47</sup> Poly(vinyl alcohol) (PVOH, Selvol 205, degree of hydrolysis 88%, ex Sekisui Chemicals Co., Japan), hydroxypropyl methylcellulose (HPMC, E15LV, ex Parchem Chemicals, United States), NaAlginate (alginate, Vivastar CS002, ex JRS, Germany), glycerol (CremerGLYC 3109921, ex Cremer Ole, Germany) and sorbitol (Neosorb<sup>®</sup> P 100 T, Roquette, France) were used without further purification. Biodegradable poly(lactic acid) (PLA, BoPLA-Folie NTSS 25 NT/25 μm, Pütz GmbH, Germany) films were used as substrates without further surface treatment.

#### 4.1.2 | Sample preparation

Hec was added to double-distilled water to obtain a 6 wt % Hec suspension. The suspension was placed for 7 days

in an overhead shaker to guarantee complete delamination into single Hec nanosheets.

One hundred grams of each of the three plasticized polymer suspensions (PVOH, HPMC, and alginate) were prepared by adding the polymer to double-distilled water in a round flask at 30 wt% for the PVOH, 20 wt% for the HPMC, and 15 wt% for the alginate suspension. The solid content was adjusted to achieve similar viscosities for slot die coating. The solutions were kept at 85°C under reflux for 2 h while stirring at 200 rpm using a magnetic stirring bar. Then the plasticizers were added to the polymer solutions so that the solid content of each was comprised of 80 wt% polymer, 10 wt% glycerol, and 10 wt% sorbitol.

#### 4.1.3 | Slot die coating

The single water-soluble layers were produced consecutively by slot die coating (Table Coater equipped with a 1-Layer Slot Die 300 mm, AAA, TSE Troller AG, Switzerland). Prior to slot die coating, the polymer solutions and the Hec suspensions were homogenized, defoamed, and degassed under vacuum (50 mbar) for 5 min at 2500 rpm using a Speed-Mixer DAC 400.2 VAC-P (Hauschild, Germany). The applied shim ensures a coating width of 210 mm and a slot height of 165  $\mu\text{m}$ . The coating gap was adjusted according to the desired wet film thickness. The pump flow rate and the table speed were set accordingly depending on the coating gap. The vacuum table supported and fixed the PLA substrate needed for the first wet layer.

The table temperature, referred to as the drying temperature, was adjusted to the respective coated layer. The obtained wet films were dried in-line, generating a slight under pressure with an airflow of 1.5  $\text{m}^3 \text{min}^{-1}$ . The adjustable airflow was created by a Side Channel Blower Type 1SD 510 (Elektor Airsystems GmbH, Germany). A microporous surface below the airflow guarantees a soft and uniform solvent removal over the entire wet film surface.

For details on the slot die coating settings applied for each layer, please refer to the Data S1. After drying was complete, the films were peeled off the PLA carrier substrate for analysis.

## 4.2 | Characterization methods

### 4.2.1 | Small-angle x-ray scattering

SAXS experiments were performed by employing the system Ganesha Air (SAXSLAB, Denmark). The system is equipped with a rotating anode copper x-ray source MicroMax 007HF (Rigaku Corp., Japan) and a position-

sensitive detector PILATUS 300K (Dectris, Switzerland) with adjustable sample-to-detector positions covering a wide range of scattering vectors  $q$ . The measurement of the suspension was conducted in 1 mm glass capillaries (Hilgenberg, Germany) at room temperature. The resulting one-dimensional (1D) data ( $I(q)$  [ $\text{cm}^{-1}$ ] vs.  $q$  [ $\text{\AA}^{-1}$ ], with intensity  $I(q)$ ) are background corrected and displayed in absolute scale.

The birefringence of a diluted Hec suspension was checked with a self-made crossed polarizer.

### 4.2.2 | Thermogravimetric analysis

Thermogravimetric analysis measurements were conducted on a Linseis STA PT 1600 (Linseis Messgeräte GmbH, Germany). The films were dried under vacuum ( $10^{-3}$  bar) at 70°C for 7 days. The dry samples were heated up from room temperature to 1000°C under an argon atmosphere with a heating rate of 10°C  $\text{min}^{-1}$ .

### 4.2.3 | Scanning electron microscopy

SEM images of a singular Hec nanosheet (Figure 2b) were recorded using the microscope ZEISS LEO 1530 (Carl Zeiss AG, Germany) operating at 3 kV and equipped with an InLens secondary electron detector. For sample preparation, the Hec suspension was diluted to 0.001 wt% and then drop-casted on a plasma-treated silicon wafer. Subsequently, the sample was sputtered with 1.2 nm of platinum.

SEM images of the cross-sections of the films were recorded using the microscope ZEISS Ultra plus (Carl Zeiss AG, Germany) operating at 5 kV and equipped with an InLens and secondary electron detector. The cross-sections were obtained by cutting the substrate-supported films with a scalpel toward the substrate side in order to protect the films. Subsequently, the films were carefully peeled off from the substrate. The film samples were sputtered with 1.2 nm of platinum. In addition, the cross-sections of the films were analyzed via EDX by employing an UltraDry-EDX detector (Thermo Fisher Scientific, United States).

### 4.2.4 | Transmission electron microscopy

TEM images of the cross sections were recorded employing a JEOL-JEM-2200FS (JEOL GmbH, Germany) microscope. Cross sections were prepared from the peeled-off films using a JEOL EM-09100IS Cryo Ion Slicer (JEOL GmbH, Germany).

#### 4.2.5 | X-ray diffraction

Diffraction patterns were obtained on a Bragg–Brentano-type instrument (Empyrean Malvern Panalytical BV, The Netherlands). The diffractometer is equipped with a PIXcel-1D detector, and Cu  $K_\alpha$  radiation ( $\lambda = 1.54187 \text{ \AA}$ ) was used. The patterns were analyzed by applying Malvern Panalytical's Highscore Plus software.

#### 4.2.6 | Water-solubility tests

The water-solubility of the films was tested according to the method "MSTM 205 Solubility Test with Plastic Holder." The setup is displayed in Figure S4. An average of three measurements for each film was taken.

#### 4.2.7 | Barrier properties

OTR were determined on the system OX-TRAN 2/21 (Mocon, United States) at 65% RH and 23°C. A mixture of 98 vol% nitrogen and 2 vol% hydrogen as carrier gas and pure oxygen (>99.95 vol%, Linde Sauerstoff 3.5) as permeant were used. WVTR were determined on the system PERMA-TRAN-W 3/33 (Mocon, United States) at 85% RH and 23°C. All samples were sufficiently equilibrated to guarantee moisture conditioning.

#### 4.2.8 | Coating thickness

The total film thickness was determined by employing High-Accuracy Digimatic Micrometer (Mitutoyo, Japan) with a measuring range of 0–25 mm and a resolution of 0.1  $\mu\text{m}$ . A mean value of 10 measuring points within the permeability measurement area of the film was taken.

#### 4.2.9 | Mechanical properties

Stress–strain tests were performed with a tensile instrument (Zwick/Roell, BT1-FR0.5TN.D14). The samples for the tensile measurement were cut to a size of 3 mm  $\times$  30 mm for a pristine effective tensile length of 10 mm. Prior to testing, the samples were equilibrated at 53% RH in a desiccator for 5 days. The test was performed with a crosshead speed of 5 mm  $\text{min}^{-1}$  at room temperature for at least 10 measurements. The slope of the linear region of the stress–strain curves was used to determine the elasticity modulus. All samples were measured at least 5 times, with the statistical average given as the result.

#### 4.2.10 | Optical properties

Optical properties were analyzed on a BYK-Gardner Haze-Gard Plus (BYK-Gardner GmbH, Germany). An average of five measurements per film sample were taken for transmittance, haze, and clarity values.

#### 4.2.11 | Biodegradation properties

The prepared films were tested for biodegradation in wastewater sludge under aerobic environment in triplicate for 33 days. The test method was based on DIN ISO 14851:2019. Activated sludge (after nitrification) collected from the wastewater treatment plant at Bayreuth, Germany, was used in the experiment as an inoculum. Aniline was used as the positive sample. Activated sludge in the same concentration was used as a control. Around 70 mg of the films were added in 100 mL test medium, with 95 mL of standard medium and 5 mL of supernatant of activated sludge. The Micro-Oxymax Respirometer furnished with a paramagnetic  $\text{O}_2$  and  $\text{CO}_2$  sensor (Columbus Instruments International, United States) was used for this biodegradation test.

The percentage of biodegradation was analyzed by observing the production of  $\text{CO}_2$  using the following equation:

$$\begin{aligned} \% \text{Biodegradation} &= \frac{(\text{mgCO}_2 \text{ produced})_{\text{T}} - (\text{mgCO}_2 \text{ produced})_{\text{B}}}{\text{ThCO}_2} \quad (1) \\ &\times 100 \end{aligned}$$

where  $(\text{mgCO}_2 \text{ produced})_{\text{T}}$  and  $(\text{mgCO}_2 \text{ produced})_{\text{B}}$  were the amounts of  $\text{CO}_2$  evolved in the test material and blank flask, respectively, given in milligrams.  $\text{ThCO}_2$  is the theoretical amount of  $\text{CO}_2$  expected to be evolved by the test material when completely mineralized and is calculated by:

$$\text{ThCO}_2 = \text{Specimen (mg)} \times \frac{\text{TOC (\%)}}{100} \times \frac{44}{12} \quad (2)$$

where 44 is the molecular weight of  $\text{CO}_2$  and 12 is the molecular weight of C, TOC (%) is the total carbon content of the test specimen determined by elemental analysis.

#### AUTHOR CONTRIBUTIONS

**Maximilian Röhr:** Conceptualization (lead); data curation (equal); methodology (lead); visualization (equal); writing – original draft (equal); writing – review and

editing (supporting). **Renee Timmins:** Conceptualization (equal); data curation (equal); methodology (supporting); visualization (equal); writing – original draft (equal); writing – review and editing (equal). **Dipannita Ghosh:** Formal analysis (supporting); methodology (equal); writing – review and editing (supporting). **Dominik Schuchardt:** Investigation (supporting); methodology (supporting); validation (supporting); writing – review and editing (supporting). **Sabine Rosenfeldt:** Data curation (supporting); methodology (supporting); software (equal); validation (supporting); writing – review and editing (supporting). **Simon Nürmberger:** Investigation (supporting); methodology (supporting). **Uwe Bözl:** Conceptualization (supporting); methodology (supporting); validation (supporting); writing – review and editing (supporting). **Seema Agarwal:** Funding acquisition (equal); project administration (equal); writing – review and editing (supporting). **Josef Breu:** Funding acquisition (lead); project administration (lead); supervision (lead); writing – review and editing (lead).

#### ACKNOWLEDGMENTS

This study was funded by the Deutsche Forschungsgemeinschaft (DFG, German Research Foundation) – SFB 1357-391977956. This project has received funding from the European Union's Horizon 2020 research and innovation programme under the Marie Skłodowska-Curie agreement grant No. 860720. The authors cordially thank Florian Puchtler for producing the synthetic clay and Marco Schwarzmann for recording scanning and transmission electron microscope images. Furthermore, the authors are thankful for the support of the Keylabs for Optical and Electron Microscopy and Mesoscale Characterization: Scattering Techniques of the Bavarian Polymer Institute. Open Access funding enabled and organized by Projekt DEAL.

#### CONFLICT OF INTEREST STATEMENT

The authors declare no conflict of interest.

#### DATA AVAILABILITY STATEMENT

The data that support the findings of this study are available in the supplementary material of this article.

#### ORCID

Josef Breu  <https://orcid.org/0000-0002-2547-3950>

#### REFERENCES

- [1] T. A. Cooper, *Trends in Packaging of Food, Beverages and Other Fast-Moving Consumer Goods (FMCG)*, Woodhead Publishing, Cambridge, UK **2013**, p. 58.
- [2] N. Ben Halima, *RSC Adv.* **2016**, *6*, 39823.
- [3] J. A. Giroto, R. Guardani, A. C. S. C. Teixeira, C. A. O. Nascimento, *Chem. Eng. Process.: Process Intensif.* **2006**, *45*, 523.
- [4] C.-C. Lin, L.-T. Lee, *J. Ind. Eng. Chem.* **2015**, *21*, 569.
- [5] W. Sun, L. Chen, J. Wang, *J. Adv. Oxid. Technol.* **2017**, *20*, 20170018.
- [6] E. Chiellini, A. Corti, R. Solaro, *Polym. Degrad. Stab.* **1999**, *64*, 305.
- [7] R. Solaro, A. Corti, E. Chiellini, *Polym. Adv. Technol.* **2000**, *11*, 873.
- [8] E. Chiellini, A. Corti, S. D'Antone, R. Solaro, *Prog. Polym. Sci.* **2003**, *28*, 963.
- [9] T. Vaclavkova, J. Ruzicka, M. Julinova, R. Vicha, M. Koutny, *Appl. Microbiol. Biotechnol.* **2007**, *76*, 911.
- [10] S. Mondellini, M. Schott, M. G. Löder, S. Agarwal, A. Greiner, C. Laforsch, *Sci. Total Environ.* **2022**, *847*, 157608.
- [11] H. Schonberger, A. Baumann, W. Keller, P. Pogopetris, *Am. Dyestuff Rep.* **1997**, *86*, 9.
- [12] J. Nilsen-Nygaard, E. N. Fernández, T. Radusin, B. T. Rotabakk, J. Sarfraz, N. Sharmin, M. Sivertsvik, I. Sone, M. K. Pettersen, *Compr. Rev. Food Sci. Food Saf.* **2021**, *20*, 1333.
- [13] G. A. Martáu, M. Mihai, D. C. Vodnar, *Polymer* **2019**, *11*, 1837.
- [14] K. K. Mokwena, J. Tang, *Crit. Rev. Food Sci. Nutr.* **2012**, *52*, 640.
- [15] M. S. Abdel Aziz, H. E. Salama, M. W. Sabaa, *LWT* **2018**, *96*, 455.
- [16] B. Akinalan Balik, S. Argin, J. M. Lagaron, S. Torres-Giner, *Appl. Sci.* **2019**, *9*, 5136.
- [17] C. Habel, M. Schöttle, M. Daab, N. J. Eichstaedt, D. Wagner, H. Bakhshi, S. Agarwal, M. A. Horn, J. Breu, *Macromol. Mater. Eng.* **2018**, *303*, 1800333.
- [18] J. Zhu, A. Kumar, P. Hu, C. Habel, J. Breu, S. Agarwal, *Global Chall.* **2020**, *4*, 2000030.
- [19] R. L. Timmins, A. Kumar, M. Röhr, K. Havlíček, S. Agarwal, J. Breu, *Macromol. Mater. Eng.* **2022**, *307*, 2100727.
- [20] M. Röhr, L. K. S. Federer, R. L. Timmins, S. Rosenfeldt, T. Dörres, C. Habel, J. Breu, *ACS Appl. Mater. Interfaces* **2021**, *13*, 48101.
- [21] M. Röhr, J. H. Mettke, S. Rosenfeldt, H. Schmalz, U. Mansfeld, R. L. Timmins, C. Habel, J. Breu, F. Durst, *J. Coat. Technol. Res.* **2021**, *19*, 487.
- [22] P. T. Anastas, J. C. Warner, *Green Chemistry: Theory and Practice*, Oxford University Press, Oxford, UK **1998**.
- [23] V. Dudko, O. Khoruzhenko, S. Weiß, M. Daab, P. Loch, W. Schwieger, J. Breu, *Adv. Mater. Technol.* **2022**, *8*, 2200553.
- [24] M. Stöter, D. A. Kunz, M. Schmidt, D. Hirsemann, H. Kalo, B. Putz, J. Senker, J. Breu, *Langmuir* **2013**, *29*, 1280.
- [25] S. Rosenfeldt, M. Stöter, M. Schlenk, T. Martin, R. Q. Albuquerque, S. Förster, J. Breu, *Langmuir* **2016**, *32*, 10582.
- [26] L. Boldon, F. Laliberte, L. Liu, *Nano Rev.* **2015**, *6*, 25661.
- [27] R. K. Bharadwaj, *Macromolecules* **2001**, *34*, 9189.
- [28] M. Röhr, J. H. Mettke, S. Rosenfeldt, H. Schmalz, U. Mansfeld, R. L. Timmins, C. Habel, J. Breu, F. Durst, *J. Coat. Technol. Res.* **2022**, *19*, 487.
- [29] E. L. Cussler, S. E. Hughes, W. J. Ward, R. Aris, *J. Membr. Sci.* **1988**, *38*, 161.
- [30] T. Schilling, C. Habel, S. Rosenfeldt, M. Röhr, J. Breu, *ACS Appl. Polym. Mater.* **2020**, *2*, 3010.

- [31] J. Lange, Y. Wyser, *Packag. Technol. Sci.* **2003**, *16*, 149.
- [32] Exceval™ – Attractive protection for your food. [https://www.kuraray-poval.com/fileadmin/technical\\_information/brochures/poval/Kuraray\\_Exceval\\_attractive\\_protection\\_for\\_your\\_food\\_engl.pdf](https://www.kuraray-poval.com/fileadmin/technical_information/brochures/poval/Kuraray_Exceval_attractive_protection_for_your_food_engl.pdf) (accessed: May 2023)
- [33] J. C. Grunlan, A. Grigorian, C. B. Hamilton, A. R. Mehrabi, *J. Appl. Polym. Sci.* **2004**, *93*, 1102.
- [34] R. Ghadermazi, S. Hamdipour, K. Sadeghi, R. Ghadermazi, A. Khosrowshahi Asl, *Food Sci. Nutr.* **2019**, *7*, 3363.
- [35] S. X. Weng, N. Yousefi, N. Tufenkji, *ACS Appl. Nano Mater.* **2019**, *2*, 1431.
- [36] M. Yang, Y. Xia, Y. Wang, X. Zhao, Z. Xue, F. Quan, C. Geng, Z. Zhao, *J. Appl. Polym. Sci.* **2016**, *133*, 43489.
- [37] H. Lee, B. Rukmanikrishnan, J. Lee, *Int. J. Biol. Macromol.* **2019**, *141*, 538.
- [38] M. Alboofetileh, M. Rezaei, H. Hosseini, M. Abdollahi, *J. Food Eng.* **2013**, *117*, 26.
- [39] S. Roy, J. W. Rhim, *Int. J. Biol. Macromol.* **2020**, *164*, 37.
- [40] F. Wu, M. Misra, A. K. Mohanty, *Prog. Polym. Sci.* **2021**, *117*, 101395.
- [41] Gas Barrier Properties. <https://www.mgc.co.jp/eng/products/ac/nmxd6/barrier.html> (accessed: September 2003)
- [42] A. A. Sapalidis, F. K. Katsaros, T. A. Steriotis, N. K. Kanellopoulos, *J. Appl. Polym. Sci.* **2012**, *123*, 1812.
- [43] K. E. Strawhecker, E. Manias, *Chem. Mater.* **2000**, *12*, 2943.
- [44] J.-W. Rhim, H.-M. Park, C.-S. Ha, *Prog. Polym. Sci.* **2013**, *38*, 1629.
- [45] C. G. Otoni, B. D. Lodi, M. V. Lorevice, R. C. Leitão, M. D. Ferreira, M. R. de Moura, L. H. Mattoso, *Ind. Crops Prod.* **2018**, *121*, 66.
- [46] O. Adeyeye, E. R. Sadiku, A. Babu Reddy, A. S. Ndamase, G. Makgatho, P. S. Sellamuthu, A. B. Perumal, R. B. Nambiar, V. O. Fasiku, I. D. Ibrahim, *Green Biopolymers and Their Nanocomposites*, Springer, Singapore **2019**, p. 137.
- [47] H. Kalo, M. W. Möller, M. Ziadeh, D. Dolejš, J. Breu, *Appl. Clay Sci.* **2010**, *48*, 39.

### SUPPORTING INFORMATION

Additional supporting information can be found online in the Supporting Information section at the end of this article.

**How to cite this article:** M. Röhr, R. L. Timmins, D. Ghosh, D. D. Schuchardt, S. Rosenfeldt, S. Nürnberger, U. Bözl, S. Agarwal, J. Breu, *J. Appl. Polym. Sci.* **2023**, e54418. <https://doi.org/10.1002/app.54418>

## Supporting Information

### **Green and scalable processing of water-soluble, biodegradable polymer/clay barrier films**

*Maximilian Röhrl<sup>‡1</sup>, Renee L. Timmins<sup>‡1</sup>, Dipannita Ghosh<sup>2</sup>, Dominik D. Schuchardt<sup>1</sup>, Sabine Rosenfeldt<sup>3</sup>, Simon Nürnberger<sup>1</sup>, Uwe Bölz<sup>4</sup>, Seema Agarwal<sup>2</sup> and Josef Breu<sup>\*1</sup>*

<sup>1</sup>M. Röhrl, R. L. Timmins, D. D. Schuchardt, S. Nürnberger, J. Breu

Bavarian Polymer Institute and Department of Chemistry, University of Bayreuth, Bayreuth 95447, Germany

\*E-mail (corresponding author): josef.breu@uni-bayreuth.de

ORCID ID: <https://orcid.org/0000-0002-2547-3950>

<sup>2</sup>D. Ghosh, S. Agarwal

Macromolecular Chemistry II, Bavarian Polymer Institute and Department of Chemistry, University of Bayreuth, Bayreuth 95447, Germany

<sup>3</sup>S. Rosenfeldt

Physical Chemistry I, Bavarian Polymer Institute and Department of Chemistry, University of Bayreuth, Bayreuth 95447, Germany

<sup>4</sup>U. Bölz

HPX Polymers GmbH, Tutzing 82327, Germany

‡: M.R. and R.L.T. contributed equally to this work.

## 1. Film Fabrication

### 1.1 Poly(vinyl alcohol) (PVOH)-based water-soluble film

For PVOH-based films, the drying temperature was set to 60 °C. The first water-soluble polymer layer was coated from a 30 wt% PVOH solution on a poly(lactide) (PLA) film. The coating gap was adjusted to 205  $\mu\text{m}$ , and the pump flow rate was set to 2.52  $\text{ml min}^{-1}$  and the table speed to 0.1  $\text{m min}^{-1}$  accordingly. The film was dried for 15 min. The composition of the dry film was 80% PVOH, 10% glycerol, and 10% sorbitol.

The water-dispersible nanosheet layer was then added on top by coating a 6 wt% Hec suspension. The coating gap was adjusted to 385  $\mu\text{m}$ , and the pump flow rate was set to 4.6  $\text{ml min}^{-1}$  and the table speed to 0.1  $\text{m min}^{-1}$  accordingly. The film was removed from the table and dried for 7 days under ambient conditions. The composition of the dry nanosheet layer was 100% Hec.

A second single water-soluble polymer layer was coated from a 30 wt% PVOH solution on top of the Hec barrier layer. The coating gap was adjusted to 250  $\mu\text{m}$ , and the pump flow rate was set to 2.52  $\text{ml min}^{-1}$  and the table speed to 0.1  $\text{m min}^{-1}$  accordingly. The film was dried for 30 min, and the composition of the dry film was 80% PVOH, 10% glycerol, and 10% sorbitol.

### 1.2 Hydroxypropyl methylcellulose (HPMC)-based water-soluble film

For HPMC-based films, the drying temperature was set to 20 °C. The first water-soluble polymer layer was coated from a 20 wt% HPMC solution on a PLA film. The coating gap was adjusted to 450  $\mu\text{m}$ , and the pump flow rate was set to 5.9  $\text{ml min}^{-1}$  and the table speed to 0.1  $\text{m min}^{-1}$  accordingly. The film was dried for 1 h, and the composition of the dry film was 80% HPMC, 10% glycerol, and 10% sorbitol.

The water-dispersible nanosheet layer was then added on top by coating a 6 wt% Hec suspension. The coating gap was adjusted to 385  $\mu\text{m}$ , and the pump flow rate was set to 4.6  $\text{ml min}^{-1}$  and the table speed to 0.1  $\text{m min}^{-1}$  accordingly. The film was removed from the table and dried for 7 days under ambient conditions. The composition of the dry nanosheet layer was 100% Hec.

A second single water-soluble polymer layer was coated from a 20 wt% HPMC solution on top of the Hec barrier layer. The coating gap was adjusted to 480  $\mu\text{m}$ , and the pump flow rate was set to 5.9  $\text{ml min}^{-1}$  and the table speed to 0.1  $\text{m min}^{-1}$  accordingly. The film

was dried for 2 h, and the composition of the dry film was 80% HPMC, 10% glycerol, and 10% sorbitol.

### **1.3 NaAlginate-based water-soluble film**

For alginate-based films, the drying temperature was set to 20 °C. Prior to slot die coating, the alginate suspension and the slot die were heated using a heat gun. The first water-soluble polymer layer was coated from a heated 15 wt% Alginate solution on a PLA film. The coating gap was adjusted to 475  $\mu\text{m}$ , and the pump flow rate was set to 1.92  $\text{ml min}^{-1}$  and the table speed to 0.03  $\text{m min}^{-1}$  accordingly. The film was dried for 1 h, and the composition of the dry film was 80% Alginate, 10% glycerol, and 10% sorbitol.

The water-dispersible nanosheet layer was then added on top by coating a 6 wt% Hec suspension. The coating gap was adjusted to 385  $\mu\text{m}$ , and the pump flow rate was set to 4.6  $\text{ml min}^{-1}$  and the table speed to 0.1  $\text{m min}^{-1}$  accordingly. The film was removed from the table and dried for 7 days under room conditions. The composition of the dry nanosheet layer was 100% Hec.

A second single water-soluble polymer layer was coated from a heated 15 wt% Alginate solution on top of the Hec barrier layer. The coating gap was adjusted to 500  $\mu\text{m}$ , and the pump flow rate was set to 1.92  $\text{ml min}^{-1}$  and the table speed to 0.03  $\text{m min}^{-1}$  accordingly. The film was dried for 2 h, and the composition of the dry film was 80% Alginate, 10% glycerol, and 10% sorbitol.

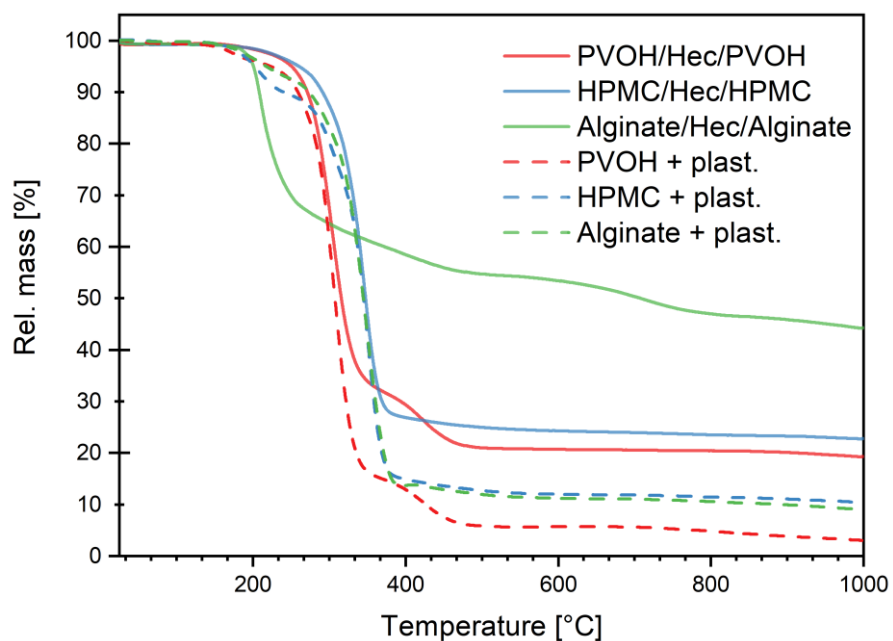


**Figure S1.** TGA curves of water-soluble films. The mass loss corresponds to the degradation of the polymer layers. The solid residue can be assigned to neat Hec minus the residue from corresponding neat plasticized polymer films (dotted lines). The water-soluble films are made of approximately 21 wt% Hec for the PVOH, 22 wt% Hec for HPMC, and 40 wt% for the Alginate case.

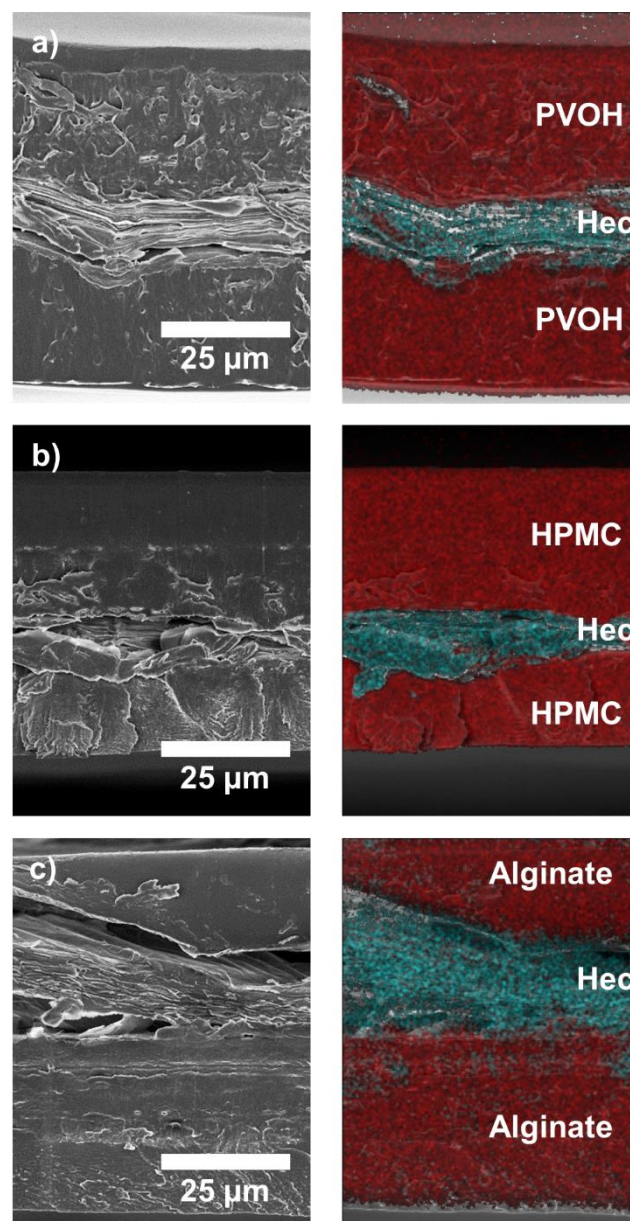


**Figure S2.** SEM cross-sections of the foils. a) PVOH/Hec/PVOH, b) HPMC/Hec/HPMC and c) Alginate/Hec/Alginate. The respective right images show the elemental distribution of Si (cyan) and C (red) *via* EDX spectroscopy.

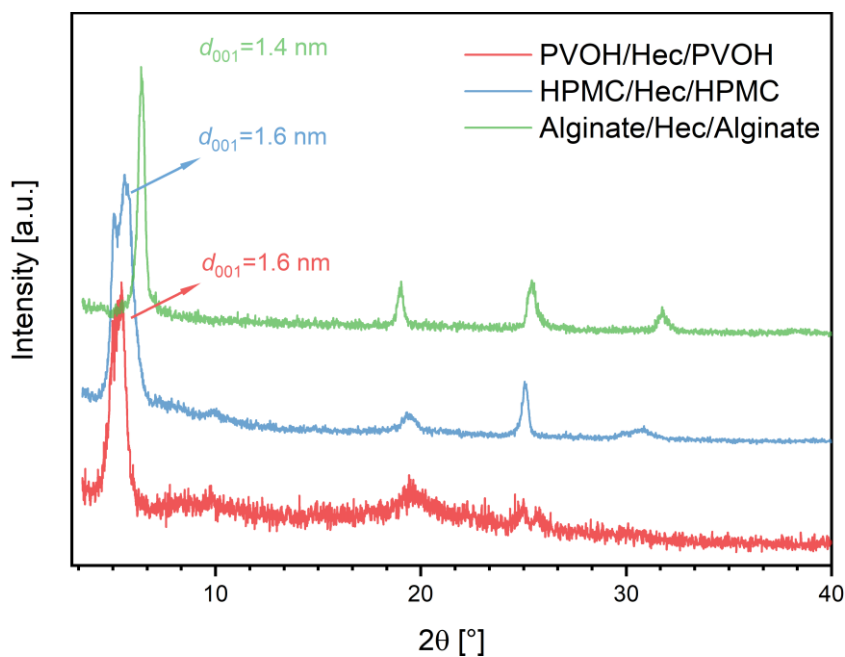


**Figure S3.** XRD pattern of water-soluble films. The  $d_{001}$  corresponds to a two-water layer hydrate of the interlayer sodium cation of neat Hec nanosheets, *i.e.* no intercalation of polymer occurred during the coating process. The polymers show typical amorphous pattern.

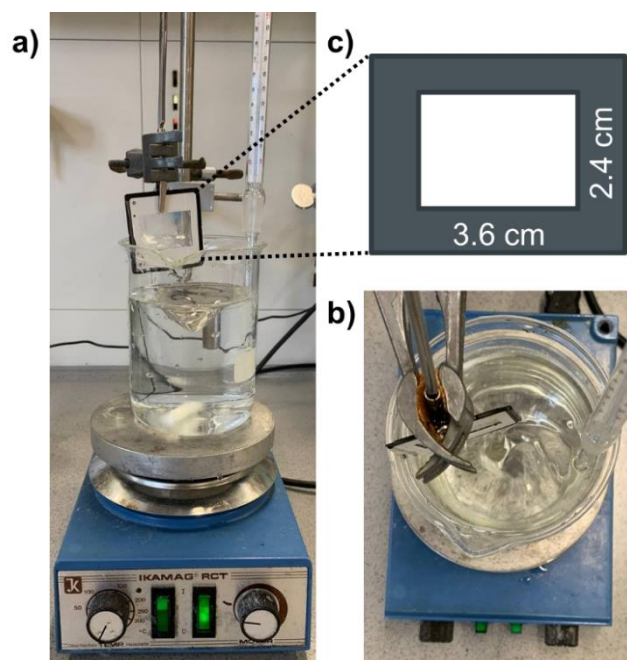


**Figure S4.** Test setup for the water-solubility tests according to MSTM-205: Solubility Test with Plastic Holder. a) Front view, b) Top view, and c) Dimensions of the sample holder.

**Table S1.** Mechanical properties of plasticized polymers (10 wt% sorbitol, 10 wt% glycerol) and their layered films with Hec. Values are a statistical average from measuring at least 6 runs.

<i>Sample:</i>	<i>PVOH</i>	<i>PVOH/ Hec/ PVOH</i>	<i>HPMC</i>	<i>HPMC/ Hec/ HPMC</i>	<i>Alginate</i>	<i>Alginate/ Hec/ Alginate</i>
<i>Tensile Strength (MPa)</i>	5.6	27	15	43	23	35
<i>Elongation at break (%)</i>	260	71	8.1	14	12	5.0
<i>Elastic Modulus (MPa)</i>	21	570	790	970	390	1100

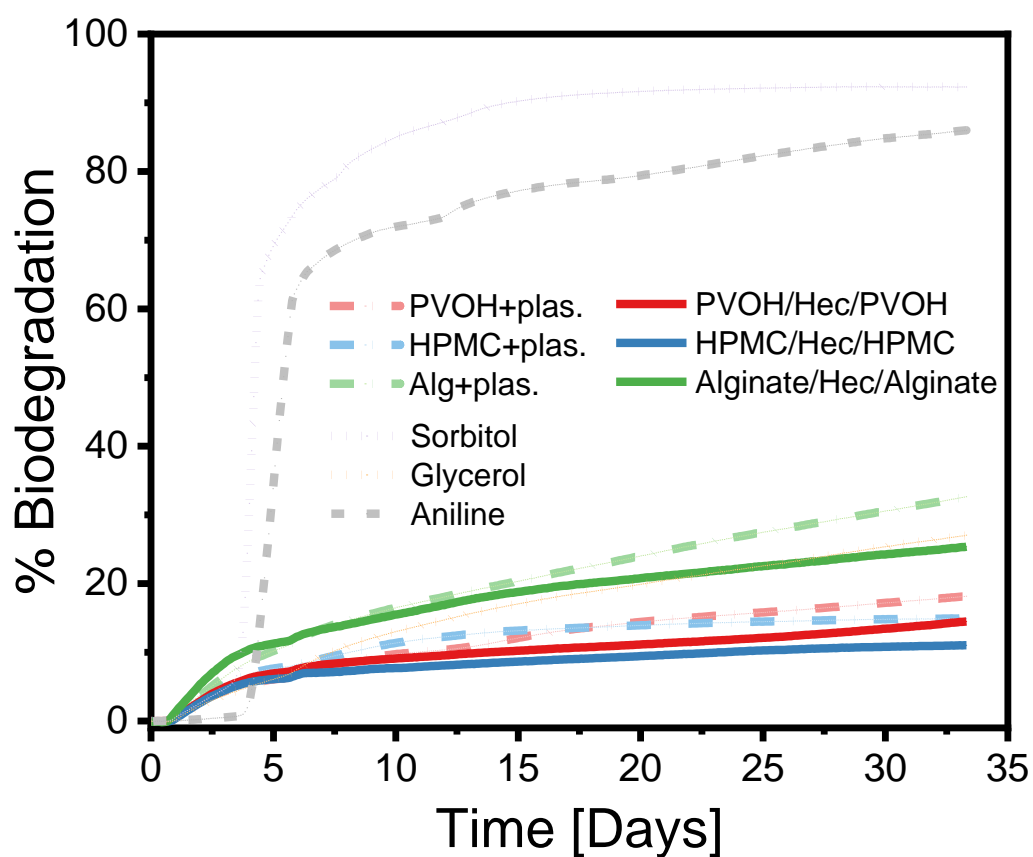


**Figure S5.** Biodegradation measured in terms of conversion to CO<sub>2</sub> for plasticized polymer films (10 wt% glycerol, 10 wt% sorbitol), the plasticized polymers as a layered film with Hec, the neat plasticizers, and aniline as the internal positive standard.



## 7. List of Publications

- Habel, C.; Tsurko, E. S.; Timmins, R. L.; Hutschreuther, J.; Kunz, R.; Schuchardt, D. D.; Rosenfeldt, S.; Altstadt, V.; Breu, J., Lightweight Ultra-High-Barrier Liners for Helium and Hydrogen. *ACS Nano* **2020**, 14 (6), 7018-7024.
- Venkateshaiah, A.; Havlíček, K.; Timmins, R. L.; Röhr, M.; Waclawek, S.; Nguyen, N. H.; Černík, M.; Padil, V. V.; Agarwal, S., Alkenyl succinic anhydride modified tree-gum kondagogu: A bio-based material with potential for food packaging. *Carbohydrate Polymers* **2021**, 266, 118126.
- Röhr, M.; Federer, L. K. S.; Timmins, R. L.; Rosenfeldt, S.; Dorres, T.; Habel, C.; Breu, J., Disorder-Order Transition-Improving the Moisture Sensitivity of Waterborne Nanocomposite Barriers. *ACS Appl Mater Interfaces* **2021**, 13(40), 48101-48109.
- Venkateshaiah, A.; Timmins, R. L.; Sehl, E.; Waclawek, S.; Černík, M.; Padil, V. V.; Agarwal, S., High Barrier, Biodegradable Nanocomposite Films based on Clay Coated and Chemically Modified Gum Kondagogu. *Macromolecular Materials and Engineering* **2022**, 2200008.
- Röhr, M.; Mettke, J. H.; Rosenfeldt, S.; Schmalz, H.; Mansfeld, U.; Timmins, R. L.; Habel, C.; Breu, J.; Durst, F., Shear orientation of nematic phases of clay nanosheets: processing of barrier coatings. *Journal of Coatings Technology and Research* **2022**, 19(2), 487-495.
- Timmins, R. L.; Kumar, A.; Röhr, M.; Havlíček, K.; Agarwal, S.; Breu, J., High Barrier Nanocomposite Film with Accelerated Biodegradation by Clay Swelling Induced Fragmentation. *Macromolecular Materials and Engineering* **2022**, 2100727.
- Venkateshaiah, A.; Sehl, E.; Timmins, R. L.; Waclawek, S.; Černík, M.; Agarwal, S.; Padil, V. V., Dialdehyde Modified Tree Gum Karaya: A Sustainable Green Crosslinker for Gelatin-Based Edible Films. *Advanced Sustainable Systems* **2022**, 2100423.
- Sehl, E.; Timmins, R. L.; Ghosh, D.; Breu, J.; Agarwal, S., Stretchable and Fast Composting Polyester Films with High-Performance Oxygen Barrier. *ACS Applied Polymer Materials* **2022**, 4 (9), 6675-6686.
- Dudko, V.; Timmins R. L.; Khoruzhenko O.; Röhr M.; Greve C.; Rosenfeldt S.; Tammelin T.; Agarwal S.; Herzig E.M.; Breu J., Spontaneous Delamination of Affordable Natural Vermiculite as a High Barrier Filler for Biodegradable Food Packaging *Materials Advances* **2022**, 3 (24), 9052-9062.



## 8. Acknowledgements

I would like to end this thesis by thanking those who have supported me along the way.

First, a special thank you to my supervisor, Prof. Dr. Josef Brey, for the opportunity to join his group and represent Anorganische Chemie 1 within the Microplastic collaborative research center. I will always appreciate the guidance and great expectations that pushed me to do my best work.

I would also like to express sincere gratitude to Prof. Dr. Seema Agarwal for her kind guidance, patience, and expertise that has greatly elevated this work. My gratitude extends to my colleagues in the Macromolecular Chemie II group that have carried out biodegradation testing and polymer analysis for our fruitful collaboration projects (Anil, Elmar, and Dipannita).

Furthermore, I would like to thank the members of the SFB 1357 Microplastics for their inspirational dedication to understanding and combating such a momentous environmental challenge through interdisciplinary collaboration. Likewise, I thank the Deutsche Forschungsgemeinschaft for funding the project.

Next, I would like to express gratitude to my lab colleagues for not only their scientific input, but also helping me learn the German way (especially Sebastian who has answered countless questions from me). Thank you to my co-authors Maxi and Volodymyr and thank you to Olena for amazing creative input. Additionally I want to give a huge thanks to Marco for all the ion-slicing and imaging, as well as Florian for Hec synthesis, clay purification, and general technical help.

My heartfelt thanks to my friends in the US who have remained one of my greatest sources of strength despite being across the ocean, especially Emily.

To my Mom and Dad, thank you so much for your love and support as I took this unexpected path. Also to my younger sisters, Carlee and Katee, whom I am incredibly proud to watch grow into awesome people.

Finally, thank you to my partner Ken from the bottom of my heart. Not only would these last three years not have been possible without you, but the experiences we have had along the way have been unforgettable. Thank you for your unwavering support and encouragement through all the ups and downs.

## *Acknowledgements*

---

## 9. Author's statement

### (Eidesstattliche) Versicherungen und Erklärungen

(§ 9 Satz 2 Nr. 3 PromO BayNAT)

*Hiermit versichere ich eidesstattlich, dass ich die Arbeit selbstständig verfasst und keine anderen als die von mir angegebenen Quellen und Hilfsmittel benutzt habe (vgl. Art. 64 Abs. 1 Satz 6 BayHSchG).*

(§ 9 Satz 2 Nr. 3 PromO BayNAT)

*Hiermit erkläre ich, dass ich die Dissertation nicht bereits zur Erlangung eines akademischen Grades eingereicht habe und dass ich nicht bereits diese oder eine gleichartige Doktorprüfung endgültig nicht bestanden habe.*

(§ 9 Satz 2 Nr. 4 PromO BayNAT)

*Hiermit erkläre ich, dass ich Hilfe von gewerblichen Promotionsberatern bzw. -vermittlern oder ähnlichen Dienstleistern weder bisher in Anspruch genommen habe noch künftig in Anspruch nehmen werde.*

(§ 9 Satz 2 Nr. 7 PromO BayNAT)

*Hiermit erkläre ich mein Einverständnis, dass die elektronische Fassung meiner Dissertation unter Wahrung meiner Urheberrechte und des Datenschutzes einer gesonderten Überprüfung unterzogen werden kann.*

(§ 9 Satz 2 Nr. 8 PromO BayNAT)

*Hiermit erkläre ich mein Einverständnis, dass bei Verdacht wissenschaftlichen Fehlverhaltens Ermittlungen durch universitätsinterne Organe der wissenschaftlichen Selbstkontrolle stattfinden können.*

.....  
Ort, Datum

.....  
Renee Timmins